5-24-2017 12:00 AM

Electrokinetic Consolidation of Oil Sands Tailings: An Experimental and Numerical Study

Yu Guo, *The University of Western Ontario*

Supervisor: Dr. Julie Q. Shang, *The University of Western Ontario*

A thesis submitted in partial fulfillment of the requirements for the Doctor of Philosophy degree in Civil and Environmental Engineering

ABSTRACT

The management of fine oil sands tailings, known as mature fine tailings (MFT), is a major challenge for the oil industry in the Northern Alberta, Canada. Dewatering and consolidation of MFT are slow and time consuming due to high water content and low permeability of MFT. The electrokinetic (EK) dewatering treatment has shown to be effective on oil sands tailings based on the results of previous researches. Therefore, this thesis is focusing on experimental and numerical studies of EK dewatering of oil sands tailings. The thesis includes three parts, i.e., EK dewatering of oil sands tailings and kaolinite slurry, EK and chemical (quicklime and Portland cement) combined treatment, and development of a one-dimensional large strain EK consolidation model.

In the first part, the EK dewatering experiments are designed and executed on oil sands tailings and slurries of kaolinite, which is the major clay mineral in the Alberta oil sands tailings, with vertically installed electrodes. The analyses are carried to obtain the regression equations of the dewatering trends for the results of oil sands tailings and kaolinite slurries, including the water drainage, water/solid content, energy consumptions, etc. The effects of applied voltage gradient and initial water content on EK dewatering are studied via the regression equations. The material saturation, especially at the anode, is found to be the key factor controlling the water flow generated by electrokinetics. Once the degree of saturation of the material at the anode drops below 80%, the most efficient stage for EK dewatering will end.

The effects of EK and chemical combined treatment of MFT are evaluated in the 2nd part in this research. The addition of quicklime or Portland cement minimizes the difference of water content and undrained shear strength of MFT between the anode and cathode, whereas it also reduces EK induced water flow. It is concluded that EK and chemical combined treatment of MFT may be beneficial at a low chemical dosage (1% quicklime or cement).

In the 3rd part of this study, a one-dimensional large strain EK consolidation model (LSEK-1D) is developed for oil sands tailings. The model predictions are in consistency with the experimental results in terms of the final settlements and consolidation times. Moreover, the effects of sample initial heights and applied current densities on consolidation times are evaluated via the model. The results indicate that the consolidation times of oil sands tailings are shorter than those based

on the conventional small strain consolidation theory, and the application of EK combined with surcharge pressure can significantly reduce the consolidation time of oil sands tailings.

Keywords: Electrokinetics (EK), Electroosmosis (EO), Dewatering, Consolidation, Oil sands tailings, Mature fine tailings (MFT), Fluid fine tailings (FFT), Chemical stabilization, Numerical modelling, Large strain EK consolidation.

CO-AUTHORSHIP

This thesis was prepared in accordance with the guidelines and regulations for a manuscript format stipulated by the Faculty of Graduate Studies at Western University. The following chapters will be modified and submitted to scientific journals have been co-authored as:

Chapter 3: Electrokinetic dewatering of oil sands tailings: data regression and saturation analysis

The contributions of the co-authors are:

Yu Guo: Carried out the experiments, analyzed the results of the laboratory study and wrote the draft and final version of the paper.

Shang, J.Q.: made major revision of paper.

Chapter 4: Experimental study and Regression analysis on electrokinetic dewatering of kaolinite slurry

The contributions of the co-authors are:

Yu Guo: Carried out the experiments, analyzed the results of the laboratory study and wrote the draft and final version of the paper.

Shang, J.Q.: made major revision of paper.

Chang Liu: helped to carry out the experiments.

Chapter 5: Electrokinetic and chemical treatment of mature fine tailings (MFT) from oil sands processing: dewatering and strengthening

The contributions of the co-authors are:

Yu Guo: Carried out the experiments, analyzed the results of the laboratory study and wrote the draft and final version of the paper.

Shang, J.Q.: made major revision of paper.

Yixuan Wang: helped to carry out the experiments

Chapter 6: One-dimensional large strain electroosmotic consolidation model

The contributions of the co-authors are:

Yu Guo: Carried out the experiments, analyzed the results of the laboratory study and wrote the draft and final version of the paper.

Shang, J.Q.: contributed advice on modelling and made major revision of paper.

ACKNOWLEDGEMENTS

I would like to express my sincere gratitude and appreciation to my supervisor, Dr. Julie Q. Shang for her great guidance, encouragement, understanding and patience. It has been a great experience to work in her group. I also want to gratefully thank Dr. K.Y. Lo, Dr. Silvana Micic for their advice during my research. With their help, my knowledge expanded greatly. Their help is not only for my research but also for my future career. It was a great pleasure for me to work with them.

I would like to thanks NSERC, ESSO URA and COSIA for their financial support in this research.

Grateful thanks are expressed to the faculty, staff, fellow graduate students, especially to Ms. Stephanie Lawrence, Ms. Cynthia Quintus, Ms. M. Richards, Mr. T. Stephens and Mr. W. Logan, Ms. C. Marshall, Ms. K. Edwards, and Ms. S. McKay. I would like to thank my friends, Cheng Zhao, Yan Ye, Dr. Raquibul Alam, Dr. Taesang Ahn , Yixuan Wang, Mingyue Liu, Wei Xiang, and Cheng Qian for their continuous support and help.

Genuine gratitude will give to my best friends, David Herbert, Irene Herbert, Trent Herbert. They are patient and kind, and always selflessly support and help me.

I am especially grateful to my parents, my wife Daoping Guo for their endless love and encouragement. Finally, and most importantly, I am thankful for the Lord's great strength and love that help me in everything.

DEDICATION

Dedicated to

The Memory of My Grandparents

TABLE OF CONTENTS

LIST OF TABLES

LIST OF FIGURES

LIST OF SYMBOLS

a_v: the coefficient of compressibility (kPa)

A: empirical parameter in the constitutive relationships for e-σ'

B: empirical parameter in the constitutive relationships for e-σ'

c_0: the molar concentration of electrolyte (mol/m^3),

C: empirical parameter in the constitutive relationships for e-k_h

CH: high plasticity clay

CHWE: Clark hot water extraction process

C_{su}: empirical coefficient for regression equation of undrained shear strength (kPa)

CT: Composite tailings

C_v: the coefficient of consolidation (m^2/s)

D: empirical parameter in the constitutive relationships for e-k_h

D_v: empirical parameter describes the maximum reduction of dewatering for EK

D_w: the maximum reduction in water content at anode during EK treatment

e: the void ratio

e_0: initial void ratio

e_i: valence

E: voltage gradient (V/m)

EK: electrokinetics

EKG: electro-kinetic geosynthetics

EO: electroosmosis

EVD: electrokinetic vertical drains

E_z: macroscopic electric field intensity (V/m)

F: Faraday constant (96487 C/mol)

FFT: fluid fine tailings

F_w: the body force per unit volume (kPa/m)

g: the acceleration of gravity (9.8 m/s^2)

G_s: specific gravity

h: total head (m)

h_z: elevation head (m)

H_0: initial height of the sample (m)

H_{dr}: initial drainage path (m)

H-S model: the Helmholtz and Smoluchowski model

i: current density (A/m^2)

i_c: applied current density (A/m^2)

i_s: streaming current (A/m^2)

I: electrical current (A)

j_{rel}: flux of water relative to the moving solid phase

k: the intrinsic permeability (m^2)

k_e: coefficient of electroosmotic permeability (m^2/sV)

k_i: electroosmotic transport coefficient (m^3/Ah)

k_h: hydraulic conductivity (m/s)

K_m: relative permittivity of free solvent

L: the length of the sample in the EK cell (m)

LEE: Low Energy Extraction process

LL: liquid limit (%)

LSEK-1D: the one dimensional large strain EK consolidation model

m_v: the coefficient of volume compressibility (kPa)

MFT: mature fine oil sands tailings

MFT-A: samples of mature fine tailings used in this study

MH: elastic silt

n: porosity of the soil, n=e/(1+e)

NST: non-segregating tailings

p_{ext}: the constant gas pressure immediately above the deposit (kPa)

P: power consumption per unit volume of bulk tailings (kW/m^3)

P_m: the maximum power consumptions per unit volume of bulk tailings (kW/m^3)

PL: plastic limit (%)

PVD: prefabricated vertical drain

q_e: the water discharge rate by electroosmosis (m^3/h)

q_{eo}: the EO flow velocity (m/s)

R: the gas constant (8.314 J/(mol·K))

REV: the representative elementary volume

s_c: solid content, which has a relationship between water content, described as: s = 1/(1 + w) (wt%)

s: location presented in material coordinate system

S: the settlement of the sample (m)

S_d: the degree of saturation (%)

S_{max}: is the maximum consolidation settlement (m)

S_u: undrained shear strength (kPa)

t: time (hour)

t_{50}: characteristic time obtained trough experiments, when normalized water drainage, $V_w/V_0=D_v/2$ (hour)

T: the absolute temperature (K)

T_{end}: characteristic time when EK induced water flow stops (hours)

T_{tran}: characteristic time when the rate of EK induced water flow changes (hours)

T_v: dimensionless time factor

u: pore-water pressure (kPa)

u_{eo}: EK induced excess pore water pressure (kPa)

u_{ex}: the excess pore water pressure (kPa)

u_{hyrd}: the hydrostatic pore water pressure (kPa)

U: electrical voltage (potential) (V)

U_{av}: average degree of consolidation (%)

USCS: Unite Soil Classification System

v_e: the average velocity of liquid phase relative to that of the moving solid phase (m^2/sV)

v_s: solid phase velocity (m/s)

v_w: pore water flow velocity (m/s)

V_0: initial volume of tailings slurry (mL)

V_w: volume of water discharge (mL)

V_w/V_0: Normalized EK water drainage (%)

w: water content, w = mass of water/mass of solid (wt%)

w_0: initial water content of tailings (wt%)

w_f: the lowest of normalized water content at anode the EK can reach

w(t): water content at any treatment time (wt%)

$w(t)/w_0$: normalized water content (%)

W: energy consumption per unit volume of bulk tailings slurry (kWh/m^3)

W_{in}: the weight of water inflow

W_m: maximum energy consumption per unit volume of bulk tailings slurry (kWh/m^3)

W_{out}: the weight of water outflow

x: the distance to the cathode (m)

x/L: the normalized distance to the cathode

z: location presented in Eulerian coordinate system in one dimension

α: the mechanical response of the soil skeleton

γ_w: the unit weight of water (9.8 kN/m^3)

γ_s: the unit weight of soil solid (kN/m^3)

Γ: electrical conductance (S)

ε: the permittivity of the pore fluid (C/V·m)

ε_0: permittivity of vacuum (8.854×1-12 F/m)

ζ: the zeta potential of soil (V)

κ: material electrical conductivity (S/m)

κ_0: initial material electrical conductivity (S/m)

κ^{-1}: the electrical double layer thickness (m)

λ_P: reduction rate of power consumptions (hour^{-1})

λ_{su}: empirical coefficient for regression equation of undrained shear strength (hour^{-1})

λ_w: reduction rate of normalized water content (hour^{-1})

μ: the liquid phase viscosity (kg/(s·m))

ξ: location presented in Lagrangian coordinate system in one dimension

ρ_b: the bulk density of the soil (kg/m^3)

ρ_w: the density of water (1×10^3 kg/m^3)

σ: normal stress (kPa)

σ': effective stress (kPa)

ψ: porewater pressure (kPa)

Chapter 1 Introduction

1.1. Background

The oil sands industry in Canada has been developing for over 40 years and are expected to grow in the future. During this process, many concerns, such as the geotechnical risk, local groundwater contamination, and greenhouse gas emission have been raised on tailings (Sobkowicz 2012, Small et al. 2015). Oil sands tailings, the by-products after oil sands processing, are mixtures of sand, silt, clay, water, residual bitumen and other hydrocarbons. The current tailings management is focusing on several aspects, i.e., production, storage, and reclamation of fluid fine tailings (Sobkowicz 2012). One of challenges in the tailings management is to accelerate the dewatering rate and minimize fluid fine tailings (FFT). The existing tailings require many large tailings ponds for storage, and must be consolidated in order to reclaim the land occupied by these tailings ponds. A major challenge for the dewatering and consolidation treatment is to deal with the mature fine tailings (MFT), which typically have the solid content of about 30% and naturally remain in a very stable condition.

Electrokinetics (EK) is one of the potential technologies that can be used to accelerate the dewatering of the tailings. EK has been applied in geotechnical and environmental engineering for years, such as improving the soft ground (Casagrande 1959, 1983, Fetzer 1967, Shang 1997, Rittirong and Shang 2005) and dewatering the waste slurry (Tuan et al. 2012). A preliminary study on the feasibility of EK dewatering on oil sands mature fine tailings has been carried out (Guo and Shang 2014). The one-dimensional bench scale dewatering tests were carried out with horizontally installed electrodes. The results indicate that EK can significantly accelerate the dewatering rate of MFT. This study is the continuation of the previous study (Guo and Shang 2014), focusing on experimental and theoretical aspects of electrokinetic dewatering on oil sands tailings and kaolinite slurries.

1.2. Research objectives

The goals of this research are to study the EK dewatering of oil sands tailings and kaolinite slurries via vertically installed electrodes, and to develop a large strain one-dimensional model for EK

consolidation of oil sands tailings and other highly compressible geomaterials. The specific objectives of the study include:

1) Design experiments to study the EK dewatering effects on oil sands tailings via the vertically installed electrodes to simulate field applications in tailings ponds.

2) Study the general trends of EK dewatering on oil sands tailings as well as on kaolinite slurries, including the water drainage, solid content, applied voltage and current, energy consumptions, etc., via data regressions of experimental results.

3) Study the mechanism of EK flow as related to the degree of saturation of oil sand tailings and kaolinite slurries.

4) Investigate the combined effects of EK and chemical stabilization (quicklime and Portland cement) on MFT.

5) Develop a one-dimensional large strain EK consolidation model and verify and validate the model via the experimental results of EK dewatering on oil sands tailings.

1.3. Thesis outline

The thesis contains seven chapters. The contents present in each chapter are summarized as follows:

- ***Chapter 1:*** Introduce the background of the research, research objectives, thesis outline and original contributions of the study.

- ***Chapter 2*****:** Present a literature review, including the basic knowledge of oil sands and associated tailings management technologies, and fundamentals of electrokinetics.

- ***Chapter 3*****:** Describe the experimental study of EK dewatering on oil sands tailings via the vertically installed electrodes and conduct data analysis via regression. An in-depth discussion of EK flow as affected by the material saturation is presented.

- ***Chapter 4:*** Describe the experimental study on kaolinite slurry. The effects of voltage gradient on energy consumption are analyzed via data regression. The effects of kaolinite sample saturation on EK induced water flow are analyzed.

- ***Chapter 5:*** Study the combined treatments of EK and chemical stabilization (quicklime and Portland cement) on oil sands tailings. The analysis is focusing on changes in water content and undrained shears strength.

- ***Chapter 6:*** Develop a one dimensional large strain EK consolidation model (LSEK-1D), and validate the model with the data obtained from EK dewatering experiments on oil sands tailings in terms of final settlement and consolidation time. The effects of the initial sample height and applied current density on the EK consolidation time are analyzed via the LSEK-1D model.

- ***Chapter 7:*** Summarize the key aspects, draw conclusions, and make recommendations for future research.

Chapters 3, 4, 5 and 6 are presented in the format of manuscripts. The topics are different but related to each other and prepared for publication. Hence there might be overlaps in the introduction and experimental sections in these chapters.

1.4. Original contributions

The original contributions of this study are:

- Experimental study of the EK dewatering on oil sands tailings and kaolinite slurry via vertically installed electrodes to simulate the field conditions.

- A data processing technique involving normalization and regression to obtain mathematical equations for the general trends of EK dewatering process.

- Identification of the limiting factor, i.e. the degree of saturation, quantitatively for EK flow in oil sands tailings and kaolinite slurries.

- Evaluation and interpretation of the combined effects of EK treatment and chemical stabilization (quicklime and Portland cement) on oil sands tailings.

- Development of a one dimensional large strain EK consolidation model (LSEK-1D) for oil sands tailings, and verification and validation of the model with experimental data on oil sands tailings in the first time.

References

Casagrande, L. (1959). Review of past and current work on electroosmotic stabilization of soils. In Harvard Soil Mechanics Series, 45, Harvard University Cambridge, Massachusetts, USA (reprinted November 1959 with a supplement of June 1957).

Casagrande, L. (1983). Stabilization of soil by means of electroosmosis: state-of-the-art. Journal of the Boston Society of Civil Engineers, ASCE, 69, No. 2, 255–302.

Fetzer, C. A. (1967). Electro-osmotic stabilization of west branch dam. Journal of the Soil Mechanics and Foundations Division, 93, No. 4, 85-106.

Guo, Y., and Shang, J. Q. (2014). A study on electrokinetic dewatering of oil sands tailings. Environmental Geotechnics, 1, No. 2, 121-134.

Rittirong, A., and Shang, J. (2005). Electroosmotic stabilization. Elsevier Geo-Engineering Book Series, 3, 967-996.

Shang, J. Q. (1997). Electrokinetic dewatering of clay slurries as engineered soil covers. Canadian Geotechnical Journal, 34, No. 1, 78-86.

Small, C. C., Cho, S., Hashisho, Z., and Ulrich, A. C. (2015). Emissions from oil sands tailings ponds: Review of tailings pond parameters and emission estimates. Journal of Petroleum Science and Engineering, 127, 490-501.

Sobkowicz, J. (2012). Oil Sands Tailings Technology Deployment Roadmap Project Report – Volume 1: Project Summary. Available at http://www.cosia.ca/uploads/documents/id9/Tailings%20Roadmap%20Volume%201%20June%202012.pdf.

Tuan, P. A., Mika, S., and Pirjo, I. (2012). Sewage sludge electro-dewatering treatment—a review. Drying Technology, 30, No. 7, 691-706.

Chapter 2 Literature review

2.1. Management of oil sands tailings

Oil sands, which are unconventional petroleum reserves, are partially consolidated sandstone or loose sand deposits of bitumen. Compared with conventional oil, bitumen has high density and viscosity. Enormous capacity of oil sands, 2100 billion barrels of oil, has been estimated (Demaison et al. 1977, Shaw et al. 1996). Oil sands deposits are found around the world, including Canada, Venezuela, USA, Trinidad, Madagascar, Albania, Russia and Romania (Shaw et al. 1996, Chalaturnyk et al. 2002). Canada has the third largest reserves of crude oil, among which 165 billion barrels are in oil sands (AER 2016, CAPP 2016). Surface mining (Fig. 2.1) and in-situ extraction (Fig. 2.2) are two main methods used for oil recovery (CAPP 2016). The surface mining is used to recover shallow oil sands deposits (typically less than 75 meters below the ground surface) (Charpentier et al. 2009, ADOE 2016). For deeper deposits, bitumen is pumped to surface after being heated or diluted in-situ (Charpentier et al. 2009, ADOE 2016).

Older facilities (such as Suncor and Syncrude Base mines) use the Clark hot water extraction (CHWE) process to separate bitumen from the ore obtained in surface mining (Sobkowicz. 2012). In the process, oil sands are dispersed with water, steam, and caustic (NaOH) (Mikula et al. 1996). Therefore, extraction of the bitumen generates large amount of liquid wastes. It is estimated that to produce one barrel of synthetic crude oil, about 2 tonnes of ore are needed and about 1.8 tonnes of solid waste and 2 m^3 wastewater are generated (Mikula et al. 1996). A simplified illustration of oil sands mining and bitumen extraction operations processes is shown in Fig. 2.3. More recently, the Low Energy Extraction (LEE) process developed by Syncurde has been used in newer facilities (Sobkowicz 2012).

It was reported that the Alberta oil sands industry produced 1.184 million barrels per day in 2008 (Giesy et al. 2010) and about 2.3 million barrels per day in 2014 (ADOE 2016, AER 2016). Among these, 56% of crude oil are produced by surface mining in 2008 and reduced to 47% in 2014 (ADOE 2016). Enormous amounts of tailings have been produced due to surface mining of oil sands. Small et al. (2015) reported that tailings ponds occupied about 176 km^2. A net cumulative footprint, including dykes, berms, beaches, and in-pit ponds, is about 220 km^2 in the Lower

Athabasca Region (GOA 2015). Thus, nowadays the management of oil sands tailings has become one of the major challenges in the oil sands industry.

2.1.1. Oil sands tailings characteristics

Tailings are the by-products after mining processing. Oil sands tailings are discharged in the form of slurry, which is a mixture of water, sand, silt, clay and residual bitumen. The discharged tailings slurry contains about 55 wt% solid, which consists 82wt% sand, 17wt% fines (smaller than 44 μm) and 1wt% residual bitumen, which is transported and deposited in tailings ponds via pipelines (Chalaturnyk et al. 2002). The coarse sized particles segregate from fines, and form the dike. The remaining fines run off into the tailings ponds, accumulate and settle with time. The solid content of these fines quickly reaches to 20 wt% and further to 30 wt% after a few years (Chalaturnyk et al. 2002). These fine tailings are called mature fine tailings (MFT), which have a stable structure and will remain fluid state for decades (Kasperki 1992). It is estimated that it will take thousands of years to reach full consolidation if untreated (Mikula et al. 1996).

The mineralogy governs both hydraulic and mechanical behaviors of MFT. In the McMurray Formation, quartz sand is the major component of Athabasca oil sands (Shaw et al. 1996). The dominant clay minerals in this formation are kaolinite and illite with traces of smectities, chloride, vermiculite and mixed-layer clays (Mossop 1980, Mikula et al. 1996, Chalaturnyk et al. 2002, Mikula et al. 1996, Kaminsky 2008, Guo and Shang 2014, Bourgès-Gastaud et al. 2017).

A brief summary of the MFT properties is listed in Table 2.1, cited from different sources. The average solid content of MFT is about 33%, corresponding to the water content of 203% and void ratio of 5, reported by BGC Engineering Inc. (2010). The specific gravities range from about 2.3 to 2.6, as seen in Table 2.1. The liquid limit is from 40% to 70% and the plastic limit is 10% to 20% (BGC Engineering Inc. 2010). It is noted that the water content is 3 to 5 times over the liquid limit, indicating that the MFT is in the liquid state and has a virtually zero shear strength. The residual bitumen content ranges from 1 to 7 wt% by total mass and the particle size of MFT is varied from case to case, as seen in Table 2.1. The hydraulic conductivity reported by BGC Engineering Inc. (2010) is in the range of 1×10^{-6} to 1×10^{-9} m/s. The measured hydraulic conductivities of oil sands tailings (Jeeravipoolvarn et al. 2009, Guo and Shang 2014) are within

this range. Since the MFT is stable in nature (Mikula et al. 1996, BGC Engineering Inc. 2010), the consolidation is very slow in tailings ponds.

2.1.2. Technologies of oil sands tailings management

Two fundamental factors affect the selection of the tailings management technology, i.e., the cost required to meet the performance criteria, as well as the objective and the risks associated with the selected methods (COSIA 2012).

COSIA (2012) reported four types of disposal method for oil sands tailings and some of the current process methods used to release water from fine tailings.

- ***Thin layered, fines-dominated deposits***: The tailings are discharged into disposal site in thin layers (thin lifts), which are typically 100-500 mm thick, after initial dewatering via chemical or mechanical treatment. Further dewatering of tailings depends on natural process of atmospheric evaporation and free-thaw cycles.

- ***Deep, fines-dominated deposits***: After initial dewatering via mainly polymer flocculation, the tailings are discharged continuously into a deep disposal sites, and further dewatering is primarily attributed to self-weight consolidation.

- ***Fines-enriched sand deposits***: Composite tailings (CT) or non-segregating tailings (NST) are formed by mixing fine tailings with coarse materials and flocculants or coagulants. The materials usually have higher hydraulic conductivity and lower compressibility than fine tailings. Further dewatering relies on self-weight consolidation.

- ***Water capped fines deposits***: In this method, the MFT is placed in a completed mine pit and capped with water. Then a natural lake system can be established once the quality of water reaches the environmental criteria.

BCG Engineering Inc. (2010) presented a detailed review of current technologies for oil sands tailings management. The technologies were classified into five categories:

- ***Physical/Mechanical Processes***: The physical/mechanical processes include thermal, electrical treatment, prefabricated vertical drain (PVD) and other mechanical forces (pressure, centrifuge, vacuum filtration) to accelerate the dewatering of MFT.

  Filtration and centrifugation are mature and commercialized technologies to dewater tailings in the mining industry (Sobkowicz 2012). Some researches were performed in last decades by using filtration (Xu et al. 2008, Zhang 2010, Wang et al. 2010, Alamgir et al. 2012, Wang et al. 2014), and centrifuge (Mikula et al. 2009, Rima 2013, Azam and Rima 2014, Sorta 2015) on oil sands tailings. An Experimental study on using PVD to dewater oil sands tailings was reported by Yao (2016). Electrokinetic dewatering researches on oil sands tailings were reported by (Guo and Shang 2014, Zhang 2016, Bourgès-Gastaud et al. 2017).

- ***Natural Process***: In this method, the dewatering of oil sands tailings relies on the natural process, such as self-weight consolidation (Jeeravipoolvarn et al. 2009, Jeeravipoolvarn 2010), atmospheric evaporation (Yao 2016) and free-thaw cycles (Proskin et al. 2010, 2012).

- ***Chemical/Biological treatment:*** In chemical treatment, flocculants or coagulants are used to modify the surface properties of tailings particles, thus leading to flocculation and coagulation of MFT and reduction in water content. Biological treatment involves using bacterial action to densify MFT. Many researches are carried out by using flocculants or coagulants to improve the thickening and dewatering of oil sands tailings (Pourrezaei and El-Din 2008, Sworska and Laskowski 2000, Beier et al. 2103, Farkish and Fall 2014, Islam and Shang 2017).

- ***Mixtures/Co-disposal***: Fine tailings are mixed with other soil or waste materials of coarse sizes, to increase the density and hydraulic conductivity of tailings. Composite tailings (CT) or non-segregating tailings (NST) mentioned above are the typical products. Flocculants or coagulants are also added during mixing.

- ***Permanent Storage***: Tailings are water capped in a completed mine pit to form a lake connecting to local hydrological system or back filled into underground mine caverns.

Sobkowicz (2012) reported the ongoing technology development of oil sands tailings. In this report, developments of the technologies for tailings management are summarized in terms of tailings technology suites. The technology suite means a series of technologies involved in the entire tailings plan for a specific mine site (Sobkowicz 2012). The technologies associated with its development stages are classified into six categories (as seen in Appendix A in Sobkowicz 2012):

- Mining
- Extraction and Bitumen recovery
- Tailings processing
- Deposition
- Water treatment
- Reclamation

Some of the technologies are used in other mining industries, but less than half of the technologies mentioned in the report are currently mature and commercialized for oil sands (Sobkowicz 2012).

2.2. Electrokinetics

Electrokinetics (EK) dewatering of MFT is studied in this research. EK has been applied in geotechnical engineering to consolidate soft clays since 1950s (Casagrande 1949, Bjerrum et al. 1967, Fetzer 1967, Chappell and Burton 1975, Wade 1976, Lo et al. 1991 Bergado et al. 2000, Chew et al. 2004, Rittirong et al. 2008, Jones et al. 2011). More recently, electrokinetics has been studied to dewater mine tailings (Fourie et al. 2007, Fourie and Jones 2010) and oil sands tailings (Guo and Shang 2014, EKS 2014, 2016, Bourgès-Gastaud et al. 2017).

2.2.1. Fundamentals of electrokinetics

Electrokinetics (EK) consists of mainly three phenomena, as seen in Fig. 2.4:

- ***Electroosmosis (EO):*** Electroosmosis refers to the movement of the pore fluid under the DC electric field in a stationary porous media, such as clay, slurry, tailings, etc.

- ***Electrophoresis:*** Electrophoresis is the movement of a colloidal particle with charged surfaces in a stationary fluid under an electric force (Smoluchowski 1924, Masliyah and Bhattacharjee 2006).

- ***Electromigration***: Electromigration refers to the movement of dissolved ions under an electrical force.

For soils, the clay surfaces are negatively charged due to isomorphous substitution. The silicon (Si^{4+}) in the clay crystal structure is substituted by lower valence ion (such as Al^{3+}, Mg^{2+}), resulting in a net negative charge in the surface. In the soil-water-electrolyte system, the electrical double layer is formed because the negatively charged clay particle surface attracts the cations and repulse anions. The ion distributions at the charged clay particle surface are described via the theory of electrical double layer, i.e., a fixed inner layer (Stern-layer) and a diffusive outer layer (Gouy-layer). The widely used Gouy-Chapman-Stern double layer model, is illustrated in Fig. 2.5 (Shang et al. 1994, Mitchell and Soga 2005, Masliyah and Bhattacharjee 2006). The electrical double layer thickness (κ^{-1}) (m) is defined as (Shang et al. 1994, Mitchell and Soga 2005, Masliyah and Bhattacharjee 2006):

$$\kappa = \sqrt{\frac{2c_0 e^2 F^2}{\varepsilon_0 K_m RT}} \tag{2.1}$$

where c_0 is the molar concentration of electrolyte (mol/m^3), e is valence, F is Faraday constant (96487 C/mol), ε_0 is permittivity of vacuum (8.854×1^{-12} F/m), K_m is relative permittivity of free solvent, R is gas constant (8.314 J/(mol·K)), and T is absolute temperature (K).

A quantitative determination of the potential distribution in the Gouy-Chapman-Stern double layer model was given by Shang et al. (1994).

The presence of electrical double layer is essential for the EO flow in the soils. The Helmholtz and Smoluchowski (H-S) model is widely used to describe the electroosmosis in soil. Based on the theory, the liquid-filled capillary in soil is treated as an electrical condenser with the negative charges on the surface of particles and counterchanges concentrated in a layer in the liquid closed to the particle surface, as seen in Fig. 2.6 (Mitchell and Soga 2005). The moved layer of counterions is assumed to drag the water through the capillary via plug flow under the electric field. This water flow is known as EO water flow. A comparison between hydraulic flow and EO flow is shown in Fig. 2.6 (Mitchell and Soga 2005). The fluid flow due to electroosmosis is expressed in an empirical relationship by analogy with Darcy's law (Casagrande 1949, Mitchell and Soga 2005):

$$q_{eo} = k_e E \tag{2.2}$$

where q_{eo} is the EO flow velocity (m/s), E is the voltage gradient (V/m), and k_e is the coefficient of electroosmotic permeability ($m^2/s \cdot V$), which can be expressed as below according to the H-S model (Mitchell and Soga 2005):

$$k_e = \frac{\zeta \varepsilon}{\mu} n \tag{2.3}$$

where, ζ (V) is the zeta potential of soil, ε (C/V·m) is the permittivity of the pore fluid, n is the porosity of the porous medium and μ ($N \cdot s/m^2$) is the viscosity of the pore fluid.

Eq. 2.3 cannot be used to estimate the coefficient of electroosmotic permeability, k_e, directly, since the H-S model does not consider the soil capillary tortuosity (Shang 1997). Therefore, the coefficient of electroosmotic permeability, k_e, must be measured through experiments (Mohamedelhassan and Shang 2001, Mohamedelhassan and Shang 2003, Guo and Shang 2014).

The zeta potential, ζ, is the potential measured at the shear surface between the fixed Stern layer and diffusive Gouy layer, as seen in Fig. 2.5. It is usually measured in experiments and used to characterize the surface potential of the clay particles. Shang (1997) reported the linear relationship

between the coefficient of electroosmotic permeability, k_e, and the zeta potential of natural clay. Thus, the measurement of the zeta potential can be used as a quick method to evaluate the feasibility of EK treatment on soils.

The main factors, which affect the electroosmotic flow in soils, include the soil zeta potential, porewater salinity and pH, which have been discussed extensively in the literature, e.g. Iwata et al. (2013), Malekzadeh et al. (2016).

2.2.2. EK consolidation and model

Electroosmosis consolidation has been studied extensively via laboratory and field works for over five decades (Casagrande 1959, 1983, Bjerrum et al. 1967, Esrig and Gemeinhardt 1967, Esrig 1968, Fetzer 1967, Lockhart and Hart 1988, Lo and Ho 1991, Chew et al. 2004, Fourie et al. 2007). However, in the oil sands industry, this technology is not widely accepted and still remains at the stage of research (Sobkowicz 2012).

The modeling of electroosmotic dewatering and consolidation is very important for the prediction of consolidation time and dewatering effect. Esrig (1968) proposed the theory of excess pore water pressure generated due to EK via superposition of the fluid flow generated by both electrical field and hydraulic gradient, expressed as:

$$u_{eo} = \frac{k_e}{k_h}\gamma_w U(z) \tag{2.4}$$

where u_{eo} is the excess pore water pressure generated due to electroosmosis (kPa), k_e (m^2/sV) is coefficient of electroosmotic permeability, k_h is the hydraulic conductivity (m/s), γ_w is the unit weight of water (kN/m^3), U(z) is the electrical potential at position z from the cathode (V).

Based on the same principle of Terzaghi's consolidation theory, the one-dimensional EK consolidation model was introduced by Esrig (1968):

$$u_e(z,t) = \frac{k_e}{k_h}\left[-\gamma_w U(z) + \frac{2}{\pi^2}\gamma_w \sum_{n=0}^{\infty} \frac{(-1)^n}{(n+\frac{1}{2})^2} \sin\frac{(n+\frac{1}{2})\pi z}{L} * \exp\left[-(n+\frac{1}{2})^2\pi^2 T_V\right]\right]$$

(2.5)

where γ_w is the unit weight of water (kN/m^3), z is the location from the cathode (m), T_v is dimensionless time factor defined as:

$$T_V = \frac{c_V t}{H^2}$$

(2.6)

where C_v is the coefficient of consolidation (m^2/s), t is the time (s), and H is the length of the drainage path (m).

The Esrig's work has been extended by many researchers. Wan and Mitchell (1976) proposed an analytical solution for electroosmosis combined with direct loading in one-dimensional condition. Lewis and Humpheson (1973) applied the finite element method to analyze the electroosmosis consolidation. Shang (1998a, b) introduced a two-dimensional EO consolidation model and presented an analytical solution. Rittriong and Shang (2008) applied the finite differential method to solve two dimensional EO consolidation. Yuan et al. (2012) proposed a finite element model for multi-dimensional domain. Later Yuan et al. (2013) used the finite element method coupled with modified Cam Clay model to simulate the nonlinear behavior of clay during electroosmotic consolidation. Su and Wang (2003) proposed a 2-D electroosmotic consolidation model in the horizontal plane. Hu and Wu (2014) proposed a 3-D mathematical model based on Biot's multi-dimensional consolidation theory.

The models mentioned above are developed based on the small strain consolidation theory with a constant consolidation coefficient, i.e., a constant hydraulic conductivity. However, the small strain theory encounters difficulties when dealing with extra soft materials, such as marine clay, sewage slurry, mature fine tailings. A consolidation theory based on the large strain analysis was firstly proposed by Gibson et al. (1967). A close form solution was derived under the assumption of a constant large strain coefficient of consolidation, C_F. The numerical solution was given by

considering the linear relationship between the void ratio and C_F. Since then many researches have carried out studies on large strain consolidation of geomaterials (Monte and Krizek 1976, Gibson et al. 1981, Lee and Sills 1981, Been and Sills 1981, Cargill 1986, Xie and Leo 2004, Bo et al. 2010, 2011, Ito and Azam 2013).

Feldkamp and Belhomme (1990) developed an EK consolidation theory by considering large strain deformation based on the Gibson (1967) theory. More recently, Hu et al. (2012) proposed an EK consolidation model via nonlinear variation of soil parameters. Yuan and Hicks (2013) used the finite element method to simulate the large strain electroosmotic consolidation, which predicts faster pore water pressure development and smaller finial settlements. Yuan and Hicks (2016) extend the large strain electroosmotic consolidation model by coupling with the modified Cam Clay model and verified with the cases reported by Bjerrum et al. (1967), Feldkamp and Belhomme (1990), Mohamedelhassan and Shang (2002).

Two practical approaches, pointed out by Krizek and Somogyi (1984), can be used to improve the accuracy of the model, i.e., modify the model or improve material property relationships. Material property relationships for many model analyses involve empirical estimations. This will increase the discrepancies between the model prediction and observation. Therefore, in this thesis, a large strain EK consolidation model for oil sands tailings is developed, with consideration of nonlinearity of the oil sand tailings behavior, such as the hydraulic conductivity, stress-strain relationship, coefficient of electroosmotic permeability and tailings electrical conductivity.

References

Alam, R., and Shang, J. Q. (2017). Removal of bitumen from mature oil sands tailings slurries by electro-flotation. Journal of Water Process Engineering,15, 116-123.

Alamgir, A., Harbottle, D., Masliyah, J., and Xu, Z. (2012). Al-PAM assisted filtration system for abatement of mature fine tailings. Chemical engineering science, 80, 91-99.

Alberta Energy Regulator (AER) (2016). ST98-2016 executive summary Alberta's energy reserves 2015 & Supply/Demand outlook 2016-2025. Available at http://www1.aer.ca/st98/data/executive_summary/ST98-2016_Executive_Summary.pdf

Alberta Department of Energy (ADOE) (2016). Oil sands production profile 2004 – 2014. Available at http://www.energy.alberta.ca/Org/pdfs/InitiativeOSPP.pdf

Azam, S., and Rima, U. S. (2014). Oil sand tailings characterization for centrifuge dewatering. Environmental Geotechnics, 1, No. 3, 189-196.

Been, K., and Sills, G. C. (1981). Self-weight consolidation of soft soils: an experimental and theoretical study. Géotechnique, 31, No. 4, 519-535.

Beier, N., Wilson, W., Dunmola, A., and Sego, D. (2013). Impact of flocculation-based dewatering on the shear strength of oil sands fine tailings. Canadian Geotechnical Journal, 50, No. 9, 1001-1007.

Bergado, D. T., Balasubramaniam, A. S., Patawaran, M. A. B., and Kwunpreuk, W. (2000). Electroosmotic consolidation of soft Bangkok clay with prefabricated vertical drains. Ground Improvement, 4, No.4, 153-163.

BGC Engineering Inc. 2010. Oil sands tailings technology review. Oil sands research and information network (OSRIN), University of Alberta, School of Energy and the Environment, Edmonton, Alberta; 2010. p. 136.

Bjerrum, L., Moum, J., and Eide, O. (1967) Application of electroosmosis to a foundation problem in a Norwegian quick clay. Géotechnique, 17, No. 3, 214–235

Bo, M. M., Choa, V., and Wong, K. S. (2010). Constant rate of loading test on ultra-soft soil. ASTM geotechnical testing journal, 33, No.3, 192-200.

Bo, M. W., Choa, V., Wong, K. S., and Arulrajah, A. (2011). Laboratory validation of ultra-soft soil deformation model. Geotechnical and Geological Engineering, 29, No.1, 65-74.

Bourgès-Gastaud, S., Dolez, P., Blond, E., and Touze-Foltz, N. (2017). Dewatering of oil sands tailings with an electrokinetic geocomposite. Minerals Engineering, 100, 177-186.

Cameselle, C., Belhadj, B., Akretche, D. E., and Gouveia, S. (2013). Advances in electrokinetic remediation for the removal of organic contaminants in soils. Intech Open Access Publisher.

Canadian Association of Petroleum Producers (CAPP) (2016). The facts on Canada's oil sands. Available at http://www.capp.ca/publications-and-statistics/publications/296225

Cargill, K. W. (1986). The large strain, controlled rate of strain (LSCRS) device for consolidation testing of soft fine-grained soils (No. WES/TR/GL-86-13). Army Engineer Waterways Experiment Station Vicksburg Geotechnical Lab.

Casagrande, L. (1949) Electroosmosis in soil. Géotechnique, 1, No.3,159–177.

Casagrande, L. (1959). Review of past and current work on electroosmotic stabilization of soils. In Harvard Soil Mechanics Series, 45, Harvard University Cambridge, Massachusetts, USA (reprinted November 1959 with a supplement of June 1957).

Casagrande, L. (1983). Stabilization of soil by means of electroosmosis: state-of-the-art. Journal of the Boston Society of Civil Engineers, ASCE, 69, No. 2, 255–302.

Chappell, B.A. and Burton, P.L. (1975). Electro-osmosis applied to unstable embankment, J. Geotech. Eng. Div., ASCE, 101, No. 8, 733–740.

Chalaturnyk, R. J., Don Scott, J., and Özüm, B. (2002). Management of oil sands tailings. Petroleum Science and Technology, 20, No. 9-10, 1025-1046.

Charpentier, A. D., Bergerson, J. A., and MacLean, H. L. (2009). Understanding the Canadian oil sands industry's greenhouse gas emissions. Environmental research letters, 4, No. 1, 014005.

Chew, S. H., Karunaratne, G. P., Kuma, V. M., Lim, L. H., Toh, M. L., and Hee, A. M. (2004). A field trial for soft clay consolidation using electric vertical drains. Geotextiles and Geomembranes, 22, No. 1, 17-35.

COSIA (2012). Technical guide for fluid fine tailings management. Available at: http://www.cosia.ca/uploads/documents/id7/TechGuideFluidTailingsMgmt_Aug2012.pdf

Demaison, G. J. (1977). Tar sands and supergiant oil fields. In the Oil Sands of Canada-Venezuela 1977, ed. D.A. Redford and A.G. Winestock, Special Volume 17, 9-16. Calgary, Alberta: Canadian Institute of Mining, Metallurgy and Petroleum.

Electrokinetic solutions Inc. (EKS) (2014). EKR testing and development technical report presented to Shell Canada. Available at: http://electrokineticsolutions.com/wp-content/uploads/sites/2/2014/06/Shell-Testing-Report-April-2014.pdf

Electrokinetic solutions Inc. (EKS) (2016). Final report: EKR testing and development Phase II presented to Shell Canada. Available at: http://electrokineticsolutions.com/wp-content/uploads/sites/2/2014/06/AI-EES-C-FER-Test-Report-Final-Public-7-Jan-2016.pdf

Esrig, M. I. (1968). Pore pressures, consolidation, and electrokinetics. Journal of the Soil Mechanics and Foundations Division, 94, No. 4, 899-922.

Esrig, M. I., and Gemeinhardt, J. P. (1967). Electrokinetic stabilization of an illitic clay. Journal of the Soil Mechanics and Foundations Division, 93, No. 3, 129-136.

Farkish, A. (2013). SAP based dewatering of oil sands mature fine tailings. M.ASc. Thesis, University of Ottawa, Ottawa, Canada

Farkish, A., and Fall, M. (2014). Consolidation and hydraulic conductivity of oil sand mature fine tailings dewatered by using super absorbent polymer. Journal of Geotechnical and Geoenvironmental Engineering, 140, No. 7, 1-6.

Feldkamp, J. R., and Belhomme, G. M. (1990). Large-strain electrokinetic consolidation: theory and experiment in one dimension. Géotechnique, 40, No. 4, 557-568.

Fetzer, C. A. (1967). Electro-osmotic stabilization of west branch dam. Journal of the Soil Mechanics and Foundations Division, 93, No. 4, 85-106.

Fourie, A. B., and Jones, C. J. F. P. (2010). Improved estimates of power consumption during dewatering of mine tailings using electrokinetic geosynthetics (EKGs). Geotextiles and Geomembranes, 28, No.2, 181-190.

Fourie, A. B., Johns, D. G., and Jones, C. F. (2007). Dewatering of mine tailings using electrokinetic geosynthetics. Canadian Geotechnical Journal, 44, No. 2, 160-172.

Gibson, R. E., England, G. L., and Hussey, M. J. L. (1967). The theory of one-dimensional consolidation of saturated clays. Géotechnique, 17, No. 3, 261-273.

Gibson, R. E., Schiffman, R. L., and Cargill, K. W. (1981). The theory of one-dimensional consolidation of saturated clays. II. Finite nonlinear consolidation of thick homogeneous layers. Canadian geotechnical journal, 18, No. 2, 280-293.

Giesy, J. P., Anderson, J. C., & Wiseman, S. B. (2010). Alberta oil sands development. Proceedings of the National Academy of Sciences, 107, No. 3, 951-952.

Government of Alberta (GOA) (2015) Lower Athabasca Region: Tailings Management Framework for the mineable Athabasca oil sands. Available at: http://open.alberta.ca/publications/9781460121740

Guo, Y. (2012). Electrokinetic dewatering of oil sands tailings. M.Esc. Thesis, University of Western Ontarion, London, Canada

Guo, Y., and Shang, J. Q. (2014). A study on electrokinetic dewatering of oil sands tailings. Environmental Geotechnics, 1, No. 2, 121-134.

Hu, L., and Wu, H. (2014). Mathematical model of electro-osmotic consolidation for soft ground improvement. Géotechnique, 64, No. 2, 155-164.

Hu, L., Wu, W., and Wu, H. (2012). Numerical model of electro-osmotic consolidation in clay. Géotechnique, 62, No. 6, 537-541.

Ito, M., and Azam, S. (2013). Large-strain consolidation modeling of mine waste tailings. Environmental Systems Research, 2, No. 1, 1-12.

Islam, S., and Shang, J. Q. (2017). Electrokinetic thickening of mature fine oil sands tailings. Environmental Geotechnics, 4, No. 1, 40-55.

Iwata, M., Tanaka, T., and Jami, M. S. (2013). Application of electroosmosis for sludge dewatering—A review. Drying Technology, 31, No.2, 170-184.

Javan Roshtkhari, S. (2016). Application of rhamnolipid and microbial activities for improving the sedimentation of oil sand tailings. Ph.D. Thesis, Concordia University, Montreal, Canada

Jeeravipoolvarn, S. (2010). Geotechnical behavior of in-line thickened oil sands tailings. PhD thesis, University of Alberta, Edmonton, Alberta.

Jeeravipoolvarn, S., Scott, J. D., and Chalaturnyk, R. J. (2009). 10 m standpipe tests on oil sands tailings: long-term experimental results and prediction. Canadian geotechnical journal, 46, No. 8, 875-888.

Jones, C. J., Lamont-Black, J., and Glendinning, S. (2011). Electrokinetic geosynthetics in hydraulic applications. Geotextiles and Geomembranes, 29, No.4, 381-390.

Kasperski, K. L. (1992). A review of properties and treatment of oil sands tailings. AOSTRA Journal of Research, 8, 11-53.

Kaminsky, H. A. W. (2008). Characterization of an Athabasca oil sand ore and process streams. Ph.D. Thesis, University of Alberta, Edmonton, Canada.

Krizek, R. J., and Somogyi, F. (1984). Perspectives on modelling consolidation of dredged materials. Sedimentation consolidation models: predictions and validation: In proceedings of a symposium, R.N. Yong and F.C. Townsend Eds, ASCE, New York, 296-332.

Lee, K., and Sills, G. C. (1981). The consolidation of a soil stratum, including self-weight effects and large strains. International journal for numerical and analytical methods in geomechanics, 5, No. 4, 405-428.

Lewis, R. W., and Humpheson, C. (1973). Numerical analysis of electro-osmotic flow in soils. Journal of the Soil Mechanics and Foundations Division, 99, No. 8, 603-616.

Lo, K.Y. and Ho, K.S. (1991) The effects of electroosmotic field treatment on the soil properties of a soft sensitive clay, Canadian Geotechnical Journal, 28, 763–770.

Lo, K. Y., Ho, K. S., and Inculet, I. I. (1991). Field test of electroosmotic strengthening of soft sensitive clay. Canadian Geotechnical Journal, 28, No. 1, 74-83.

Lockhart, N. C.,and Hart, G. H. (1988). Electro-osmotic dewatering of fine suspensions: the efficacy of current interruptions. Drying Technology, 6, No. 3, 415-423.

Malekzadeh, M., Lovisa, J., and Sivakugan, N. (2016). An overview of electrokinetic consolidation of soils. Geotechnical and Geological Engineering, 34, No. 3, 759-776

Masliyah, J.H., and Bhattacharjee, S. (2006). Electrokinetic and colloid transport phenomena. John Wiley and Sons, Inc., Hoboken, NJ.

Mikula, R. J., Kasperski, K. L., Burns, R. D., and MacKinnon, M. D. (1996). Nature and fate of oil sands fine tailings. In: Schramm, L.L. (Ed.), Suspensions: Fundamentals and Applications in the Petroleum Industry. ACS, Washington, DC, 677–723.

Mikula, R. J., Munoz, V. A., and Omotoso, O. (2009). Centrifugation options for production of dry stackable tailings in surface-mined oil sands tailings management. Journal of Canadian Petroleum Technology, 48, No. 9, 19-23.

Mitchell, J., and Soga, K. (2005). Fundamentals of soil behavior. John Wiley and Sons, Inc., Hoboken, NJ.

Mohamedelhassan, E., and Shang, J.Q. (2001) Effects of electrode materials and current intermittence in electroosmosis. Ground Improvement, 5, No. 1, 3–11.

Mohamedelhassan, E., and Shang, J. Q. (2002). Feasibility assessment of electro-osmotic consolidation on marine sediment. Proceedings of the Institution of Civil Engineers-Ground Improvement, 6, No. 4, 145-152.

Mohamedelhassan, E., and Shang, J. Q. (2003). Electrokinetics-generated pore fluid and ionic transport in an offshore calcareous soil. Canadian Geotechnical Journal, 40, No. 6, 1185-1199.

Monte, J. L., and Krizek, R. J. (1976). One-dimensional mathematical model for large-strain consolidation. Géotechnique, 26, No. 3, 495-510.

Mossop, G. D. (1980). Geology of the Athabasca oil sands. Science, 207, No. 4427, 145-152.

Pourrezaei, P., and El-Din, M.G. (2008). Coagulation-flocculation pre-treatment of oil sands process affected water. 1st International oil sands tailings conference (IOSTC), Edmonton, Alberta, Canada.

Proskin, S., Sego, D., and Alostaz, M. (2010) Freeze-thaw and consolidation tests on Suncor mature fine tailings (MFT). Cold Regions Science and Technology, 63, No. 3, 110-120.

Proskin, S., Sego, D., and Alostaz, M. (2012). Oil sands MFT properties and freeze-thaw effects. Journal of Cold Regions Engineering, 26, No. 2, 29–54.

Rima, U. S. (2013). Characterization and centrifuge dewatering of oil sands fine tailings. M.ASc. Thesis, University of Regina.

Rittirong, A., and Shang, J. Q. (2008). Numerical analysis for electro-osmotic consolidation in two-dimensional electric field. In the Eighteenth International Offshore and Polar Engineering Conference. International Society of Offshore and Polar Engineers.

Rittirong, A., Douglas, R. S., Shang, J. Q., and Lee, E. C. (2008). Electrokinetic improvement of soft clay using electrical vertical drains. Geosynthetics International, 15, No.5, 369-381.

Shang, J. Q. (1997). Zeta potential and electroosmotic permeability of clay soils. Canadian Geotechnical Journal, 34, No. 4, 627-631.

Shang, J. Q. (1998a). Electroosmosis-enhanced preloading consolidation via vertical drains. Canadian Geotechnical Journal, 35, No. 3, 491-499.

Shang, J. Q. (1998b). Two-dimensional electro-osmotic consolidation. Proceedings of the ICE-Ground Improvement, 2, No. 1, 17-25.

Shang, J.Q., and Lo, K.Y., and Quigley, R.M. (1994). Quantitative determination of potential distribution in Stern-Gouy double-layer model. Canadian Geotechnical Journal, 31, 624-634

Shaw, R.C., Schramm, L.L., Czarnecki, J. (1996). Suspensions in the hot water extraction process for Canadian oil sands. In: Schramm, L.L. (Ed.), Suspensions: Fundamentals and Applications in the Petroleum Industry. ACS, Washington, DC, 639–675.

Small, C. C., Cho, S., Hashisho, Z., and Ulrich, A. C. (2015). Emissions from oil sands tailings ponds: Review of tailings pond parameters and emission estimates. Journal of Petroleum Science and Engineering, 127, 490-501.

Smoluchowski, M. (1924). Contribution à la théorie de l'endosmose électrique et de quelques phénomènes corrélatifs. Pisma Mariana Smoluchowskiego, 1(1), 403-420.

Sobkowicz, J. (2012). Oil sands tailings technology deployment roadmap project report – Volume 1: Project summary. Available at http://www.cosia.ca/uploads/documents/id9/Tailings%20Roadmap%20Volume%201%20June%202012.pdf.

Sorta, A. R. (2015). Centrifugal modelling of oil sands tailings consolidation, Ph.D. thesis, University of Alberta.

Sworska, A., Laskowski, J. S., and Cymerman, G. (2000). Flocculation of the Syncrude fine tailings: Part I. Effect of pH, polymer dosage and Mg^{2+} and Ca^{2+} cations. International journal of mineral processing, 60, No.2, 143-152.

Su, J. Q., and Wang, Z. (2003). The two-dimensional consolidation theory of electro-osmosis. Géotechnique, 53, No. 8, 759-763.

Wade, M.H. (1976). Slope stability by electro-osmosis. Proceedings of 29th Canadian Geotechnical Conference, Vancouver, Section 10, 44–66.

Wan, T. Y., and Mitchell, J. K. (1976). Electro-osmotic consolidation of soils. Journal of the geotechnical engineering division, 102, No. 5, 473-491.

Wang, C., Harbottle, D., Liu, Q., and Xu, Z. (2014). Current state of fine mineral tailings treatment: A critical review on theory and practice. Minerals Engineering, 58, 113-131.

Wang, X. T., Feng, X., Xu, Z., and Masliyah, J. H. (2010). Polymer aids for settling and filtration of oil sands tailings. The Canadian Journal of Chemical Engineering, 88, No. 3, 403-410.

Xie, K. H., and Leo, C. J. (2004). Analytical solutions of one-dimensional large strain consolidation of saturated and homogeneous clays. Computers and Geotechnics, 31, No. 4, 301-314.

Xu, Y., Dabros, T., and Kan, J. (2008). Filterability of oil sands tailings. Process Safety and Environmental Protection, 86, No. 4, 268-276.

Yao, Y. (2016). Dewatering behavior of fine oil sands tailings: an experimental study. Ph.D. Thesis, Delft University of Technology, Delft, Netherlands.

Yuan, J., Hicks, M. A., and Dijkstra, J. (2012). Multi-dimensional electro-omosis consolidation of clays. In TC 211 International Symposium & Short Courses" Recent Research, Advances & Execution Aspects of Ground Improvement Improvement Works, Brussels, Belgium, 30 May-1 June 2012. ISSMGE Technical Commitee TC 211.

Yuan, J., Hicks, M. A., and Dijkstra, J. (2013). Numerical model of elasto-plastic electro-osmosis consolidation of clays. Poromechanics V, Vienna, Austria. ASCE, 2076-2085.

Yuan, J., and Hicks, M. A. (2013). Large deformation elastic electro-osmosis consolidation of clays. Computers and Geotechnics, 54, 60-68.

Yuan, J., and Hicks, M. A. (2016). Numerical simulation of elasto-plastic electro-osmosis consolidation at large strain. Acta Geotechnica, 1-17.

Zhang, C. (2010). Cross flow filtration of oil sands total tailings. M.Sc Thesis, University of Alberta, Edmonton, Canada.

Zhang, R. (2016). Electrokinetics and vacuum combined dewatering of oil sand tailings. M.Esc. Thesis, Western University, London, Canada

Table 2.1 Summary of properties of oil sands tailings

Properties		BGC Engineering Inc (2010)	Jeeravipoolvarn et al. (2009)	Farkish (2013), Farkish and Fall (2014)	Guo (2012) Guo and Shang (2014)	Yao (2016)	Javan Roshtkhari (2016)	Alam and Shang (2017)
Water content, w (wt%)		203	227	156	171	213	124	158
Solid content, s (wt%)		33	30	39	37	32	45	39
Void ratio, e		5	5.2	3.8	4.39	4.9	-	4.26
Specific gravity, G_s		-	2.28	2.45	2.51	2.30	-	2.58
Atterberg limit	Liquid limit, LL (%)	40-75	-	51.2	51.6	48-61	68	54.4
	Plastic limit, PL (%)	10-20	-	37.2	29.1	26-29	31	36.0
	Plastic index, PI (%)	-	-	14	22.5	22-33	37	18.4
Hydraulic conductivity, k_h (m/s)		1×10^{-6}~1×10^{-9}	$1.8\times10^{-9}e^{3.824}$	-	1.81×10^{-9} (e=2.03)			-
Organic content (wt% by total mass)		-	3.1	-	5.4 (14.7% by dry mass)	1-2	7.4	5.4 (17.9% by dry mass)
Grain size	Sand	-	11.0	4	0	0-7	28	0
	Silt	-	89.0	77	80	43-55	72	81
	Clay	-		19	20	45-50		19
	D_{10} (µm)	-	-	-	0.85	-	-	1.09
	D_{30} (µm)	-	-	-	-	0.8	-	-
	D_{50} (µm)	-	-	-	7.15	2.2	-	8.03
	D_{60} (µm)	-	-	-	-	4.8	-	-
	D_{90} (µm)	-	-	-	27.9	-	-	26.86

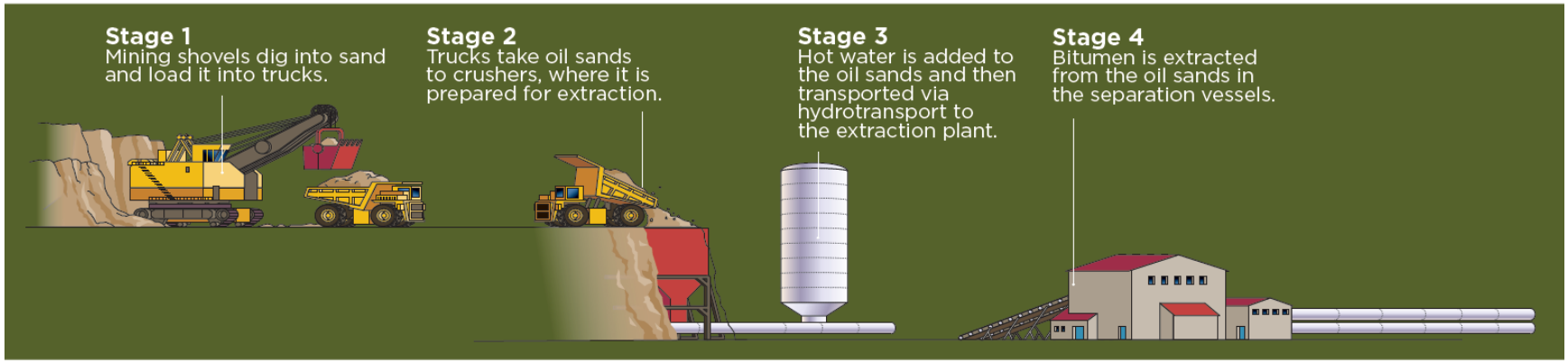

Figure 2.1 A simple illustration of the surface mining of oil sands (CAPP 2016)

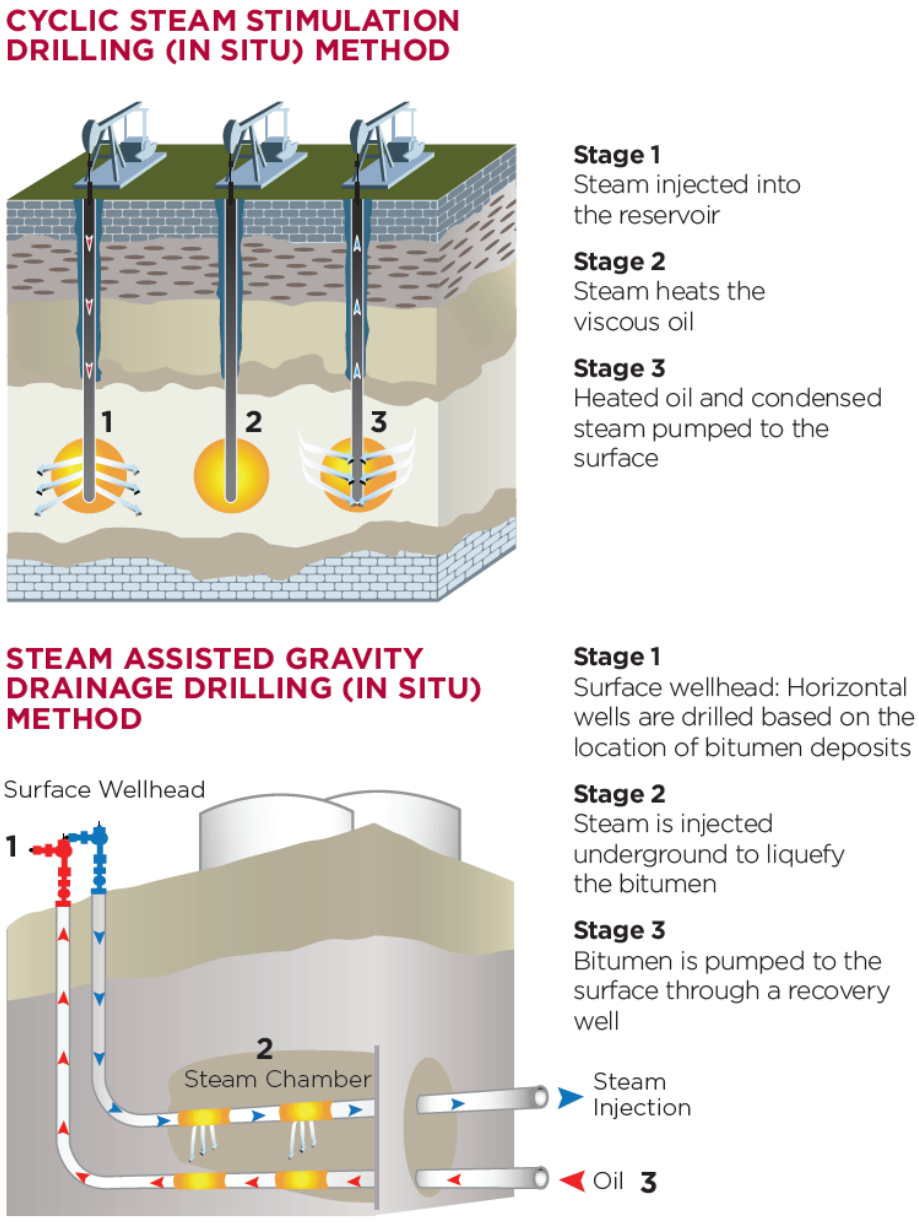

Figure 2.2 A simple illustration of the in site mining of oil sands (CAPP 2016)

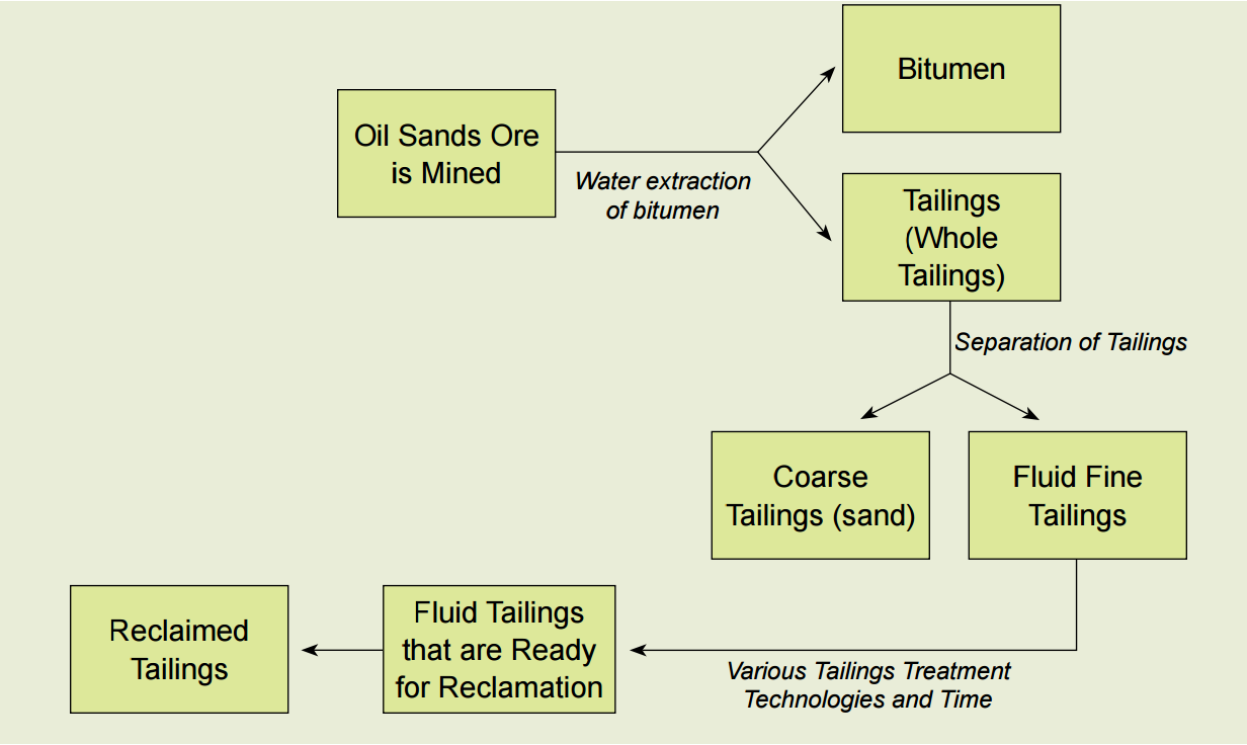

Figure 2.3 A flow chart for the simplified illustration of oil sands mining and bitumen extraction operations (GOA 2015)

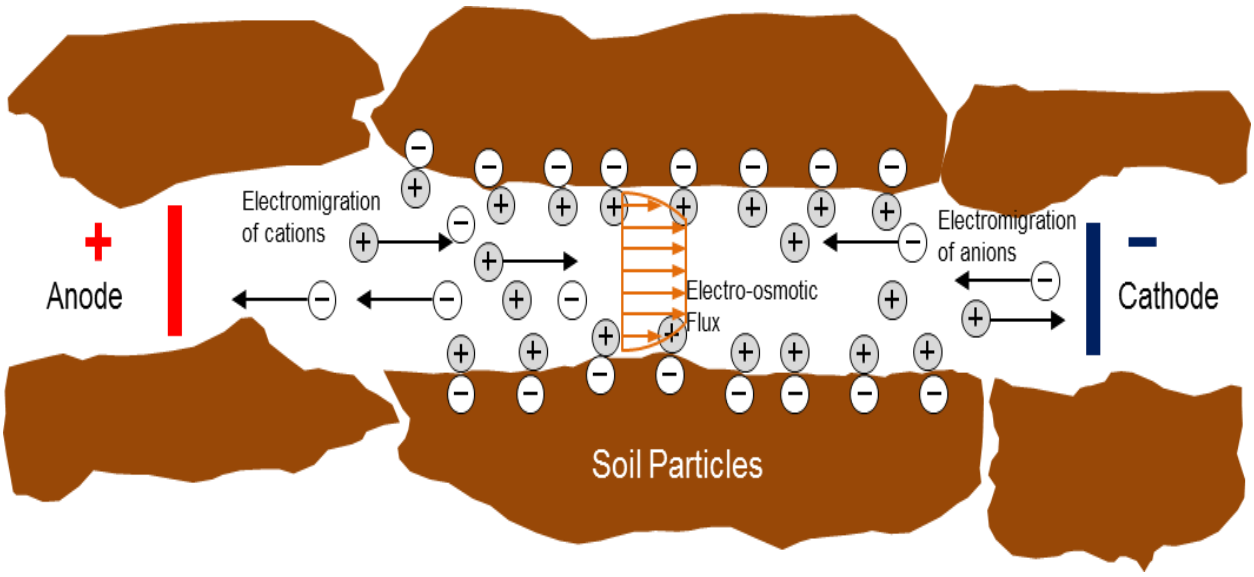

Figure 2.4 Electrokinetic transport phenomena in a single capillary of soil (Cameselle et al. 2013)

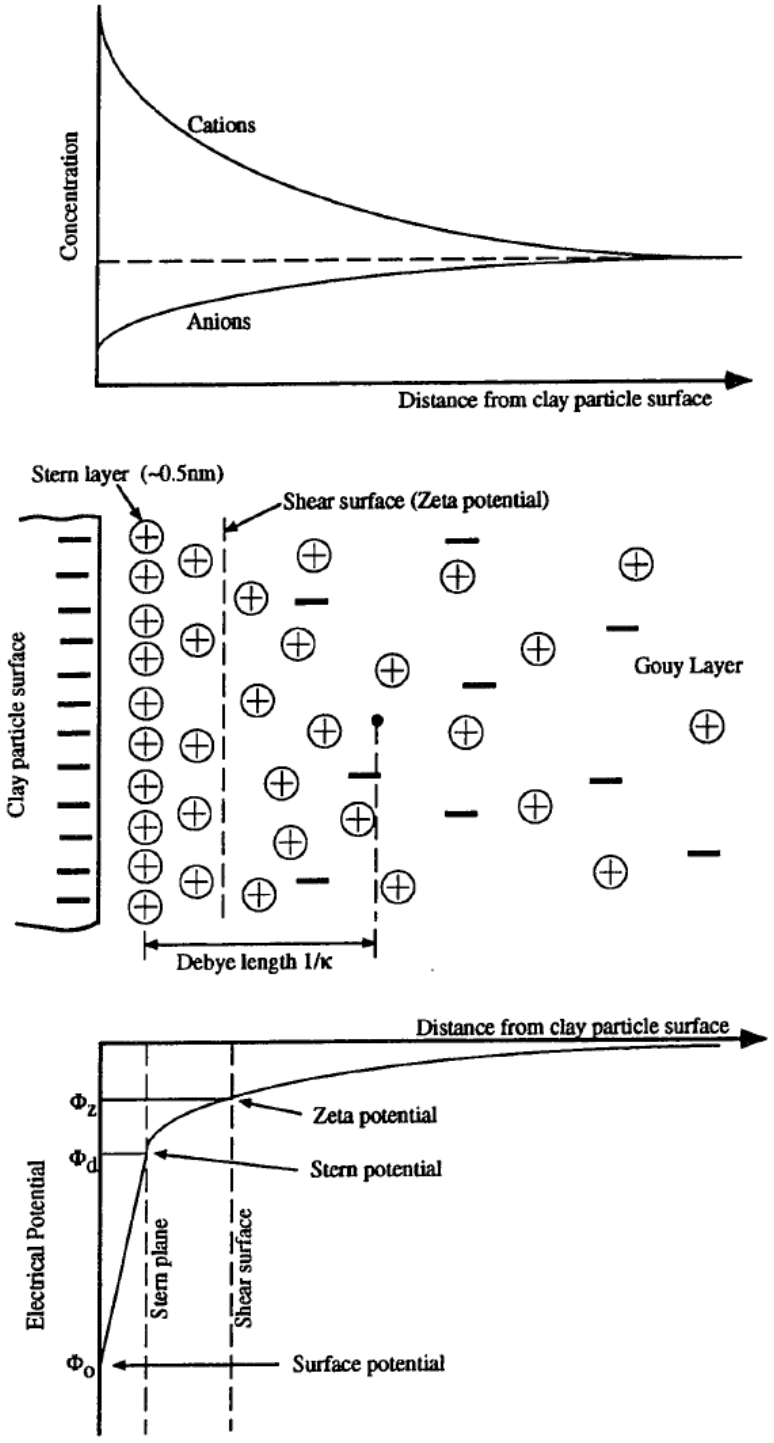

Figure 2.5 The Gouy-Chapman-Stern model for double layer theory presented in Guo (2012)

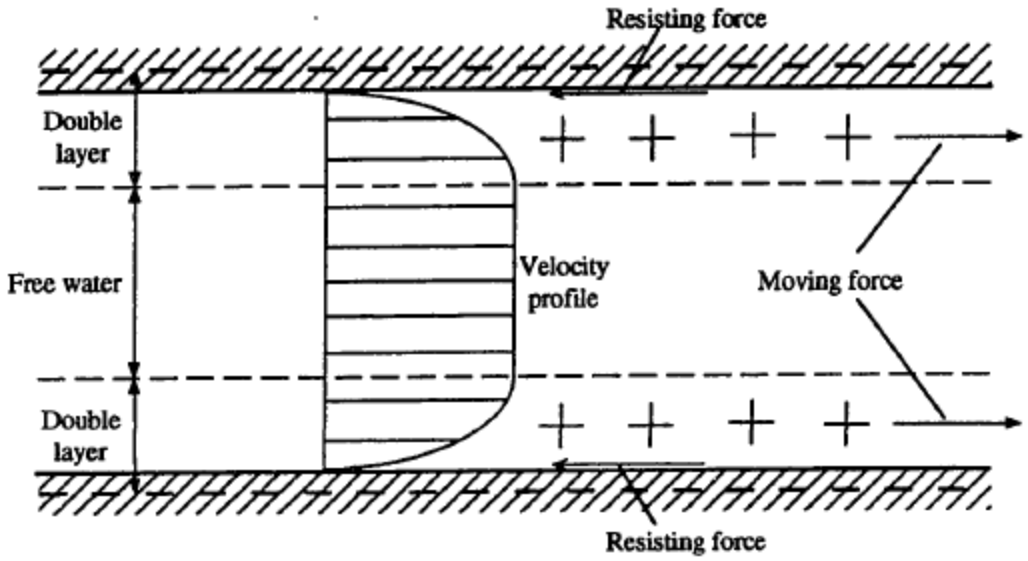

(a) Electroosmotic flow

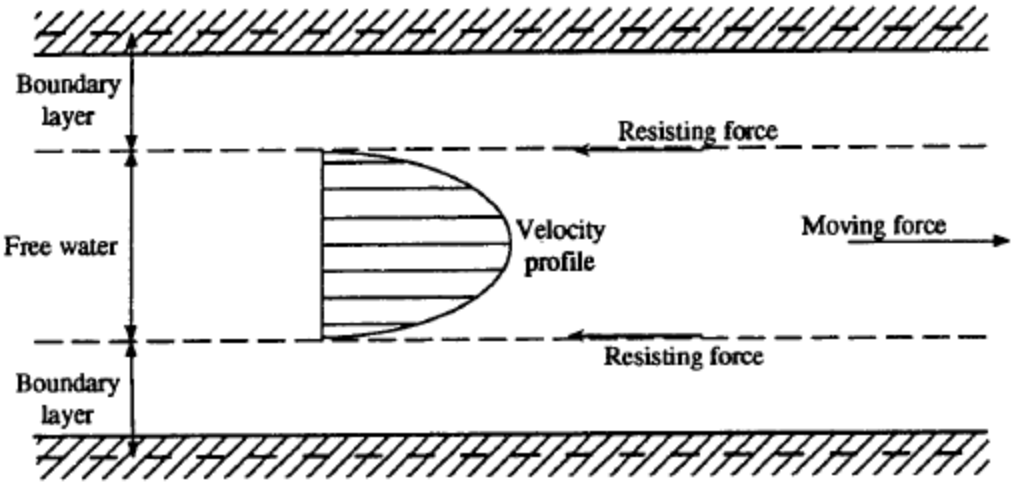

(b) Hydraulic flow

Figure 2.6 Comparison between electroosmotic flow and hydraulic flow in a capillary presented in Guo (2012)

Chapter 3 Electrokinetic dewatering of oil sands tailings: data regression and saturation analysis

3.1.Introduction

Electrokinetics (EK) is a promising soil improvement method. Laboratory studies and field applications of EK treatment on soft clays, mine tailings and waste slurry have been reported since 1950s (Casagrande 1949, 1959, 1983; Mohamedelhassan and Shang 2001, Micic et al. 2001, 2002, Chew et al. 2004, Shang et al. 2004, Fourie et al. 2007, Glendinning et al. 2007, Fourier and Jones 2010, Jones et al. 2011, Lee and Shang 2013, Guo and Shang 2014). The effects such as reducing soil water content and increasing undrained shear strength, have been studied on different types of soils (Bjerrum et al. 1967, Lo et al. 1991a, 1991b, Micic et al. 2002, Rittirong et al. 2008, Guo and Shang 2014). In 1960s, Bejerrum et al. (1967) applied the EK to stabilize quick clay on an excavation site near Oslo, Norway. Later the EK field tests on a soft sensitive Champlain clay in Ottawa valley, Canada, were reported by Lo et al. (1991a, 1991b). More recently Micic et al. (2001, 2002) reported a lab experimental study on electrokinetic strengthening soft marine clay recovered from the southeast coast of Korean Peninsulas. Field applications of EK for soil improvement is reviewed by Rittirong and Shang (2005).

Mohamedelhassan and Shang (2001) proposed an experimental device to measure the coefficient of electroosmotic permeability, k_e (m^2/sV), based on the vertical installed electrodes. Other essential soil parameters, such as the hydraulic conductivity, k_h (m/s), material electrical conductivity, κ (S/m), and voltage distribution, can also be measured on the device. The dimensionally stable anode (DSA) has been used in lab experiments for electrokinetic tests due to its advantages such as corrosion resistance and small voltage loss (Guo and Shang 2014, Liu and Shang 2014, Chien et al. 2014, Ou et al. 2015). In recent years the electrokinetic vertical drains (EVD) and electrokinetic geosynthetics (EKG) have been developed and studied in lab tests and field trials (Bergado et al. 2000, Glendinning et al. 2005a, 2005b, 2007, Jones et al. 2008, 2011, Rittirong et al. 2008, Shang 2011). The applications of EK dewatering on other geo materials such as mine tailings and sewage

sludge are also reported (Raats et al. 2002, Yang et al. 2005, Fourie et al. 2007, Glendinning et al. 2007, Jone et al. 2011, Guo and Shang 2014, Iwata 2013).

An important consideration for EK applications is the cost. The electrokinetic treatment is considered cost efficient for soft silt clay or soft clayey silt with relatively low hydraulic conductivities. Grey and Mitchell (1967) suggested using electroosmotic transport coefficient, k_i (m^3/Ah), to calculate the power consumption per unit volume of water discharge, which is expressed as:

$$\frac{P}{q_e} = \frac{U}{k_i} \times 10^{-3} \tag{3.1}$$

where P is the power consumption (kW); q_e is the water discharge rate by electroosmosis (m^3/h), U is the electrical potential (V), k_i is electroosmotic transport coefficient (m^3/Ah), which can be calculated from the coefficient of electroosmotic permeability, k_e, and material electrical conductivity, κ:

$$k_i = \frac{k_e}{\kappa} \tag{3.2}$$

The coefficient of electroosmotic permeability, k_e (m^2/sV), varies within a relatively narrow range, about 5×10^{-9} in average for most type of clays (Casagrande 1949, Grey and Mitchell 1967, Mitchell and Soga 2005).

However, it should be noted that during an electrokinetic dewatering process, the soil properties, including the coefficient of electroosmotic permeability, k_e, and electrical conductivity, κ, change with time, thus k_i is not a constant.

It is well understood that during an electrokinetic treatment, soil parameters, such as the water content, shear strength, and electrical conductivity will change with treatment time. The voltage gradient, current density and treatment time are the most important parameters for electrokinetic treatment, as they are closely related to the total energy consumption and finial dewatering effects. The water is driven from anode and discharged at cathode during EK dewatering. In the previous study of EK dewatering on oil sands tailings, it is found that once the water content of soil at anode reached to a certain point, the water discharge

would stop, which is mainly attributed to the fact that soil become unsaturated with significantly reduced hydraulic conductivity and increased electrical resistance (Guo and Shang 2014). In many laboratory studies (Esmaeily et al. 2006, Shang 1997) and field applications (Bjerrum et al. 1967, Lo et al. 1991a), it was also found that the water contents of the soils reduced and the electrical resistances of soils increased significantly at the anode, thus increasing energy consumption. However, there is limited information about quantitative analysis of the saturation status of the materials during EK treatment in the literature. Therefore, the saturation status of soils, especially near the anode, which is considered as the reason for the reduction of efficiency for EK dewatering treatment, need to be studied in detail.

The study is conducted on mature fine oil sand tailings (MFT), which are the fine fraction of oil sands tailings after separation and segregation. MFT contains significant fraction of clay minerals, including kaolinite (40–70 wt%), illite (28–45 wt%) and traces of montmorillonite (Chalaturnyk et al. 2002). Because of the high clay content and fine particle size the MFT has low hydraulic conductivity, which leads to slow consolidation. Due to the high water content (low solid content) and slow consolidation, the tailings without treatments would remain at a liquid state for decades. The previous study (Guo and Shang 2014) has shown the EK treatment can dewater MFT effectively. It was observed that the EK dewatering tests resulted in significant reductions in water content and consolidation time and increases in overall undrained shear strength of fine oil sands tailings.

In this study, the laboratory experiments are designed to simulate the conditions of EK field treatment with vertical installed electrodes. The effects of voltage gradient and treatment time on the material properties, such as the water content, and material electrical conductivity, are studied, since it is necessary and important for efficient application of EK. A data processing method is proposed, which involves normalization and regression. The degree of saturation in tailings during the EK treatment is analyzed to understand its effects on EK dewatering. Moreover, the effective treatment period, which is an important design parameter for large scale applications of EK technology, is analyzed in relation to the development of unsaturation in oil sands tailings.

3.2.Experiments

3.2.1. Properties of oil sands tailings

The oil sands tailings used in this study are recovered from the tailings pond, courtesy of Syncrude Canada (MFT-A). The properties of oil sands tailings have been studied by Guo and Shang (2014) and Islam and Shang (2017). The characteristics of MFT-A are summarized in Table 3.1. MFT-A has the initial solid content* (the mass ratio of solids/bulk tailings) from 27% to 40%, which is equivalent to the water content (the mass ratio of water/dry solids) 260% to 140%.

3.2.2. EK dewatering tests

The EK dewatering tests are designed to simulate the field application of EK treatment with vertically installed electrodes. All tests are conducted under the voltage-control method, i.e., the voltage is kept constant during the experiments.

The EK dewatering cell, which is modified from Liu and Shang (2014), is used in this research. The apparatus consists of a plexiglass tank with the dimensions of 350×100×250 mm (length × width × height), as shown in Fig. 3.1. Two vertical electrode plates are installed on the right and left sides of the tank with a spacing of 295 mm. The electrodes are covered with filter papers and geotextiles to prevent the leakage of tailings particles. The MFT-A sample is placed in EK dewatering cell between two vertical electrodes. A horizontal flow is generated by EK under this electrode configuration. The top surface of the tailings sample is set as a free boundary, which allows the free settlement during the EK treatment. The DSA (dimensionally stable anode, Ti/IrOx mesh) and stainless steel (SS316) mesh cathode are used as the anode and cathode, respectively. There are two drainage holes at the left and right edges of the tank for water collection. The water discharge is through the drainage holes connected via a plastic tube to a graduated cylinder for measurement.

* Solid content, s_c, has a relationship with the water content, w, $s_c = 1/ (1 + w)$ (wt%)

The conditions of EK dewatering tests are summarized in Table 3.2. The initial water content was measured, following ASTM D2216-10 (ASTM 2010), and recorded before each test. The original tailings slurry without any pre-treatment was poured into the tank. The initial height of the sample was measured to calculate the initial volume of the sample. Then a DC current was applied for EK dewatering treatment. The polarity of the electrodes remained the same during each test. The first variable studied in the tests was the voltage gradients, which were set at 50 V/m and 100 V/m. The DC current and water drainage were recorded in real time during treatment. There was no surcharge loading on the tailings sample. The EK dewatering cell was sealed by plastic wrap to prevent evaporation. The settlement of tailings was measured by a ruler attached on the front panel of the EK dewatering tank and used for saturation analysis. The second variable investigated in this study is the treatment time. The tailings underwent the EK treatment for a pre-determined time. Then the tailings samples were taken at the anode, center and cathode sides to measure water contents (ASTM D2216-10; ASTM 2010). The details of sampling, including numbers of samples and sampling time, are summarized in Table 3.3. As seen in Table 3.3, 2 to 3 samples were taken in 5 tests in the first 25 hours. To avoid disturbance, small amount of sample was collected by using a syringe at the anode, center and cathode, respectively, since the tailings remained nearly in a liquid state in the first 25 hours. Afterwards samples were taken at the end of the tests without any disturbance.

3.3. Results and regression analysis

3.3.1. Water drainage during EK dewatering tests

Table 3.4 presents a summary of results of EK dewatering tests. Since the initial volume of tailings slurry was slightly different for each test, the water collected during a test was normalized and plotted in terms of V_w/V_0 for comparison, in which V_w is the volume of water discharge, and V_0 is the initial volume of tailings slurry. Figs. 3.2 and 3.3 present the water drainage under the voltage gradients of 50 V/m and 100 V/m, respectively. It is clear that the voltage gradient of 100 V/m generated a higher rate of water discharge than that of the voltage gradient of 50 V/m at the beginning of the tests. However, the total volumes of water discharge under both voltage gradients of 50V/m and 100V/m were nearly identical

at the end of tests. The regression analysis of the water discharge under the voltage gradient of 50V/m and 100V/m is carried out and the results are shown in Fig. 3.4. The EK water discharge at different treatment time under 50V/m and 100V/m can be represented in following equations:

Under 50V/m

$$V_w/V_0 = \frac{0.740\ t}{130.0 + t} \qquad R^2 = 0.970 \qquad (3.3)$$

Under 100V/m

$$V_w/V_0 = \frac{0.695\ t}{62.2 + t} \qquad R^2 = 0.963 \qquad (3.4)$$

where V_w/V_0 is the volumetric ratio of water discharge to the initial tailings slurry, t is the treatment time in hours.

The general trend for water drainage after EK dewatering treatment can be expressed as:

$$V_w/V_0 = \frac{D_v\ t}{t_{50} + t} = \frac{D_v}{\frac{t_{50}}{t} + 1} \qquad (3.5)$$

where D_v and t_{50} are parameters obtained through experiments. D_v represents the maximum reduction of volume for EK dewatering when time approaches infinity. According to Eq. 3.5, $V_w/V_0 = D_v$ when time t approaches infinity, and at time $t = t_{50}$, $V_w/V_0 = D_v/2$, hence t_{50} represents the time to reach 50% of the volume reduction ($D_v/2$). The maximum water drainage from an EK treatment can be expressed as:

$$V_w = D_v V_0\ (t \to \infty) \qquad (3.6)$$

3.3.2. Water content changes during EK dewatering tests

The post-treatment water content of soil is a function of the location to cathode, which has been observed in many researches in laboratory experiments (Lo et al. 1991b, Guo and Shang 2014) and field tests (Bjerrum et al. 1967, Lo et al. 1991a).

In this study, the tailings samples in the testing tank were divided into three sections, i.e., near anode, at center and near cathode because the sample condition was different with the locations. Figs. 3.5 and 3.6 show the water contents of MFT-A versus time at the vicinity of anode (Figs. 3.5a; 3.6a), center (Figs. 3.5b; 3.6b), and cathode (Figs. 3.5c; 3.6c) after EK dewatering tests under the voltage gradients of 50V/m and 100V/m, respectively. In Fig. 3.7, the results were normalized against the initial water content of the sample, $w(t)/w_0$, in which w(t) is the water content after EK dewatering testing at any treatment time *t*, and w_0 is the initial water content of MFT-A samples. Fig. 3.7a shows the normalized water content changes at the vicinity of the anode. The water content of sample at the anode reduced quickly at the beginning of the EK dewatering tests. After time passed t_{50}, defined in Eq. 3.5, the normalized water contents, $w(t)/w_0$, approached to a plateau at the anode, about 20 ~ 30%, corresponding to the solid content of 60%~70%, under both 50V/m and 100V/m. Further treatment did not reduce the water content of sample at the anode significantly. In the center of the sample, the normalized water content, $w(t)/w_0$ remained at about 60%~70% (45%~50% in solid content), as shown in Fig. 3.7b until the end of EK test. In contrast, as shown in Fig. 3.7c, the sample water content at the cathode remained almost constant during the entire treatment period. The similar results, i.e., relatively constant water content at the cathode after EK treatment, have been reported on sensitive clays by Bjerrum et al. (1967) and Lo et al. (1991a).

The reduction of water content with time at the anode and center locations yields an exponential decay, which can be expressed as:

Under a voltage gradient of 50V/m:

At the anode

$$w(t)/_{w_0} = 0.230 + 0.790e^{-0.0169t} \qquad R^2 = 0.930 \qquad (3.7)$$

At the center

$$w(t)/_{w_0} = e^{-0.004t} \qquad R^2 = 0.872 \qquad (3.8)$$

Under the voltage gradient of 100 V/m:

At the anode

$$w(t)/_{w_0} = 0.198 + 0.801e^{-0.0391t} \qquad R^2 = 0.984 \qquad (3.9)$$

At the center

$$w(t)/_{w_0} = e^{-0.006t} \qquad R^2 = 0.879 \qquad (3.10)$$

The general regression equation for at the anode can be expressed as:

$$w(t)/_{w_0} = w_f + D_w e^{-\lambda_w t} \qquad (3.11)$$

where w_f, D_w and λ_w (hour^{-1}) are empirical parameters. w_f represents the lowest normalized water content after the EK dewatering treatment when the treatment time, t, approaches to infinity. D_w represents the maximum reduction in water content ($w_f + D_w \approx 1$), and λ_w represents the rate of dewatering.

The reason for the exponential decay of the water content is because the rate of water content reduction reduced linearly with the decrease in water content.

3.3.3. Power consumption

The power consumption of EK treatment is directly related to the cost. The electrical conductivity is the key parameter to estimate the power consumption. The electrical conductivity of MFT, κ (S/m), was calculated through the applied voltage gradient, E, (V/m) and current density, j, (A/m^2) during EK treatment. The current density and electrical

conductivity, κ, are plotted in Fig. 3.8. It can be seen that the MFT-A has an initial electrical conductivity of 0.17 S/m. The regression analysis for the electrical conductivity under voltage gradients of 50V/m and 100V/m are shown in Fig. 3.8a and 3.8b, respectively. The regression equations are expressed as follows:

Under 50 V/m

$$\kappa = 0.17e^{-0.01t} \qquad R^2 = 0.902 \tag{3.12}$$

Under 100 V/m

$$\kappa = 0.17e^{-0.019t} \qquad R^2 = 0.904 \tag{3.13}$$

The power consumption (P, W/m^3) is defined as the power consumption per unit volume of MFT at the initial water content:

$$P = \frac{\Gamma U^2}{v_i} \tag{3.14}$$

where U is the voltage (V), Γ is the electrical conductance (Γ =I/U) (S), and v_i is the initial volume of the sample (m^3). The results of power consumptions versus time are shown in Fig. 3.9.

An exponential decay function was fitted to interpolate the power consumption with time during EK dewatering tests. The experimental data and regression curves are plotted in Fig. 3.10, and expressed in the following equations:

Under 50 V/m

$$\mathrm{P}(kW/m^3) = 0.392e^{-0.0113t} \quad R^2 = 0.904 \tag{3.15}$$

Under 100 V/m

$$\mathrm{P}(kW/m^3) = 1.612e^{-0.0192t} \quad R^2 = 0.871 \tag{3.16}$$

where t is time in hours.

The energy consumptions under voltage gradients of 100 and 50 V/m can be estimated by integrating the power consumption equation over time:

For 50V/m

$$\mathrm{W}\ (kWh/m^3\ ) = 34.7(1 - e^{-0.0113t}) \tag{3.17}$$

For 100V/m

$$\mathrm{W}(kWh/m^3) \ = 84.0(1 - e^{-0.0192t}) \tag{3.18}$$

The general equations for power consumption, P (kW/m^3), and energy consumption, W (kWh), can be expressed as follows:

$$\mathrm{P}(kW/m^3) = P_m e^{-\lambda_P t} = E^2 \kappa_0 e^{-\lambda_P t} \tag{3.19}$$

$$\mathrm{W}(kWh/m^3) = \frac{E^2 \kappa_0}{\lambda_P}\left(1 - e^{-\lambda_P t}\right) \tag{3.20}$$

where P_m (kW/m^3) is the maximum power consumptions at the beginning of the treatment ($P_m = E^2\kappa_0$), E is the voltage gradient, κ_0 is the initial material electrical conductivity, and λ_P (hour^{-1}) is the rate of power consumption decay. According to Eq. 3.19, it is noted that the power requirement for EK treatment reduces with time. In the meantime, Eq. 3.20 shows the maximum energy consumption in the EK treatment is $\frac{E^2\kappa_0}{\lambda_P}$ when time approaches infinity.

3.4.Discussion

Based on the experiment results, the flow rate of EK drainage changed with time (Fig. 3.4). During the treatment, the water content of tailings reduced more rapidly at the anode, as shown in Fig. 3.7a. The electrical conductivity also reduced, as seen in Fig. 3.8. Under a constant voltage gradient, this led to reduced current, hence reduced dewatering effect. Similar observations were reported in EK tests on clays (Lo et al. 1991a, Bjerrum et al. 1967). It has been recognized that during EK dewatering geo-materials became unsaturated (Guo and Shang 2014, Shang 1997). In order to quantitatively investigate this effect, the

degrees of saturation, S_d (%), of MFT samples in the EK cell at different time intervals are plotted in Figs. 3.11 and 3.12, together with the results of water discharge for 50V/m and 100V/m, respectively. In the figures, x is the distance to the cathode, and the horizontal axis is the normalized distance, i.e., x/L, in which L is the length of the EK cell.

As observed in Fig. 3.4, for voltage gradients of 50V/m and 100 V/m respectively, the water discharge can be broadly divided into three stages, i.e., 1). Linear flow, indicated by the time from the beginning of the EK treatment (T_0) to T_{tran}, which is the time when flow rate changes and become nonlinear. T_{tran} marks the beginning of the transitional flow stage; 2). Transitional flow, marked by the time period from T_{tran} to T_{end}, where T_{end} is the time when the flow stops; and 3). End of flow, indicated by the treatment time after T_{end}. In the linear flow stage, the EK dewatering maintained at a constant flow rate, as seen in Figs. 3.11a and 3.12a, for 50V/m and 100V/m respectively. The transitional stage is observed through the slowdown of flow rate after a certain period time of treatment, T_{tran}, as seen in the Figs. 3.11a and 3.12a, where the results of water discharge become non-linear. Finally, the water discharge stops, marked the end of dewatering process, at time T_{end}, indicated with the water discharge approaching to a plateau.

As shown in Fig. 3.11, under the voltage gradient of 50 V/m, the degree of saturation, S_d, of the sample at the anode (x/L = 0.9) remained nearly 100% in the first 25 hours, and at this stage the flow of water discharge was in the linear flow stage. When treatment time passed 25 hours and reached to 50 hours, the degree of saturation, S_d, at the anode (x/L = 0.9) reduced quickly from 100% to 80%. During this time period the flow is still in the linear flow stage as seen in Fig. 3.11a. Once the time passed 50 hours, the degree of saturation, S_d, at the anode (x/L=0.9) reduced significantly. The time, T_{tran}, when the degree of saturation, S_d, at the anode (x/L=0.9) reached to 80%, marks the start of the transitional flow stage as seen in Fig. 3.11a. After 125 hours (around t_{50}), the degree of saturation, S_d, at the anode (x/L=0.9) reached about 40% and remained constant for the rest of treatment. At this time the flow was still within the transitional stage as seen in Fig. 3.11a.

Meanwhile, at the center (x/L=0.5) of the EK cell, it was observed from Fig. 3.11b that the degree of saturation, S_d, remained 100% in the first 25 hours then reduced slowly. After

125 hours, the degree of saturation, S_d, quickly reduced to below 80%, then the EK flow ended. According to the Fig. 3.11a, the T_{end} is about 200 hours. At the cathode (x/L=0), it can be clearly seen from Fig. 3.11b that the sample remained saturated over the entire treatment period.

The similar observation is found in Fig. 3.12 for EK dewatering tests under 100V/m. At the anode (x/L=0.9), the sample remained saturated 100% under EK treatment for 5 hours and shortly dropped below 80% after 25 hours, corresponding to time T_{tran}. Compared to the test under the voltage gradient of 50 V/m, the higher voltage generates much rapid reduction of saturation at the anode (x/L=0.9), resulting in a shorter period of the linear flow stage (about 30 hours) compared to 50 hours for the test under the voltage gradient of 50V/m. The degree of saturation, S_d, at anode (x/L=0.9), as seen in Fig. 3.12b, significantly reduced to about 40% during the period for transitional flow stage from 30 hours to 125 hours, as seen in Fig. 3.12a. A much shorter duration of transitional flow stage was observed under voltage gradient of 100V/m, compared to those for 50 V/m. When the degree of saturation, S_d, reached to 80% at center (x/L=0.5), the flow stopped, as seen in Fig. 3.12. In contrast, the degree of saturation, S_d, remained saturated during the entire treatment period. Figure 3.13a shows the original tailings status at the beginning of the test, while Figs. 3.13b and 3.13c show the tailings conditions during and after the treatment, respectively.

The above results of voltage gradient of 50 and 100 V/m can be concluded that:

1.The linear flow regime lasted from commencing the treatment until the degree of saturation, S_d, at anode (x/L=0.9) reduced to 80%.

2.The flow stopped when the degree of saturation, S_d, at the center of tailings sample (x/L=0.5) reduced to 80%.

This process is summarized as:

$$T_{0_{S_d=100\%}} \xrightarrow[stage]{Linear\ flow} T_{tran} \quad {\scriptstyle S_d<80\%\ at\ anode\ (x/L=0.9)} \xrightarrow[stage]{Transitional\ flow} T_{end} \quad {\scriptstyle S_d<80\%\ at\ center(x/L=0.5)} \xrightarrow[stage]{End\ flow} End$$

The reductions of tailings water content and electrical conductivity were observed in the tests. In the linear flow stage, both the water content at anode (Fig. 3.7a) and electrical conductivity (Fig. 3.8) decreased linearly until the transitional flow stage, $T_{tran.}$, was reached. Then during transitional flow stage their reduction paces slowed down, which are indicated by the change of slope of results in Figs. 3.7a and 3.8. Finally, in the end flow stage ($t = T_{end}$), the normalized water content at the anode reached to a plateau about 30%, and electrical conductivity reduced to 0.02 S/m.

The degrees of saturation are plotted along with time in Fig. 3.14 for samples at anode, center and cathode respectively, under voltage gradients of 50V/m and 100V/m. Based on Fig. 3.14, it can be noted that the characteristic time t_{50} (defined in Eq. 3.5 and shown in Fig. 3.4) is the time when degree of saturation of the sample at anode (x/l=0.9) reduced to 40%. It should be noted that the characteristic times, t_{50}, T_{tran}, $T_{end,}$ were obtained through the test results under this testing configuration and not normalized. Further studies are needed on scaling effects.

Overall, EK dewatering flow is nonlinear with treatment time and will stop after certain treatment time. The change of EK discharge rate is primarily governed by the saturation status of sample. For MFT-A, when degree of saturation, S_d=80% at anode (x/L=0.9) was observed, the EK flow changed from linear to nonlinear and entered into transitional flow stage. When the degree of saturation, S_d, of the sample at center (x/L=0.5) dropped to 80% the EK flow reached a stop. It should be noted that this transform is independent to the applied voltage gradient. Therefore, for MFT-A, the S_d=80% at center (x/L=0.5) could serve as a indicator of the end of treatment. As results, the EK dewatering treatment may be terminated when the treatment time reached T_{end}. The degree of saturation in tailings sample governs the transition of EK flow stages. Thus, it can serve as a guideline for large scale applications to determine the effective treatment time.

3.5.Conclusion

In this study, an experimental study on EK dewatering was carried on fine oil sands tailings (MFT-A). The vertical installed electrodes were used to generate the horizontal water flow. Data were collected and regression analyses were carried on the EK water drainage, tailings

water content, material electrical conductivity, and power consumption of EK treatment. The saturation of the sample was studied as a function of the distance to electrodes. It is observed that the EK induced water flow can be classified in three stages, i.e., 1) the linear flow, 2) the transitional flow, and 3) the end flow. It is identified that the rate of EK water was controlled by the saturation status of the sample.

This study has led to the following conclusions:

- The water content distribution of oil sands tailings after EK treatment is non-uniform. The water content of tailings sample reduced significantly at the anode, whereas it remains at the nearly constant at the vicinity of cathode. The changes in water content during the EK treatment at anode and center can be expressed via exponential decay functions.

- The relationship between the power consumption and treatment time can be expressed via an exponential decay function.

- The EK induced water flow can be further classified in three stages, i.e., 1) the linear flow, 2) the transitional flow, and 3) the end flow. The linear flow stage lasted from beginning of the treatment until the degree of saturation, S_d, reached 80% at the anode (x/L=0.9). When the degree of saturation, S_d, at the center (x/L=0.5), reduced to 80%, the EK flow reached a stop. Therefore, the degree of saturation of tailings sample may serve as a guideline for large scale application to determine the effective treatment time.

- The times of the linear flow stage and transitional flow stage are identified as T_{tran} and T_{end}, respectively. These characteristic times may also be used as a guidance for EK treatment with further study on the scaling effects.

References

ASTM (2010). D2166-10: Standard test methods for laboratory determination of water (moisture) content of soil and rock by mass. ASTM International, West Conshohocken, PA, 2010, https://doi.org/10.1520/D2216-10

Bergado, D. T., Balasubramaniam, A. S., Patawaran, M. A. B., and Kwunpreuk, W. (2000). Electroosmotic consolidation of soft Bangkok clay with prefabricated vertical drains. Ground Improvement, 4, No.4, 153-163.

Bjerrum, L., Moum, J., and Eide, O. (1967). Application of electroosmosis to a foundation problem in a Norwegian quick clay. Géotechnique, 17, No.3, 214–235.

Casagrande, L. (1949). Electroosmosis in soil. Géotechnique, 1, No.3,159–177.

Casagrande, L. (1959). Review of past and current work on electroosmotic stabilization of soils. In Harvard Soil Mechanics Series, 45, Harvard University Cambridge, Massachusetts, USA (reprinted November 1959 with a supplement of June 1957).

Casagrande, L. (1983). Stabilization of soil by means of electroosmosis: state-of-the-art. Journal of the Boston Society of Civil Engineers, ASCE 69, No.2, 255–302.

Chalaturnyk, R. J., Don Scott, J., and Özüm, B. (2002). Management of oil sands tailings. Petroleum Science and Technology, 20, No. 9-10, 1025-1046.

Chew, S. H., Karunaratne, G. P., Kuma, V. M., Lim, L. H., Toh, M. L., and Hee, A. M. (2004). A field trial for soft clay consolidation using electric vertical drains. Geotextiles and Geomembranes, 22, No.1, 17-35.

Chien, S. C., Ou, C. Y., and Lo, W. W. (2014). Electroosmotic chemical treatment of clay with interbedded sand. Proceedings of the Institution of Civil Engineers-Geotechnical Engineering, 167, No.1, 62-71.

Esmaeily, A., Elektorowicz, M., Habibi, S., and Oleszkiewicz, J. (2006). Dewatering and coliform inactivation in biosolids using electrokinetic phenomena. Journal of Environmental Engineering and Science, 5, No. 3, 197-202.

Fourie, A. B., and Jones, C. J. F. P. (2010). Improved estimates of power consumption during dewatering of mine tailings using electrokinetic geosynthetics (EKGs). Geotextiles and Geomembranes, 28, No.2, 181-190.

Fourie, A. B., Johns, D. G., and Jones, C. F. (2007). Dewatering of mine tailings using electrokinetic geosynthetics. Canadian Geotechnical Journal, 44, No.2, 160-172.

Glendinning, S., Jones, C. J., and Pugh, R. C. (2005a). Reinforced soil using cohesive fill and electrokinetic geosynthetics. International Journal of Geomechanics, 5, No.2, 138-146.

Glendinning, S., Jones, C. J., and Lamont-Black, J. (2005b). The use of electrokinetic geosynthetics (EKG) to improve soft soils. Elsevier Geo-Engineering Book Series, 3, 997-1043.

Glendinning, S., Lamont-Black, J., and Jones, C. J. (2007). Treatment of sewage sludge using electrokinetic geosynthetics. Journal of Hazardous Materials, 139, No.3, 491-499.

Gray, D.H., and Mitchell, J.K. (1967). Fundamental aspects of electroosmosis in soils, Journal of the Soil Mechanics and Foundation Division, 93, No.SM 6, 209-236, Closure Discussion (1969), 95, No.SM 3, 875-879.

Guo, Y. and Shang, J.Q. (2014). A study on electrokinetic dewatering of oil sands tailings. Environmental Geotechnics, 1, No.2, 121-134.

Islam, S., and Shang, J. Q. (2017). Electrokinetic thickening of mature fine oil sands tailings. Environmental Geotechnics, 4, No.1, 40-55.

Iwata, M., Tanaka, T., and Jami, M. S. (2013). Application of electroosmosis for sludge dewatering—A review. Drying Technology, 31, No.2, 170-184.

Jones, C. J. F. P., Lamont-Black, J., Glendinning, S., Bergado, D., Eng, T., Fourie, A., Hu, L., Pugh, C., Romantshuk, M., Simpanen, S., and Zhuang, Y. (2008). Recent research and applications in the use of electrokinetic geosynthetics. In Proceedings of 4th european geosynthetics conference. EuroGeo4, Keynote paper: Edinburgh, UK.

Jones, C. J., Lamont-Black, J., and Glendinning, S. (2011). Electrokinetic geosynthetics in hydraulic applications. Geotextiles and Geomembranes, 29, No. 4, 381-390.

Lee, J. K., and Shang, J. Q. (2013). Electrical vertical drains in geotechnical engineering applications. Geotechnical Engineering Journal of the SEAGS & AGSSEA, 44, No, 4, 24-35.

Liu, P., and Shang, J. Q. (2014). Improvement of marine sediment by combined electrokinetic and chemical treatment. International Journal of Offshore and Polar Engineering, 24, No. 3, 232-240.

Lo, K. Y., Ho, K. S., and Inculet, I. I. (1991a). Field test of electroosmotic strengthening of soft sensitive clay. Canadian Geotechnical Journal, 28, No. 1, 74-83.

Lo, K. Y., Inculet, I. I., and Ho, K. S. (1991b). Electroosmotic strengthening of soft sensitive clays. Canadian Geotechnical Journal, 28, No. 1, 62-73.

Micic, S., Shang, J. Q., Lo, K. Y., Lee, Y. N., and Lee, S. W. (2001). Electrokinetic strengthening of a marine sediment using intermittent current. Canadian Geotechnical Journal, 38, No. 2, 287-302.

Micic, S., Shang, J. Q., and Lo, K. Y. (2002). Electrokinetic strengthening of marine clay adjacent to offshore foundations. International Journal of Offshore and Polar Engineering, 12, No. 1, 64-73.

Mitchell, J.K., and Soga K. (2005). Fundamental of soil behavior, 3rd edn. Wiley, Hoboken, New Jersey, USA.

Mohamedelhassan, E., and Shang, J. Q. (2001). Effects of electrode materials and current intermittence in electroosmosis. Proceedings of the Institution of Civil Engineers-Ground Improvement, 5, No. 1, 3-11.

Ou, C. Y., Chien, S. C., Yang, C. C., and Chen, C. T. (2015). Mechanism of soil cementation by electroosmotic chemical treatment. Applied Clay Science, 104, 135-142.

Raats, M. H. M., Van Diemen, A. J. G., Laven, J., and Stein, H. N. (2002). Full scale electrokinetic dewatering of waste sludge. Colloids and Surfaces A: Physicochemical and Engineering Aspects, 210, No. 2, 231-241.

Rittirong, A., and Shang, J. (2005). Electroosmotic stabilization. Elsevier Geo-Engineering Book Series, 3, 967-996.

Rittirong, A., Douglas, R. S., Shang, J. Q., and Lee, E. C. (2008). Electrokinetic improvement of soft clay using electrical vertical drains. Geosynthetics International, 15, No. 5, 369-381.

Shang, J. Q. (1997). Electokinetic dewatering of clay slurries as engineered soil covers. Canadian Geotechnical Journal, 34, No. 1, 78-86.

Shang, J. Q. (2011). Electrokinetics: engineering applications and recent development. In Advances in Unsaturated Soil, Geo-Hazard, and Geo-Environmental Engineering, ASCE, No. 217, 1-8.

Shang, J. Q., Mohamedelhassan, E., and Ismail, M. (2004). Electrochemical cementation of offshore calcareous soil. Canadian geotechnical journal, 41, No.5, 877-893.

Yang, L., Nakhla, G., and Bassi, A. (2005). Electrokinetic dewatering of oily sludges. Journal of hazardous materials, 125, No. 1, 130-140.

Table 3.1 Tailings Properties (Guo and Shang 2014)

Properties		Oil sands tailings
Specific gravity, G_s		2.51
Hydraulic conductivity, k_h (m/s) (at e = 2.03)		1.81×10^{-9}
Atterberg limits	Plastic limit, PL (%)	29.1
	Liquid limit, LL (%)	51.6
	Plasticity index, PI (%)	22.5
Carbonate content (%)		<1
Grain size	D_{10} (μm)	0.85
	D_{50} (μm)	7.15
	D_{90} (μm)	27.9
	Sand (%)	0.00
	Silt (%)	80.00
	Clay (%)	20.00
Pore water pH		8.88
Pore water electrical conductivity (mS/cm)		3.59

Table 3.2 EK dewatering tests conditions

Conditions		
Tests No.	EKD-0-50-series	EKD-0-100-series
Voltage gradient (V/m)	50	100
Surcharge (kPa)	0	
Tailings sample size (cm)	Recorded Height(H_0)× 29.5 (length) × 10 (width)	
Water Discharge (mL)	Recorded	
Current (A)	Recorded	
Electrodes	SS316 mesh cathode , Ti/IrOx mesh anode	

Table 3.3 Summary of sampling for water content measurement

Test No.	Voltage gradient (V/m)	Numbers of sampling	Time of sampling (hours)
EKD-0-50-50a	50	4	5; 10; 20; 50
EKD-0-50-50b		4	5; 10; 20; 50
EKD-0-50-51		1	51
EKD-0-50-70		1	70
EKD-0-50-100a		1	100
EKD-0-50-100b		1	100
EKD-0-50-125a		1	125
EKD-0-50-125b		1	125
EKD-0-50-156		3	5;25.2;156
EKD-0-50-168		3	5;25.2;168
EKD-0-50-170		1	170
EKD-0-50-245		1	245
EKD-0-100-24	100	1	24
EKD-0-100-50a		1	50
EKD-0-100-50b		1	50
EKD-0-100-70		1	70
EKD-0-100-100		1	100
EKD-0-100-122		3	5;25;122
EKD-0-100-125		1	125
EKD-0-100-165		1	165

Table 3.4 Summarized EK dewatering results

Test No.	Voltage gradient (V/m)	Testing duration (hours)	H_0 (cm)	V_w/V_0 (%)	Total Water Discharge (mL)
EKD-0-50-50a	50	50	10	25.46	751
EKD-0-50-50b		50	10	19.42	573
EKD-0-50-51		51	10.5	15.40	477
EKD-0-50-70		70	10.8	27.72	883
EKD-0-50-100a		100	10.5	30.81	909
EKD-0-50-100b		100	10.5	29.93	927
EKD-0-50-125a		125	10.4	35.17	1079
EKD-0-50-125b		125	11.8	33.50	1166
EKD-0-50-156		156	10	38.71	1142
EKD-0-50-168		168	11.5	33.37	1132
EKD-0-50-170		170	19.5	41.63	2395
EKD-0-50-245		245	20.5	49.19	2975
EKD-0-100-24	100	24	10.5	20.15	468
EKD-0-100-50a		50	11	22.90	743
EKD-0-100-50b		50	11.5	34.52	1171
EKD-0-100-70		70	11	37.35	1212
EKD-0-100-100		100	9.9	36.40	1063
EKD-0-100-122		122	12.9	45.30	1724
EKD-0-100-125		125	10.5	42.52	1317
EKD-0-100-165		165	21	49.39	3059

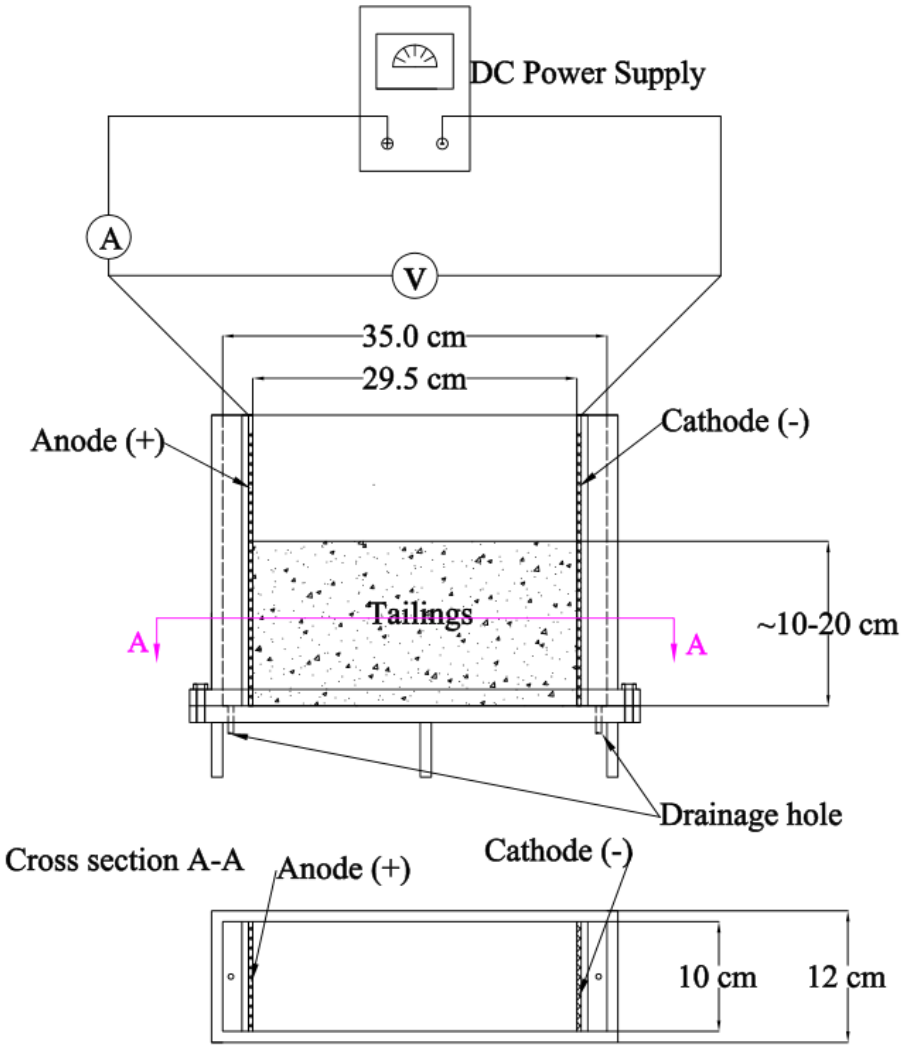

Figure 3.1 Schematic diagram of an EK dewatering cell with vertical installed electrodes

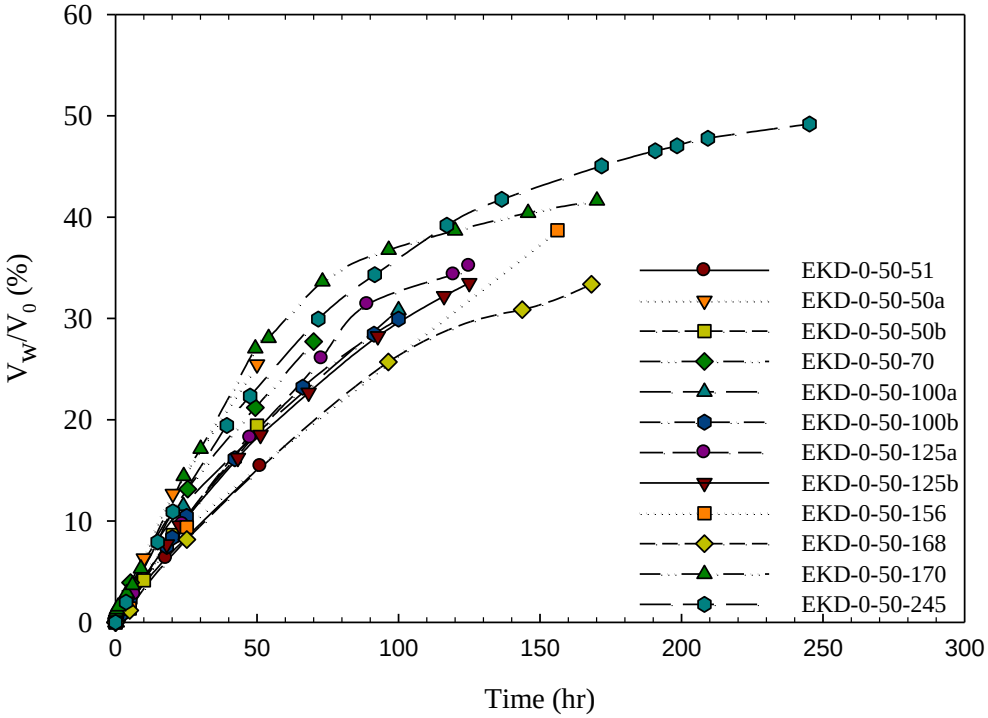

Figure 3.2 Water discharge with time under a voltage gradient of 50V/m

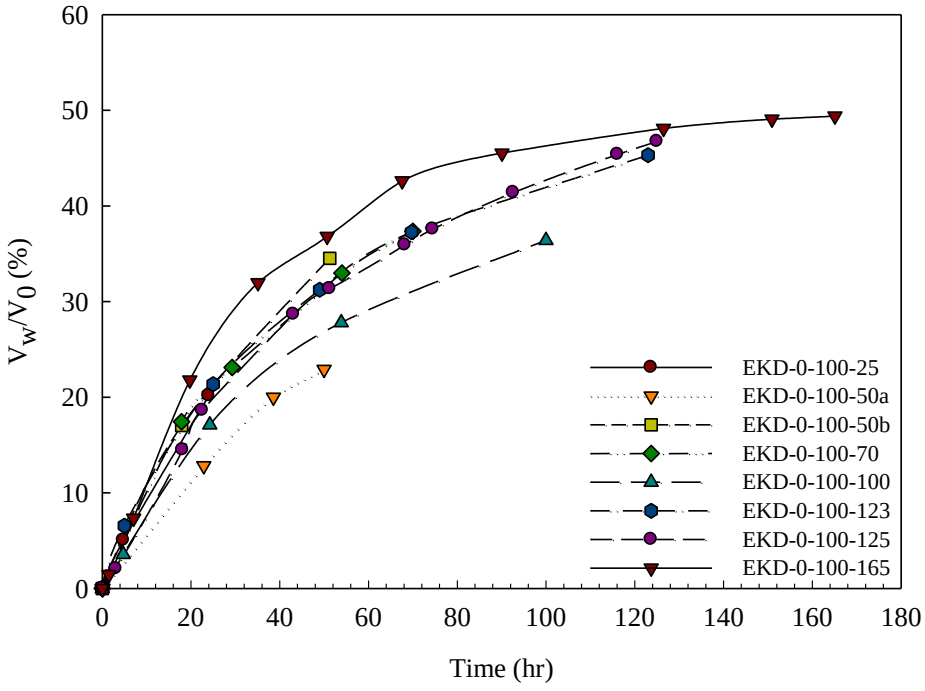

Figure 3.3 Water discharge with time under a voltage gradient of 100V/m

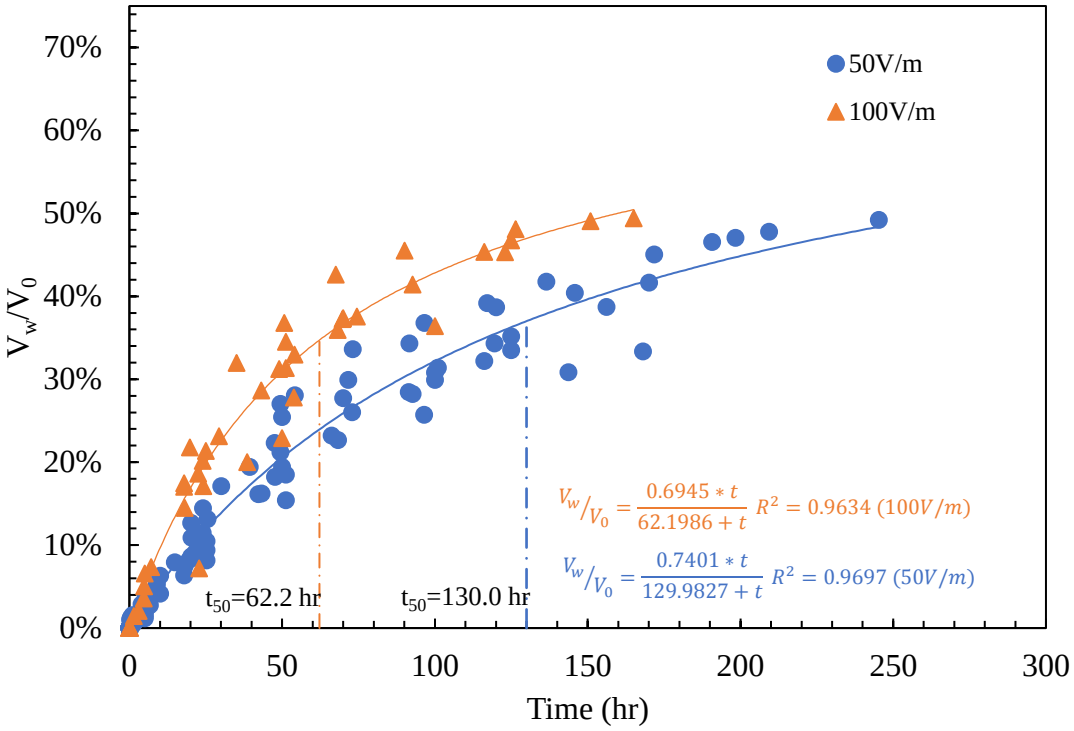

Figure 3.4 Regression trend of water discharge for voltage gradient of 50V/m and 100V/m

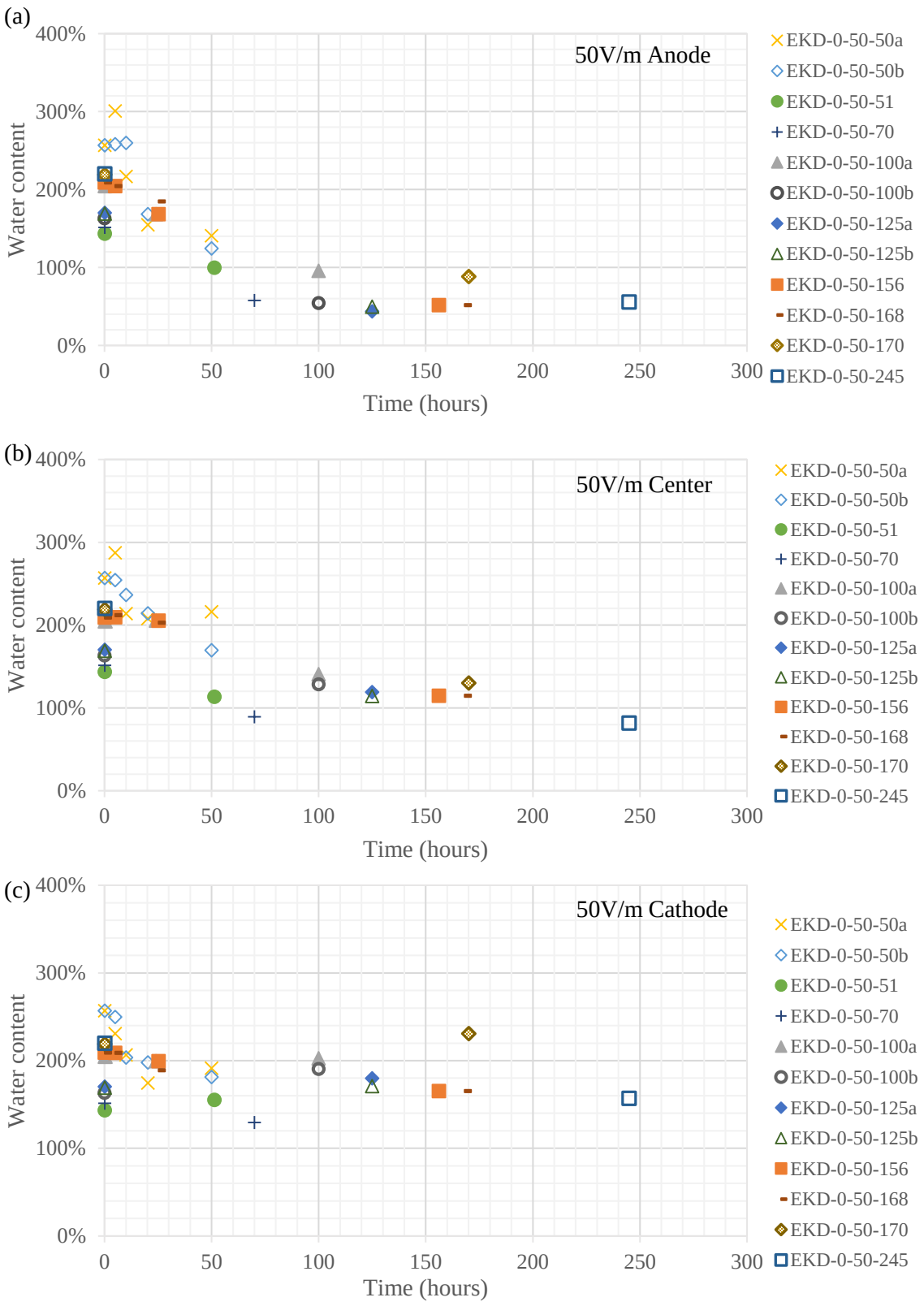

Figure 3.5 Water content changes with the time during EK dewatering tests under a voltage gradient of 50V/m (a) sample at anode, (b) sample at the center, and (c) sample at the cathode

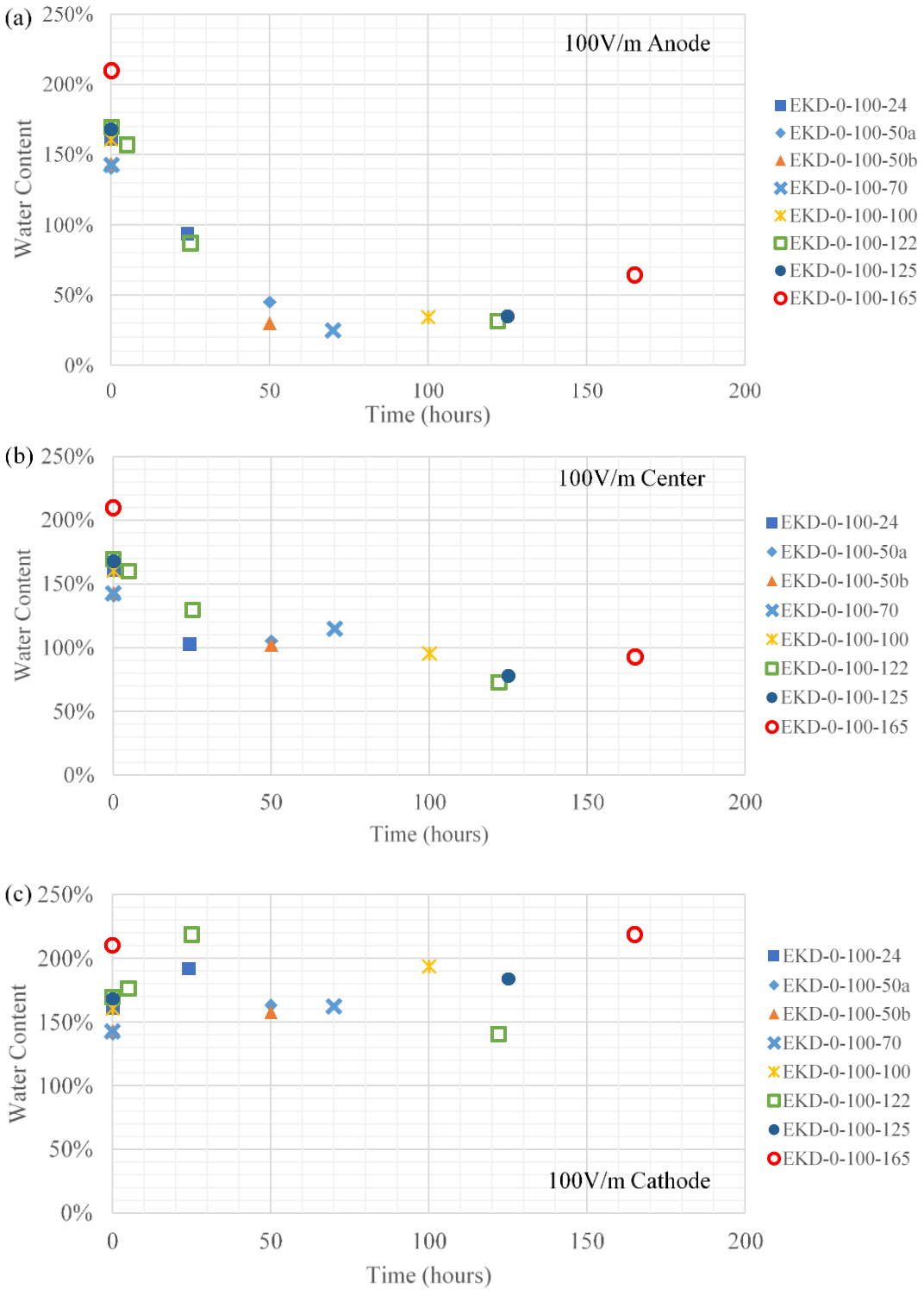

Figure 3.6 Water content changes with the time during EK dewatering tests under a voltage gradient of 100V/m (a) sample at anode, (b) sample at the center, and (c) sample at the cathode

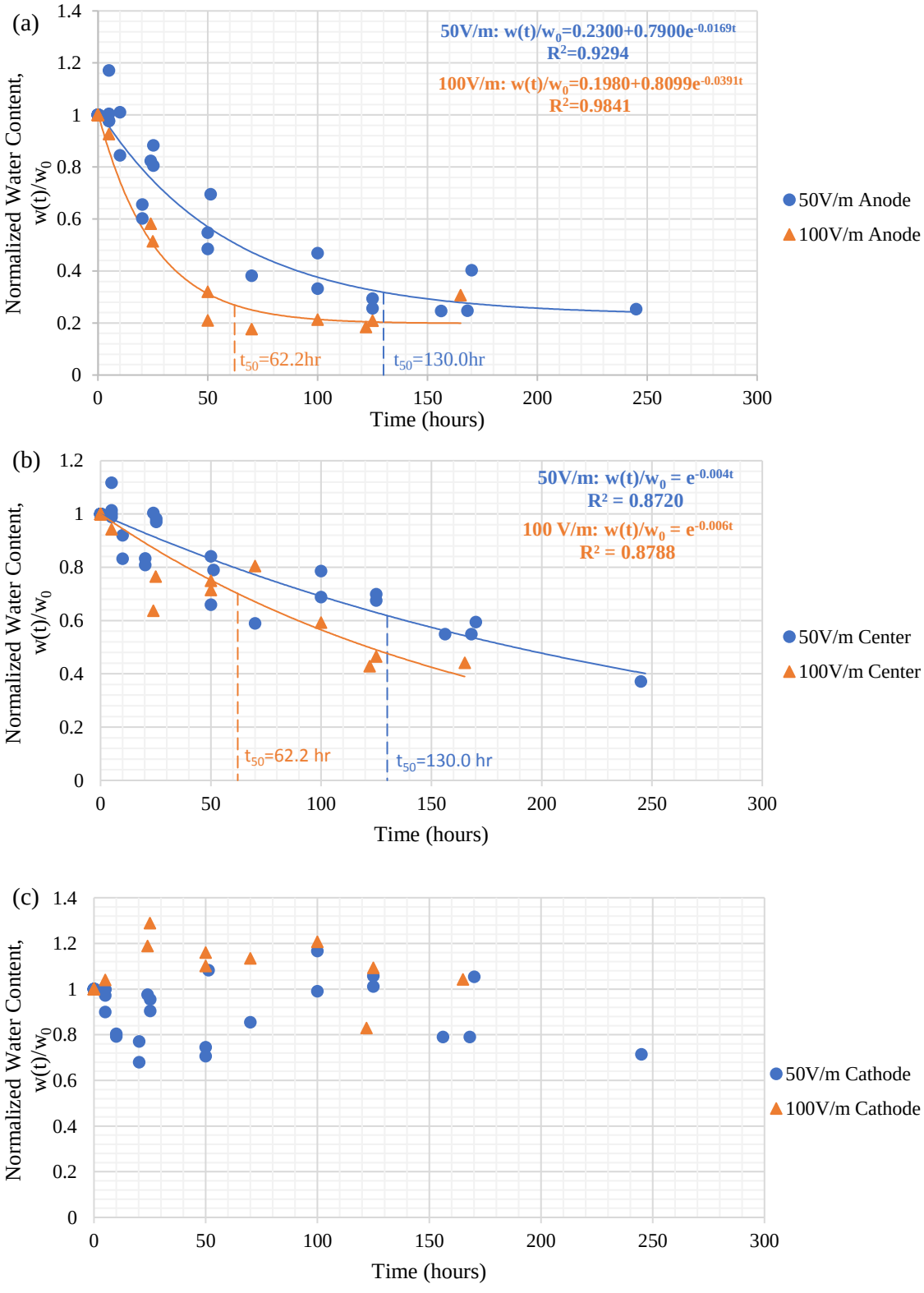

Figure 3.7 Normalized water content, $w(t)/w_0$ with the time during EK dewatering tests (a) sample at anode, (b) sample at the center, and (c) sample at the cathode

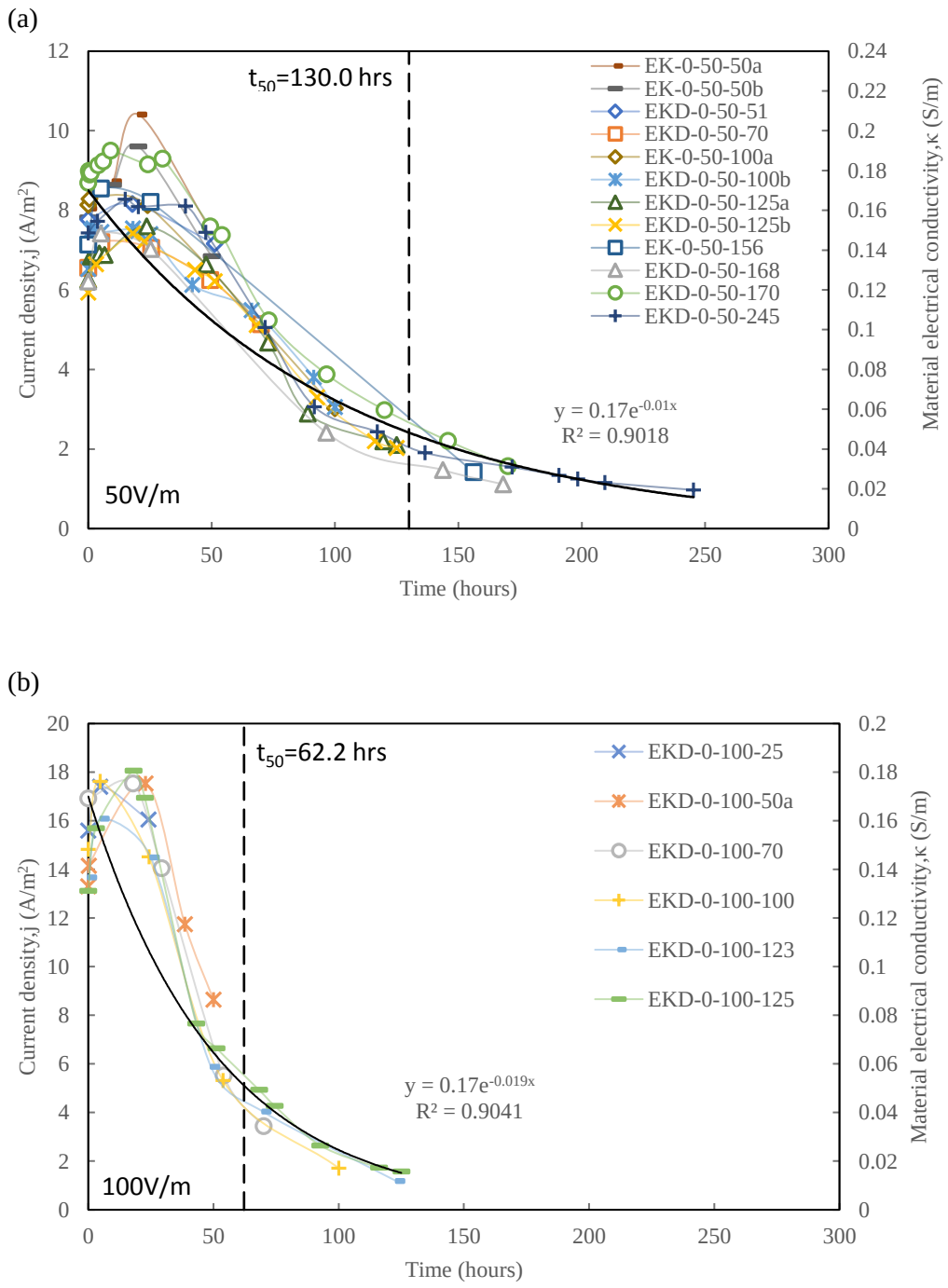

Figure 3.8 Recorded current density and material electrical conductivity during EK dewatering tests, (a) for voltage gradient of 50V/m, (b) for voltage gradient of 100V/m

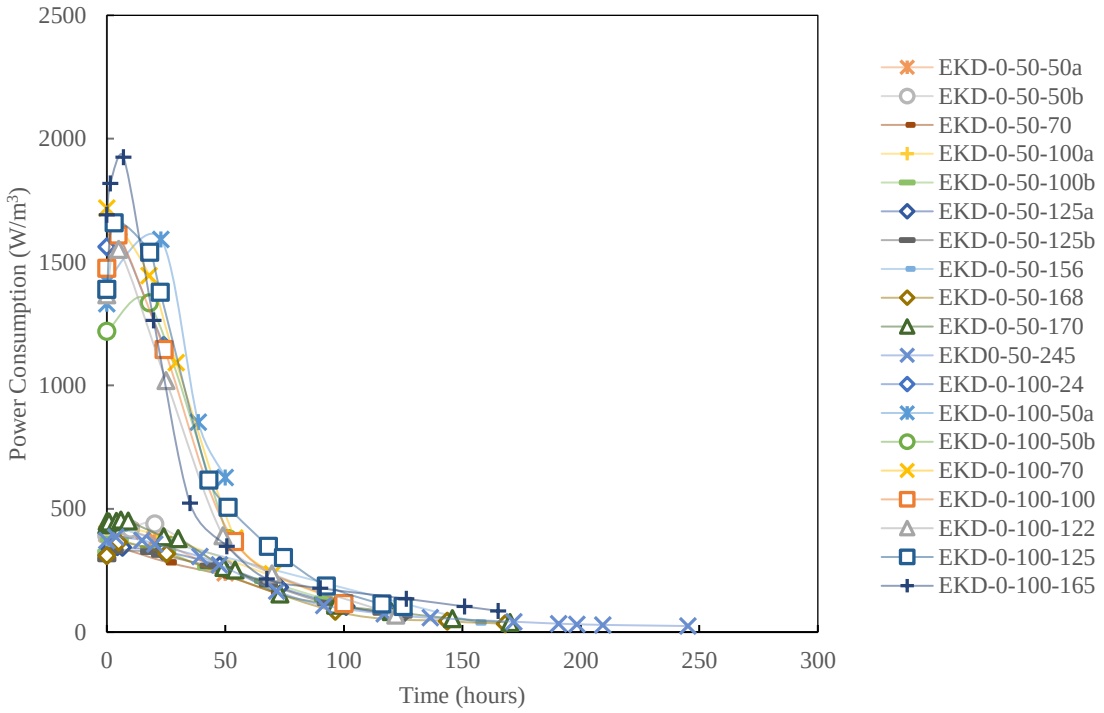

Figure 3.9 Power consumptions calculated from EK dewatering tests

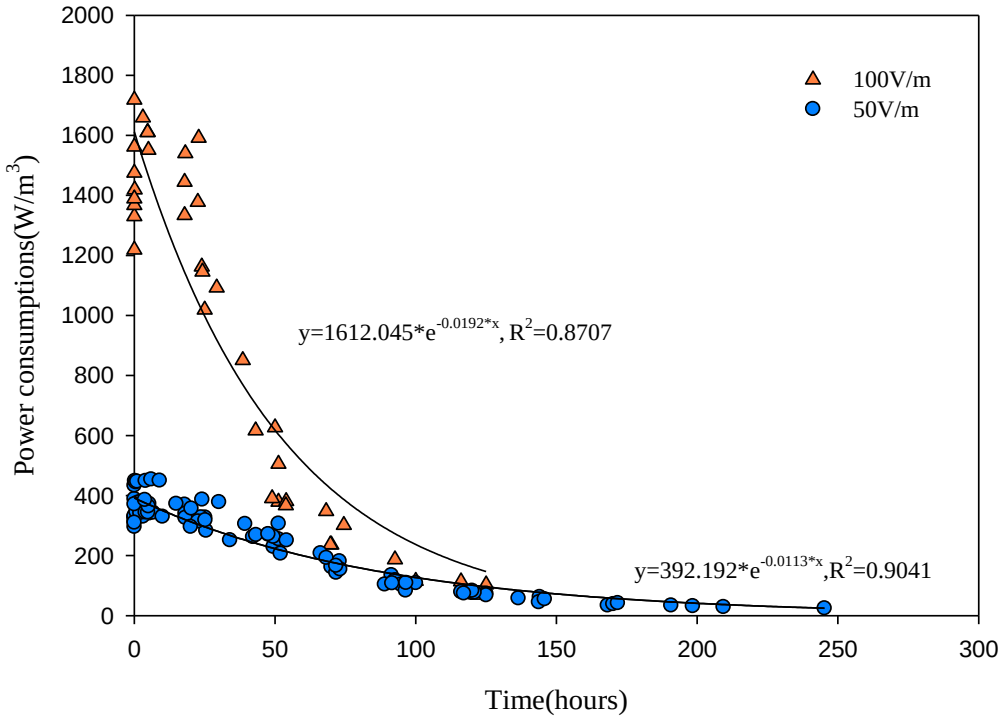

Figure 3.10 Regression analysis of power consumptions for EK dewatering tests

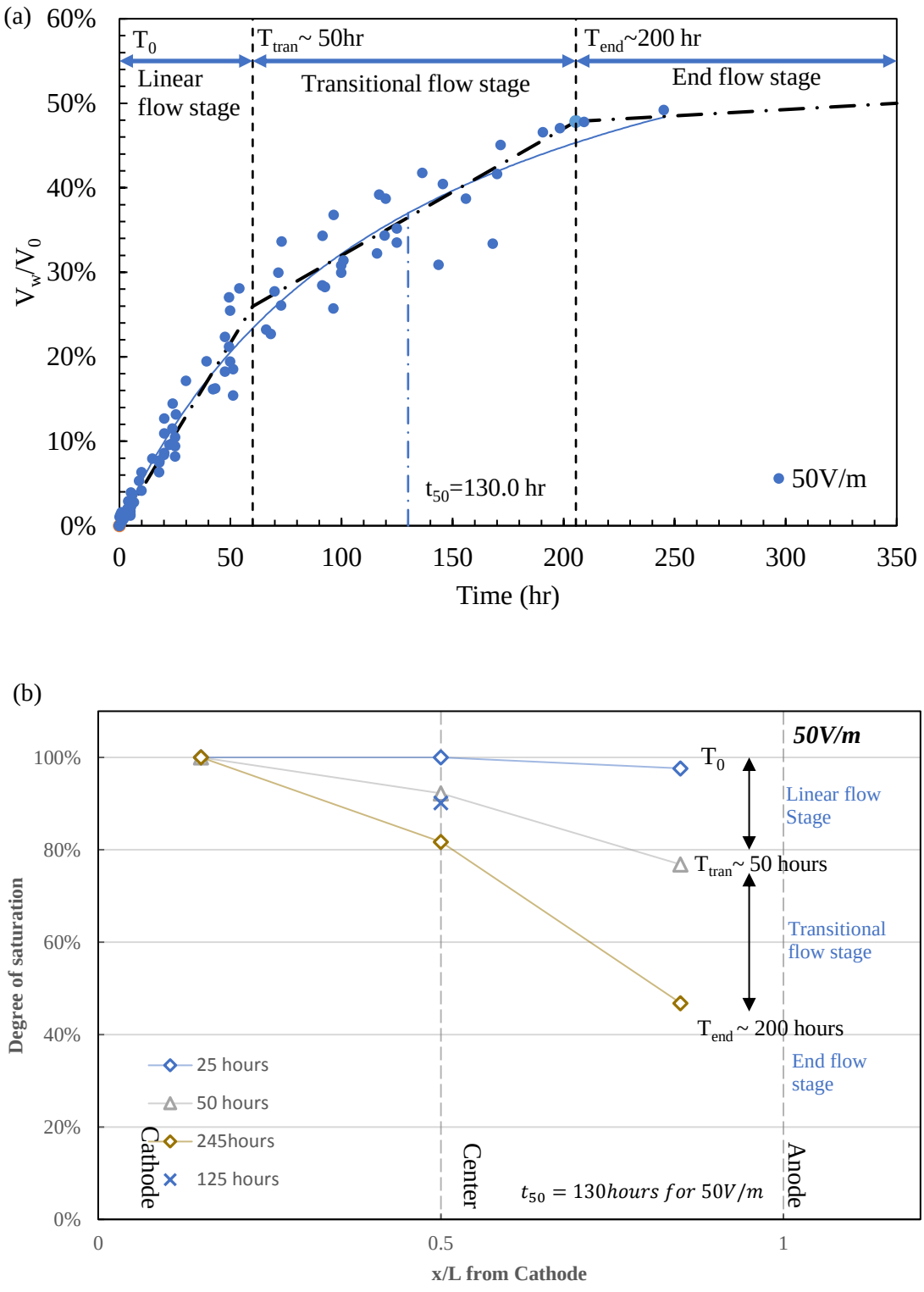

Figure 3.11 The analysis of (a). EK dewatering flow stages, and (b). degree of saturation through the Oil sands tailings for 50V/m

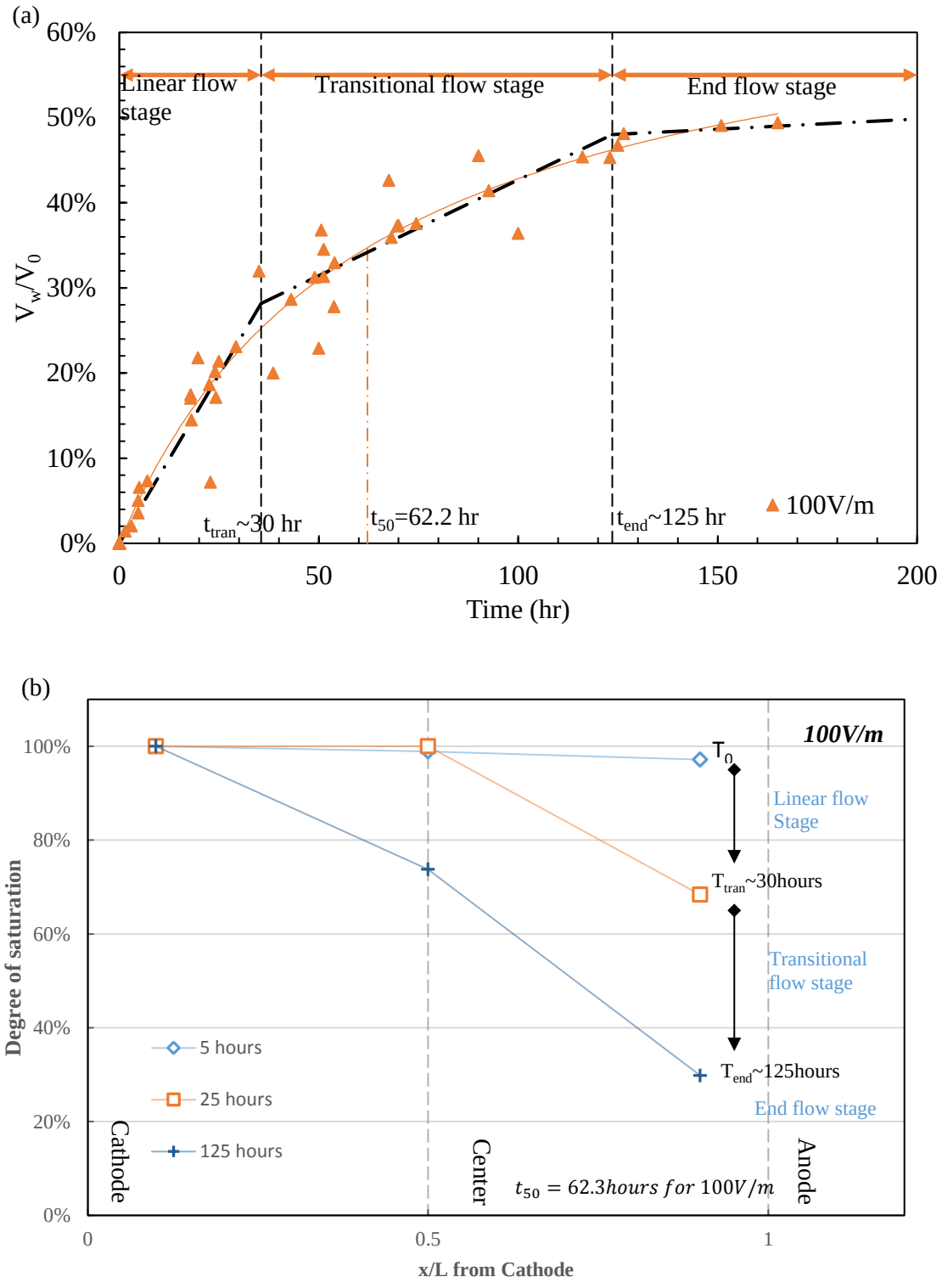

Figure 3.12 The analysis of (a). EK dewatering flow stages, and (b). degree of saturation through the Oil sands tailings for 100V/m

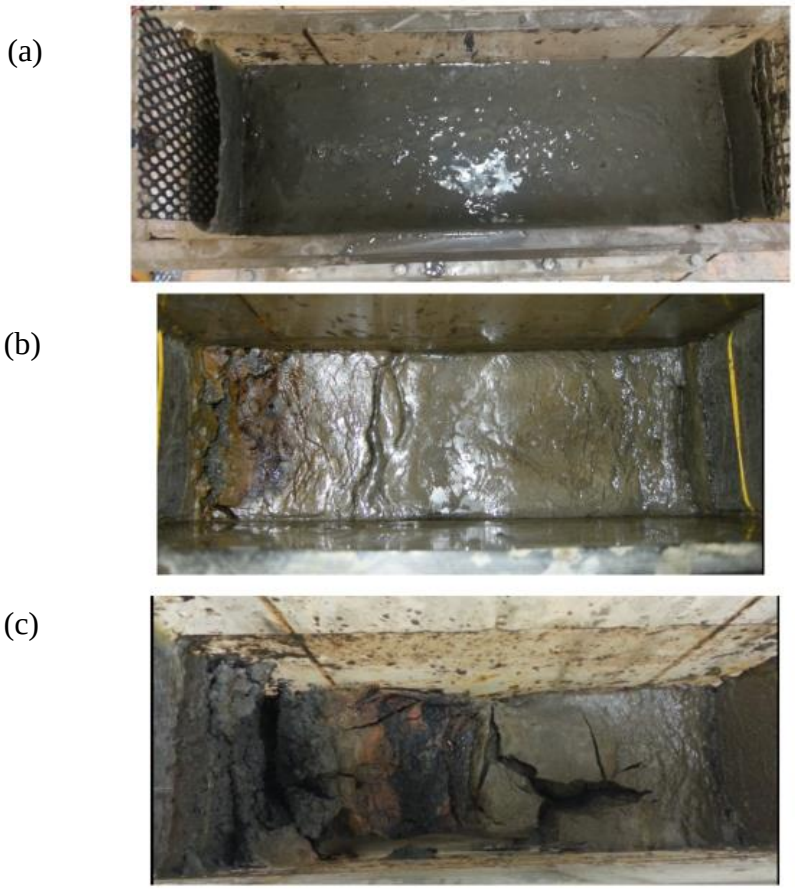

Figure 3.13 Photos for oil sands tailings (a) at the beginning of the treatment, (b) during the treatment, and (c) at the end of the treatment

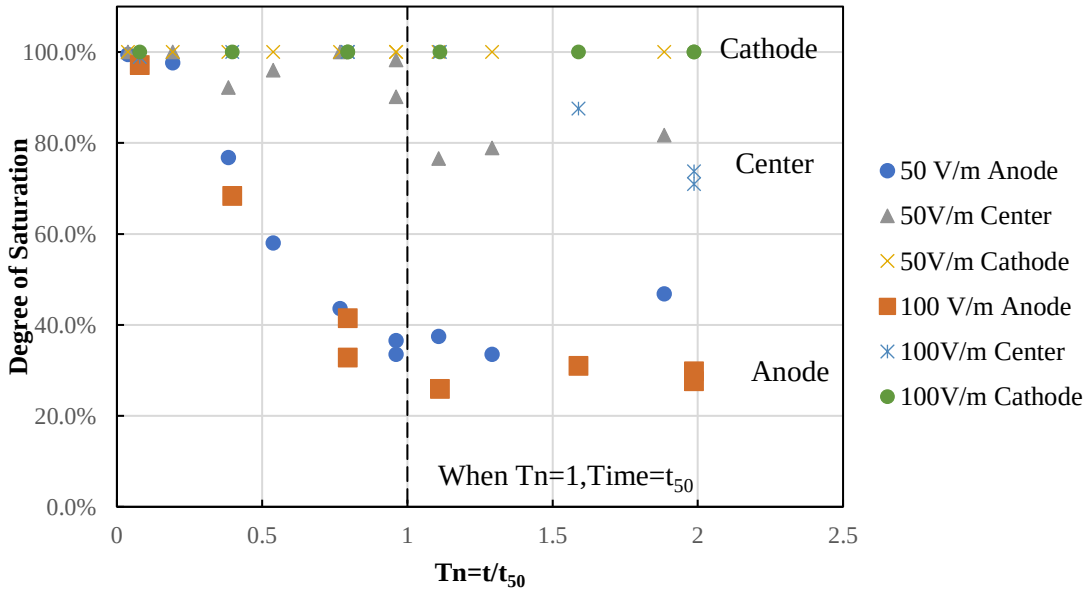

Figure 3.14 Saturation analysis for 50V and 100 V plotted with time

Chapter 4 Experimental study and regression analysis on electrokinetic dewatering of kaolinite slurry

4.1.Introduction

Dewatering and consolidation of highly compressible geo-materials are challenges facing geotechnical engineers and mining industry. Electrokinetics (EK) is a promising dewatering method on a wide variety of materials, such as soft clay, mine tailings, and wastewater sludge (Casagrande 1949, 1959, Bjerrum et al. 1967, Sunderland 1987, Lo et al. 1991a, b, Raats et al. 2002, Glendinning et al. 2005, Fourie et al. 2007, Rittriong et al. 2008, Guo and Shang 2014). In Chapter 3, a regression analysis was carried out on experimental results of EK dewatering of oil sands tailings. The reason for this study is to verify the proposed method on more commonly encountered geomaterials. Kaolinite is a clay mineral commonly existing in soft clays and mine tailings. Therefore, the first objective of this study is to find the regression equations of EK dewatering on the kaolinite slurry at well controlled conditions.

The degree of saturation of the samples was analyzed in Chapter 3 to study the influencing factors governing the EK dewatering process. Thus, the second objective in this study is to assess the effects of sample saturation on EK treatment of kaolinite slurry.

Historically, attempts have been made to improve the performance and reduce the energy cost of EK dewatering, such as polarity reversal (Bergado et al. 2000, Lo et al. 1991b) and intermittent current (Micic et al. 2001, Mohamedelhassan and Shang 2001). The energy consumption is closely related to the applied voltage gradient and current density. A wide range of voltage gradients used for EK treatment are reported in the literature (Lo et al. 1991a, b, Micic et al. 2001, Fourie et al. 2007). Mitchell and Soga (2005) suggested that a reasonable spacing (2-3 m) and voltage (50V-150V) are required to generate a significant negative pore water pressure. Thus, the corresponding voltage gradient suggested by Mitchell and Soga (2005) is from 15-75V/m. A high voltage gradient may reduce the treatment time but lead to high energy cost. So, the third objective of this study is to analyze the effects of voltage gradients and initial water contents of kaolinite slurry on EK water

drainage and energy consumption, which is especially important for the application of EK dewatering treatment.

Kaolinite is a common clay mineral. EK dewatering on kaolinite containing geomaterials has been found very effective (Lockhard 1983a, b, Fourie et al. 2007, Guo and Shang 2014). This study is focusing on EK dewatering of kaolinite slurry to enhance the understanding for EK dewatering of geo-materials containing kaolinite, such as oil sands tailings.

The EK dewatering tests in this research are carried out in a laboratory setting, and the results are analyzed via data regression. The general trends of water contents, power consumptions, and treatment time under different electrical potentials are established. The effects of voltage gradient on EK water drainage and energy consumption are analyzed via the regression trends obtained in this study. The degree of saturation of the kaolinite samples at the anode is analyzed, relating with the EK generated water flow. The influence of the initial water content of the kaolinite slurry in the EK dewatering process is also investigated.

4.2. Experiments

4.2.1. Design consideration

The experiments were carried out in two categories in an electrokinetic dewatering cell with vertically installed electrodes. The variables in tests series include the voltage gradient, initial water content of kaolinite slurry, and treatment time. The voltage-controlled method was used in the experiments, i.e. the voltage gradient is kept constant during a test while the current is recorded as a function of time. The electrical conductivity of the sample, κ, and power consumptions, P, were calculated in real time. In the first category of experiments (KV), four series of tests with the voltage gradients of 25V/m (KV-25), 50V/m (KV-50), 75V/m (KV-75), and 100 V/m (KV-100) were conducted on kaolinite slurry with a water content 100% (50% in solid content[2]) to evaluate the influence of voltage gradients on EK dewatering. In the second category of experiments (KW), two series of tests were

[2] Solid content, s_c, has a relationship with water content, w, as: $s_c=1/(1+w)$ (wt%)

carried out, using kaolinite slurry with two initial water contents, i.e. 100% (50% in solid content) (KW-100 series, which is the same as KV-50 series) and 150% (40% in solid content) (KW-150 series) under a constant voltage gradient of 50V/m. In each series, tests were terminated after pre-determined durations to study the effect of treatment time. Table 4.1 summarizes the testing conditions of all tests in both categories.

4.2.2. Experimental apparatus

The EK dewatering cell used in this study was introduced in Chapter 3 (Fig. 4.1). The experimental system consists of an EK dewatering cell, a DC power supply, and a graduated cylinder to collect and measure water drainage from dewatering process. The EK dewatering cell consists of a Plexiglas tank (35 cm L × 10 cm W × 25 cm H), and two electrodes. The anode is made of a dimensionally stable anode (DSA) mesh (expended titanium coated with iridium oxide) and the cathode is made of a woven wire stainless steel mesh (SS316). Electrodes are covered with geotextile fabric to prevent the leakage of the slurry solids. The system is sealed during a dewatering test to avoid water evaporation.

4.2.3. Sample preparation and testing procedure

Basic properties of kaolinite slurry are listed in Table 4.2. To prepare a test, about 3 kg dried pulverized kaolinite powder (EPK Kaolin from Edgar Minerals, Inc.) and tap water were added into a bucket and well mixed with an electric mixer to achieve a target water content. Then the EK dewatering cell was assembled and well-mixed kaolinite slurry was poured into the cell for the EK dewatering test. A DC power supply was connected to electrodes to generate a target voltage gradient cross the cell and maintained throughout the test. There was no surcharge applied on top of the cell during the experiment. Water was discharged into a graduated cylinder via two plastic tubes at the bottom of the cell.

The initial water content of sample was measured prior to each test, following ASTM D2166-10 (ASTM 2010a). The original height of the sample in the cell was measured to calculate the initial volume. The electric current and water drainage were recorded in real time during the test. After a predetermined treatment time, the power was terminated, and the finial solid (water) content, undrained shear strength, and Atterberg limits (ASTM

D4318-10e1; ASTM 2010b) were measured at the anode, center and cathode sides, respectively.

4.3. Results and Analysis

4.3.1. Water drainage

A summary of dewatering results is presented in Table 4.3. For comparison, the water drainage was normalized to the initial sample volume, i.e., V_w/V_0, the ratio of water discharge to the initial volume of slurry. The results of water discharge are presented in Figs. 4.2 and 4.3 for KV series and KW series of tests, respectively. It is observed that water drained quickly at the beginning of an EK dewatering test, and slowed down gradually and finally reached a stop at certain treatment time. For example, in test KV-100, the water discharged quickly in the first 50 hours with an almost constant flow rate, then the flow rate reduced and approached zero after 150 hours. The similar results were recorded in KV-75 tests. For tests KV-50 (KW-100), KV-25 and KW-150, the constant flow was also observed in the initial stage, whereas the stop of the EK drainage was not observed because the treatment time was not long enough. The normalized results, which indicate the volume reduction due to EK dewatering, were about 25%~30% for KV series tests and 40% for KW-150 test.

As discussed in Chapter 3, the relationship between the normalized water drainage of oil sands tailings and EK treatment time can be expressed as (Eq. 3.5 in Chapter 3):

$$V_w/V_0 = \frac{D_v t}{t_{50} + t} \tag{4.1}$$

where D_v and t_{50} are parameters obtained through experiments. D_v represents the maximum reduction of sample volume due to EK dewatering when time approaches infinity, and t_{50} is the time (hours) to reach 50% volume reduction ($D_v/2$) by EK dewatering. The parameters D_v, and t_{50} for KV series and KW series of tests are summarized in Table 4.4.

It is noted that at the same initial water content, for example w_0=100%, parameter D_v, which represents the maximum dewatering effect, is similar under different voltage

gradients, i.e. it varies from 0.34 to 0.38 under voltage gradients from 25 to 100 V/m, as seen in Fig. 4.4. On the other hand, when the initial water content increased to 150%, the maximum water drainage increased as well (Fig. 4.3), indicated by D_v = 0.53 for KW-150 series and 0.34 for KW-100 series. From Figs. 4.3 and 4.4, the values of parameter t_{50} for KW series of tests are similar, i.e., 61.9 hours for KW-150 and 67.4 hours for KW-100. It should be noted that the voltage gradient for these tests was 50V/m.

It is also noted that the high voltage gradient will lead to fast water drainage and low value of t_{50}. In comparison, t_{50} =36.3 hours for 100V/m, whereas t_{50} =216.3 hours for 25V/m. This means that the high voltage will shorten the time of EK drainage.

According study in Chapter 3, the average water content for oil sands tailings is about 200%, thus leading to higher maximum water discharge, D_v (about 0.7) than those for kaolinite slurry, as seen in Fig. 4.4. Similar with kaolinite slurry, the low value of t_{50} was obtained at high voltage gradient for oil sands tailings. But at the same voltage gradient, the t_{50} for oil sands tailings is higher than it for kaolinite slurry. For example, at voltage gradient of 100V/m, the t_{50} for oil sands tailings was 62.2 hours, which is higher than t_{50} (36.3 hours) in KV-100 tests. The possible reasons for the difference are due to the differences in mineral composition and pore water chemistry between oil sands tailings and kaolinite slurry.

It is concluded that during an EK dewatering test the initial water content of samples affects the maximum water discharge, and the voltage gradient governs the duration required to achieve the max water drainage.

4.3.2. Water content

During an EK dewatering test, water is driven by electric current from anode and discharged at the cathode. Thus, the water content at the anode reduced quickly with time. For different types of geomaterials, the water content of the sample at the cathode can be lower than or remain the same as the initial value. This phenomenon has been recognized in both theoretical development and experimental data (Guo and Shang 2014, Shang 1997, Bjerrum et al. 1967; Lo et al. 1991a). As discussed in Chapter 3, the changes in water

content of the sample at the anode during an EK dewatering test were expressed via an exponential decay function (Eq. 3.11 in Chapter 3):

$$w(t)/w_0 = w_f + D_w e^{-\lambda_w t} \quad (4.2)$$

where $w(t)/w_0$ is the normalized water content, in which $w(t)$ is the water content of the sample after dewatering time, t, w_0 is the initial water content of the sample; w_f, D_w, and λ_w are empirical parameters obtained from experiments. w_f represents the lowest normalized water content after EK dewatering treatment when the treatment time, t, approaches to infinity; D_w represents the maximum reduction in water content ($w_f + D_w \approx 1$); and λ_w represents the rate of dewatering.

For all tests in the KV series with the sample initial water content of 100%, the normalized water contents, $w(t)/w_0$, versus treatment time at the anode are plotted in Fig. 4.5 with data regression equations. The values of w_f, D_w, and λ_w are listed in Table 4.5 for KV series tests.

It is noted that the proposed regression equation (Eq.4.2) fits well with the results of sample water content at the anode, as shown in Fig. 4.5. As shown higher voltage gradients lead to more rapid dewatering at the anode. Under 100V/m, the water content at the anode approached to a plateau shortly after 50 hours, whereas under the voltage gradient of 25 V/m, the rate of water content reduction was constant over 170 hours. The water content changes at center and vicinity of cathode are plotted in Fig. A1.1 and A1.2 in Appendix 1. The results indicate that the changes of normalized water content of the sample at the center and cathode are less than that at the anode.

For KW-150 test series, Fig. 4.6 presents the water content reduction of the samples at the anode with the initial water content of 150%. The regression equation for the water content in KW-150 test series is shown in the figure, and the fitted values of parameters, D_w, w_f, and λ_w, are also listed in Table 4.5. The results of the water contents of the samples at the center and cathode are plotted in Fig. A1.3 in Appendix 1.

Fig. 4.7 plots the reduction rate, λ_w, at different voltage gradients, E for the samples with the same initial water content of 100%. From Fig. 4.7, it is noted that the change of

reduction rate, λ_w, is nearly linear with the applied voltage gradient. The higher initial water content will lead to more rapid reduction in the water content at anode. On the other hand, it is noted that under the same voltage gradient of 50V/m, the value of λ_w for KW-150 test series with the initial water content of 150% is 0.017 (Table 4.5), which is slightly higher than λ_w = 0.014 from KW-100 test series with the initial water content of 100%.

4.3.3. Power consumptions

The power consumption is a key parameter in the EK design. Under a constant applied voltage gradient, the power consumption is closely related to the electrical conductivity of the sample. The current density reduces with the decrease in the electrical conductivity of the sample, thus leading to a reduction in dewatering efficiency. The Power consumptions of all lab tests are calculated according to the current density, j(A/m^2), and the voltage gradient, E(V/m), recorded during experiments. Current densities, j(A/m^2), and calculated electrical conductivities, κ (S/m), are shown in Figs. A1.4 and A1.5 in Appendix 1 for KV series and KW series, respectively. Power consumptions and accumulated energy consumptions under different voltage gradient (in KV series tests) are shown in Fig. 4.8. For KW series of tests, which have the initial water contents of 100% and 150%, power consumptions and accumulated energy consumptions are calculated and presented in Fig. 4.9. As discussed in Chapter 3, the relationship between power consumptions per unit volume at the specific initial water content and treatment time can be expressed via an exponential function (Eq. 3.19 in Chapter 3):

$$\mathrm{P}(kW/m^3) = P_m e^{-\lambda_P t} \qquad (4.3)$$

where P_m is the maximum power consumptions (kW/m^3). The values of parameters P_m and λ_p are listed in Table 4.6 for KV and KW series of tests.

According to results in Figs. 4.8 and 4.9, the proposed regression equation (Eq. 3.19) presented in Chapter 3 can also describe the power consumption reduction for kaolinite slurry during EK dewatering treatment. Hence Eq. 4.3 is used for the analysis of EK dewatering efficiency in a later section.

4.3.4. Undrained shear strength and Atterberg limits

During a dewatering process of geomaterials, the water content will decrease and the shear strength increase. A comparison of the undrained shear strength of kaolinite samples at the vicinities of anode and cathode for KV and KW series of tests is plotted in Figs. 4.10a and 4.10b, respectively. It is observed that the undrained shear strength of the sample at the anode increases exponentially with time during the EK treatment period. As observed from the figure, the exponential increases in undrained shear strength of kaolinite sample at the anode with time can be expressed by the following regression equation:

$$S_u = C_{su} e^{\lambda_{su} t} \tag{4.4}$$

where S_u is the undrained shear strength (kPa), C_{su}, and λ_{su} are empirical coefficients obtained through experiments, and t is the treatment time (hours). The values of parameters C_{su}, and λ_{su} for KV and KW series tests are listed in Table 4.7.

As shown in Fig. 4.10a, the increase in the undrained shear strength of the sample at the anode is most significant, from virtually 0 to 15 kPa, under the voltage gradient of 100V/m in KV-100 series of tests. In KV-25 series, the voltage gradient is the lowest in the KV test category, i.e., 25 V/m, the shear strength increase is minimum, i.e., from virtually 0 kPa to 3.5 kPa. The undrained shear strength of the sample at the vicinity of cathode remains below 2 kPa.

Under the voltage gradient of 50V/m, the samples with the initial water content of 100% (KW-100 series) had higher undrained shear strength at the anode than those in KW-150 series (initial water content of 150%) during the same treatment period, as seen in Fig. 4.10b. After 175 hours treatment, the undrain shear strength of the sample at the anode is about 4.5 kPa and 1 kPa for tests KW-100 and KW-150, respectively. The undrained shear strength of the sample at the cathode remained less than 1 kPa for both KW-100 and KW-150 series.

The undrained shear strength of the sample is also plotted against the water content for KV and KW series tests, as seen in Figs. 4.11. The relationship between undrained shear

strength and water content (S_u-w line) of the kaolinite is generated according to the results by Rassat et al. (2003) and expressed as:

$$S_u = 108.52e^{-6.761w} \quad (4.5)$$

where S_u is the undrained shear strength (kPa), and w is the water content (%). As shown in Fig.4.11a, at the voltage gradient of 100 V/m (KV-100 series tests), the points moved above the Su-w line, indicating that the sample at the anode had significant EK strength gain under the same water content. As seen in the figure, all data from KV-25 series tests are located near the S_u-w line, meaning that no EK strengthening effect under the voltage gradient of 25V/m (KV-25 series tests). As observed, the EK strengthening effect increases with the increase in the applied voltage gradient in the range of 50 to 100 V/m.

On the other hand, the data near the cathode in KV series are all along the S_u-w line, as seen in Fig.4.11b, indicating no EK strengthening effect occurred at the cathode. Hence it is concluded that the undrained shear strength of the sample at the cathode is only dependent of the water content.

For EK treatments with different initial water contents, as seen in Fig. 4.11a, samples at the anode had strength gains in both KW-100 an KW-150 series tests. On the other hand, the sample at the cathode did not show any EK strengthening effect in the KW series tests, as seen in Fig. 4.11b. The difference between the undrained shear strength of the samples in KW-150 and KW-100 tests is mainly attributed to the difference in water content. As shown in Fig. 4.11, the water content of the kaolinite samples was about 60-80% for KW-100 and 75-90% for KW-150, respectively, after EK dewatering.

The increase in the undrained shear strength of soils has been observed after EK treatment in many researches (Bjerrum et al. 1967, Lo and Ho 1991, Lo et al. 1991b, Abiera et al. 1999, Bergado et al. 2000). Historical research has found that the undrained shear strength of the soil can be estimated via empirical correlation based on the liquidity index (Wroth and Wood 1978, Budhu 2005).

The liquidity indices of the sample after EK treatment are listed in Table 4.8. In KV series tests, the liquidity index has an initial value of 2 and 3.5 with the initial water content of

100% and 150%. It can be found that, generally, the liquidity indices of the sample are lower at the vicinity of anode than center and cathode after EK treatment, indicating that the undrained shear strength of the sample is higher closed to the anode than center and cathode. This trend is coincident with the undrained shear strength results after EK treatment. For example, in KV-100 series test, the liquidity indices of kaolinite samples were 0.8~0.3 after 50~175 hours treatment at the anode, and significant reduced with the increase in treatment time. Whereas, they were about 1.2~0.7 and 1.0~0.8 at the center and cathode, respectively, and remained almost constant after 75 hours treatment. Similar results were found in KV-75, KV-50 and KV-25 tests. It is also found that the liquidity index decreased with the increase in applied voltage gradient within the same treatment period. For instance, as seen in Table 4.8, after 175 hours treatment, the liquidity index of the sample was 0.3 at voltage gradient of 100V/m and 0.7 at the voltage gradient of 50V/m. For the high initial water content (150% in KW-150 tests), after EK treatment, the liquidity indices of the sample were 2.1~1.3 (50~175 hours treatment), which is higher than those (1.7-0.7) obtained in KW-100 tests (100% initial water content).

The EK strengthening effects are mainly attributed to water content reduction due to EK induced consolidation and soils hardening by electrochemical reaction at electrodes (Rittrong et al. 2008). The electrochemical reaction at electrodes altered the soil behavior primarily reflected by a change in Atterberg limits. Both the reduction of water content and increase in Atterberg limits induce a reduction of liquidity index and increase the undrained shear strength. Hence the Atterberg limits were analyzed to examine the effects of electrochemical reaction on kaolinite samples.

The raw data of the Atterberg limits of the sample at the vicinities of anode, center and cathode are plotted with treatment time in Figs. 4.5, A1.1 and A1.2. From Fig. 4.5, a slight increase of the liquid limit was noted near the anode, and the plastic limit was unchanged. Under the voltage gradient 100 V/m, the sample showed more significant increase in the liquid limit than those under low voltage gradients. The Atterberg limits of post-treated samples are also plotted in the Casagrande plasticity chart, as shown in Fig. 4.12. The plastic limit for untreated kaolinite was 32.4%, and the liquid limit was 65.8% and the point for untreated kaolinite is located on the A-line. It is observed that the points for the EK

treated kaolinite samples at the center and cathode after treatment are close to untreated samples, indicating that the Atterberg limits of the sample did not have significant change during the treatment period. This can be also observed from Figs. A1.1 and A1.2 in Appendix 1. On the other hand, the results at the anode shift above the A-line, indicating an increase in the plasticity of the samples. The same observation has been reported on oil sands tailings (Guo and Shang 2014).

In summary, for kaolinite slurry at the anode, the EK strengthening effects are attributed to both reduction in water content and the increase in plasticity due to electrochemical reactions. On the other hand, the EK treatment has minor effects on plasticity of the sample at the center and cathode. Thus, it is concluded that the increase in the undrained shear strength is primarily attributed to the reduction of water content due to EK dewatering. Some studies (Micic et al. 2001, Shang et al. 2004, Mohamedelhassan et al. 2005, Rittrong et al. 2008) found that the undrained shear strength increased at the cathode in carbonate rich geomaterials, due to amorphous cementation.

4.3.5. Degree of saturation

The saturation of kaolinite samples was analyzed after EK dewatering tests. As discussed in Chapter 3, the change of saturation has a key effect on the EK dewatering process. The EK generated water drainage can be classified in three stages (Chapter 3, Section 3.4), i.e.,

1). The Linear flow stage, marked from the beginning of experiments until T_{tran}, which is the time when the flow rate of EK drainage starts to change and become non-linear;

2). The Transitional flow stage, indicated by the time from T_{tran} to T_{end}, which is the time when the flow rate approaches to zero; and

3). The End of flow stage, when the treatment time passes T_{end}.

The transition of the flow stage is related to the degree of saturation of the sample, particularly at the anode. The samples saturation at the anode are plotted versus treatment time, as shown in Fig. 4.13. The EK water drainage associated with the flow stages are also plotted in these figures. The characteristic times, i.e., T_{tran}, T_{end} and t_{50}, and corresponding

degree of saturation, S, at the anode obtained in this study are summarized in Table 4.9. It should be noted that the characteristic times obtained in this study were not normalized, thus they are only valid for the experimental configuration described in this study. A further study is necessary for the scaling effects.

Under the voltage gradient of 100 V/m, as seen in Fig. 4.13(a), the degree of saturation of the sample at the anode is plotted with the EK water drainage. As seen the linear flow stage (0 to T_{tran},) lasted about 30 hours. Then the EK drainage entered the transitional flow stage from 30 hours (T_{tran}) to 105 hours (T_{end}), then the water flow stopped. A regression trend line of the degree of saturation, S_d, of the sample at the anode is also shown in Fig. 4.13(a). It can be seen that the time for the beginning of transitional stage, T_{tran}, marked when the degree of saturation, S_d of the sample at the anode reduced to about 78%, and the time at flow rate approaches to zero, T_{end}, is reached when the sample saturation at the anode reduced to about 60%, in KV-100 series of tests.

Similar results were obtained from results of KV-75 series of tests under the voltage gradient of 75V/m, as seen in Fig. 4.13(b), which shows that the water discharge is linear between 0 and 50 hours, i.e. T_{tran} = 50 hours. In KV-75 series of tests, the transitional flow stage began when the degree of saturation, S_d, of the sample at the anode (x/L=0.9) reduced to about 76%, and lasted 125 hours (T_{end}). At T_{end}, the time when the EK flow completed stopped, the saturation at the anode was about 59%.

As seen from Figs. 4.13(c) to 4.13(e), the $T_{tran,}$ which is the time when the flow rate of EK drainage started to change and become non-linear, was about 50, 150, and 60 hours for KV-50 (KW-100), KV-25, and KW-150 tests series, respectively. The corresponding degrees of saturation of the sample were 83%, 83% and 87% at the anode. However, the treatment time was not long enough to find the T_{end} for KV-50 (KW-100), KV-25, and KW-150 tests series. The degree of saturation, S_d, of the sample at the anode was about 70% in KV-50 series of tests at the end of treatment (175 hours). It is 77% for KV-25 tests at 350 hours, and 74% for KW-150 series at 175 hours.

It is concluded that when the degree of saturation, S_d, of the kaolinite slurry sample at the anode decreases to about 82%, the EK flow changes from the linear flow stage to

transitional flow stage, and when the sample saturation at the anode reaches to about 60%, the EK flow stops.

In Chapter 3 for oil sands tailings, it was found that the linear flow stage lasted from commencing the treatment until the degree of saturation, S_d, at anode reduced to 80%, which is similar with the results for kaolinite slurry.

4.3.6. Effects of voltage gradient and initial water content on energy consumptions

The treatment time and voltage gradient are key parameters for EK dewatering. A high voltage gradient leads to a shorter treatment time, and vice versa. So, the effects of voltage gradient and initial water content on energy consumptions were analyzed in this study by using the characteristic times obtained under these experimental conditions.

Fig. 4.14 shows T_{tran}, (the time of beginning of transitional stage), and T_{end} (the time for the ending of EK drainage), are related to voltage gradients for kaolinite slurry (w=100%). When the voltage gradient, E, was under 50V/m, an increase in the voltage gradient significantly shortened the time to reach zero flow, T_{end}. However, when the voltage gradient was higher than 50V/m, further increase in the voltage gradient had a limited effect on reducing the treatment time.

The energy consumption for EK treatment is affected by both voltage gradient and treatment time, and it can be calculated by integrating the power consumption equation (Eq. 4.4) to time, t, (Chapter 3) and expressed:

$$W(kWh/m^3) = W_m\left(1 - e^{-\lambda_P t}\right)\times 10^{-3} \qquad (4.6)$$

where W_m is the maximum energy consumption, which is calculated as $\frac{P_m}{\lambda_P}$, and listed in Table 4.6 for KV and KW series tests. The W_m obtained in this study ranged from 2.5 to 13.8 kWh/m^3 at the voltage gradient from 25 to 100 V/m.

It is clear that the energy consumption, W is related to the reduction rate of the power consumption, λ_p, and the maximum power consumption, P_m. λ_p is linearly increased with

the voltage gradient, as shown in Fig. 4.15. On the other hand, P_m increases with the voltage gradient, E, in a quadratic function, and is related to κ_0, which is the initial electrical conductivity of the kaolinite sample (κ_0= 0.027 S/m) (Eq. 3.19) as shown in Fig. 4.15. The accumulated energy consumptions at real time are plotted in Figs. 4.8 and 4.9. Energy consumptions under different voltage gradients are compared in three ways, i.e., 1) the maximum energy consumption under a specific voltage gradient, 2) the energy consumption at T_{tran}, i.e., the end of the linear flow stage, and 3) the energy consumption at the same post-treated water content for different voltage gradients.

Firstly, the maximum power consumptions at different voltage gradients are plotted in Fig. 4.16. It is noted that the maximum energy consumption, W_m, is proportional to the square of voltage gradients. The maximum energy consumption in KV-100 series of tests is about 14 kWh/m^3, which is 7 times higher than that under the voltage gradient of 25V/m, i.e., 2 kWh/m^3, whereas W_m under 100V/m is about twice higher than that under 50V/m.

EK dewatering treatment is most effective in the linear flow stage, i.e., when T_{tran} reaches, the flow rate of EK drainage starts to change and become non-linear with time. The energy consumption at T_{tran} under different voltage gradients is analyzed and plotted in Fig. 4.16. A quadratic relationship is found between the energy consumption, W at T_{tran}, and the voltage gradient, E. It is noted that when the voltage gradient increased from 50V/m to 100V/m, the corresponding T_{tran} was reduced from 50 hours to 30 hours (Fig. 4.14), and the energy consumption is increased from 2.2 to 5.5kWh/m^3 (Fig. 4.16). When the voltage gradient increased from 25V/m to 50V/m, the T_{tran} was significantly reduced from 150 to 50 hours, as seen in Fig. 4.14. Meanwhile, the power consumption was increased from 1.1 to 2.2 kWh/m^3 according to Fig. 4.16.

To better understand the EK dewatering performance associated with energy consumptions, the average water content of the sample is plotted versus energy consumptions at the same time for KV and KW series in Figs. 4.17a and 4.17b, respectively. The average water content is calculated based on the volume reduction of the sample via the regression equation of normalized water drainage, V_w/V_0 (%) (Eq. 4.1). The dotted lines are the trajectories of data for the water content-energy consumptions along with the time for KV

and KW series tests during the treatment. The points are the data of the water content-energy consumptions at the characteristic times, i.e., t_{50}, T_{tran}, and T_{end}.

As shown from the experimental results, under the experimental condition described in this study, the energy required to reach a certain average water content of the sample can be found through the trajectory lines for different applied voltage gradient. From Fig. 4.17a, at each characteristic time, the average water contents of the samples were within a similar level. For example, at T_{tran}, the average water contents of the samples for KV series tests were about 80%. At characteristic times of t_{50} and T_{end} the water contents were about 75% and 60%, respectively. To reach any certain water content, it is recognized that the treatment under higher voltage gradient (for example KV-100) will required more energy than those under lower voltage gradient (KV-75, 50 and 25), as seen in Fig. 4.17a. In contrast, the high voltage gradient reduced the treatment time. As seen in Fig. 4.14, the characteristic time, T_{tran} for KV-100 is about 30 hours, but for KV-25 is about 150 hours under the current testing configuration.

For the treatment with different initial water content, as seen from Fig. 4.9, the power consumption for KW-150 series was less than KW-100. The energy consumptions for two series of tests at T_{tran}, calculated according to Eq. 4.6, were 2.2 and 2.1 kWh/m^3 with the initial water content of 100% and 150%, respectively. However, the water contents of the sample at T_{tran} were different for KW-100 and KW-150 series tests. The average water content of the sample was about 80% for KW-100 tests and 100% for KW-150 tests. According to Fig. 4.17b, more energy is required for the samples with higher initial water content (w_0=150%) to reach the same final water content as those with low initial water content (w_0=100%). For example, at characteristic time of T_{end} (165 hours), which is the time when EK flow stops, the average water content of the sample for KW-150 tests (77%) was similar to the water content of the sample in KW-100 tests (80%) at T_{tran} (50 hours). Therefore, to achieve the same final water content, the sample with high initial water content needs longer treatment time, thus leading to more energy consumptions.

Overall, the results show that it is important to consider for both voltage gradient and treatment time in the design of EK dewatering, depending on factors such as target final water content, scale of the sample, and project time requirement, etc.

4.4. Conclusion

EK dewatering tests on kaolinite slurry under different voltage gradients and initial water contents were performed and analyzed by using the proposed regression model for oil sands tailings described in Chapter 3. The regression equations obtained from data on oil sands tailings were verified on kaolinite slurry. The degrees of saturation of samples at the anode were analyzed in the EK dewatering process. A detailed analysis of energy consumption under different voltage gradients and treatment time was carried out under the experiment condition described in this research. The following conclusions are made based on the results of experiments:

- The regression model developed for oil sands tailings is applicable for EK dewatering of kaolinite-tap water slurry.
- The initial water content of kaolinite slurry governs the maximum water discharge, while the voltage gradient controls the rate of dewatering.
- The liquid limit of the kaolinite sample at the anode increased due to EK treatment, but the plastic limit was unchanged. The higher voltage gradient (100V/m) induced more rapid change in the liquid limit compared with the lower voltage gradient (25V/m).
- The undrained shear strength of the sample at the anode increased exponentially within the treatment period, and the EK strengthening effect is more significant at higher voltage gradient and longer treatment time.
- The EK strengthening effect at the anode is attributed to water content reduction due to EK induced consolidation and material hardening by electrochemical reaction, whereas the EK strengthening effect at the cathode is primarily due to EK dewatering for the kaolinite slurry.
- EK induced water flow in the kaolinite slurry can be expressed via the regression equation and further classified into three stages, i.e., 1) the linear flow, 2) the

transitional flow, and 3) the end of flow. The linear flow stage lasted from the beginning of the treatment until the degree of saturation, S_d, reached 82% at the anode. When the degree of saturation, S_d, at the anode, reduced to 60%, the EK flow reached a stop.

- With the same initial water content and experimental configuration, the treatment under high voltage gradient needs more energy but less treatment time than those with low voltage gradient to reach the same post-treated water content.
- Under the same applied voltage gradient and experimental configuration, the treatment with high initial water content needs longer time and more energy to reach the same final water content than those with low initial water content.

Reference

Abiera, H. O., Miura, N., Bergado, D. T., and Nomura, T. (1999). Effects of using electro-conductive PVD in the consolidation of reconstituted Ariake clay. Geotechnical Engineering, 30, No. 2, 67-83.

ASTM (2010a). D2166-10: Standard test methods for laboratory determination of water (moisture) content of soil and rock by mass. ASTM International, West Conshohocken, PA, 2010, https://doi.org/10.1520/D2216-10

ASTM (2010b). D4318-10e1: Standard test methods for liquid limit, plastic limit, and plasticity index of soils, ASTM International, West Conshohocken, PA, 2010, https://doi.org/10.1520/D4318

Bergado, D. T., Balasubramaniam, A. S., Patawaran, M. A. B., and Kwunpreuk, W. (2000). Electroosmotic consolidation of soft Bangkok clay with prefabricated vertical drains. Ground Improvement, 4, No.4, 153-163.

Bjerrum, L., Moum, J., and Eide, O. (1967). Application of electroosmosis to a foundation problem in a Norwegian quick clay. Géotechnique, 17, No.3, 214–235.

Budhu, M. (2005). Soil mechanics and foundations, 2nd edn. Wiley, Hoboken, New Jersey, USA.

Casagrande, L. (1949). Electroosmosis in soil. Géotechnique, 1, No.3,159–177.

Casagrande, L. (1959). Review of past and current work on electroosmotic stabilization of soils. In Harvard Soil Mechanics Series, 45, Harvard University Cambridge, Massachusetts, USA (reprinted November 1959 with a supplement of June 1957).

Fourie, A. B., Johns, D. G., and Jones, C. F. (2007). Dewatering of mine tailings using electrokinetic geosynthetics. Canadian Geotechnical Journal, 44, No.2, 160-172.

Glendinning, S., Lamont-Black, J., and Jones, C. J. (2007). Treatment of sewage sludge using electrokinetic geosynthetics. Journal of Hazardous Materials, 139, No.3, 491-499.

Guo, Y. and Shang, J.Q. (2014) A study on electrokinetic dewatering of oil sands tailings. Environmental Geotechnics, 1, No.2, 121-134.

Lo, K.Y., and Ho, K.S., (1991). The effects of electroosmotic field treatment on the soil properties of a soft sensitive clay. Canadian Geotechnical Journal, 28, No.6, 763-770.

Lo, K. Y., Ho, K. S., and Inculet, I. I. (1991a). Field test of electroosmotic strengthening of soft sensitive clay. Canadian Geotechnical Journal, 28, No.1, 74-83.

Lo, K. Y., Inculet, I. I., and Ho, K. S. (1991b). Electroosmotic strengthening of soft sensitive clays. Canadian Geotechnical Journal, 28, No.1, 62-73.

Lockhart, N.C. (1983a). Electroosmotic dewatering of clays. I. Influence of voltage. Colloids and Surfaces, 6, No.3, 229-238.

Lockhart, N.C., (1983b). Electro-osmotic dewatering of fine tailings from mineral processing. International journal of mineral processing, 10, No.2, 131-140.

Micic, S., Shang, J. Q., Lo, K. Y., Lee, Y. N., and Lee, S. W. (2001). Electrokinetic strengthening of a marine sediment using intermittent current. Canadian Geotechnical Journal, 38, No.2, 287-302.

Mitchell, J.K., and Soga K. (2005). Fundamental of soil behavior, 3rd edn. Wiley, Hoboken, New Jersey, USA.

Mohamedelhassan, E., and Shang, J. Q. (2001). Effects of electrode materials and current intermittence in electroosmosis. Proceedings of the Institution of Civil Engineers-Ground Improvement, 5, No.1, 3-11.

Mohamedelhassan, E., Shang, J. Q., Ismail, M. A., and Randolph, M. F. (2005). Electrochemical cementation of calcareous sand for offshore foundations. International Journal of Offshore and Polar Engineering, 15, No. 01, 71-79.

Raats, M. H. M., Van Diemen, A. J. G., Laven, J., and Stein, H. N. (2002). Full scale electrokinetic dewatering of waste sludge. Colloids and Surfaces A: Physicochemical and Engineering Aspects, 210, No.2, 231-241.

Rassat, S. D., Bagaasen, L. M., Mahoney, L. A., Russell, R. L., Caldwell, D. D., and Mendoza, D. P. (2003). Physical and liquid chemical simulant formulations for transuranic wastes in Hanford Single-Shell Tanks. PNNL-14333, National Technical Information Service, US Dept. of Commerce, Springfield, VA p. iv.

Rittirong, A., Douglas, R. S., Shang, J. Q., and Lee, E. C. (2008). Electrokinetic improvement of soft clay using electrical vertical drains. Geosynthetics International, 15, No.5, 369-381.

Shang, J. Q. (1997). Electrokinetic sedimentation: a theoretical and experimental study. Canadian Geotechnical Journal, 34, No. 2, 305-314.

Shang, J. Q., Mohamedelhassan, E., and Ismail, M. (2004). Electrochemical cementation of offshore calcareous soil. Canadian geotechnical journal, 41, No. 5, 877-893.

Sunderland, J.G. (1987). Electrokinetic dewatering and thickening. II. Thickening of ball clay. Journal of applied electrochemistry, 17, No.5, 1048-1056.

Wroth, C. P., and Wood, D. M. (1978). The correlation of index properties with some basic engineering properties of soils. Canadian Geotechnical Journal, 15, No. 2, 137-145.

Table 4.1 EK dewatering tests conditions

Conditions						
Categories.	KV				KW	
Series	KV-100	KV-75	KV-50	KV-25	KW-100	KW-150
Voltage gradient (V/m)	100	75	50	25	50	
Initial water content	100				100	150
Surcharge (kPa)	0					
Sample size (cm)	Recorded Height(H_0) × 29.5 (length) × 10 (width)					
Water Discharge (mL)	Recorded					
Current (A)	Recorded					
Electrodes	SS316 mesh cathode, Ti/IrOx mesh anode					

Table 4.2 Kaolinite properties

Properties	**Kaolinite slurry**
Water content (%)	100% or 150%
Specific gravity, G_s	2.65
Plastic limit (%)	32.4
Liquid limit (%)	65.8
Plasticity index (%)	33.4
Liquidity index	2.0 or 3.5
Pore fluid	Tap water
Water electrical conductivity (µS/cm)	200-350

Table 4.3 Summary of the EK dewatering tests for kaolinite slurry

Series	Test No.	Initial water content (%)	Voltage gradient (V/m)	Testing time (hours)	H_0 (cm)	V_w/V_0 (%)	V_w (mL)
KV-100	EKD-kt-0-100-50	100	100	50	12.5	25.0	923
	EKD-kt-0-100-75			75	12.5	28.5	1049
	EKD-kt-0-100-100			100	12.5	29.9	1102
	EKD-kt-0-100-125			125	11.8	29.8	1038
	EKD-kt-0-100-150			150	12.0	30.3	1074
	EKD-kt-0-100-175			175	12.0	30.9	1093
KV-75	EKD-kt-0-75-25	100	75	25	9.0	12.2	323
	EKD-kt-0-75-75			75	11.5	24.5	830
	EKD-kt-0-75-125			125	10.5	27.8	862
	EKD-kt-0-75-175			175	8.6	27.6	700
KV-50 (KW-100)	EKD-kt-0-50-25	100	50	25	10.5	7.8	241
	EKD-kt-0-50-50			50	11.7	15.3	527
	EKD-kt-0-50-75			75	10.8	17.5	556
	EKD-kt-0-50-100			100	12.5	20.3	749
	EKD-kt-0-50-125			125	11.5	21.2	720
	EKD-kt-0-50-150			150	9.0	22.6	601
	EKD-kt-0-50-175			175	8.5	24.3	609
KV-25	EKD-kt-0-25-25	100	25	25	9.0	3.6	94
	EKD-kt-0-25-50			50	11.5	6.8	229
	EKD-kt-0-25-75			75	11.2	9.1	301
	EKD-kt-0-25-100			100	10.2	12.2	368
	EKD-kt-0-25-125			125	11.2	14.8	490
	EKD-kt-0-25-150			150	11.0	15.7	509
	EKD-kt-0-25-175			175	11.8	18.0	627
	EKD-kt-0-25-350			350	10.1	22.5	670
KW-150	EKD-kt-0-50-50-150	150	50	50	12.0	24.8	876
	EKD-kt-0-50-75-150			75	12.2	30.7	1105
	EKD-kt-0-50-100-150			100	11.5	33.5	1137
	EKD-kt-0-50-125-150			125	12.5	33.5	1237
	EKD-kt-0-50-150-150			150	11	38.2	1239
	EKD-kt-0-50-175-150			175	10	38.9	1149

Table 4.4 Summary of the parameters for the regression equation of normalized water drainage

Test No.	D_v	t_{50}	R^2	Regression Equation
KV-100	0.387	36.3	0.989	$V_w/V_0 = \frac{0.387t}{36.3+t}$ $(T4.1)$
KV-75	0.381	51.2	0.987	$V_w/V_0 = \frac{0.381t}{51.2+t}$ $(T4.2)$
KV-50(KW-100)	0.336	67.4	0.995	$V_w/V_0 = \frac{0.336t}{67.4+t}$ $(T4.3)$
KV-25	0.385	216.3	0.994	$V_w/V_0 = \frac{0.385t}{216.3+t}$ $(T4.4)$
KW-150	0.534	61.9	0.995	$V_w/V_0 = \frac{0.534t}{61.9+t}$ $(T4.5)$

Table 4.5 Summary of the parameters for the regression equation of normalized water content at the anode

Test No.	W_f	D_w	λ_w	R^2	Regression Equation
KV-100	0.495	0.507	0.0297	0.986	$w_t/w_0 = 0.495 + 0.507e^{-0.0297t}$ $(T4.6)$
KV-75	0.506	0.490	0.0181	0.998	$w_t/w_0 = 0.506 + 0.490e^{-0.0181t}$ $(T4.7)$
KV-50(KW-100)	0.660	0.405	0.0142	0.970	$w_t/w_0 = 0.603 + 0.405e^{-0.0142t}$ $(T4.8)$
KV-25	0.495	0.514	0.0040	0.994	$w_t/w_0 = 0.495 + 0.514e^{-0.0040t}$ $(T4.9)$
KW-150	0.503	0.497	0.0170	0.989	$w_t/w_0 = 0.503 + 0.497e^{-0.0170t}$ $(T4.10)$

Table 4.6 Summary of the parameters for the regression equation of power consumptions and energy consumptions

Test No.	P_m	W_m	λ_p	R^2	Regression Equation
KV-100	233.1	13.8	0.0169	0.930	$P\left(W/m^3\right) = 233.1e^{-0.0169t}$ $(T4.11)$
					$W\left(kWh/m^3\right) = 13.8(1 - e^{-0.0169t})$ $(T4.12)$
KV-75	106.9	7.9	0.0136	0.983	$P\left(W/m^3\right) = 106.9e^{-0.0136t}$ $(T4.13)$
					$W\left(kWh/m^3\right) = 7.9(1 - e^{-0.0136t})$ $(T4.14)$
KV-50(KW-100)	54.6	6.1	0.0089	0.913	$P\left(W/m^3\right) = 54.6e^{-0.0089t}$ $(T4.15)$
					$W\left(kWh/m^3\right) = 6.1(1 - e^{-0.0089t})$ $(T4.16)$
KV-25	10.1	2.5	0.0041	0.818	$P\left(W/m^3\right) = 10.1e^{-0.0041t}$ $(T4.17)$
					$W\left(kWh/m^3\right) = 2.5(1 - e^{-0.0041t})$ $(T4.18)$
KW-150	48.4	4.4	0.0111	0.946	$P\left(W/m^3\right) = 48.4e^{-0.0111t}$ $(T4.19)$
					$W\left(kWh/m^3\right) = 4.4(1 - e^{-0.0111t})$ $(T4.20)$

Table 4.7 Summary of the parameters for the regression equation of undrained shear strength

Test No.	C_{Su}	λ_{su}	R^2	Regression Equation
KV-100	1.205	0.0154	0.906	$S_u(kPa) = 1.205e^{-0.0154t}$ $(T4.21)$
KV-75	0.540	0.0186	0.940	$S_u(kPa) = 0.540e^{-0.0186t}$ $(T4.22)$
KV-50(KW-100)	0.261	0.0160	0.902	$S_u(kPa) = 0.261e^{-0.0160t}$ $(T4.23)$
KV-25	0.095	0.0109	0.948	$S_u(kPa) = 0.095e^{-0.0109t}$ $(T4.24)$
KW-150	0.044	0.0193	0.967	$S_u(kPa) = 0.0435e^{-0.0193t}$ $(T4.25)$

Table 4.8 Summary of liquidity indices of the kaolinite samples after EK treatment

Test series	Test No.	Voltage gradient (V/m)	Treatment time (hours)	Liquidity index		
				Anode	Center	Cathode
KV-100	EKD-kt-0-100-50	100	50	0.8	1.2	0.9
	EKD-kt-0-100-75		75	0.5	0.9	1.0
	EKD-kt-0-100-100		100	0.5	0.7	1.0
	EKD-kt-0-100-125		125	0.6	0.8	1.0
	EKD-kt-0-100-150		150	0.4	0.8	0.8
	EKD-kt-0-100-175		175	0.3	0.9	1.0
KV-75	EKD-kt-0-75-25	75	25	1.2	1.9	1.7
	EKD-kt-0-75-75		75	0.8	1.3	1.2
	EKD-kt-0-75-125		125	0.6	1.3	1.0
	EKD-kt-0-75-175		175	0.5	1.4	1.2
KV-50 (KW-100)	EKD-kt-0-50-25	50	25	1.7	2.1	1.9
	EKD-kt-0-50-50		50	1.2	1.8	1.7
	EKD-kt-0-50-75		75	1.1	1.7	1.4
	EKD-kt-0-50-100		100	1.0	1.4	1.2
	EKD-kt-0-50-125		125	1.0	1.2	1.2
	EKD-kt-0-50-150		150	0.8	1.1	1.3
	EKD-kt-0-50-175		175	0.7	0.9	1.2
KV-25	EKD-kt-0-25-25	25	25	1.9	2.2	2.1
	EKD-kt-0-25-50		50	1.7	2.1	1.8
	EKD-kt-0-25-75		75	1.6	1.9	1.8
	EKD-kt-0-25-100		100	1.5	1.8	1.6
	EKD-kt-0-25-125		125	1.4	1.6	1.5
	EKD-kt-0-25-150		150	1.3	1.5	1.4
	EKD-kt-0-25-175		175	1.1	1.4	1.3
	EKD-kt-0-25-350		350	0.7	1.0	1.5
KW-150	EKD-kt-0-50-50-150	50	50	2.1	3.3	1.9
	EKD-kt-0-50-75-150		75	1.6	2.4	1.8
	EKD-kt-0-50-100-150		100	1.6	2.1	1.7
	EKD-kt-0-50-125-150		125	1.6	1.6	1.8
	EKD-kt-0-50-150-150		150	1.2	1.4	1.5
	EKD-kt-0-50-175-150		175	1.3	1.7	1.9

Table 4.9 Summary of characteristic times and water content at the anode

	Characteristic Times			Degree of Saturation at the anode	
Test No.	t_{50}	T_{tran}	T_{end}	S_d ($t=T_{tran}$)	S_d($t=T_{end}$)
KV-100	36.3	30	105	78.0%	62.4%
KV-75	51.2	50	125	76.2%	59.0%
KV-50 (KW-100)	67.4	50	-	82.7%	-
KV-25	216.3	150	-	83.4%	-
KW-150	61.9	60	-	87.4%	-
Average	-	-	-	81.5%	60.7%

"*", the value is estimated.
"-", the value is not available.

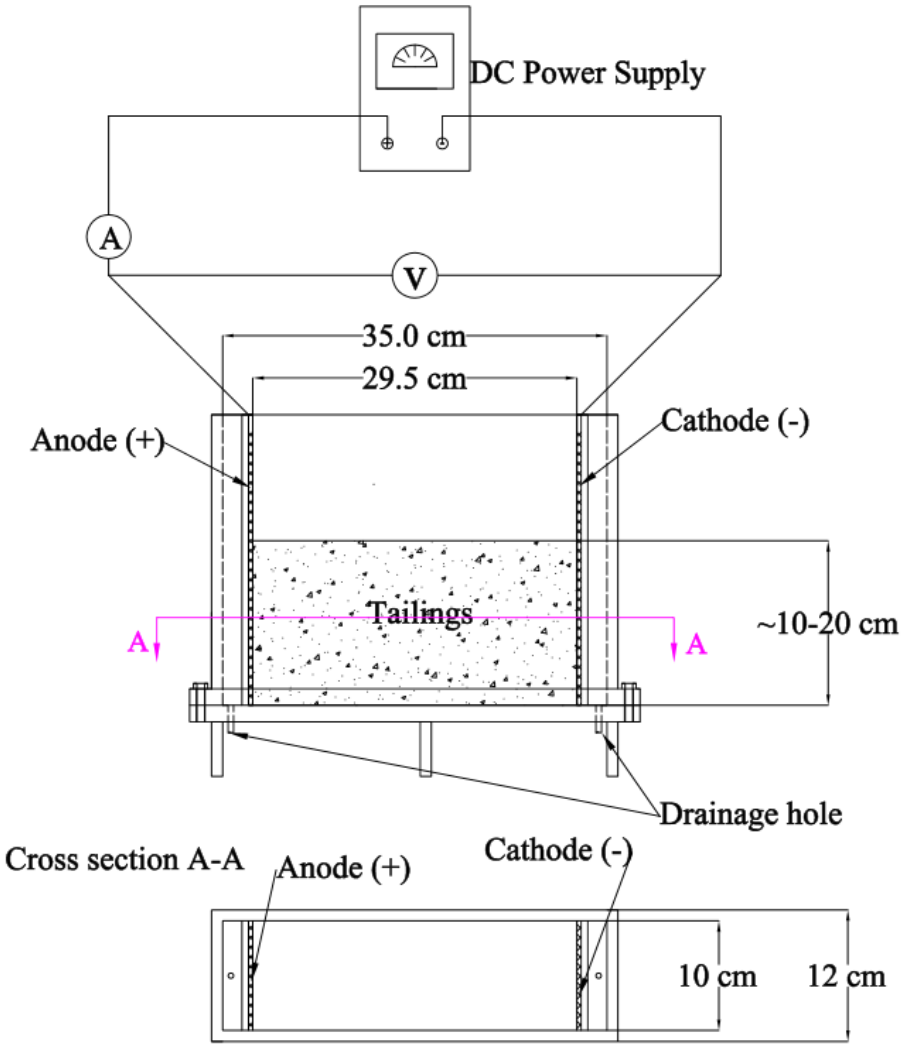

Figure 4.1 Schematic diagram of an EK dewatering cell with vertical installed electrodes

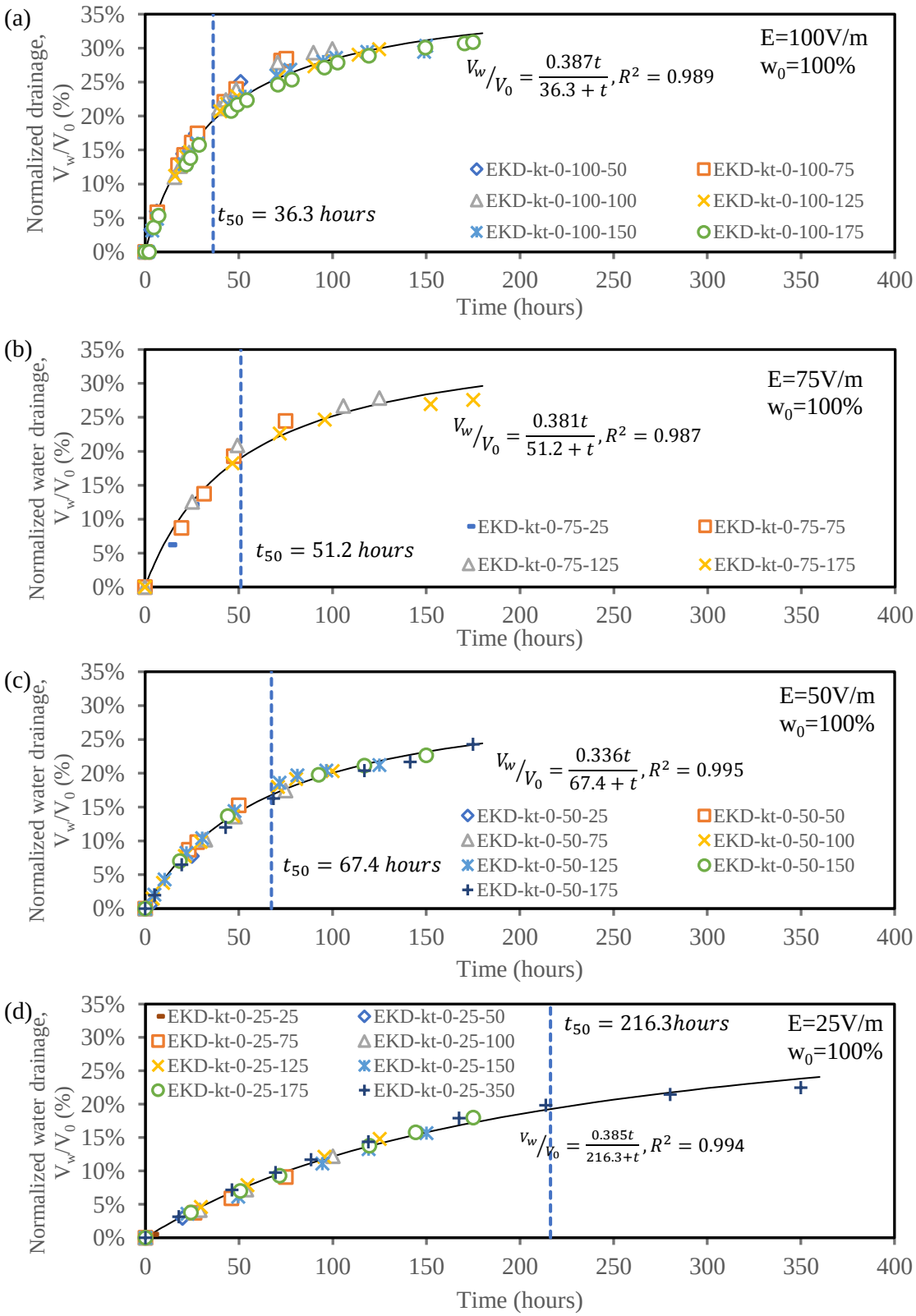

Figure 4.2 Normalized water drainage, V_w/V_0 of Kaolinite slurry for KV series tests (a) KV-100; (b) KV-75; (c) KV-50; (d) KV-25.

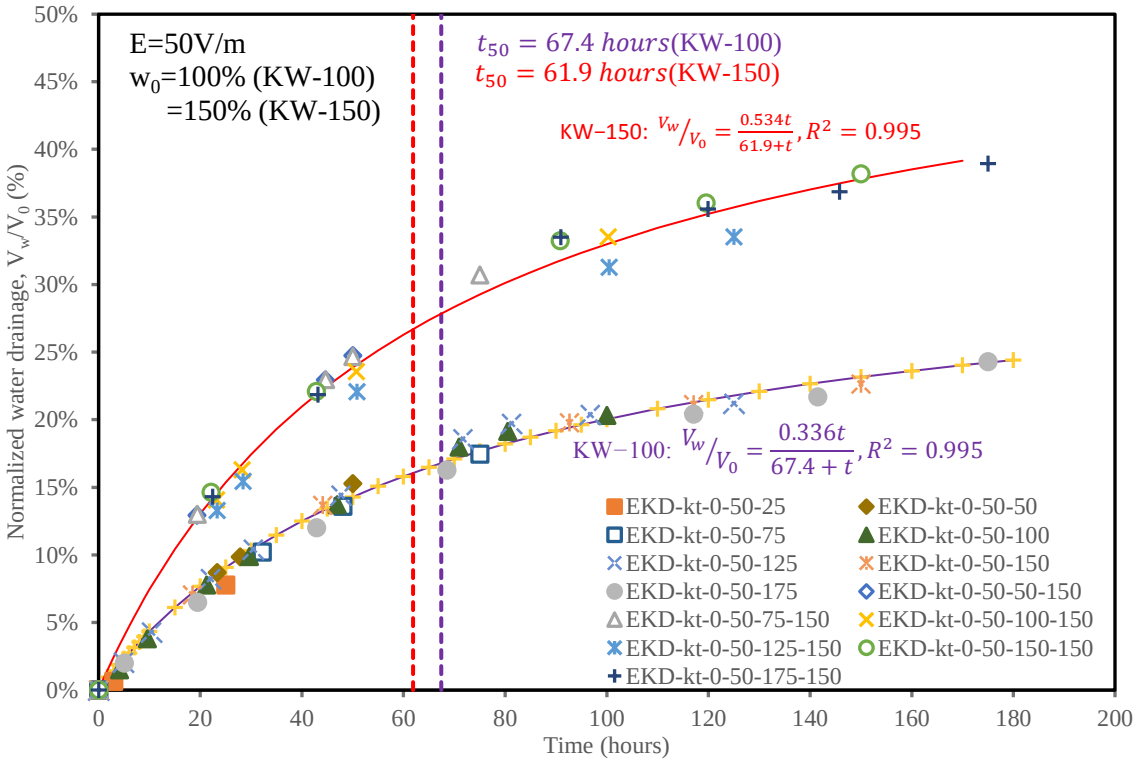

Figure 4.3 Normalized water drainage, V_w/V_0 of Kaolinite slurry for KW series tests

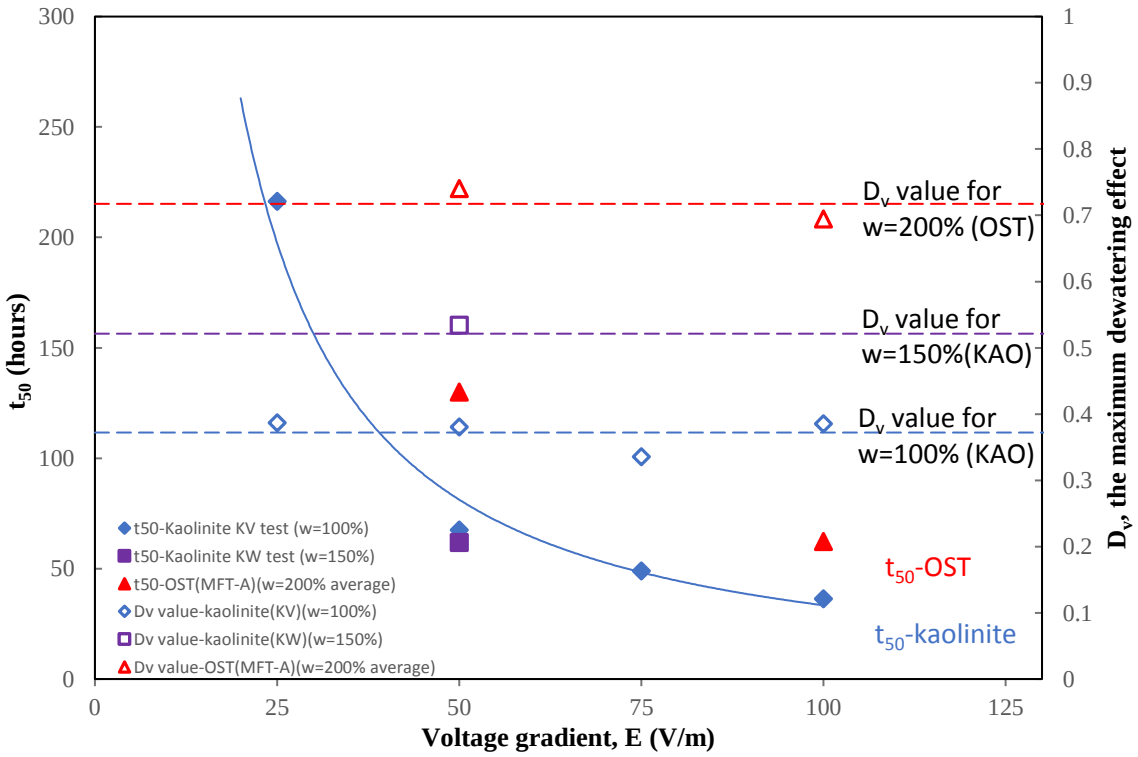

Figure 4.4 Water drainage parameters, t_{50} and D_v versus voltage gradient, E

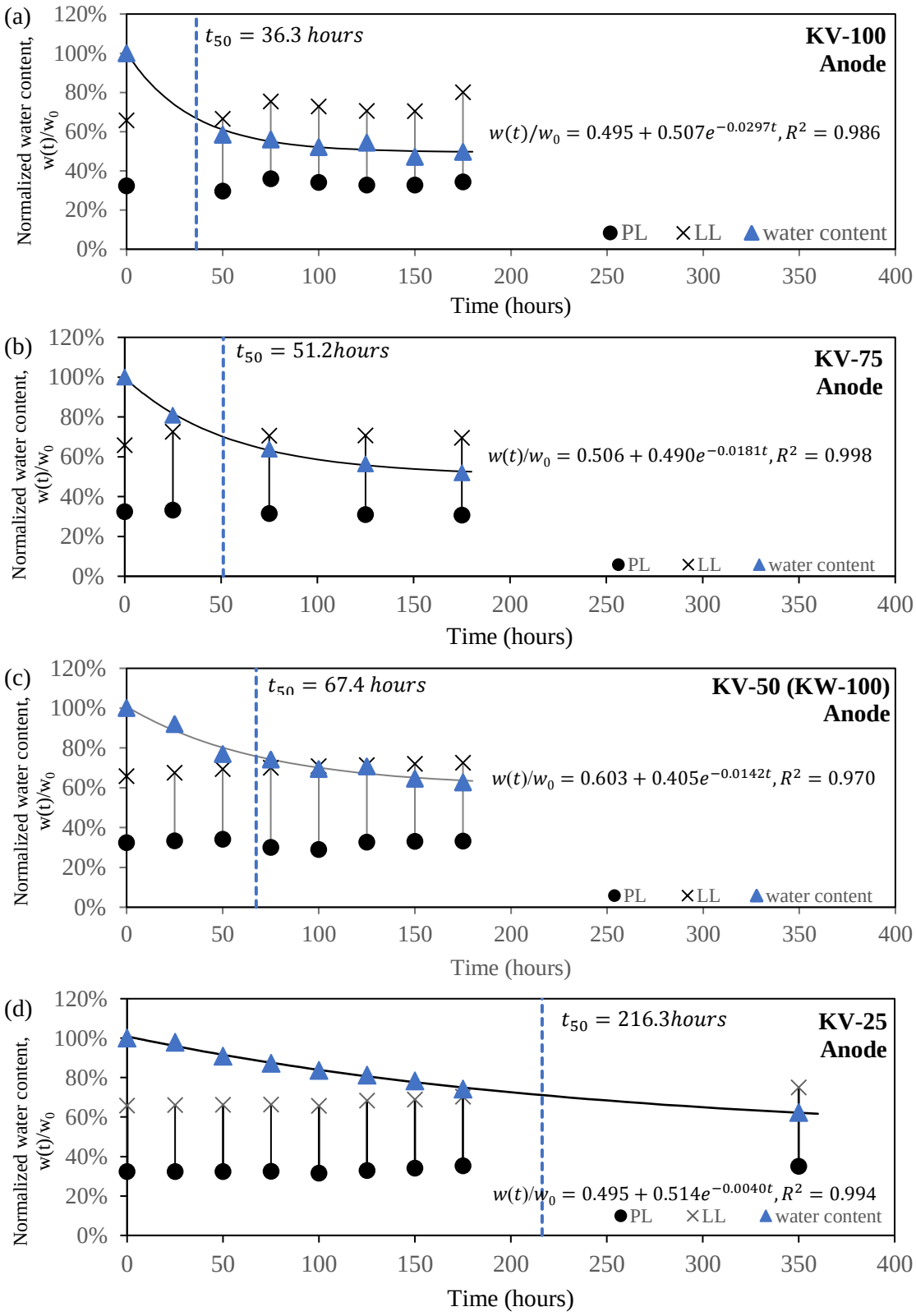

Figure 4.5 Normalized water content, w(t)/w₀, of the kaolinite sample at anode for KV series tests (a) KV-100; (b) KV-75; (c) KV-50; (d) KV-25.

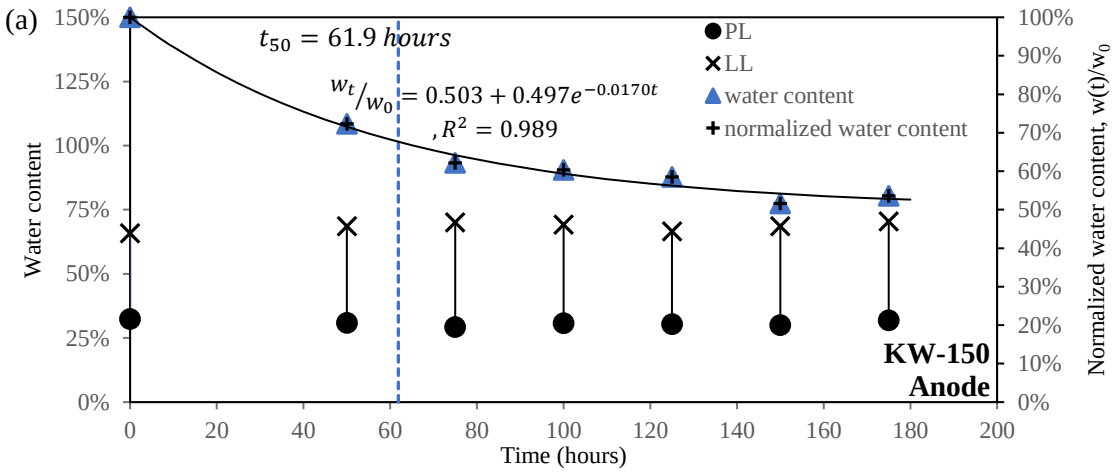

Figure 4.6 Water content reduction of Kaolinite slurry at (a) anode, (b) center, and (c) cathode for test series of KW-150

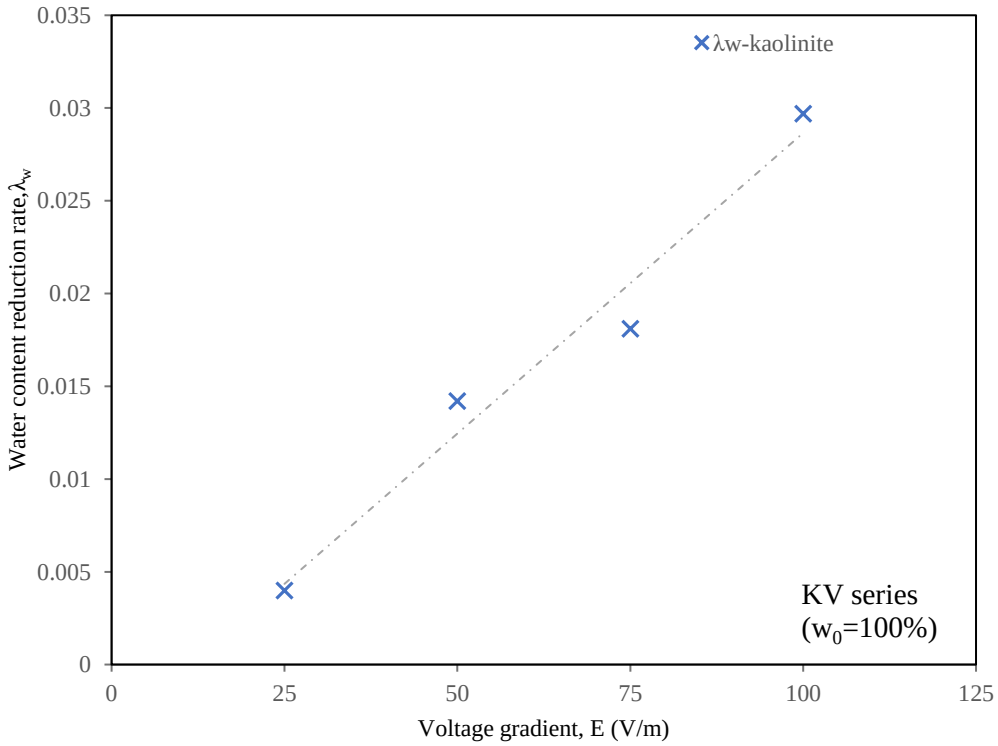

Figure 4.7 Relationship between water content reduction rate, λ_w, and voltage gradient, E

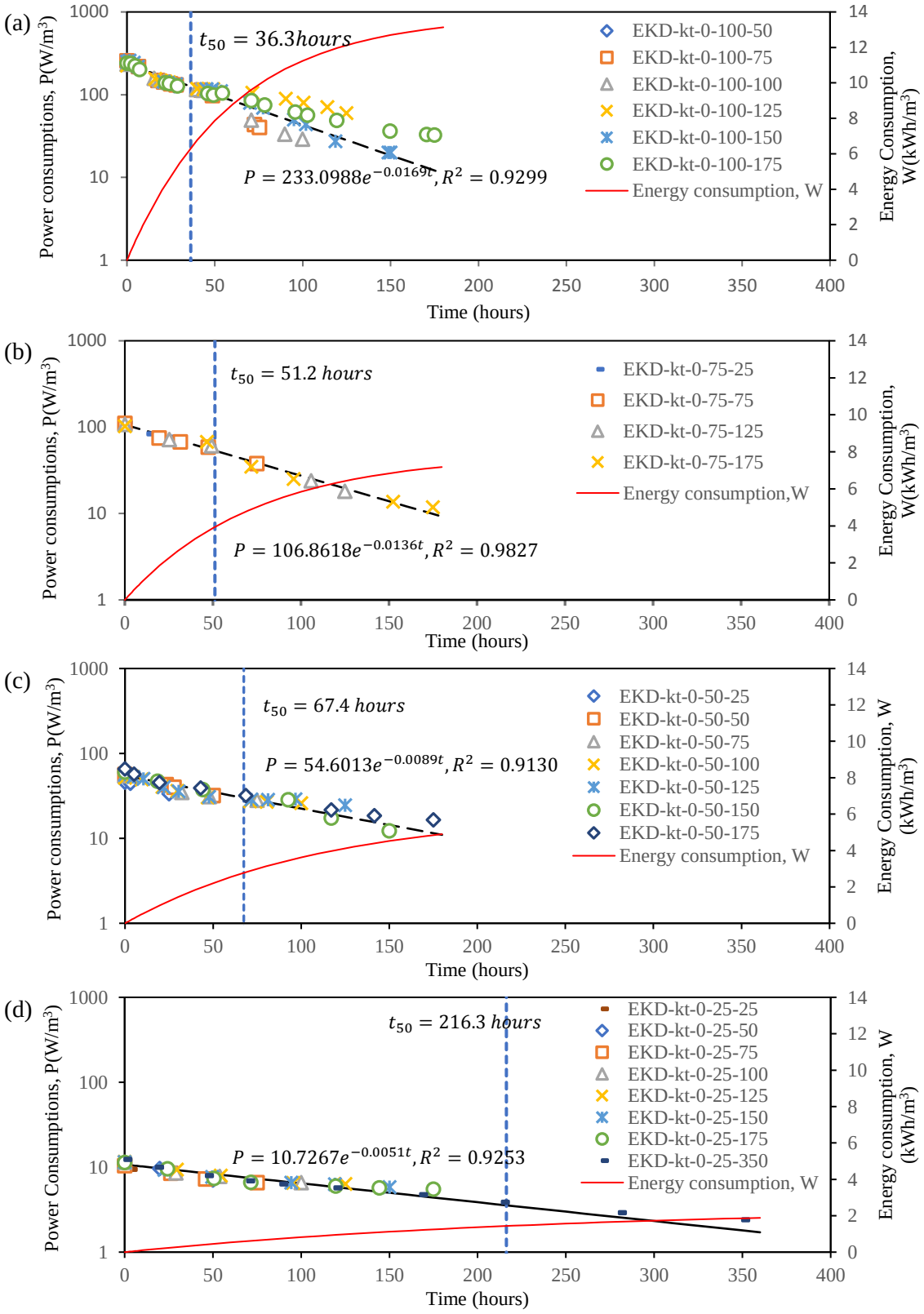

Figure 4.8 Power consumption and accumulated energy consumptions of Kaolinite slurry for KV series tests (a) KV-100; (b) KV-75; (c) KV-50; (d) KV-25

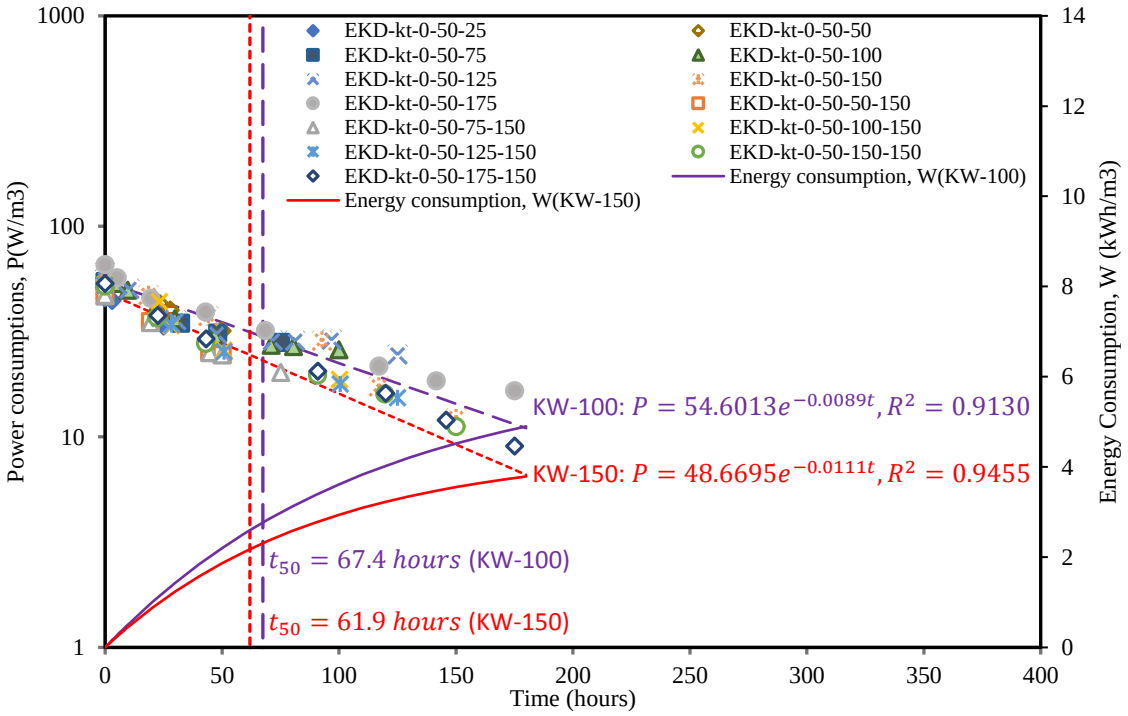

Figure 4.9 Power consumption and accumulated energy consumptions of Kaolinite slurry for KW series tests

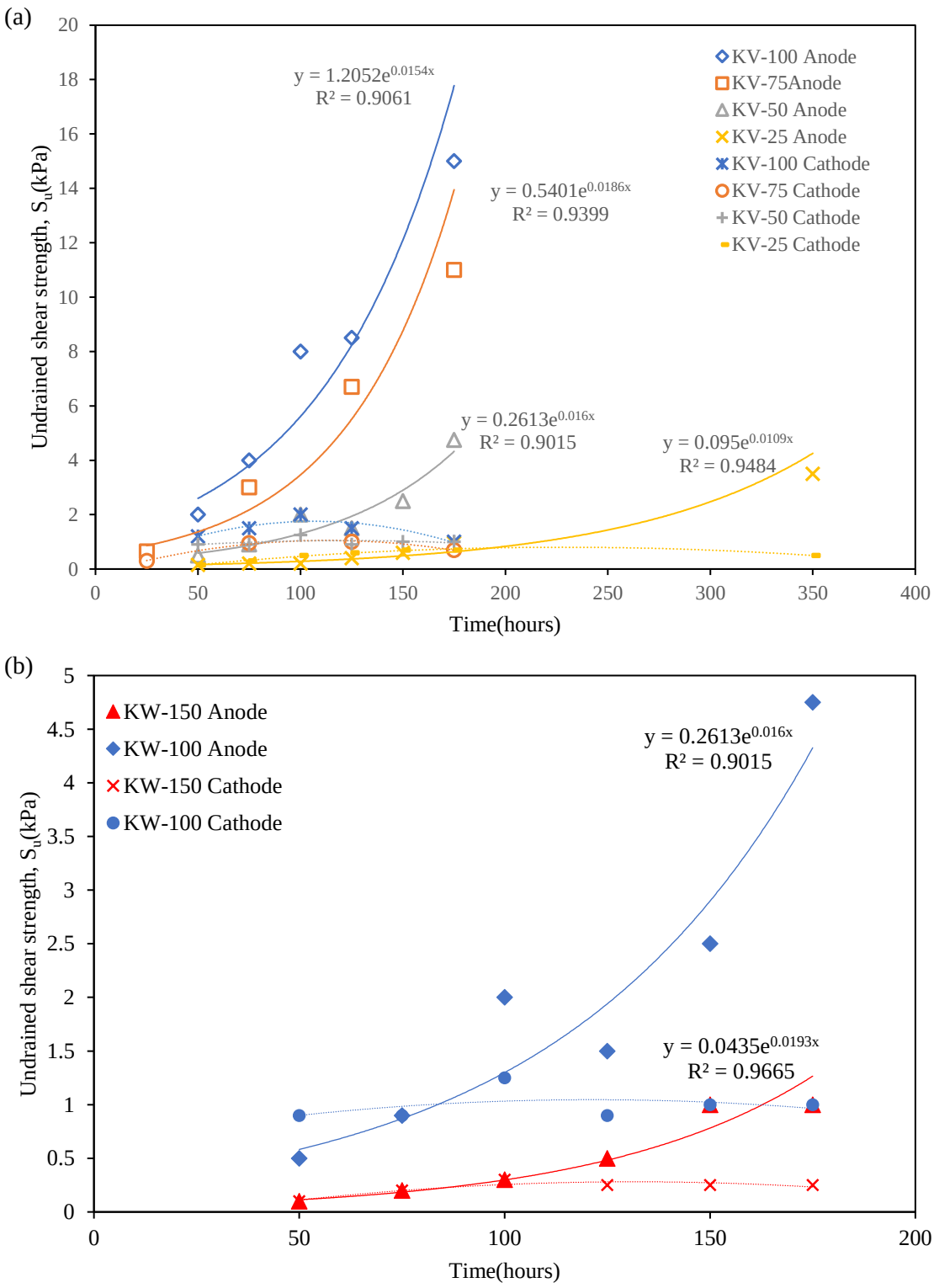

Figure 4.10 Undrained shear strength, S_u versus time for (a) KV series tests, and (b) KW series tests

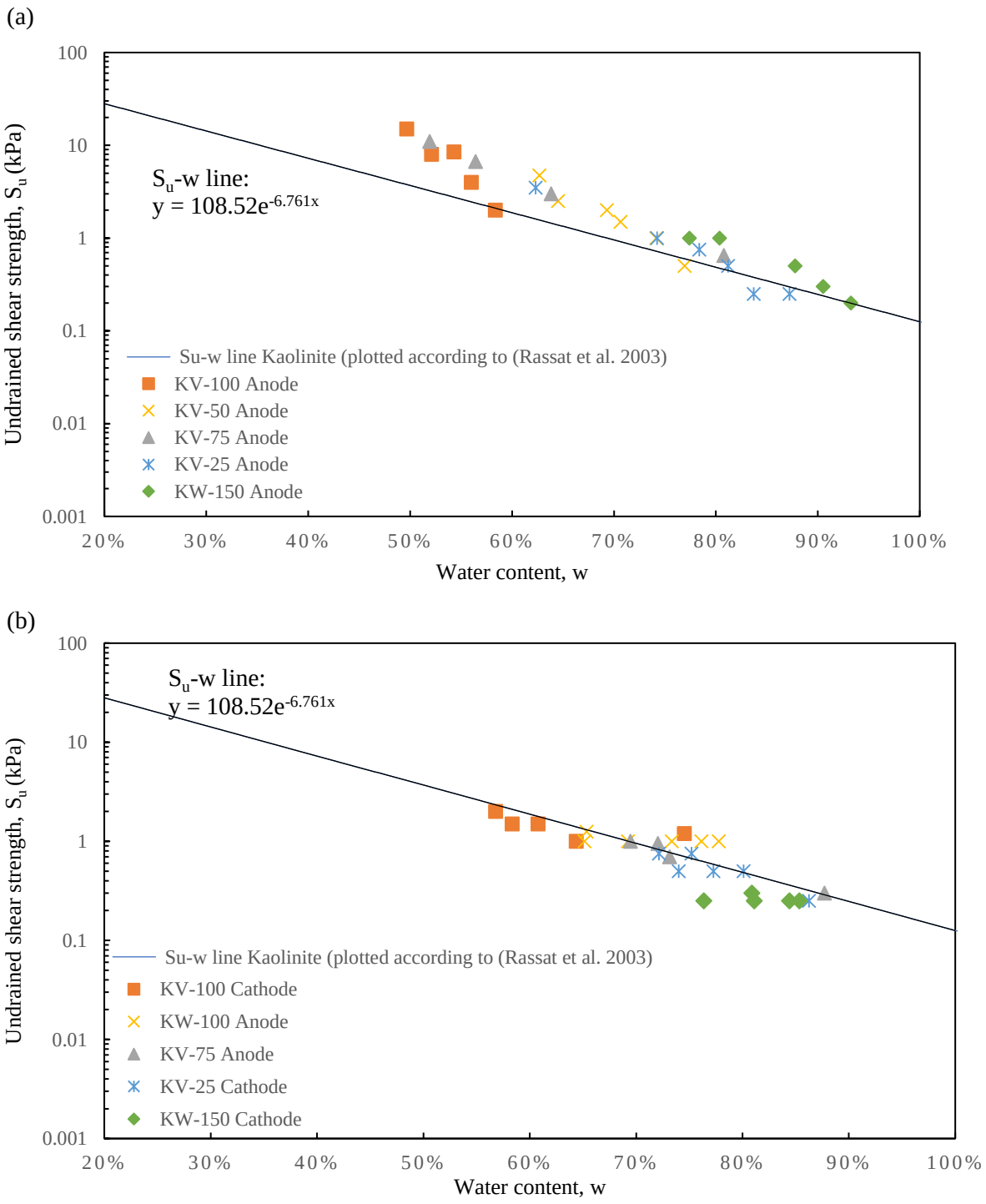

Figure 4.11 Undrained shear strength of the sample at (a) the anode and (b) the cathode plotted against water content for KV series tests

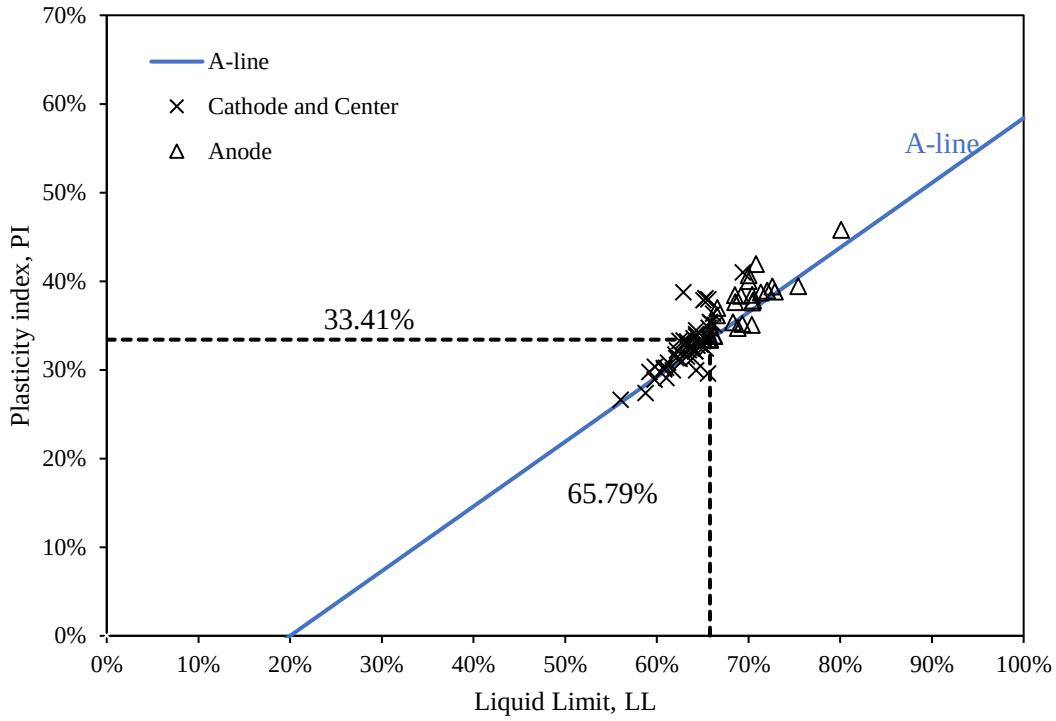

Figure 4.12 Casagrande Plasticity chart

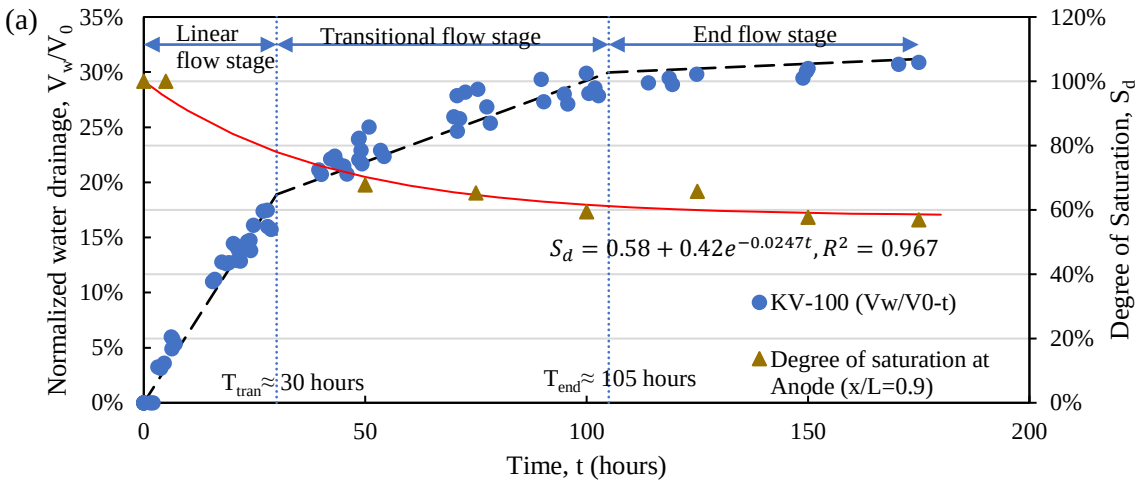
(a)
Linear flow stage
Transitional flow stage
End flow stage
$S_d = 0.58 + 0.42e^{-0.0247t}, R^2 = 0.967$
KV-100 (Vw/V0-t)
Degree of saturation at Anode (x/L=0.9)
T_{tran}≈ 30 hours
T_{end}≈ 105 hours
Normalized water drainage, V_w/V_0
Degree of Saturation, S_d
Time, t (hours)

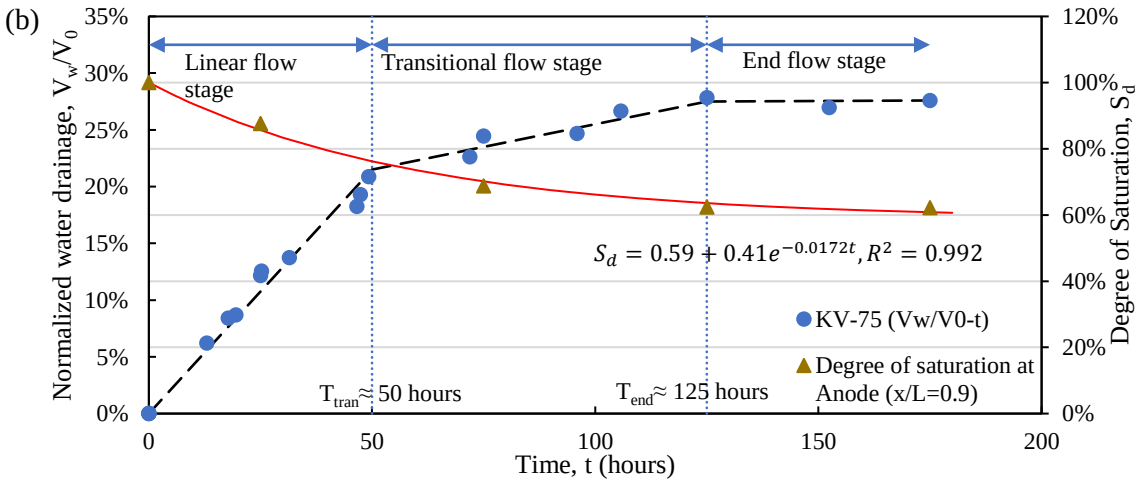
(b)
Linear flow stage
Transitional flow stage
End flow stage
$S_d = 0.59 + 0.41e^{-0.0172t}, R^2 = 0.992$
KV-75 (Vw/V0-t)
Degree of saturation at Anode (x/L=0.9)
T_{tran}≈ 50 hours
T_{end}≈ 125 hours
Normalized water drainage, V_w/V_0
Degree of Saturation, S_d
Time, t (hours)

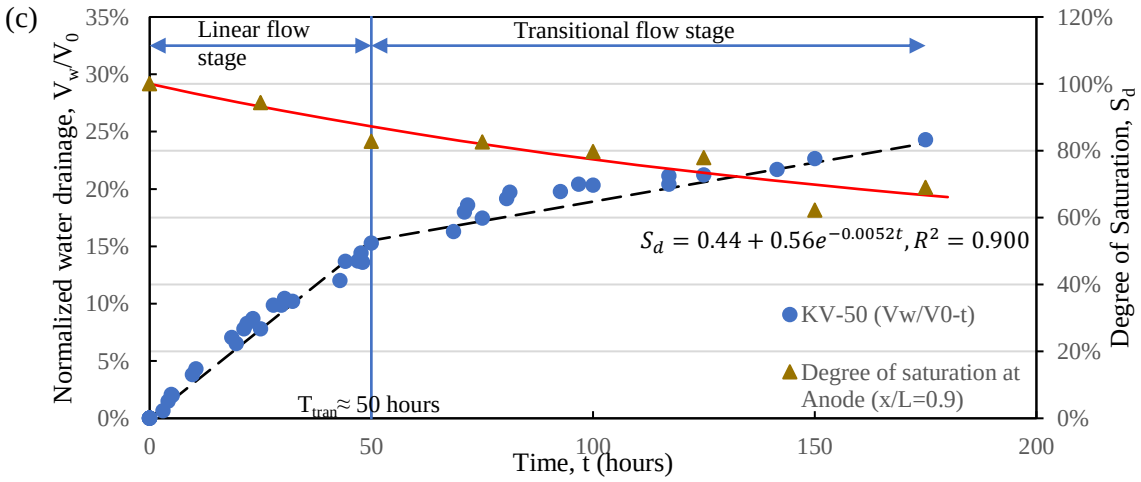
(c)
Linear flow stage
Transitional flow stage
$S_d = 0.44 + 0.56e^{-0.0052t}, R^2 = 0.900$
KV-50 (Vw/V0-t)
Degree of saturation at Anode (x/L=0.9)
T_{tran}≈ 50 hours
Normalized water drainage, V_w/V_0
Degree of Saturation, S_d
Time, t (hours)

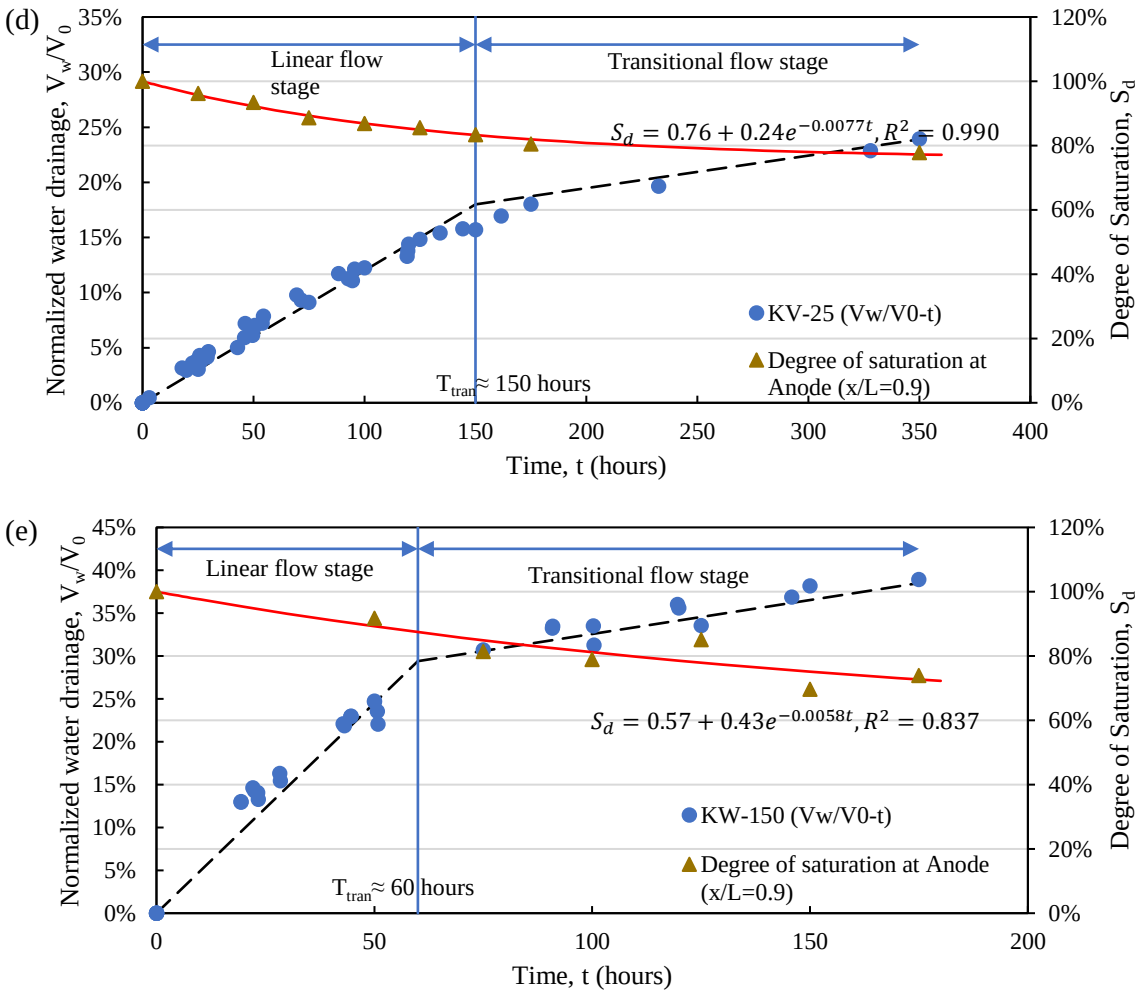

Figure 4.13 The degrees of saturation of the kaolinite at the anode versus time in (a) KV-100, (b) KV-75, (c)KV-50(KW-100), (d) KV-25, and (e) KW-150

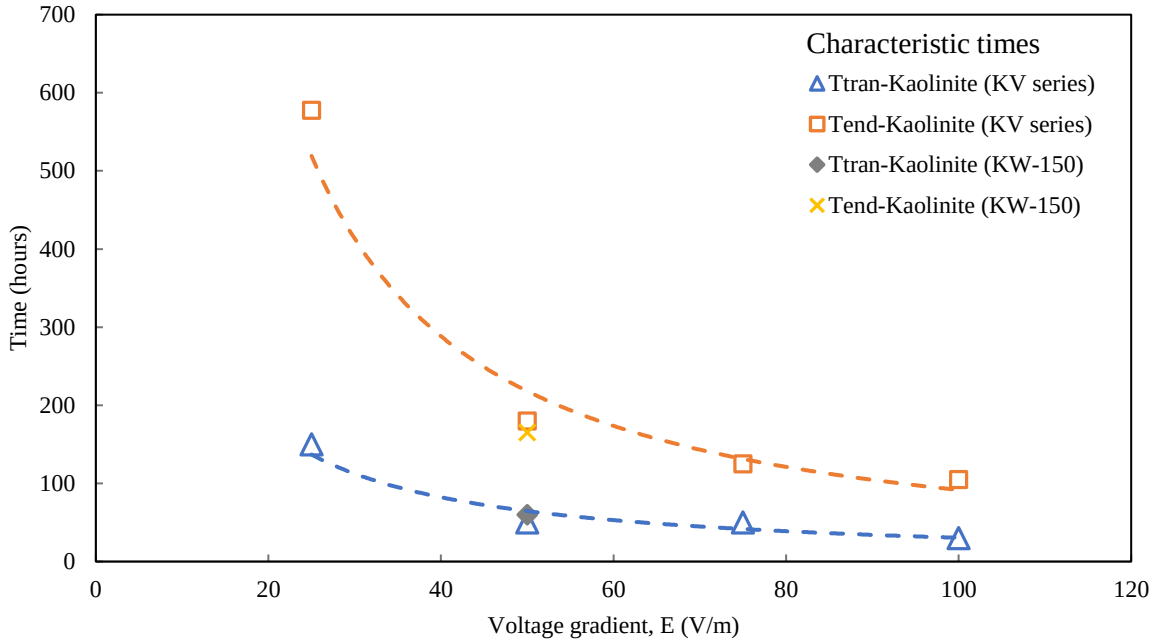

Figure 4.14 Characteristic time T_{tran} and T_{end} vs. voltage gradients, E

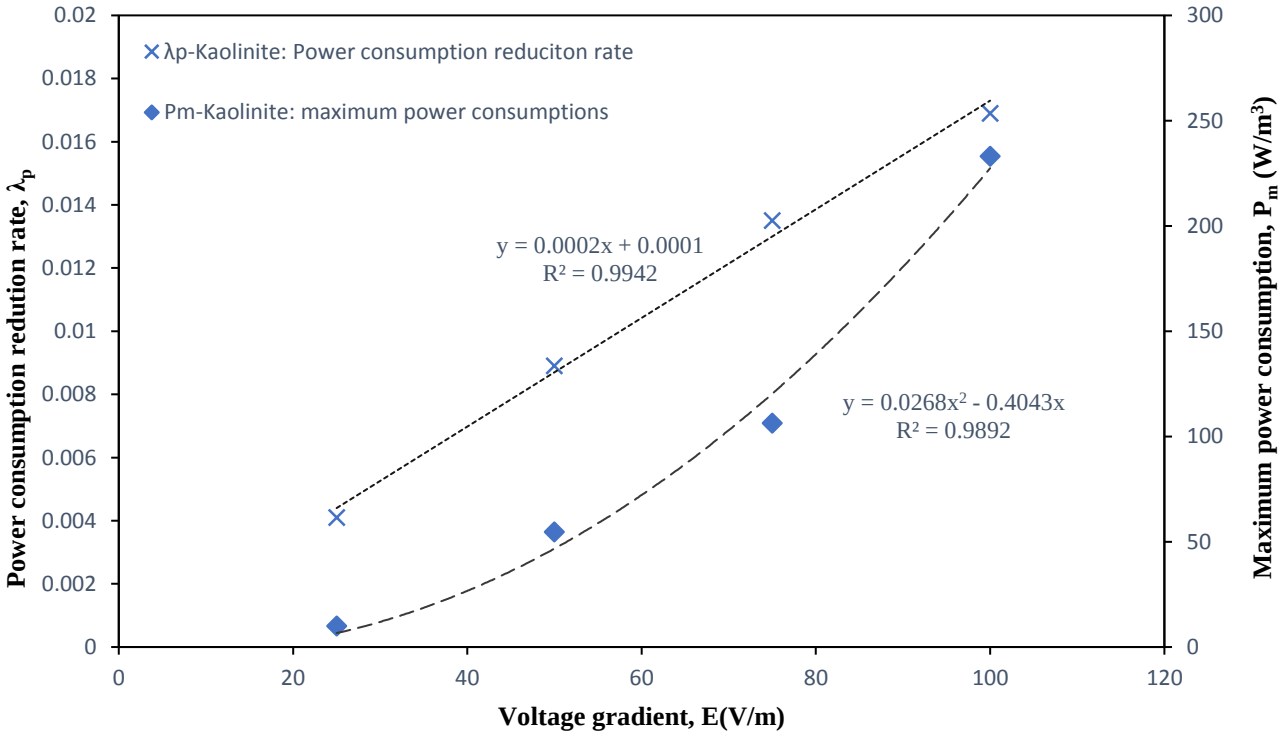

Figure 4.15 Power consumption reduction rate, λ_p and the maximum power consumption, P_m at different voltage gradient, E

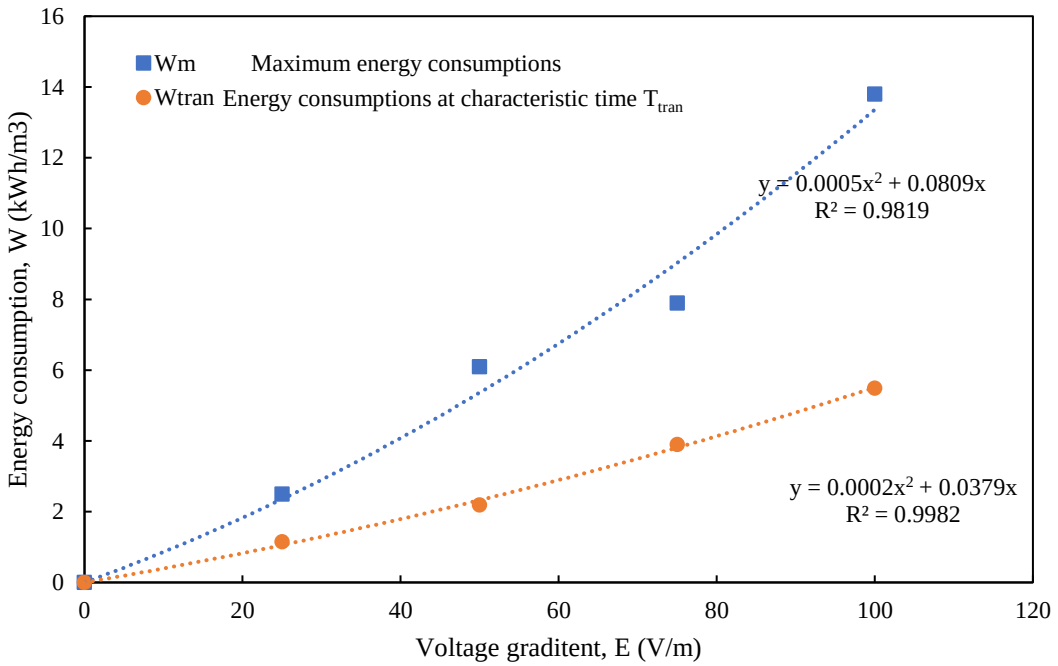

Figure 4.16 Maximum energy consumption, W_m and energy consumption at T_{tran} versus voltage gradient, E (V/m)

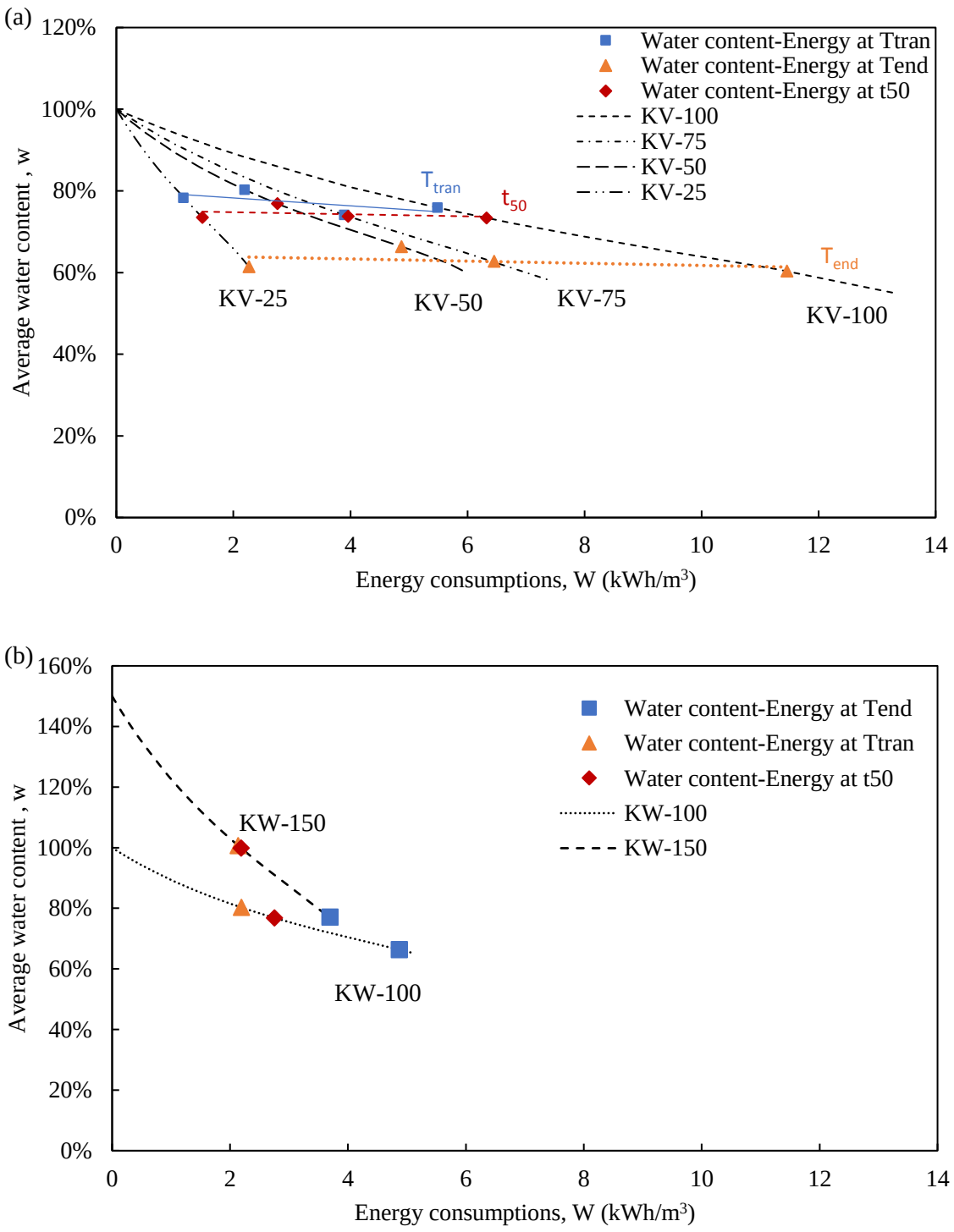

Figure 4.17 Trajectories of average water content, w (%) versus energy consumptions, W (kWh/m^3) of the sample in (a) KV series tests, and (b) KW series tests

Chapter 5 Electrokinetic and chemical treatment of mature fine tailings (MFT) from oil sands processing: dewatering and strengthening

5.1. Introduction

Oil sands deposits in Alberta are the third-largest crude oil reserve in the world. With the oil sands industry development and expansion, large amounts of tailings, which mainly consist of a mixture of residual bitumen, water, quartz sands and clays, are produced during bitumen recovery from oil sands and discharged into surface tailings ponds. The accumulated oil sands tailings end up occupying about 176 km^2 of tailings ponds across the Athabasca oil sands region (Small et al. 2015). Due to environmental issues, such as disturbance of landscape, greenhouse gas emission, ground water contamination, etc., there is a demand to reduce the total amount of tailings and reclaim existing tailings ponds. Mature fine tailings (MFT) or fluid fine tailings (FFT) are formed in tailings ponds after separating from coarse particles and long term sedimentation. MFT, which contain about 70% water and 30% silt and clay size solids, is a major challenge facing oil sands industry because of the difficulty of the consolidation by nature (BGC Engineering 2010). Researches have been devoted to find an effective method to treat oil sands tailings, including coagulation and flocculation (Pourrezaei and El-Din 2008, Sworska and Laskowski 2000, Beier et al. 2103, Islam and Shang 2017), centrifugation (Rima 2013, Sorta 2015), filtration (Xu et al. 2008, Wang et al. 2010), electrokinetics (Guo and Shang 2014, Zhang 2016) etc., but not every technology is commercialized and considered reliable at this stage (Wang et al. 2014).

Electrokinetics (EK) is one of the dewatering techniques for oil sands tailings treatment. It has been studied and used in geotechnical engineering field to treat the soft clays (Casagrande 1959, Bergado et al. 2000, Chew et al. 2004a), marine sediments (Micic et al. 2001, 2002), sensitive clays (Bjerrum et al. 1967, Lo et al. 1991a, 1991b), mine tailings (Fourie et al. 2007, Fourie and Jones, 2010), etc., for many years. Some researches of electrokinetic dewatering (or electrofiltration) have been conducted to dewater oil sands mature fine tailings (MFT) and reported by Guo and Shang (2014), Zhang (2016) and in Chapter 3. During EK dewatering process, the water in oil sands tailings is driven by DC current from the anode and discharged at the cathode. The research performed by Guo and Shang (2014) indicated that EK can accelerate dewatering

rate and improve oil sands tailings. In Chapter 3, the results of EK dewatering tests indicate that EK generated up to 50% volume reduction of oil sands mature fine tailings (MFT). Through these studies, it has been shown that EK can significantly reduce water contents of tailings samples at the anode, but had minor effects at the cathode (Guo and Shang 2014, and Chapter 3). It has also been found that during the EK dewatering, once an unsaturation zone of the sample is generated at the anode, EK dewatering process would stop, thus the dewatering effects is limited at the center and cathode **(**Guo and Shang 2014, Chapter 3). Therefore, further research and development are needed to improve the properties of tailings at the cathode.

Chemical stabilization has been used in geotechnical engineering to strengthen soft soils since early 1960s (Mitchell and Hooper 1961, Mitchell 1976, Saitoh et al. 1985, Hausmann 1990, Bell 1979, 1996, Lorenzo and Bergado, 2004). Cement and lime are two commonly used chemical additives in ground improvement. Hydration reactions, which occur immediately when cement or lime is in contact with soil water, control the early strength gain. The secondary reactions, i.e., soil-cement or soil-lime reactions, are slower and may continue for months (Hausmann 1990). In a recent study by Liu and Shang (2013) the combined electrokienetic and chemical treatment were used to strengthen a marine sediment, in which significant strengthening and shorter treatment time were observed in the experiments.

In this study, the electrokinetic and chemical stabilization are applied on oil sands mature fine tailings (MFT) to evaluate their combined dewatering and strengthening effects. The chemical additives used in this research are quicklime (Carmeuse Lime (Canada) ltd.) and Portland cement (Type HS, Lafarge Canada Inc.). The post treatment evaluation includes the Atterberg limits, undrained shear strength, water content, pH and electrical conductivity of pore water, and zeta potential of tailings particles. The results are compared between chemical treated MFT and original MFT. The effects of chemical additives on EK dewatering are assessed from the comparison between EK combined chemical treatment and EK treatment alone.

5.2. Experiments

The bulk MFT slurry with the natural water content of 165% in average was recovered from Fort McMurray, AB, and used in this study. The geotechnical properties of oil sands tailings are

summarized in Table 5.1 (Guo and Shang 2014). Two series of experiments, i.e., 1). Chemical treatment and 2). EK treatment, were carried out in this research. In the first series of study, quicklime and cement were used as the chemical additives, which were mixed with oil sands tailings (MFT-A) at different mixing ratios (mass ratio of bulk MFT to dry chemical). The water content and Atterberg limits of MFT samples after mixing were measured. In the second series of study, EK dewatering tests were carried out on chemical added MFT to assess the combined effects on oil sands tailings. The detailed experimental design is shown in Table 5.2.

5.2.1. Experimental apparatus

Plastic cylindrical molds were used in the first step of study, as seen in Fig. 5.1. It has an inner diameter of 50 mm and height of 100 mm. An air tight cap was placed on top of the mold during the curing period to prevent evaporation.

The EK dewatering cell, as shown in Fig. 5.2, was used to carry out dewatering tests. The cell has been used in the study presented in Chapter 3 and in previous studies (Mohamedelhasand and Shang 2002, Liu and Shang 2014). The device has a plexiglass tank with dimensions of 350×100×250 mm (Length ×Width × Height). The electrodes are placed at right and left side in the tank. The distance between the anode and cathode is 295 mm. The anode is made of IrO_x coated Titanium mesh, and a stainless-steel S.S. 316 is used as the cathode. The sample is placed between the electrodes. The initial height of the sample was measured before each test. The surcharge load is placed via a loading plate on the top of the sample. The water drainage from both anode and cathode sides is collected and measured via a graduated cylinder.

5.2.2. Quicklime and Portland cement treatment

Quicklime (Carmeuse Lime (Canada) Ltd.) and Portland cement (Type HS, Lafarge Canada Inc.) were added to bulk oil sands tailings slurry at different mixing ratios, defined as the ratio of the mass of bulk tailings to the dry mass of chemical additives. The water content of oil sands tailings was measured before the tests. In this study, the mixing ratios of quicklime and MFT (MFT: QL) were 9.5:0.5, 9:1, 8.5:1.5, and 8:2, corresponding to the quicklime content of 5%, 10%, 15%, and 20%. The mixing ratios of Portland cement treated MFT were 9.9:0.1, 9.5:0.5, and 9:1, which are 1%, 5% and 10% in terms of cement content.

Chemical additives were pulverized prior to mixing with tailings. The chemical and tailings were stirred thoroughly in a mixer, transferred into nine molds, and cured in the capped molds under the room temperature for 0, 7, 14 and 28 days, with the triplicate for each curing time. The water content (ASTM D2166-10; ASTM 2010a) and Atterberg limits (ASTM D4318-10e1; ASTM 2010b) after the specific curing period were measured.

5.2.3. EK cell tests

The mixtures of MFT and chemicals (quicklime or cement) at the mixing ratios 9:1 (10% chemical content) and 9.9:0.1 (1% chemical content) were selected for EK cell tests. The samples were mixed thoroughly in a mixer and then poured into two EK dewatering cells (Fig. 5.2). A geotextile sheet was placed on top of the sample as the top drainage. The electrodes were covered with filter papers and geotextiles for filtration and separation. A surcharge loading was added gradually to reach 5 kPa in 48 hours and sustained during the EK cell test. In one cell, a DC current was applied under a voltage gradient of 50V/m for 120 hours after 48 hours consolidation under 5 kPa surcharge. The volume of water drainage, voltage, and current were recorded during the testing period. The second EK cell was used as a control without application of DC current. The total volume of water drainage, undrained shear strength and water content were measured after 7 days on samples in both cells. The undrained shear strength was measured via a laboratory vane shear tester. The vane shear tester has the smallest division on the dial of 1 kPa and visual interpretation of about 0.25 kPa. The EK cell test conditions were summarized in Table 5.3.

5.3. Results and Discussion

5.3.1. Chemical treatment of oil sands tailings

5.3.1.1. Water content and mixing ratio

Results of water content of chemical treated MFT are summarized in Table 5.4. The original MFT sample has an average water content of 165% (38% in solid content). Fig. 5.3 shows the average water content of the chemical treated MFT sample at different curing time. It is noted that the water content of MFT reduced immediately after adding quicklime or cement (0 day) due to hydration reactions, and then remained nearly constant for the rest of curing period. According to

Fig. 5.3a, for the quicklime content of 5%, 10%, 15% and 20%, the average water contents of quicklime treated MFT were 142%, 119%, 83% and 68%, respectively, corresponding to a solid content of 41%, 46%, 55%, and 60%. For cement treated MFT samples, the average water contents were 155%, 135% and 114%, for the cement content of 1%, 5% and 10%, respectively, as seen in Fig. 5.3b and Table 5.4. The corresponding solid contents were 39%, 43% and 47%. The average water contents of chemical treated tailings are plotted against the percentage of chemical additives in Fig. 5.4. The post-treatment water content of the sample is proportional to the percentage of chemical additives. The cement treated MFT samples had slightly lower water contents than those treated with quicklime. For example, the post-treatment water content of MFT sample with 5% of cement (the mixing ratio of 9.5:0.5) was 142%, while the water content of quicklime treated MFT sample was 135% at the same mixing ratio. For mixing ratio of 9:1 (10% of chemical additives in bulk sample), the water content of treated MFT were 114% and 119% for cement and quicklime, respectively.

5.3.1.2. Atterberg limits

The Atterberg limits of chemical treated samples were measured at each curing time and are listed in Table 5.5 and plotted in Figs. 5.5 and 5.6 for quicklime or cement treated MFT, respectively.

The original MFT has the liquid limit of 51.6% and the plastic limit of 29.1%. From Fig. 5.5 it is noted that both liquid limit and plastic limit of MFT were increased after adding quicklime. The plastic limit of quicklime treated MFT samples increased to about 50% in average. The increase in the plastic limit of MFT is not significantly affected by quicklime content from 5% to 20%, and curing time, as seen in Fig.5.5. In contrast, the increase in the liquid limit of quicklime treated MFT is related to both the mixing ratio and curing time. For example, at the highest mixing ratio of 8:2 (20% quicklime content) in this study, the liquid limit of quicklime treated MFT at 7 days was 84.9% and further increased to 93% after 28 days curing (Fig. 5.5a). In contrast, the liquid limit was 98.4% at 7 days and increased to 111.6% after curing for 28 days for the 5% quicklime treated MFT sample (Fig. 5.5d). It is noted that the more significant increase in liquid limit was observed at lower quicklime content.

Fig. 5.6 presents the changes of the Atterberg limits of cement treated MFT. The plastic limit of treated MFT increased with the increase of mixing ratio and curing time. At the lowest mixing

ratio of 9.9:0.1, the plastic limit of cement treated MFT was 24% at 7 days and slightly rose to 28% after 14 days curing (Fig. 5.6 c). At the mixing ratio of 9:1, the plastic limit of treated MFT was 40% at 7 days, and further increased to 56% at 28 days (Fig. 5.6a). The results of liquid limit of treated MFT shows the similar trend. The liquid limits of treated MFT were 90.3%, 104.9%, and 114.3% at 7 days at cement content of 1%, 5%, and 10% and 9:1, respectively, and further increased to 100.8%, 125.7% and 122.0% after 14 days.

In general, both the liquid limit and the plastic limit increased after adding quicklime or cement. Specifically, for quicklime treated MFT, the increase of plastic limit was not significantly affected by mixing ratio and curing time, and the increase of the liquid limit was more at lower quicklime content. For cement treated MFT, both plastic and liquid limits increased with the increase in the mixing ratio and curing time.

In conclusion, for the treatment of cement or quicklime only, the post-treated water content of the sample is proportional to the percentage of chemical additives. For cement treated MFT samples, the water contents were observed lower than those treated with quicklime at the same mixing ratio. The Atterberg limits of the sample increased after adding the chemical additives. For quicklime treated MFT, the increase in plastic limit was not affected by percentage of quicklime and curing time, but the more significant increase in liquid limit was observed at the lower percentage of quicklime. In contrast, both plastic and liquid limit increased with the increase in the cement percentage and curing time, for cement treated MFT samples.

5.3.2. EK combined with chemical treatment

Figs. 5.7 and 5.8 present the results of EK dewatering tests of MFT with quicklime or cement added, respectively. The volume of water drainage during EK treatment for quicklime or cement treated MFT are plotted in Figs. 5.7a and 5.8a. For a better comparison, the normalized water drainage, V_w/V_0, where V_w is the volume of water drainage and V_0 is the initial volume of bulk sample, is presented in Figs. 5.7b and 5.8b. The normalized water drainage also indicates the volume reduction of the sample due to dewatering. The results of EK combined with chemical additives are compared with those obtained in two controlled experiments, including chemical treated MFT dewatering under a surcharge of 5 kPa and the treatment of EK alone on untreated MFT, to reveal the effects of chemical additives on EK dewatering.

The total water drainage for chemical treated MFT under the consolidation of 5 kPa surcharge only was measured at the end of 7 days for the first control tests (C-QL and C-CM series tests). In the second control test (EK-0-50-125) with EK dewatering only, there was no surcharge loading on top to the sample.

The dewatering results for quicklime treated MFT sample are shown in Fig. 5.7 for the mixing ratio of 9:1 (10% quicklime) and 9.9:0.1 (1% quicklime). As shown in Fig. 5.7a, at the high quicklime content (10% quicklime), the volume of water drainage was 70 ml after 7 days consolidation under 5 kPa surcharge alone in the first control test (Test: C-QL-5-0-10). The normalized water drainage, V_w/V_0, which reflects the volume reduction of the sample due to dewatering, was 1.8%, as seen in Fig. 5.7b. With the combined treatment of EK and quicklime, the volume of water drainage reached 93ml, corresponding to the normalized volume change, V_w/V_0, of 2.34% (Test: EK+QL-5-50-10). For the sample with low quicklime content (1%), the water drainage was larger than those with high quicklime content (10%). The volume of water drainage was 104ml after 5kPa consolidation in the first control test (Test: C-QL-5-0-1), and it was 257ml observed in EK combined treatment (Test: EK+QL-5-50-1). The corresponding normalized water drainage, V_w/V_0, was 4.2% and 10.25% in the test with 5 kPa consolidation only and EK treatment, respectively. On the other hand, the largest volume reduction, i.e., 30%, of the MFT sample was observed in the second controlled test (Test: EK-0-50-125), i.e., the EK dewatering on original MFT without adding chemicals (0% quicklime).

Similar results were observed in dewatering tests of cement treated MFT. Fig. 5.8 shows results of EK dewatering on MFT samples with cement added. As shown in Fig. 5.8a, at the high cement content (10% cement), the water drainage under 5 kPa surcharge was 334ml, corresponding to the normalized water drainage of 9.9% (Test: C-CM-5-0-10), as seen in Fig. 5.8b. Based on Fig. 5.8b, EK dewatering flow was completely eliminated after adding 10% cement into MFT. The normalized water drainage obtained in EK dewatering was 9.9% (Test: EK+CM-5-50-10), the same as was obtained in the control test. Similar with the experiments on quicklime treated MFT, at the lower cement content (1%), EK treatment generated more water drainage. As seen in Fig. 5.8b, the normalized water drainage was 9.3% (354ml in Test: C-CM-5-0-1), and it increased to about 25% (1428ml) in the EK combined treatment (EK+CM-5-50-1). On the other hand, EK treatment alone (Test: EK-0-50-125) can achieve more volume reduction (about 30%) in 125 hours.

As evidenced from experiments, the quicklime or cement reduced the EK generated water flow in MFT samples, thus reduced dewatering effects. The EK flow is inversely related to the chemical dosage.

Above observations can be further verified from water contents of MFT after tests. Table 5.6 summarizes the water contents of MFT samples after the EK dewatering tests. When the chemical content (10% chemical additives) was high, the water contents at the end of controlled test were 114% and 96% for quicklime or cement treated MFT sample, respectively. After EK dewatering tests, the water contents were similar or even higher than those without EK treatment. As seen in Table 5.6, the water contents were 112% and 114% at the anode and cathode, respectively, for quicklime treated MFT samples. The corresponding water content reductions of the sample due to EK are 1.8% at the anode and 0% closed to the cathode. Similarly, for the cement treated MFT, the water contents were 99% and 101% at the vicinity of anode and cathode, respectively. Compared with the water content obtained in control tests, the water content reductions of the cement treated sample due to EK are -2.7% and -4.7% at the anode and cathode, respectively. The results indicate that the EK dewatering effect had been eliminated by adding high percentage of chemical additives.

The EK treatment had better effect at low chemical content (1% chemical additives) in terms of water content reduction. The water contents obtained in control tests were 136% and 129% for quicklime and cement treated MFT, respectively, as seen in Table 5.6. With the EK treatment, the water contents of the sample decreased to 121% and 124% at the anode and cathode, respectively, after adding quicklime, from the original water content of 154%. For the cement treated MFT sample, the water content was 88% at the anode and 116% at the cathode with the EK treatment. On the other hand, without chemical added, the final water content of MFT after EK dewatering test reached 50% at the anode and 171% at the cathode. It is concluded that EK treatment alone can significantly reduce the water content of the sample at the anode but have minor effects on the sample at the cathode for oil sands tailings.

The results of MFT water content after dewatering treatment are plotted in Fig. 5.9. A significant difference of MFT water content between the anode and cathode side was observed in test EK-0-50-125, which is the EK treatment on original MFT under 50V/m without surcharge and chemical

additives. The water content of treated MFT at the anode was 50%, while the water content of MFT at the cathode was 171%, which is over three times of its liquid limit (51.6%). However, the water content of treated MFT was almost the same at the anode and cathode after tests with chemical additives of quicklime or cement. For example, the water contents of the sample at the anode and cathode were 99% and 101% in Test: EK+CM-5-50-10, 121% and 124% in Test: EK+QL-5-50-1, and 112% and 114% in Test: EK+QL-5-50-10. When the dosage of cement was low, i.e., in EK+CM-5-50-1 (1% cement), a difference in water content of MFT at the anode and cathode was still observed (88% and 116% at the anode and cathode, respectively) but not as significant as in the EK dewatering test with original MFT (EK-0-50-125). After EK treatment on original MFT, the sample at the cathode remained slurry and cannot sustain any load on top due to the high water content of 171%. The tailings at the cathode, therefore, need further treatment to reduce the water content. The difference of water content reduced by adding a low percentage of chemical. Then the sample can sustain a surcharge loading of 5 kPa without inducing any failure, although the final water content was not as low as 50% observed at the anode in EK treatment with original MFT (EK-0-50-125).

Based on the results, it can be noticed that the EK treatment alone has a significant dewatering effects at the anode and no effect at the vicinity of the cathode for oil sands tailings. The water content of MFT without chemical additives after EK treatment had a significant difference between the vicinity of anode and cathode. With the chemical treatment, MFT had more uniform water content distribution from the anode to cathode. But, generally, the chemical treatment with quicklime or cement reduced the EK dewatering flow. Also from these results, it is noted that the high chemical percentage leads to the low volume reduction of MFT after dewatering tests.

It is also known that the chemical treatment with quicklime or cement will generate the cementation, which contributes to the strength increase, in MFT. Therefore, the results of the undrained shear strength will be discussed in the next section for the samples after EK combined with chemical treatment.

5.3.3. Undrained shear strength and plasticity

5.3.3.1. Undrained shear strength

The undrained shear strength of treated MFT sample was measured via a laboratory vane shear tester after dewatering tests and the results are listed in Table 5.7.

For quicklime treated MFT, the undrained shear strength of the sample increased to 1.5 kPa and 2 kPa at the quicklime content of 10% and 1%, after 7 days consolidation in controlled experiment. After the EK treatment, the undrained shear strength of the sample slightly increased to 2.5 kPa at the anode and 2 kPa at the cathode at high quicklime content (10% quicklime in Test: EK+QL-5-50-10). For the lower quicklime dosage (1% quicklime in Test: EK+QL-5-50-1), a higher undrained shear strength was observed after EK treatment. The undrained shear strength of the sample reached 3.5 kPa at the vicinity of anode and 2.25 kPa at the cathode.

At the high chemical content (10%), the cement treated MFT sample (Test: C-CM-5-0-10) achieved higher strength than quicklime treated sample (Test: C-QL-5-0-10). After 7days consolidation, the undrained shear strength of the sample in Test: C-CM-5-0-10 was 5 kPa. With the EK treatment, the undrained shear strength increased to 9.25 kPa at the anode and 7.5 kPa at the cathode (10% in EK+CM-5-50-10). On the other hand, at low cement content (1%), the cement treated MFT reached 1 kPa after 7 days. After the EK treatment at the low cement content (1% in EK+CM-5-50-1), the undrained shear strength increased significantly from 1kPa to 7 kPa at the anode, and slightly from 1kPa to 1.25kPa at the cathode.

In conclusion, the shear strength gain of cement treated MFT is more significant than quicklime treated MFT. EK treatment can further increase the shear strength of chemical treated MFT samples, mainly by dewatering, at low chemical dosage.

The results of undrained shear strength of quicklime or cement treated MFT are plotted in Fig. 5.10, with the relationship between undrained shear strength and water content (S_u-w line). As shown the chemical treated MFT samples are located above the trend line, which represents the relationship between the water content and shear strength of original MFT samples. This indicates that, at the same water content, the chemical treatment generated strength gain. After chemical treatment, the sample had a shear strength over 1 kPa at the water contents ranged from 110% to 140%, with a low dosage of chemical, as seen in the results of control tests C-QL-5-0-1 and C-CM-5-0-1. The strength of samples after EK combined with chemical treatment further increased, compared with the control samples. Based on Fig. 5.10, the quicklime treated MFT had the shear

strength about 2-4 kPa, not significantly affected by the dosage of quicklime. On the other hand, the undrained shear strength of the cement treated samples was strongly affected by the cement dosage. It can be seen that the undrained shear strength was 5 kPa in control test (C-CM-0-10) and further increased to about 7.5 to 9 kPa with EK treatment at the high cement content of 10%. In contrast at low cement content of 1%, the undrained shear strength was 1 kPa in the control test and further increased to 1 to 7 kPa after EK treatment.

The sample after EK treatment alone had a significant undrained shear strength gain, up to 50 kPa at the anode. At the cathode, the shear strength of samples remained virtually zero after EK treatment. Compared with chemical treated samples, the EK treatment on original tailings without adding chemical generated more significant differences in undrained shear strength of samples between the anode and cathode than those with chemical additives.

Based on the results in Section 5.3.2 and 5.3.3, it is concluded that the EK treatment alone will reduce the water content and increase the undrained shear strength of MFT sample only at the anode. In the treatment at low chemical dosage combined with EK, the strengthening effects are attributed to both chemical grouting and EK dewatering. At the high chemical dosage, the strengthening effects are dominant by chemical grouting and the effect of EK dewatering is negligible. It is also observed that between quicklime and Portland cement, low cement dosage plus EK treatment is more effective, which generated higher undrained shear strength. The advantage of low cement dosage is to enhance strength gain at the cathode and reduce the difference of water content and shear strength between anode and cathode. Thus, it may be a good approach for EK strengthening and dewatering of MFT by adding small percentage of chemical at the cathode.

5.3.3.2. Plasticity

The results of Atterberg limits of the treated tailings are plotted in the Casagrande plasticity chart, as seen in Fig. 5.11. The point of original tailings is just slightly below the A-line, classifying the original tailings as an elastic silt (MH) in the Unite Soil Classification System (USCS). After treatment, the liquid limit of all samples increased. For the cement treated MFT samples, the points moved above the A-line (CH), indicating the increase in plasticity. For the quicklime treated MFT samples, all points shifted below the A-line (MH), indicating a decrease in plasticity. As seen in

Table 5.5, the quicklime induced more increase in plastic limit and less increase in liquid limit of MFT sample than cement. Therefore, the plasticity of cement treated MFT is observed higher than those treated with quicklime.

5.3.4. Porewater chemistry and particle zeta potential

The porewater pH and electrical conductivity (EC) of chemical treated MFT were measured after 7 days consolidation in controlled tests for both high (10%) and low (1%) chemical content. The results are shown in Fig. 5.12. The pH and EC of original MFT porewater were 8.8 and 3.59 mS/cm. The pH and EC were increased with the chemical dosage. The quicklime induced more increase in pH and EC than cement. For example, at chemical content 10% the pH and EC of the porewater were 12.8 and 32.4 mS/cm for quicklime, whereas for cement treated MFT the pH and EC of the porewater were 10.6 and 9.3 mS/cm, which is much lower than quicklime treated MFT. On the other hand, at the low chemical content (1%), the pH and EC were 9.5 and 5 mS/cm for quicklime treated MFT, and 9.3 and 4.1mS/cm for cement treated MFT. The increase of pH and EC after adding quicklime or cement is due to the hydration reaction of cement or quicklime, which produces calcium hydroxide, $Ca(OH)_2$. The hydration reaction of quicklime is governed by

$$\mathrm{CaO\ (s)\ +\ H_2O\ (l) \rightleftharpoons\ Ca(OH)_2\ (aq)\ (\Delta H_r\ =\ -63.7\ kJ/mol\ of\ CaO)} \tag{5.1}$$

The hydration reaction of the cement can produce the calcium hydroxide up to 25% of the its weight, which is less than that produced by quicklime (Hausmann 1990). Thus, at the same dosage, the quicklime generates more calcium hydroxide, which leads to higher porewater pH and EC.

At high pH condition, the clay particles in MFT tend to form a dispersed structure (Mitchell and Soga 2005). However, Wang and Siu (2006) found that at the high pH the degree of kaolinite particle flocculation increases with increases in the ionic strength because the double layers are compressed at the particle surfaces and van der Waals attraction leads to particle coagulation. The high degree of flocculation of kaolinite indicates strong interparticle attractive forces, and therefore, leads to a high measured liquid limit (LL) (Wang and Siu 2006). The zeta potential of the suspended chemical treated MFT samples was measured at various pH, and the results are plotted

in Figs. 5.13 and 5.14 for quicklime or cement treated MFT, respectively. The results of zeta potential of original MFT were reported by Guo and Shang (2014), and are also plotted in the figures. As shown the zeta potential of the MFT sample reduced after adding quicklime or cement, indicating that the double layer of the MFT particle was compressed due to the increase in porewater EC after adding quicklime or cement. The reduction in zeta potential is associated with the increase in pore water EC. It is noticed that MFT sample with 10% quicklime had the highest porewater EC (32.4 mS/cm), and the most significant reduction in the zeta potential, as seen in Fig. 5.13. At the low chemical dosage (C-QL-5-0-1 and C-CM-5-0-10), the EC increased from 3.59 mS/cm to 4.1mS/cm and 5 mS/cm for 1% cement and quicklime, respectively. The zeta potentials measured for the sample with low chemical percentage moved to above the trend line of original MFT, as seen in Figs. 5.13 and 5.14.

Thus, the mechanism proposed by Wang and Siu (2006) could be one of the reasons for the increase in the liquid limit of quicklime or cement treated MFT, which contains significant percentage of kaolinite. The Locat et al. (1996) suggested that another possible reason for the increase in soil plasticity is the development of the soil microstructure, which can retain porewater, along with the cementation of large flocs. Chew et al. (2004b) also suggested that the increase in the liquid limit is due to water trapped within intra-aggregate pores.

On the other hand, the EK flow in soil is closely related to the zeta potential (Mitchell and Soga, 2005). After adding quicklime or cement, the reduction of zeta potential of MFT sample indicates that the EK generated water flow will be reduced. This is consistent with the experimental data reported in section 5.3.2.

5.4. Conclusion

In this study, two chemical additives, i.e., cement and lime, were added to mature fine tailings (MFT) from oil sand processing, then EK treatment was carried out. Combined effects of chemical and electrokinetic treatment were assessed via the water content, undrained shear strength, plasticity, porewater pH and EC, and zeta potential of MFT particles after treatment. The conclusions based on the results of the experiments and data analysis are shown as follows:

1. The water content of MFT reduced immediately after mixing with quicklime or cement, due to hydration reaction. The post-treatment water content of MFT samples reduced linearly with the increase in the chemical dosage.

2. Both liquid and plastic limits increased after quicklime or cement treatment. The plastic limit of quicklime treated MFT was not significantly influenced by the mixing ratio and curing time. More significant increase in liquid limit was observed at lower quicklime content (1%). For cement treated MFT samples, both plastic and liquid limit increased with an increase in the mixing ratio and curing time.

3. The Portland cement is more effective in generating strength gain than quicklime.

4. The addition of quicklime or cement reduced the EK induced water flow, hence reduced dewatering effects. EK flow completely stopped at high chemical dosage (10%).

5. The low chemical dosage (1% cement or quicklime) combined with EK treatment is beneficial for the strength gain of MFT and can significantly reduce the difference in both water content and undrained shear strength of the MFT samples between the anode and the cathode by EK treatment alone.

6. The porewater pH and EC of MFT sample were increased by adding quicklime or cement. Cement treated MFT had lower porewater pH and EC than those treated with quicklime.

7. The zeta potential of MFT reduced, which is attributed to compression of electrical double layer of MFT particles by adding quicklime or cement. The reduction in zeta potential is consistent with the reduction in EK dewatering effects.

8. The Atterberg limits increased after adding quicklime or cement, which can be attributed to the increase in particle flocculation, aggregation and cementation of particles into large size clusters, and the water trapped within intra-aggregate pores.

References

ASTM (2010a). D2166-10: Standard test methods for laboratory determination of water (moisture) content of soil and rock by mass. ASTM International, West Conshohocken, PA, 2010, https://doi.org/10.1520/D2216-10

ASTM (2010b). D4318-10e1: Standard test methods for liquid limit, plastic limit, and plasticity index of soils, ASTM International, West Conshohocken, PA, 2010, https://doi.org/10.1520/D4318

Beier, N., Wilson, W., Dunmola, A., and Sego, D. (2013). Impact of flocculation-based dewatering on the shear strength of oil sands fine tailings. Canadian Geotechnical Journal, 50, No. 9, 1001-1007.

Bell, F. G. (1979). Stabilization and treatment of clay soil with lime: basic principle. Ground Engineering Journal, 12, 112-118.

Bell, F. G. (1996). Lime stabilization of clay minerals and soils. Engineering geology, 42, No. 4, 223-237.

Bergado, D. T., Balasubramaniam, A. S., Patawaran, M. A. B., and Kwunpreuk, W. (2000). Electroosmotic consolidation of soft Bangkok clay with prefabricated vertical drains. Ground Improvement, 4, No.4, 153-163.

BGC Engineering Inc. (2010). Oil sands tailings technology review. Oil sands research and information network, University of Alberta, School of Energy and the Environment, Edmonton, Alberta. OSRIN Report No. TR-1.

Bjerrum, L., Moum, J., and Eide, O. (1967). Application of electroosmosis to a foundation problem in a Norwegian quick clay. Géotechnique, 17, No.3, 214–235.

Casagrande, L. (1959). Review of past and current work on electroosmotic stabilization of soils. In Harvard Soil Mechanics Series, 45, Harvard University Cambridge, Massachusetts, USA (reprinted November 1959 with a supplement of June 1957).

Chew, S. H., Karunaratne, G. P., Kuma, V. M., Lim, L. H., Toh, M. L., and Hee, A. M. (2004a). A field trial for soft clay consolidation using electric vertical drains. Geotextiles and Geomembranes, 22, No.1, 17-35.

Chew, S. H., Kamruzzaman, A. H. M., and Lee, F. H. (2004b). Physicochemical and engineering behavior of cement treated clays. Journal of geotechnical and geoenvironmental engineering, 130, No.7, 696-706.

Fourie, A. B., and Jones, C. J. F. P. (2010). Improved estimates of power consumption during dewatering of mine tailings using electrokinetic geosynthetics (EKGs). Geotextiles and Geomembranes, 28, No.2, 181-190.

Fourie, A. B., Johns, D. G., and Jones, C. F. (2007). Dewatering of mine tailings using electrokinetic geosynthetics. Canadian Geotechnical Journal, 44, No.2, 160-172.

Guo, Y. and Shang, J.Q. (2014). A study on electrokinetic dewatering of oil sands tailings. Environmental Geotechnics, 1, No.2, 121-134.

Hausmann, M. R. (1990). Engineering principles of ground modification. McGraw-Hill.

Islam, S., and Shang, J. Q. (2017). Electrokinetic thickening of mature fine oil sands tailings. Environmental Geotechnics, 4, No. 1, 40-55.

Liu, P., and Shang, J. Q. (2014). Improvement of marine sediment by combined electrokinetic and chemical treatment. International Journal of Offshore and Polar Engineering, 24, No.3, 232-240.

Lo, K. Y., Ho, K. S., and Inculet, I. I. (1991a). Field test of electroosmotic strengthening of soft sensitive clay. Canadian Geotechnical Journal, 28, No.1, 74-83.

Lo, K. Y., Inculet, I. I., and Ho, K. S. (1991b). Electroosmotic strengthening of soft sensitive clays. Canadian Geotechnical Journal, 28, No.1, 62-73.

Locat, J., Trembaly, H., and Leroueil, S. (1996). Mechanical and hydraulic behaviour of a soft inorganic clay treated with lime. Canadian geotechnical journal, 33, No.4, 654-669.

Lorenzo, G. A., and Bergado, D. T. (2004). Fundamental parameters of cement-admixed clay-new approach. Journal of geotechnical and geoenvironmental engineering, 130, No.10, 1042-1050.

Micic, S., Shang, J. Q., Lo, K. Y., Lee, Y. N., and Lee, S. W. (2001). Electrokinetic strengthening of a marine sediment using intermittent current. Canadian Geotechnical Journal, 38, No.2, 287-302.

Micic, S., Shang, J. Q., and Lo, K. Y. (2002). Electrokinetic strengthening of marine clay adjacent to offshore foundations. International Journal of Offshore and Polar Engineering, 12, No.1, 64-73.

Mitchell, J.K. (1976). The properties of cement-stabilized soils. Proc. Residential Workshop on Materials and Methods for Low Cost Road, Rail and Reclamation Works, Leura, Australia, 365-404.

Mitchell, J. K., and Hooper, D. R. (1961). Influence of time between mixing and compaction on properties of a lime-stabilized expansive clay. Highway Research Board Bulletin, (304), HRB, National Research Council, Washington, DC, USA, 14-31.

Mitchell, J.K., and Soga K. (2005). Fundamental of soil behaviour, 3rd edn. Wiley, Hoboken, New Jersey, USA.

Mohamedelhassan, E, and Shang, JQ (2002). Feasibility assessment of electro-osmotic consolidation on marine sediment. Ground Improvement, 6, No 4, 145–152.

Pourrezaei, P., and El-Din, M.G. (2008). Coagulation-flocculation pre-treatment of oil sands process affected water. 1st International oil sands tailings conference (IOSTC), Edmonton, Alberta, Canada.

Rima, U. S. (2013). Characterization and centrifuge dewatering of oil sands fine tailings. M.ASc. Thesis, University of Regina.

Saitoh, S., Suzuki, Y., and Shirai, K. (1985). Hardening of soil improved by deep mixing method. Proceedings of 11th ICSMFE, San Francisco, August 12-16, 1985, 3,1748-1748.

Small, C. C., Cho, S., Hashisho, Z., and Ulrich, A. C. (2015). Emissions from oil sands tailings ponds: Review of tailings pond parameters and emission estimates. Journal of Petroleum Science and Engineering, 127, 490-501.

Sorta, A. R. (2015). Centrifugal modelling of oil sands tailings consolidation, Ph.D. thesis, University of Alberta.

Sworska, A., Laskowski, J. S., and Cymerman, G. (2000). Flocculation of the Syncrude fine tailings: Part I. Effect of pH, polymer dosage and Mg^{2+} and Ca^{2+} cations. International journal of mineral processing, 60, No.2, 143-152.

Wang, C., Harbottle, D., Liu, Q., and Xu, Z. (2014). Current state of fine mineral tailings treatment: a critical review on theory and practice. Minerals Engineering, 58, 113-131.

Wang, X. T., Feng, X., Xu, Z., and Masliyah, J. H. (2010). Polymer aids for settling and filtration of oil sands tailings. The Canadian Journal of Chemical Engineering, 88, No. 3, 403-410.

Wang, Y. H., and Siu, W. K. (2006). Structure characteristics and mechanical properties of kaolinite soils. I. Surface charges and structural characterizations. Canadian Geotechnical Journal, 43, No.6, 587-600.

Xu, Y., Dabros, T., and Kan, J. (2008). Filterability of oil sands tailings. Process Safety and Environmental Protection, 86, No. 4, 268-276.

Zhang, R. (2016). Electrokinetics and vacuum combined dewatering of oil sand tailings, M.Esc. thesis, The University of Western Ontario.

Table 5.1 Oil sands tailings properties (Guo and Shang 2014)

Properties		Oil sands tailings
Water content (%) (as received)		171.3%
Specific gravity, Gs		2.51
Void ratio (as received)		4.39
Dry density(Mg/m^3)		0.47
Hydraulic conductivity (m/s) (at e = 2.03)		1.81×10^{-9}
Atterberg limits	Plastic limit, PL (%)	29.1
	Liquid limit, LL (%)	51.6
	Plasticity index, PI	22.5
Organic matter (%)		14.7
Carbonate content (%)		<1
Grain size	D_{10} (μm)	0.85
	D_{50} (μm)	7.15
	D_{90} (μm)	27.9
	Sand (%)	0.00
	Silt (%)	80.00
	Clay (%)	20.00
Pore water pH		8.8
Pore water EC: mS/cm		3.59

Table 5.2 Experimental design chart

M_{MFT} / $M_{Chemical}$*			10:0	9.9:0.1	9.5:0.5	9:1	8.5:1.5	8:2
Quicklime (QL)	Curing time	0 days	-	-	QL-5-0	QL-10-0	QL-15-0	QL-20-0
		7 days	-	-	QL-5-7	QL-10-7	QL-15-7	QL-20-7
		14 days	-	-	QL-5-14	QL-10-14	QL-15-14	QL-20-14
		28 days	-	-	QL-5-28	QL-10-28	QL-15-28	QL-20-28
Cement (CM)	Curing time	7 days	-	CM-1-7	CM-5-7	CM-10-7	-	-
		14 days	-	CM-1-14	CM-5-14	CM-10-14	-	-
		28 days	-	CM-1-28	CM-5-28	CM-10-28	-	-
EK	EK + QL		-	EK+QL-5-50-1	-	EK+QL-5-50-10	-	-
	EK+CM		-	EK+CM-5-50-1	-	EK+CM-5-50-10	-	-
	EK		EK-0-50-125	-	-	-	-	-
	Control QL		-	C-QL-5-0-1	-	C-QL-5-0-10	-	-
	Control CM		-	C-CM-5-0-1	-	C-CM-5-0-10	-	-

*** M_{MFT} / $M_{Chemical}$**: mass ratio of bulk MFT to dry chemical additives

Table 5.3 Test conditions for electrokinetic dewatering

	Electrokinetic test	Control test
$M_{MFT}/M_{chemical}$	9:1 and 9.9:0.1	
Voltage gradient	50V/m	0
Drainage path	Horizontal	
Electrodes	Vertical	
Surcharge loading	Gradually applied to 5 kPa in the 1st 48 hours and kept during testing period	
EK treatment time, hr	120	0
Total treatment time, hr	168 (7 days)	
Water content	anode and cathode	center
Undrained shear strength	anode and cathode	center

Table 5.4 Summary of the water content test results after quicklime treated

		Water content (%)				Solid content (%)			
	M_{MFT} / M_{QL}	**9.5:0.5**	**9:1**	**8.5:1.5**	**8:2**	**9.5:0.5**	**9:1**	**8.5:1.5**	**8:2**
Quicklime	0 days	140.6	109.3	95.3	75.7	41.6	47.8	51.2	56.9
	7 days	150.2	129.4	77.7	66.2	40.0	43.6	56.3	60.2
	14 days	134.4	121.3	80.1	66.1	42.7	45.2	55.5	60.2
	28 days	144.3	115.6	79.8	65.4	40.9	46.4	55.6	60.5
	Average	142.4	118.9	83.2	68.4	41.3	45.7	54.7	59.4
	M_{MFT} / M_{CM}	**9.9:0.1**	**9.5:0.5**	**9:1**	**-**	**9.9:0.1**	**9.5:0.5**	**9:1**	**-**
Cement	0 days	156.3	145.5	123.4	-	39.0	40.7	44.8	-
	7 days	157.7	134.7	111.9	-	38.8	42.6	47.2	-
	14 days	153.8	133.9	109.4	-	39.4	42.8	47.8	-
	28 days	153.9	126.6	110.4	-	39.4	44.1	47.5	-
	Average	155.4	135.2	113.8		39.2	42.6	46.8	

Table 5.5 Summary of the Atterberg limits of the sample after chemical treatment

			Atterberg limit			
Quicklime	**M_{MFT} / M_{QL}**		**9.5:0.5**	**9:1**	**8.5:1.5**	**8:2**
	7days	PL (%)	44.1	47.9	50.1	48.5
		LL (%)	98.4	92.3	89.7	84.9
		PI (%)	54.3	44.4	39.6	36.4
	14days	PL (%)	50.2	54.4	51.1	55.5
		LL (%)	102.7	104.5	95.1	89.2
		PI (%)	52.5	50.1	44	33.7
	28days	PL (%)	55.5	44.2	57.3	56.6
		LL (%)	111.6	109.2	102.9	93
		PI (%)	56.1	65	45.6	36.4
Cement	**M_{MFT} / M_{CM}**		**9.9:0.1**	**9.5:0.5**	**9:1**	**-**
	7days	PL (%)	24.0	35.1	40.0	-
		LL (%)	90.3	104.9	114.3	-
		PI (%)	66.3	69.8	74.3	-
	14days	PL (%)	28.0	36.5	51.8	-
		LL (%)	100.8	125.7	122.0	-
		PI (%)	72.9	89.2	70.2	-
	28days	PL (%)	27.9	44.4	56.0	-
		LL (%)	95.6	123.6	114.5	-
		PI (%)	67.7	79.2	58.5	-

Table 5.6 Summary of the water content test results after EK treatment

Test No.	Water content					Water content reduction due to EK (%)*	
	Initial	Anode	Cathode	After mixing	Controlled	Anode	Cathode
EK+QL-5-50-1	154%	121%	124%	149%	136%	11.0%	8.8%
C-QL-5-0-1	-	-	-	-	136%	-	-
EK+QL-5-50-10	187%	112%	114%	127%	114%	1.8%	0%
C-QL-5-0-10	-	-	-	-	114%	-	-
EK+CM-5-50-1	168%	88%	116%	159%	129%	31.4%	10.0%
C-CM-5-0-1	-	-	-	-	129%	-	-
EK+CM-5-50-10	164%	99%	100.5%	124%	96%	-2.7%	-4.7%
C-CM-5-0-10	-	-	-	-	96%	-	-
EK-0-50-125	169%	50%	171%	169%	93%	46.6%	-83.7%

*Water content reduction due to EK(%) = $((w_{control}-w_{EK})/w_{Control})\times 100\%$, where $w_{control}$ is the water content at the end of controlled test, and the w_{EK} is the water content after EK dewatering.

Table 5.7 Undrained Shear strength of the sample after EK treatment

		Su (kPa)	
		EK	Controlled
		Undisturbed	Undisturbed
EK+QL-5-50-10	Anode	2.5	1.5
	Cathode	2	
EK+QL-5-50-1	Anode	3.5	2
	Cathode	2.25	
EK+CM-5-50-10	Anode	9.25	5
	Cathode	7.5	
EK+CM-5-50-1	Anode	7	1
	Cathode	1.25	

Figure 5.1 plastic cylindrical mold used in quicklime treatment

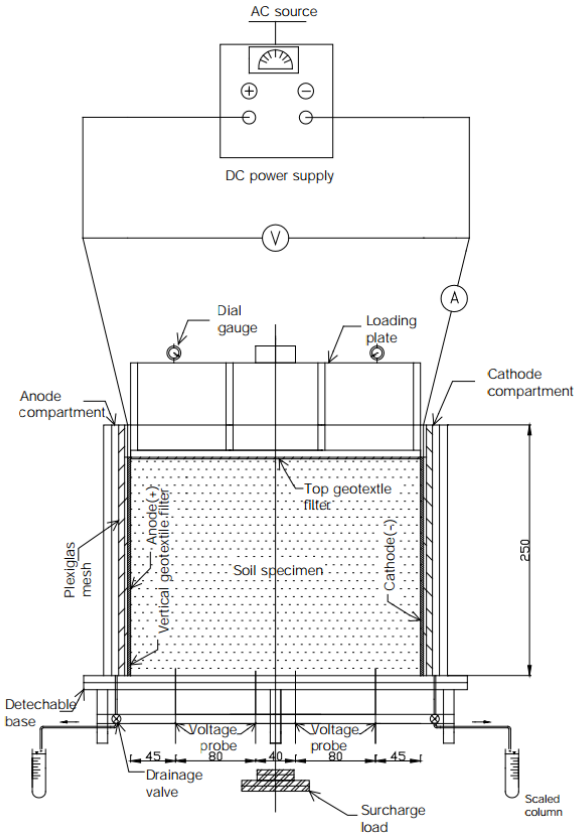

Figure 5.2 Electrokinetic dewatering cell (Dimension in mm) (Liu and Shang 2014)

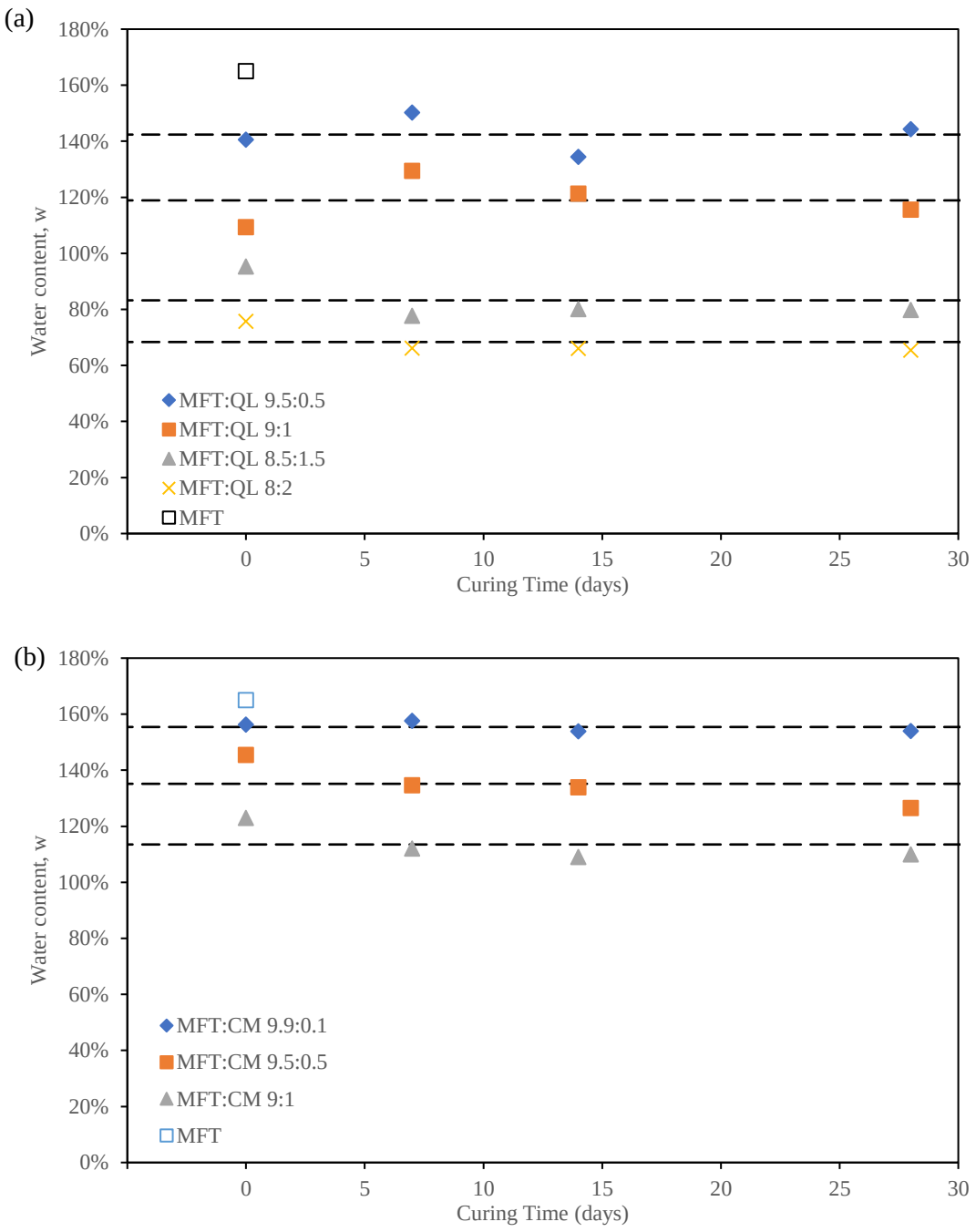

Figure 5.3 Water content of (a) quicklime and (b) cement treated MFT versus curing time

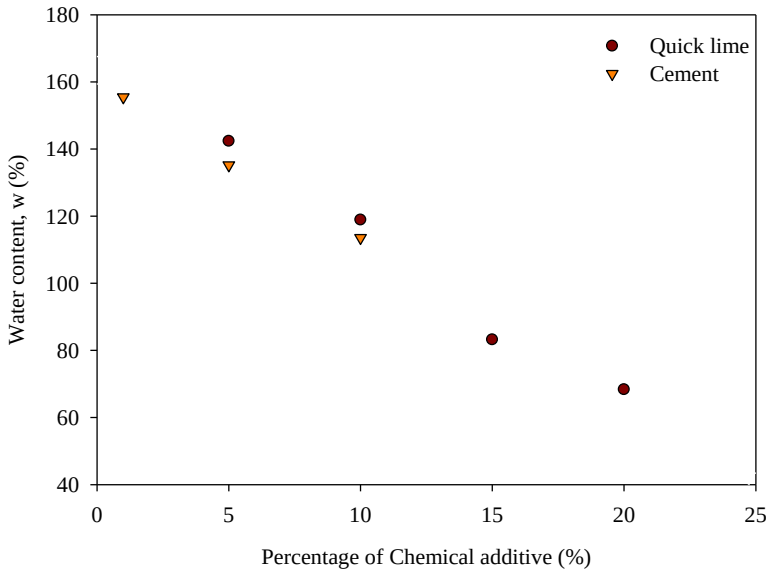

Figure 5.4 Post-treatment water content versus percentage of chemical additives

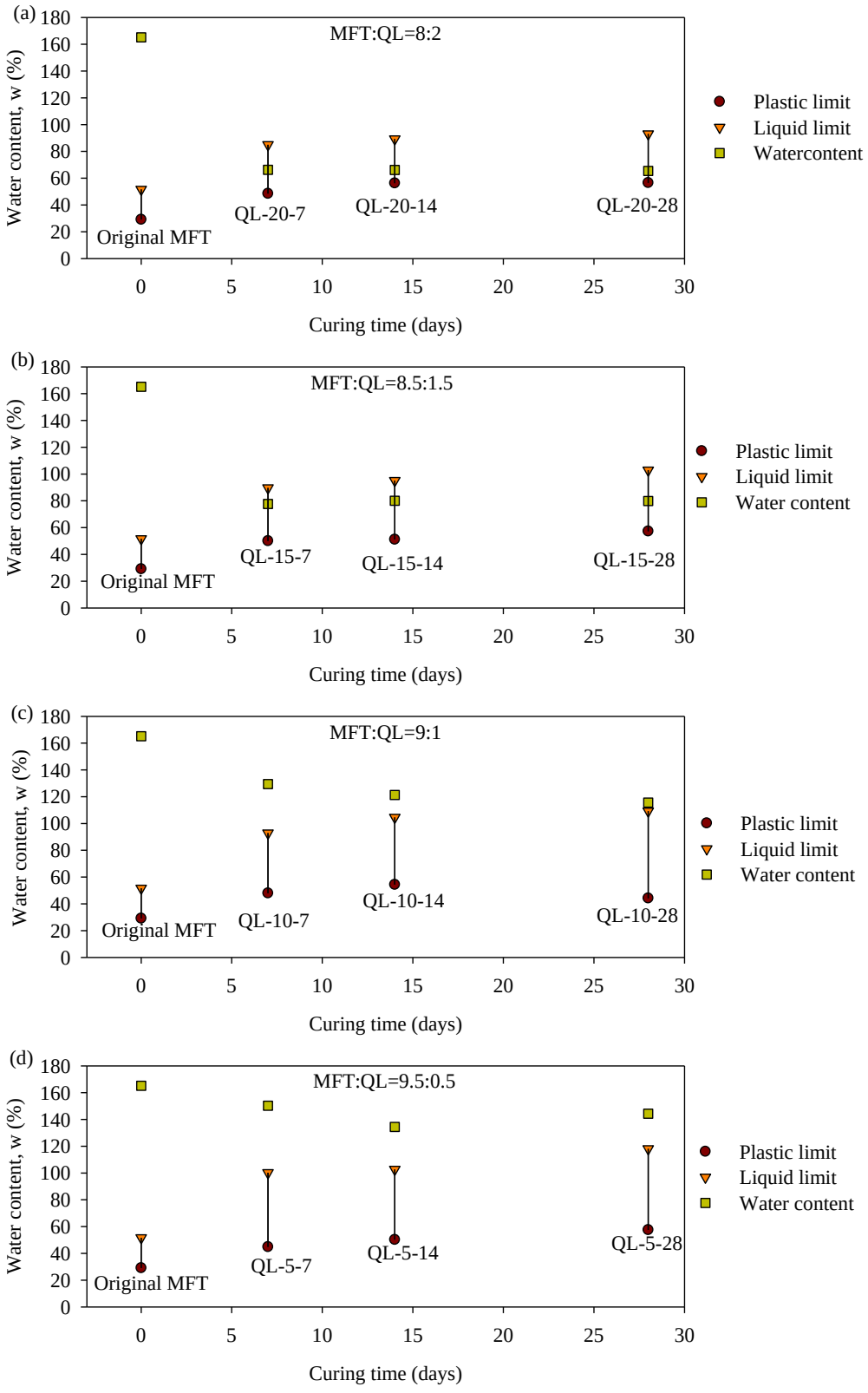

Figure 5.5 Water content and Atterberg limits of quicklime treated MFT at different curing time under the mixing ratio (a) 8:2, (b) 8.5:1.5, (c) 9:1, and (d) 9.5:0.5

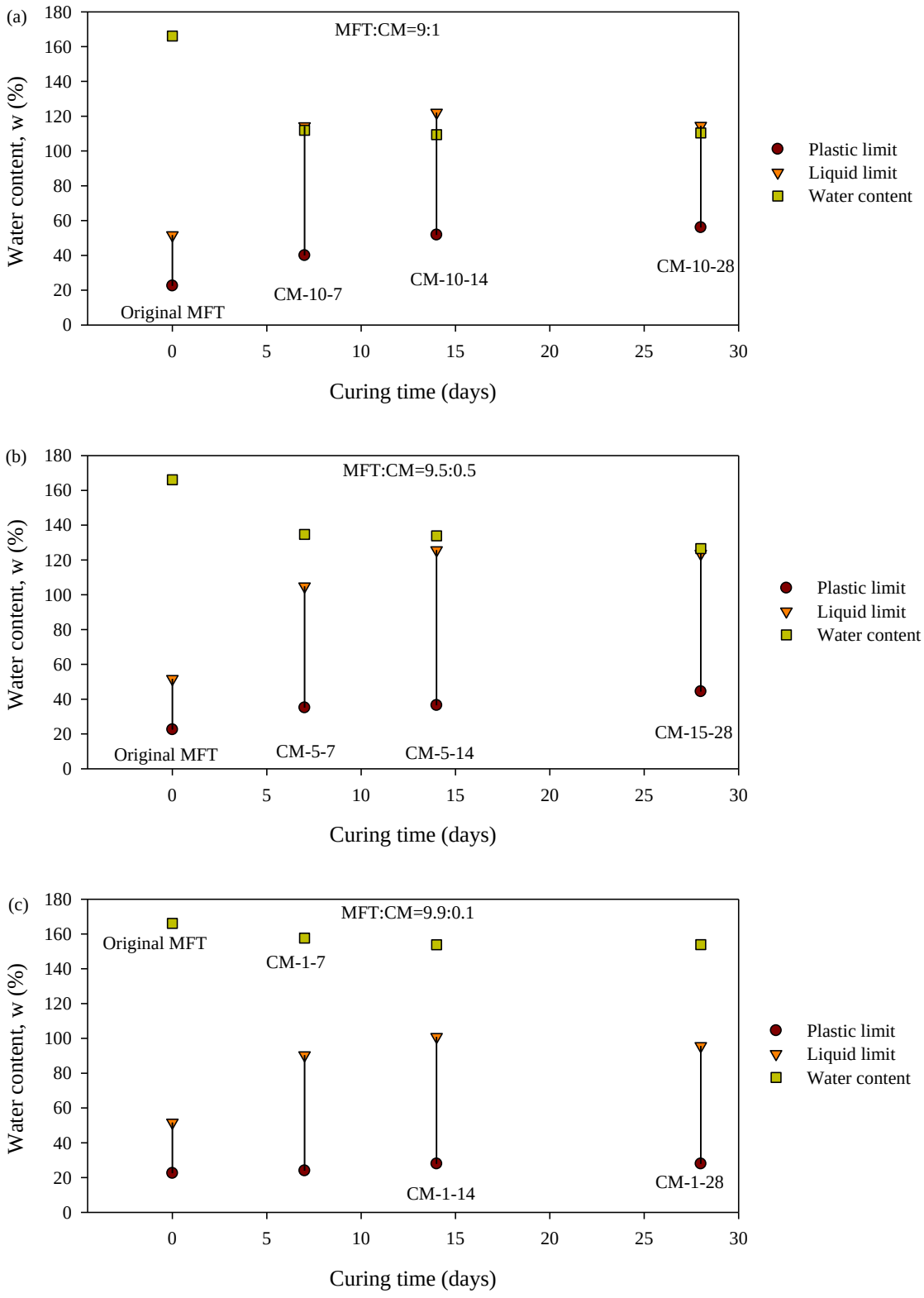

Figure 5.6Water content and Atterberg limits of cement treated MFT at different curing time under the mixing ratio (a) 9:1, (b) 9.5:0.5, and (c) 9.9:0.1

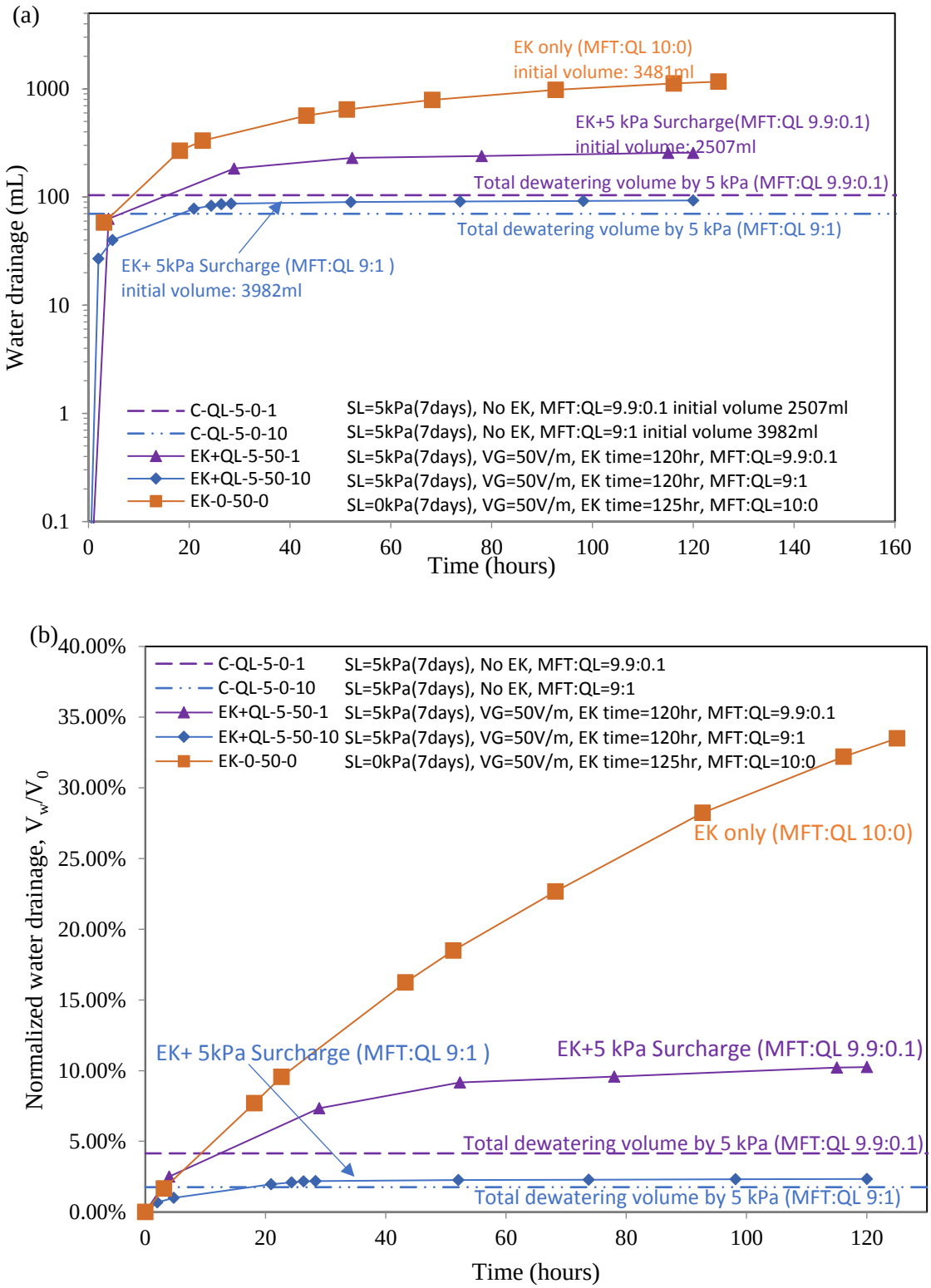

Figure 5.7 EK dewatering results of quicklime treated MFT in terms of (a) water drainage (ml) and (b) normalized water drainage, Vw/V₀ (%)

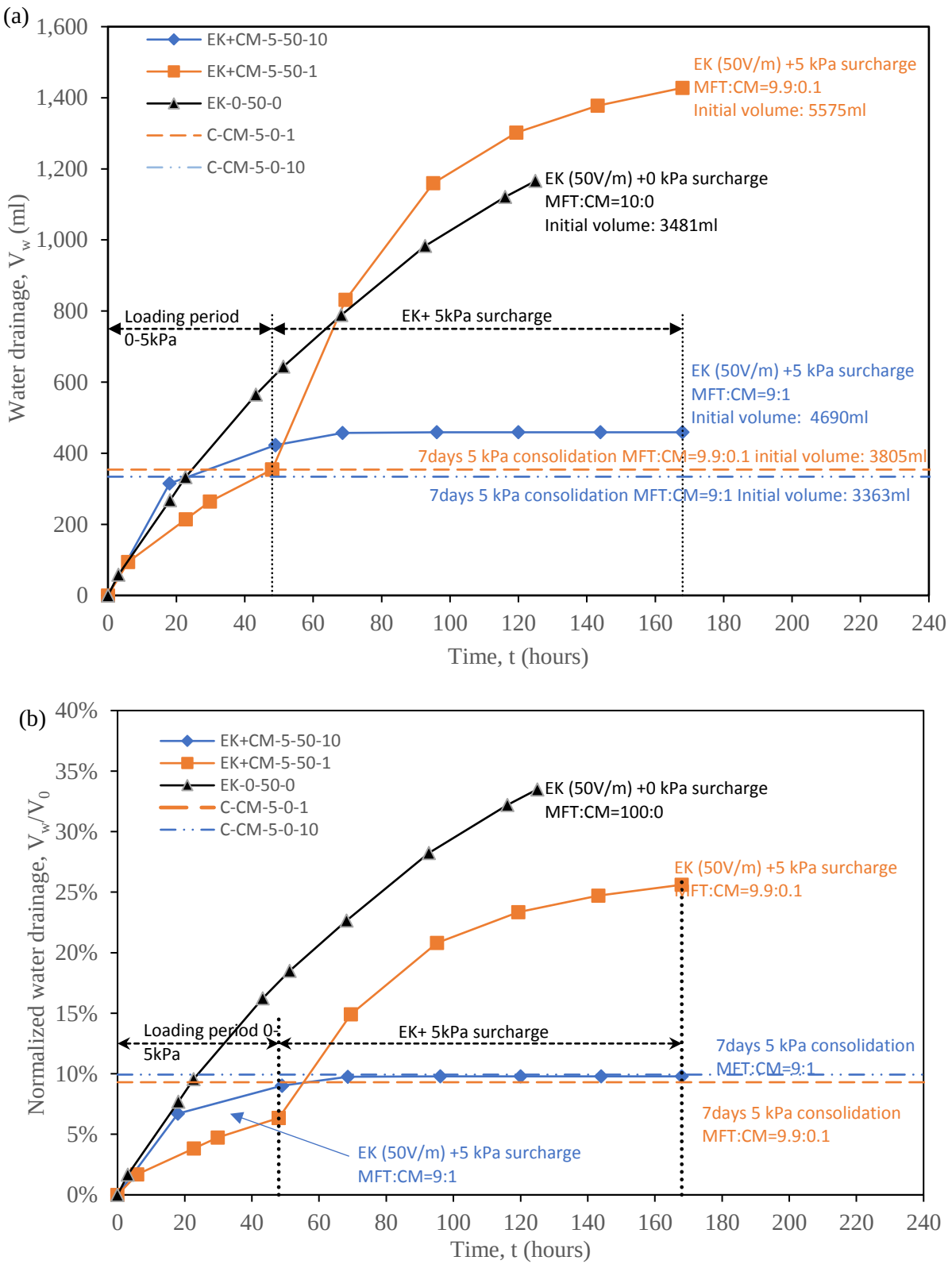

Figure 5.8 EK dewatering results of cement treated MFT in terms of (a) water drainage (ml) and (b) normalized water drainage, V_w/V_0 (%)

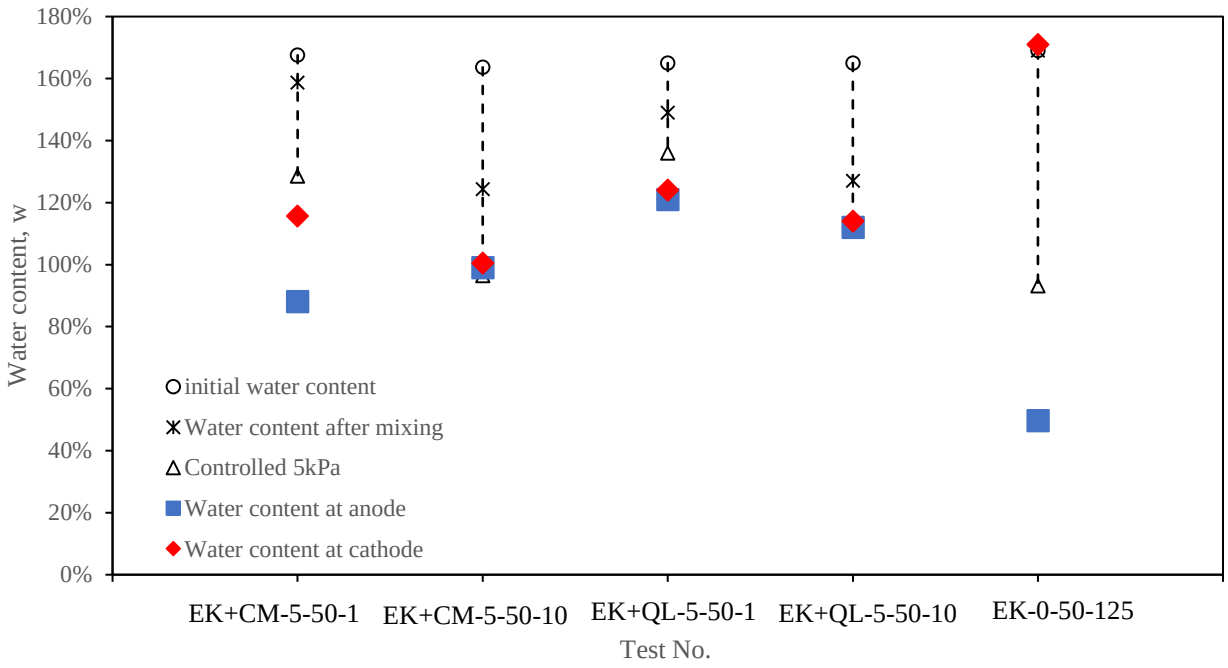

Figure 5.9 Comparison of water content of MFT samples after EK dewatering tests

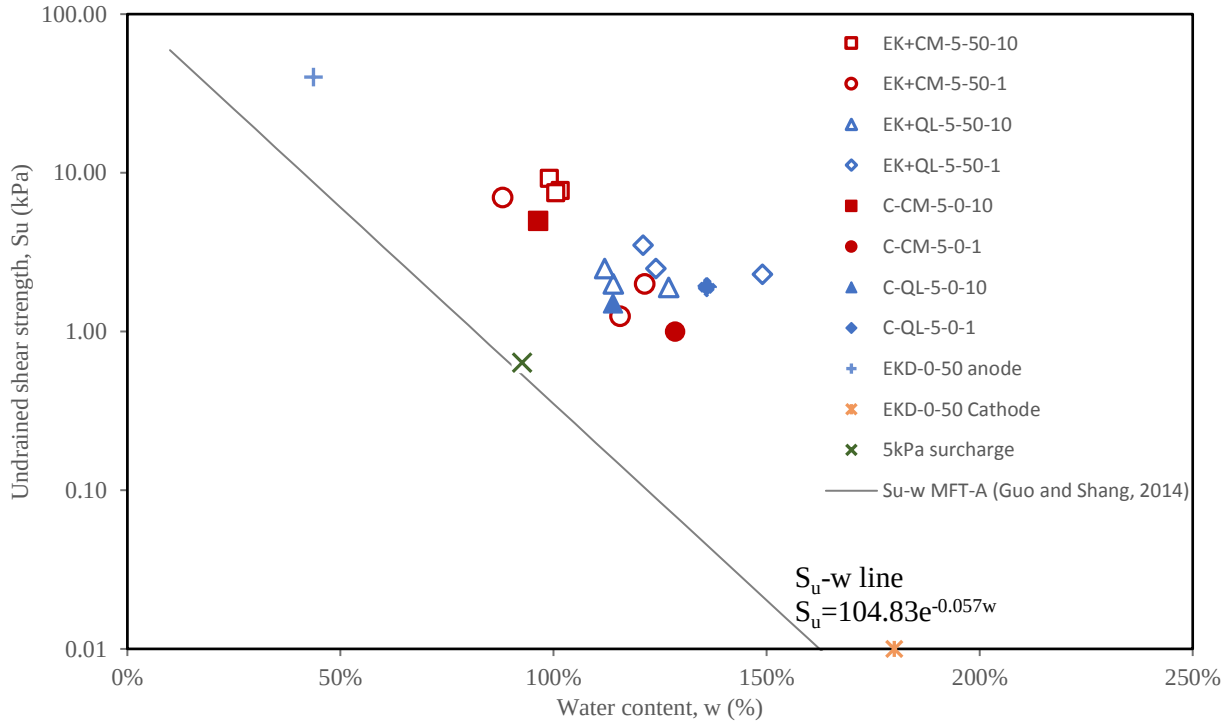

Figure 5.10 Undrained shear strength versus water content of post treated MFT

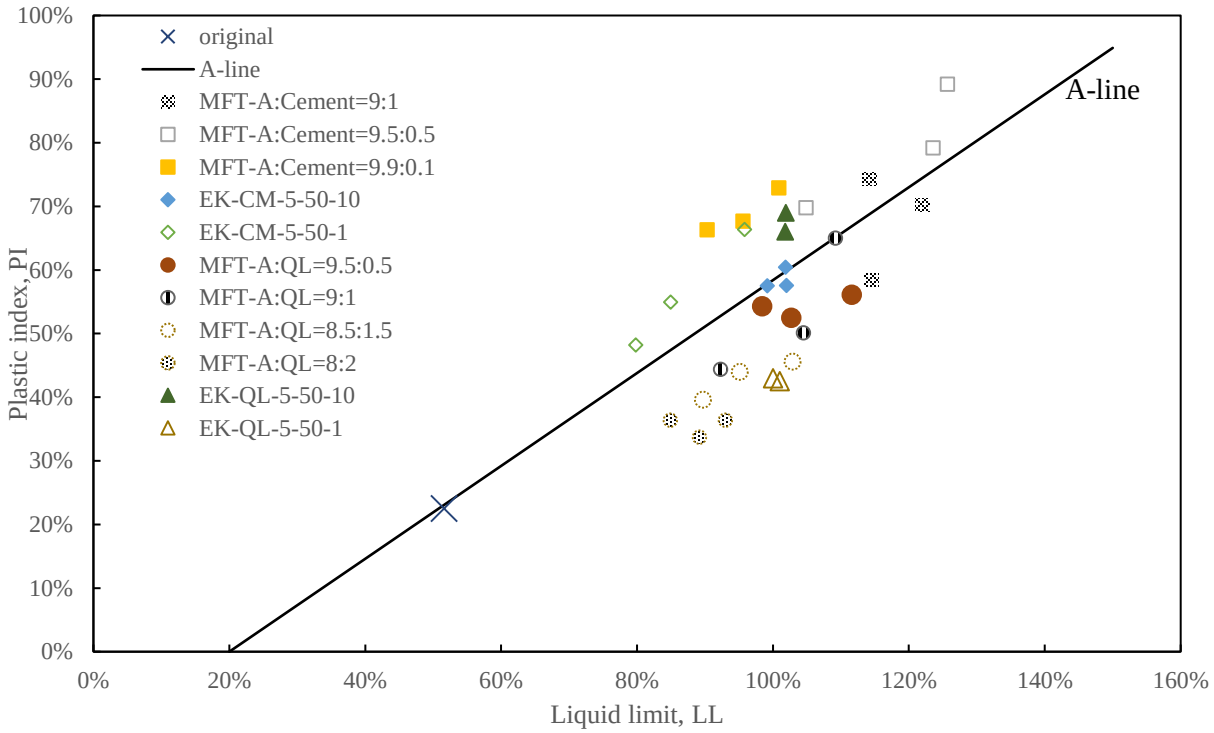

Figure 5.11 Plasticity of chemical treated MFT in Casagrande plasticity chart

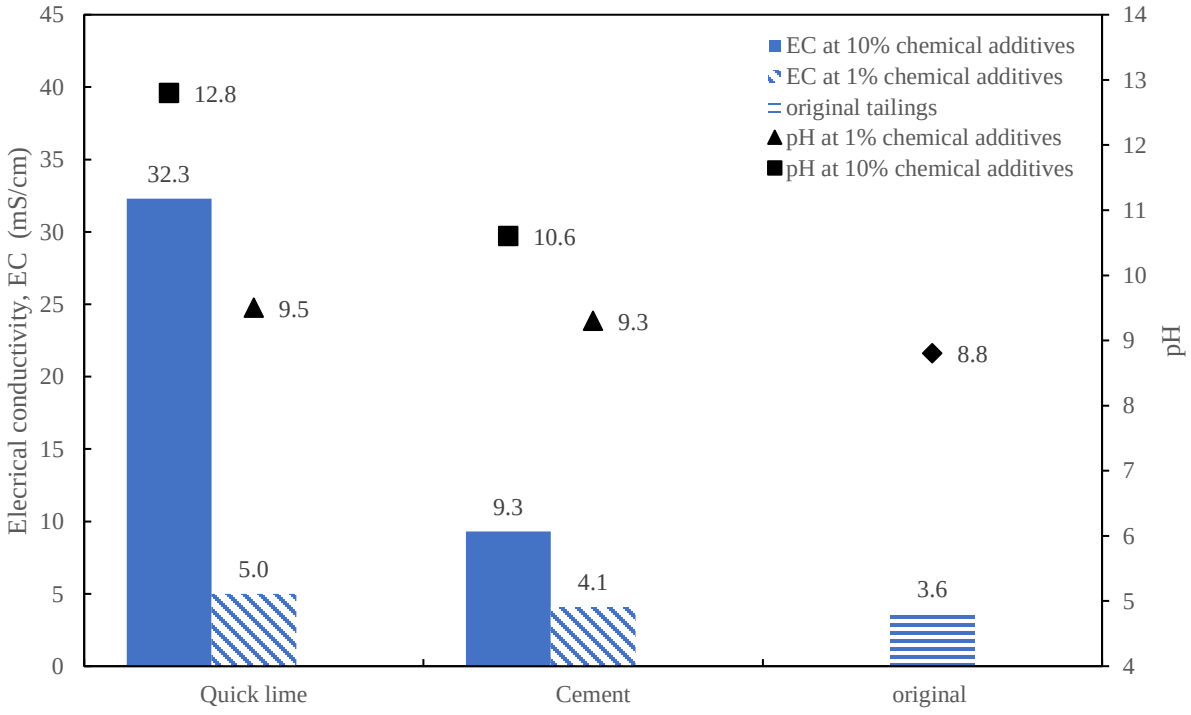

Figure 5.12 Porewater pH and EC of MFT after adding quicklime or cement

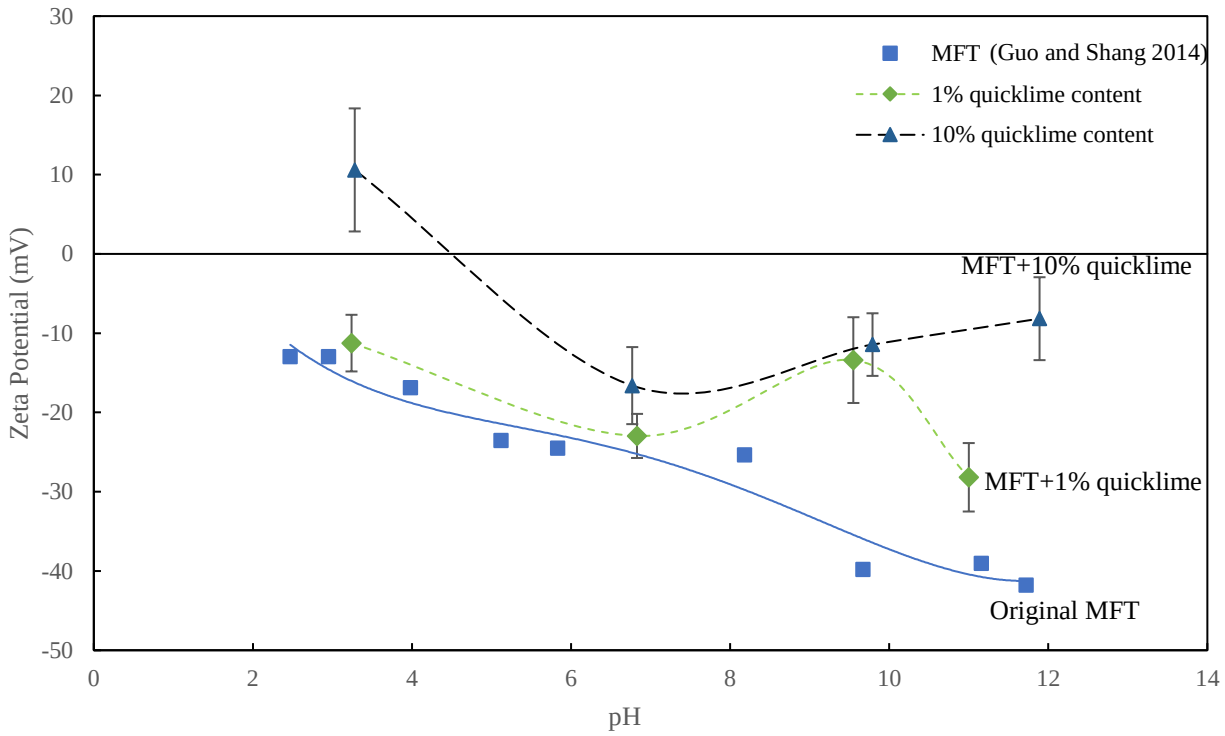

Figure 5.13 Zeta potential of MFT versus pH after adding quicklime

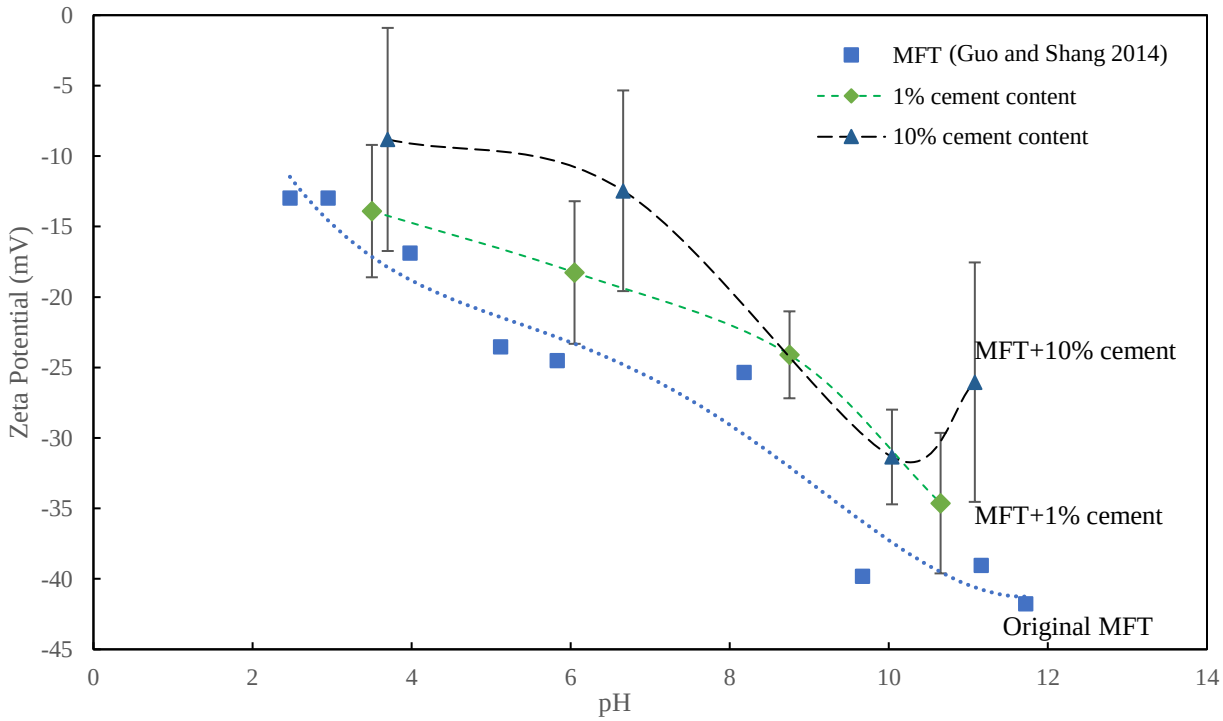

Figure 5.14 Zeta potential of MFT versus pH after adding cement

Chapter 6 One-dimensional large strain electroosmotic consolidation model

6.1. Introduction

When a saturated clay layer, such as fills, foundations, embankments, etc, is subjected to an extra loading, an excess pore water pressure is generated. The excess pore water pressure dissipates slowly, resulting in decrease of soil void ratio and settlement. Terzaghi (1943) first developed one-dimensional consolidation theory, and Biot (1941) proposed the general three-dimensional consolidation theory. In Terzaghi's theory, the governing equation for one-dimensional consolidation is shown as (Das 2008, Mitchell and Soga 2005):

$$\frac{\partial u}{\partial t} = \frac{k_h}{\gamma_w m_v}\frac{\partial^2 u}{\partial z^2} = C_v \frac{\partial^2 u}{\partial z^2} \tag{6.1}$$

where $\partial u/\partial t$ is the time derivative of excess pore-water pressure;

$\partial u/\partial z$ is the spatial derivative of excess-water pressure;

C_v [L^2T^{-1}] is the coefficient of consolidation, $C_v = \frac{k_h}{\gamma_w m_v}$;

k_h [LT^{-1}] is the hydraulic conductivity;

γ_w [9.8 kN/m^3, $ML^{-2}T^{-2}$] is the unit weight of water;

m_v [$M^{-1}LT^2$] is the coefficient of volume compressibility, $m_v = \frac{a_v}{1+e}$;

a_v [$M^{-1}LT^2$] is the coefficient of compressibility;

e [-] is the void ratio.

The Terzaghi's consolidation theory is based on the small strain theory (or infinitesimal strain theory). The deformation of clay layer is assumed to be much smaller than any relevant dimensions of soil stratum. Hence the coefficient of consolidation, C_v, is assumed to be unchanged with deformation.

Small strain consolidation theory is sufficient to predict the clay consolidation behavior, both magnitude and rate of the settlement, in most geotechnical engineering applications, such as shallow foundations, embankment, compacted fills, etc. However, the theory has encountered difficulties on extremely soft materials, such as marine sediments, fine mine tailings, sewage slurry, etc. Thus, the large strain consolidation theory has been developed (Jeeravipoolvarn 2010, Cargill 1982, Somogyi 1980, Lee and Sills 1980, Bartholomeausem et al. 2002).

Gibson et al. (1967) first derived the governing equation for one-dimensional large strain consolidation. They considered a configuration, in which the same soil particles are encapsulated in the boundaries of element; and an element of soil skeleton of unit cross-sectional area is normal to the pore fluid flow. This is known as Lagrangian point of view in continuum mechanics.

6.1.1. Coordinate systems

There are two mathematical approaches for continuum mechanics: Lagrangian and Eulerian forms.

The Eulerian coordinate system is the most commonly used in small-strain theory. The coordinates are defined in space with an origin fixed in space. On the other hand, coordinates in the Lagrangian system, which are commonly used in large-strain analysis for the convenience, are defined in solid material with an origin fixed in the material. The deformation of solid material can be described in the Eulerian (or spatial) coordinate system, e.g., the Cartesian coordinate with three axes of x^1, x^2, x^3; or the Lagrangian coordinate system with three axes of ξ^1, ξ^2, ξ^3, which is defined in and deformed with the material, as shown in Fig.6.1.

In a 1-D coordinate system, the body ABCD is shown in Fig. 6.2. The ABCD is also called the representative elementary volume (REV), i.e., the smallest volume which can represent the behaviour of entire material. There are two coordinate systems, i.e. the Eulerian coordinate system with z-axis, and the Lagrangian coordinate system with ξ-axis. Under one-dimensional condition, the volume of body ABCD deforms in the vertical direction, and the planes AB and CD are normal to the direction of deformation. In both coordinate systems, t is time, which is independent of the coordinate system selection. At the initial time $t = t_0$, the positions of AB and CD are represented by (z_1, t_0) and (z_2, t_0) in the Eulerian coordinate system, respectively. The positions of AB and CD expressed in the Lagrangian coordinate system are (ξ_1, t_0) and (ξ_2, t_0), respectively. At time t = t', body ABCD has deformed as seen in Fig. 6.2(b). Thus, the new position for plane AB in the Eulerian coordinate is (z_1', t'), and for plane CD is (z_2', t'). On the other hand, since the Lagrangian coordinate system is defined in the body of ABCD, the coordinate system will deform with the body. Thus, in the Lagrangian coordinate system, the positions of AB and CD after deformation remain unchanged and are expressed as (ξ_1, t') and (ξ_2, t') respectively.

6.1.2. Gibson's Theory

A detailed review of Gibson's theory (Gibson et al. 1967) is described in following sections.

6.1.2.1. Coordinate systems selection and relationship

For the configuration of Gibson's theory, the coordinate systems are shown in Fig. 6.3. Fig. 6.3(a) shows the Lagrangian coordinate system (ξ, t) and Eulerian coordinate system (z, t) at time t=0. Fig. 6.3(b) shows the Eulerian coordinate system (z, t) at an arbitrary time t=t. For the soil element ABCD, according to the phase relationship, the total volume of soil matrix is 1+e, in which the volume for soil solid is represented by 1, and e, the void ratio, is the volume of void. For a saturated clay, the void ratio, e, represents the volume of the pore water. The volume of bulk soil decreases during consolidation process because of net outflow of pore fluid.

Since the total volume of soil solids is always the constant during the consolidation, for convenience, the third coordinate system, i.e., material coordinates (s, t), where the

coordinate element always encapsulating the same amount of soil solid, is chosen to simplify the derivation of the governing equation in Gibson's derivation. The material coordinate system is shown in Fig. 6.3 (c). In the material coordinate system, (s, t), ds is the height of element, which is constant and independent of time.

During the consolidation process, the thickness of ABCD, dz, in the Eulerian coordinate, z, will reduce with the time, t. On the other hand, the thickness represented in the Lagrangian coordinate system will remain the same, $d\xi$. Therefore, in the Lagrangian coordinate, ξ and t are independent variables. The position of any point in the clay layer can be written as (ξ, t).

The relationship between the Lagrangian and Eulerian coordinate systems in the derivation of Gibson's theory can be found through the phase relationship. For the configuration shown in Fig. 6.3, a datum is set at the bottom of the clay layer. As seen in Fig. 6.3(a), in the Lagrangian coordinate system (ξ) at the initial time, t=0, a body representing a soil layer has a height of ξ_0. The representative elementary volume (REV hereafter) ABCD has a thickness of $d\xi$ and location of (ξ, t=0). According to the soil phase relationship shown in Fig. 6.4, the thickness $d\xi$ has a relationship with the initial void ratio, e_0:

$$d\xi = (1 + e_0)ds \tag{6.2}$$

In the Eulerian coordinate system, the REV (ABCD) has an initial thickness of $dz^{t=0}$, and location z^0, (t=0). So the thickness of $dz^{t=0}$ also has a relationship with the initial void ratio, e_0, of the REV, which is presented as:

$$dz^{t=0} = (1 + e_0)ds \tag{6.3}$$

At an arbitrary time, the thickness of REV (ABCD) in the Lagrangian coordinate remains the same. However, since the soil layer is deformed (or consolidated), the thickness and

location of the REV at time t has changed in the Eulerian system. As a result, the thickness $dz^{t=t}$ can be written as:

$$dz^{t=t} = (1 + e_t)ds \tag{6.4}$$

where e_t is the void ratio of the REV at time t.

Combining Eq. 6.3 and 6.4, the thickness dz at any arbitrary time t, can be expressed as:

$$dz = (1 + e)ds \tag{6.5}$$

where e is the void ratio of the REV at time t.

From Eq.6.2 and 6.5:

$$\frac{d\xi}{dz} = \frac{1 + e_0}{1 + e} \tag{6.6}$$

Under one-dimensional condition, ds represents the volume of the soil solids in REV (ABCD). Based on the phase relationship the relationship among dz and ds, and dξ and ds can be written as:

$$\frac{dz}{ds} = 1 + e \tag{6.7}$$

$$\frac{d\xi}{ds} = 1 + e_0 \tag{6.8}$$

According to Fig. 6.3(c), the location coordinate, s, in the material coordinate system is obtained by integration of dξ from datum plane to ξ, based on Eq. 6.8, i.e.:

$$s = \int_0^{\xi} \frac{d\xi}{1 + e_{\xi}^{t=0}} \tag{6.9}$$

where s is the location coordinate of ABCD in the material coordinate system, ξ is the location coordinate represented in the Lagrangian coordinate system, $e_{\xi}^{t=0}$ is the soil void ratio of any arbitrary location, ξ, at initial time, t=0.

Similarly, the location coordinate of REV (ABCD) in the Eulerian coordinate system can be obtained through integration of ds in Eq. 6.7:

$$z = \int_0^{s} (1 + e_s^t) ds \tag{6.10}$$

where z is the location coordinate of REV (ABCD) in the Eulerian coordinate system, e_s^t is the soil void ratio of any location in the material coordinate system at time, t.

6.1.2.2. Assumptions in Gibson's theory

In order to understand Gibson's theory for one-dimensional large strain consolidation, the assumptions made by Gibson et al. (1967), are summarized as follows:

1. The soil is saturated during the consolidation process;

2. The soil matrix consists of incompressible fluid and soil particles

3. Darcy's law is valid, which is incorporated in the theory in a form that the relative velocity of soil skeleton and pore fluid are related to the excess pore water pressure gradient.

4. The hydraulic conductivity, k_h is a function of void ratio, e, $k_h = k_h(e)$

5. The void ratio, e, and the effective stress, σ', on the soil matrix have an explicit relationship represented by σ'= σ' (e).

6.1.2.3. Force equilibrium of REV

Considering the REV ABCD, as seen in Fig. 6.2, the vertical equilibrium of element is shown in Fig. 6.5. Assuming the REV is only subjected to gravity, then at equilibrium:

$$\frac{d\sigma}{dz} + F_w = 0 \tag{6.11}$$

where σ is the normal stress [$ML^{-1}T^{-2}$] (kPa), and F_w is the body force per unit volume (self-weight) [$ML^{-2}T^{-2}$], which can be expressed by the classic phase relationship in soil mechanics:

$$F_w = \frac{e\gamma_w + \gamma_s}{1 + e} \tag{6.12}$$

where γ_w is the unit weight of water, kN/m^3, γ_s is the unit weight of soil solid, kN/m^3.

Substituting Eq. 6.12 into Eq. 6.11:

$$\frac{d\sigma}{dz} + \frac{e\gamma_w + \gamma_s}{1 + e} = 0 \tag{6.13}$$

Multiplying dz/dξ for both sides of Eq. 6.13 to transfer the Eulerian coordinate system to the Lagrangian coordinate system:

$$\frac{d\sigma}{d\xi} + \left(\frac{e\gamma_w}{1 + e} + \frac{\gamma_s}{1 + e}\right)\frac{dz}{d\xi} = 0 \tag{6.14}$$

In Eq. 6.14, the term $\frac{\gamma_w}{1+e}$ refers to the weight changes in the fluid phase, and the term $\frac{\gamma_s}{1+e}$ refers to the weight changes of the solid phase.

6.1.2.4. Fluid continuity

During consolidation, the pore water is squeezed out from the soil matrix at a velocity v_w. The large strain consolidation theory allows the movement of soil particles relative to the fluid phase. The solid phase velocity is written as v_s, (v_s = dz/dt). As shown in Fig. 6.6, the weight of water inflow into the REV (ABCD) is

$$W_{in} = n(v_w - v_s)\gamma_w \tag{6.15}$$

where W_{in} is the weight of water inflow into REV, n is the porosity of the REV, v_w-v_s is the relative velocity of the water flow (m/s), γ_w is the unit weight of water.

Similarly, the weight of water outflow is

$$W_{out} = n(v_w - v_s)\gamma_w + \frac{d}{dz}n(v_w - v_s)\gamma_w dz \tag{6.16}$$

where W_{out} is the weight of water outflow from REV (ABCD).

Subtracting Eq. 6.15 from Eq.6.16, the net weight change of water in the REV (ABCD) is

$$\Delta W = W_{in} - W_{out} = -\frac{d}{dz}n(v_w - v_s)\gamma_w dz \tag{6.17}$$

Since the net weight change of water is equal to the rate of weight change in the void:

$$-\frac{d}{dz}n(v_w - v_s)\gamma_w dz = \frac{\partial}{\partial t}(e\gamma_w)$$

(6.18)

where $e\gamma_w$ is the weight change of the pore volume, since soil is saturated.

Multiplying both sides of Eq.6.18 by dz/dξ to convert the equation from the Eulerian coordinate system to the Lagrangian coordinate system:

$$\frac{d}{d\xi}n(v_w - v_s) + \frac{\partial}{\partial t}\left(\frac{e}{1+e}\frac{dz}{d\xi}\right) = 0$$

(6.19)

where n is the porosity of the REV, v_w-v_s is the relative velocity of the water flow, e is the void ratio of the REV.

The Darcy's law is incorporated in a form of the relative velocity of soil skeleton and pore fluid, which is related to the hydraulic gradient, i.e.,

$$n(v_w - v_s) = -k_h\frac{\partial h}{\partial z}$$

(6.20)

where k_h is the hydraulic conductivity [LT^{-1}] (m/s) of the REV, h is the total head (m), [L] of REV (ABCD), which can be expressed in terms of excess pore water pressure:

$$h = \frac{u_{ex}}{\gamma_w} + h_z$$

(6.21)

where u_{ex} is the excess pore water pressure (kPa) and h_z is elevation head, which is a constant.

Eq. 6.20 can be expressed in terms of excess pore water pressure by substituting Eq. 6.21 into Eq. 6.20:

$$n(v_w - v_s) = -\frac{k_h}{\gamma_w}\frac{du_{ex}}{dz}$$

(6.22)

Converting the above equation from the Eulerian coordinate system to the Lagrangian coordinate system:

$$n(v_w - v_s)\frac{dz}{d\xi} = -\frac{k_h}{\gamma_w}\frac{du_{ex}}{dz}\frac{dz}{d\xi}$$

(6.23)

Substituting Eq. 6.6 into Eq. 6.23:

$$n(v_w - v_s) = -\frac{1 + e_0}{1 + e}\frac{k_h}{\gamma_w}\frac{du_{ex}}{d\xi}$$

(6.24)

Substituting Eq. 6.24 into Eq. 6.19:

$$\frac{d}{d\xi}\left(-\frac{1 + e_0}{1 + e}\frac{k_h}{\gamma_w}\frac{du_{ex}}{d\xi}\right) + \frac{\partial}{\partial t}\left(\frac{e}{1 + e}\frac{dz}{d\xi}\right) = 0$$

(6.25)

According to the Terzaghi's effective stress law:

$$\sigma = \sigma' + u$$

(6.26)

where u is the pore water pressure (kPa), which consists of two parts:

$$u = u_{ex} + u_{hyd}$$

(6.27)

where u_{ex} is the excess pore water pressure (kPa) due to the external loading, and u_{hyd} is the hydrostatic water pressure (kPa).

Combining Eqs. 6.26 and 6.27, the excess pore water pressure u_{ex} can be written as:

$$u_{ex} = \sigma - \sigma' - u_{hyd} \tag{6.28}$$

Hence,

$$\frac{du_{ex}}{d\xi} = \frac{d\sigma}{d\xi} - \frac{d\sigma'}{d\xi} - \frac{du_{hyd}}{d\xi} \tag{6.29}$$

Since the hydrostatic pore water pressure is a function of depth:

$$\frac{du_{hyd}}{d\xi} = \frac{du_{hyd}}{dz}\frac{dz}{d\xi} = -\frac{d(\gamma_w z)}{dz}\frac{dz}{d\xi} = -\gamma_w \frac{dz}{d\xi} \tag{6.30}$$

The negative sign is taken because the direction of coordinate is opposite to that of gravity.

Substituting Eq. 6.30 into Eq. 6.29:

$$\frac{du_{ex}}{d\xi} = \frac{d\sigma}{d\xi} - \frac{d\sigma'}{d\xi} + \gamma_w \frac{dz}{d\xi} \tag{6.31}$$

Substituting Eq. 6.14 into Eq. 6.31:

$$\frac{du_{ex}}{d\xi} = -\frac{e\gamma_w + \gamma_s}{1+e}\frac{dz}{d\xi} - \frac{d\sigma'}{d\xi} + \gamma_w \frac{dz}{d\xi} \tag{6.32}$$

Substituting Eq. 6.32 into Eq. 6.25:

$$\frac{d}{d\xi}\left[-\frac{1+e_0}{1+e}\frac{k_h}{\gamma_w}\left(-\frac{e\gamma_w+\gamma_s}{1+e}\frac{dz}{d\xi}-\frac{d\sigma'}{d\xi}+\gamma_w\frac{dz}{d\xi}\right)\right]+\frac{\partial}{\partial t}\left(\frac{e}{1+e}\frac{dz}{d\xi}\right)=0$$

(6.33)

Rearranging Eq. 6.33:

$$\frac{d}{d\xi}\left[\frac{1+e_0}{(1+e)^2}\frac{e\gamma_w+\gamma_s}{\gamma_w}k_h\frac{dz}{d\xi}+\frac{1+e_0}{1+e}\frac{k_h}{\gamma_w}\frac{d\sigma'}{d\xi}-\frac{1+e_0}{1+e}k_h\frac{dz}{d\xi}\right]+\frac{\partial}{\partial t}\left(\frac{e}{1+e}\frac{dz}{d\xi}\right)=0$$

(6.34)

Substituting Eq. 6.6 into Eq. 6.34:

$$\frac{1}{\gamma_w}\frac{d}{d\xi}\left[\frac{\gamma_s-\gamma_w}{1+e}k_h+\frac{1+e_0}{1+e}k_h\frac{d\sigma'}{d\xi}\right]+\frac{1}{1+e_0}\frac{\partial e}{\partial t}=0$$

(6.35)

Equation 6.35 is the one-dimensional governing equation for Gibson's theory in the Lagrangian coordinate system.

To take advantage of the material coordinate system, Eq. 6.35 can be converted from the Lagrangian coordinate system to the material coordinate system via Eq. 6.8:

$$\frac{1}{\gamma_w}\frac{d}{ds}\left[\frac{\gamma_s-\gamma_w}{1+e}k_h+\frac{1}{1+e}k_h\frac{d\sigma'}{ds}\right]+\frac{\partial e}{\partial t}=0$$

(6.36)

It has been assumed that the hydraulic conductivity and effective stress on the soil matrix are expressed as functions of the void ratio, i.e. $k_h(e)$, and $\sigma'(e)$. Hence Eq.6.36 can be written as:

$$\left(\frac{\gamma_s}{\gamma_w}-1\right)\frac{d}{de}\left[\frac{k_h(e)}{1+e}\right]\frac{\partial e}{\partial s}+\frac{1}{\gamma_w}\frac{d}{de}\left[\frac{k_h(e)}{1+e}\left(\frac{d\sigma'}{de}\frac{\partial e}{\partial s}\right)\right]\frac{\partial e}{\partial s}+\frac{\partial e}{\partial t}=0$$

(6.37)

In Eq. 6.37, the first term attributed to self-weight consolidation and the second term to surcharge pressure.

As mentioned before, the coefficient of consolidation, C_v, of soils is assumed to be constant in Terzaghi's consolidation theory because of small strain. Gibson's theory (Eq. 6.37) releases the restrictions and allows for non-linearity of material properties by using the relations between the hydraulic conductivity and void ratio, as well as between the stress and strain (σ'-e). Thus, the soil behavior changes during consolidation are accounted for in solving Eq. 6.37 numerically.

6.1.3. One-dimensional electrokinetic consolidation theory (Feldkamp and Belhomme, 1990)

Feldkamp and Belhomme (1990) proposed one-dimensional large strain electrokinetic consolidation theory. In the derivation, a flux of water relative to the moving solid phase is generated by both the pore water pressure and a DC electric field (Feldkamp and Belhomme 1990). The flux is written as:

$$j_{rel}=-\frac{k}{\mu}\frac{\partial \psi}{\partial z}\pm nv_eE_z$$

(6.38)

where k is the intrinsic permeability [L^2] (m^2), μ is the liquid phase viscosity [$M^1L^{-1}T^{-1}$] (kg/(s·m)), ψ is porewater pressure [$ML^{-1}T^{-2}$] (kPa), E_z is the macroscopic electric field intensity [$M^1L^1T^{-3}I^{-1}$] (V/m), n is the volume fraction of water (the porosity of the soil), v_e is the average velocity of liquid phase relative to that of the moving solid phase [$M^{-1}T^{-2}I^{-1}$] (m^2/sV) (Feldkamp and Belhomme 1990).

The porewater pressure is calculated as:

$$\psi = u_{ex} + u_{hyd} = u_{ex} + \rho_w g z$$

(6.39)

where u_{ex} is excess pore water pressure (kPa), u_{hyd} is hydrostatic pressure, ρ_w is the density of water [ML^{-3}] (kg/m^3), z is the location (m) with the axis oriented vertically upward, g is the acceleration of gravity (m/s^2).

In the derivation by Feldkamp and Belhomme (1990), the effective stress is expressed as:

$$\sigma' = p_{ext} + \sigma - u$$

(6.40)

where p_{ext} is the constant gas pressure immediately above the deposit (kPa), σ is the total overburden stress at location z, and expressed as:

$$\sigma = \int_z^L \rho_b(z) g dz$$

(6.41)

where L is the thickness of deposit (m), which is related to the time, $\rho_b(z)$ is the bulk density of the soil (kg/m^3), which depends on the location z. Substituting Eq. 6.39 and 6.40 into Eq. 6.38, the flux of water relative to the moving solid phase is expressed as:

$$j_{rel} = -\frac{k}{\mu}\left[(\rho_b - \rho_w)g + \frac{\partial \sigma'}{\partial z}\right] \pm \frac{e}{(1+e)} v_e E_z$$

(6.42)

where the porosity, n, is expressed in terms of void ratio, e, as $n = \frac{e}{1+e}$

Similar to Eq. 6.18, in the derivation by Feldkamp and Belhomme (1990), a conservation equation is expressed in the material coordinates (s, t):

$$\frac{\partial e}{\partial t} = -\frac{\partial j_{rel}}{\partial s}$$

(6.43)

Substituting Eqs. 6.5 and 6.42 into Eq. 6.43, along with the assumption of negligible consolidation under self-weight (Feldkamp and Belhomme 1990), the governing equation for EK consolidation is expressed as:

$$-\frac{\partial e}{\partial t} = \frac{1}{\mu}\frac{\partial}{\partial s}\left(\frac{d\sigma'}{\partial s}\frac{k}{1+e}\right) - \frac{\partial}{\partial s}\left(\frac{e}{1+e}v_e E_z\right)$$

(6.44)

Based on the stress-strain (σ'-e) relation during consolidation:

$$\frac{d\sigma'}{\partial s} = \frac{d\sigma'}{\partial e}\frac{\partial e}{\partial s}$$

(6.45)

Defining α(e), which is the mechanical response of the soil skeleton:

$$\alpha(e) = -\frac{1}{1+e}\frac{de}{d\sigma'}$$

(6.46)

Instead using the voltage gradient, Feldkamp and Belhomme (1990) used the current density in the derivation:

$$i = i_s + \kappa E_z$$

(6.47)

where i is the current density [IL^{-2}] (A/m^2), κ is the electrical conductivity of soil [$M^{-1}L^{-2}T^3I^3$] (S/m), i_s is the streaming current and can be neglected (Feldkamp and Belhomme

1990). Substituting Eq. 6.44 to 6.47, the governing equation for EK consolidation can be written as:

$$\frac{\partial e}{\partial t} = \frac{1}{\mu}\frac{\partial}{\partial s}\left(\frac{k(e)}{\alpha(e)(1+e)^2}\frac{\partial e}{\partial s}\right) - i\frac{\partial}{\partial s}\left(\frac{e}{1+e}\frac{v_e(e)}{\kappa(e)}\right) \tag{6.48}$$

On the right side of Eq 6.48, the first term is the contribution from the external loading and second term represents electroosmotic consolidation.

In the Feldkamp and Belhomme (1990) theory, a parameter v_e , which is the average velocity of liquid phase relative to the moving solid phase, is used in governing equation (Eq. 6.48). However, the coefficient of electroosmotic permeability, k_e, (m^2/sV) [$M^{-1}T^{-2}I^{-1}$], is more widely used than v_e (Mitchell and Soga 2005). The coefficient of electroosmotic permeability, k_e, is equal to n*ve, which presents in Eq. 6.38. The coefficient of electroosmotic permeability, k_e, can be directly measured via experiments (Mitchell and Soga 2005, Mohamedelhassan and Shang 2001, Mohamedelhassan and Shang 2003, Guo and Shang 2014). In this study, therefore, k_e is used for all calculations and modelling.

6.1.4. Esrig (1968) theory for EK generated excess porewater pressure

Esrig (1968) presented a theory for EK induced excess pore water pressure. The theory has been widely used in many applications and consolidation theories to predict the pore water pressure generated via EK (Shang 1998, Michell and Soga 2005, Shang 2011, Jones et al. 2011, Malekzadeh et al. 2016).

The Esrig (1968) theory for EK induced excess porewater pressure assumed the fluid flow generated via an electrical field and hydraulic gradient can be superimposed to obtain the total flow. Therefore, the total flow through an incompressible soil mass under one-dimensional condition can be expressed as follows (Esrig 1968):

$$\frac{\partial v_{eo}}{\partial x} + \frac{\partial v_h}{\partial x} = 0$$

(6.49)

where v_{eo} is the velocity of water flow due to electroosmosis and v_h is the velocity of flow due to any excess porewater pressure gradient, and they can be determined as:

$$v_{eo} = k_e \frac{\partial U}{\partial x}$$

(6.50)

$$v_h = \frac{k_h}{\gamma_w} \frac{\partial u}{\partial x}$$

(6.51)

in which k_e is the coefficient of electroosmotic permeability (m^2/sV), $\frac{\partial U}{\partial x}$ is the voltage gradient (V/m), k_h is the hydraulic conductivity, and γ_w is the unit weight of water (9.8 kN/m^3).

Substituting Eq. 6.50 and 6.51 into Eq. 6.49:

$$k_e \frac{\partial^2 U}{\partial x^2} + \frac{k_h}{\gamma_w} \frac{\partial^2 u}{\partial x^2} = 0$$

(6.52)

Rearranging Eq. 6.52:

$$\frac{k_e \gamma_w}{k_h} \frac{\partial^2 U}{\partial x^2} + \frac{\partial^2 u}{\partial x^2} = 0$$

(6.53)

Introducing a dummy variable η:

$$\eta = \frac{k_e \gamma_w}{k_h} U + u$$

(6.54)

Thus, Eq. 6.52 is in form of Laplace' equation in one-dimensional system:

$$\frac{\partial^2 \eta}{\partial x^2} = 0$$

(6.55)

Integrating Eq. 6.55 once:

$$\frac{\partial \eta}{\partial x} = C_1$$

(6.56)

Integrating above equation once more:

$$\eta = xC_1 + C_2$$

(6.57)

where C_1 and C_2 are the constants, which can be solved via boundary conditions.

For the closed anode and open cathode with free access to water, the boundary conditions are (Esrig 1968):

A. Cathode: x=0, U=0, u=0, and therefore η =0

B. Anode: x=L, the velocity of flow is zero so that $\frac{\partial \eta}{\partial x} = 0$

Therefore, C_2=0 and C_1=0 is calculated by substituting boundary conditions A and B into Eq. 6.56 and 6.57. Thus, η =0 is obtained, and Eq. 6.54 becomes:

$$\eta = \frac{k_e \gamma_w}{k_h} U + u = 0$$

(6.58)

Hence, at the condition of closed anode and open cathode, the excess porewater pressure due to EK is expressed as:

$$u_{eo} = -\frac{k_e \gamma_w}{k_h} U(z) \tag{6.59}$$

where U(z) is the voltage at the location at distance x from the cathode.

In this study, an EK consolidation model is developed for oil sands, based on Gibson's large strain consolidation theory coupled with Esirg (1968) theory on EK generated excess pore water pressure. The consolidation by material self-weight is also considered in the model.

6.2. One-dimensional large strain EK consolidation model

6.2.1. Governing equation

The one-dimensional large strain EK consolidation model (LSEK-1D) is derived based on the Gibson's theory and Esrig (1968) theory.

Esrig (1968) expressed that the excess pore water pressure at time, t, approaching to infinity generated by electroosmosis is represented by Eq. 6.59 for closed anode and open cathode condition.

The derivation in this study involves several assumptions, which are listed as follows

1. Soil is saturated.
2. Soil is homogenous and isotropic.
3. Incompressible fluid and soil particles.
4. The hydraulic flow is described by: $q_h = k_h \frac{\partial H}{\partial z}$.

5. The effect of electroosmosis is expressed by the excess pore water pressure at time approaching to infinity, Eq. 6.59. Although the equation represents the condition of time approaching infinity, Lo et al. (1991) have found from experiments that the pore water pressure approached equilibrium as early as about 100 minutes after the electrical field was applied. Thus, it is assumed that the time for the electroosmotic excess pore water pressure satisfying Eq. 6.59 is much shorter than the time of consolidation.

6. The maximum porewater pressure generated by EK cannot exceed the atmosphere pressure due to the possible cavitation of water in soil pores.

7. The hydraulic conductivity k_h is a function of void ratio, i.e., $k_h=k_h(e)$.

8. The soil void ratio, e, is a function of the effective stress, σ': $e = e(\sigma')$.

9. The effect of electrophoresis is negligible during EK consolidation.

The coordinate systems used for this study are Eulerian, Lagrangian and material coordinate system, the same as those in the Gibson's theory.

For the force equilibrium and fluid continuity, Eqs. 6.14 and 6.25 are presented again for convenience of discussion:

$$\frac{d\sigma}{d\xi}+\left(\frac{e\gamma_w}{1+e}+\frac{\gamma_s}{1+e}\right)\frac{dz}{d\xi}=0 \tag{6.14}$$

$$\frac{d}{d\xi}\left(-\frac{1+e_0}{1+e}\frac{k_h}{\gamma_w}\frac{du_{ex}}{d\xi}\right)+\frac{\partial}{\partial t}\left(\frac{e}{d\xi}\right)=0 \tag{6.25}$$

The excess pore water pressure generated by EK, u_{ex}, for top closed anode and bottom open cathode condition, is

$$u_{ex}=\sigma-\sigma'-u_{hyd}+u_{eo}$$

(6.60)

Substituting Eq. 6.59 into Eq. 6.60, the differential form for u_{ex} is expressed as:

$$\frac{du_{ex}}{d\xi} = \frac{d\sigma}{d\xi} - \frac{d\sigma'}{d\xi} + \gamma_w \frac{dz}{d\xi} - \frac{k_e}{k_h}\gamma_w \frac{dU(z)}{dz}\frac{dz}{d\xi}$$

(6.61)

where $\frac{dU(z)}{dz}$ is applied voltage gradient, E (V/m).

Substituting Eq.6.14 into Eq.6.61:

$$\frac{du_{ex}}{d\xi} = -\frac{e\gamma_w + \gamma_s}{1+e}\frac{dz}{d\xi} - \frac{d\sigma'}{d\xi} + \gamma_w \frac{dz}{d\xi} - \frac{k_e}{k_h}\gamma_w E \frac{dz}{d\xi}$$

(6.62)

Substituting Eq. 6.62 into Eq. 6.25:

$$\frac{d}{d\xi}\left[-\frac{1+e_0}{1+e}\frac{k_h}{\gamma_w}\left(-\frac{e\gamma_w + \gamma_s}{1+e}\frac{dz}{d\xi} - \frac{d\sigma'}{d\xi} + \gamma_w \frac{dz}{d\xi} - \frac{k_e}{k_h}\gamma_w E \frac{dz}{d\xi}\right)\right] + \frac{\partial}{\partial t}\left(\frac{e}{1+e}\frac{dz}{d\xi}\right) = 0$$

(6.63)

Simplifying above equation by the same procedure discussed in previous section for the derivation of the Gibson's theory, one may obtain the governing equation for one-dimensional large strain electroosmotic consolidation in the Lagrangian coordinate system:

$$\frac{1}{\gamma_w}\frac{d}{d\xi}\left[\frac{\gamma_s - \gamma_w}{1+e}k_h + \frac{1+e_0}{1+e}k_h\frac{d\sigma'}{d\xi} + \frac{1+e_0}{1+e}k_e\gamma_w E\frac{dz}{d\xi}\right] + \frac{1}{1+e_0}\frac{\partial e}{\partial t} = 0$$

(6.64)

To further simply above equation, the material coordinate system can be used via substituting Eq.6.6 and 6.8 into Eq. 6.64:

$$\frac{1}{\gamma_w}\frac{d}{ds}\left[\frac{\gamma_s-\gamma_w}{1+e}k_h+\frac{1}{1+e}k_h\frac{d\sigma'}{ds}+k_e\gamma_w E\right]+\frac{\partial e}{\partial t}=0$$

(6.65)

Eq. 6.65 is rearranged:

$$\left(\frac{\gamma_s}{\gamma_w}-1\right)\frac{d}{de}\left[\frac{k_h(e)}{1+e}\right]\frac{\partial e}{\partial s}+\frac{1}{\gamma_w}\frac{d}{de}\left[\frac{k_h(e)}{1+e}\left(\frac{d\sigma'}{de}\frac{\partial e}{\partial s}\right)\right]\frac{\partial e}{\partial s}+\frac{d}{de}(k_e E)\frac{\partial e}{\partial s}+\frac{\partial e}{\partial t}=0$$

(6.66)

In the process of one-dimensional electrokinetic consolidation, if the current control method is used, the current density is kept constant. Eq. 6.66 can be written in terms of the current density, i, via the relationship between the current density, i, and voltage gradient, E:

$$i=\kappa(e)E$$

(6.67)

where κ(e) is the electrical conductivity of soil, which is a function of void ratio, e. Substituting Eq. 6.67 to Eq. 6.66:

$$\left(\frac{\gamma_s}{\gamma_w}-1\right)\frac{d}{de}\left[\frac{k_h(e)}{1+e}\right]\frac{\partial e}{\partial s}+\frac{1}{\gamma_w}\frac{d}{de}\left[\frac{k_h(e)}{1+e}\left(\frac{d\sigma'}{de}\frac{\partial e}{\partial s}\right)\right]\frac{\partial e}{\partial s}+i\frac{d}{de}\left[\frac{k_e}{\kappa(e)}\right]\frac{\partial e}{\partial s}+\frac{\partial e}{\partial t}=0$$

(6.68)

Eq. 6.68 is the governing equation for one-dimensional large strain consolidation model of EK (LSEK-1D) under a constant current density. The model can incorporate surcharge loading and be solved numerically with specifically defined initial and boundary conditions.

6.2.2. Initial and boundary conditions

One initial condition and two boundary conditions are essential to solve Eq. 6.68, which are discussed below.

6.2.2.1. Initial condition

The initial void ratio distribution in the sample depends on the initial status of MFT. Two conditions for the void ratio distribution of MFT are the uniform distribution and distribution after self-weight consolidation. In the first condition, the void ratio of MFT is constant in the system. This condition is applicable shortly after deposition of MFT. This condition is adapted in the experiments and modeling in this study. The second condition is encountered long after deposition of MFT, in this case the void ratio of MFT decreases with depth.

6.2.2.2. Boundary conditions

Two boundary conditions are adapted in experiments and modeling, i.e., a free-drainage boundary and an impermeable boundary.

The free-drainage boundary is at the cathode, where the excess pore water pressure is atmosphere pressure. The void ratio, e, at the free-drainage boundary is calculated based on the effective stress, σ', at the boundary, generated by the surcharge pressure. The impermeable boundary is at the anode. Since there is no seepage flow:

$$v_w - v_s = 0 \tag{6.69}$$

Substituting Eq.6.69 to Eq.6.24:

$$\frac{du_{ex}}{d\xi} = 0 \tag{6.70}$$

Substituting Eq. 6.70 into Eq. 6.62:

$$-\frac{e\gamma_w + \gamma_s}{1+e}\frac{dz}{d\xi} - \frac{d\sigma'}{d\xi} + \gamma_w \frac{dz}{d\xi} - \frac{k_e}{k_h}\gamma_w \frac{\partial U}{\partial \xi} = 0$$

(6.71)

Substituting Eq.6.6 to 6.8 to Eq. 6.71, then

$$\frac{d\sigma'}{ds} + (\gamma_s - \gamma_w) + \frac{k_e}{k_h}\gamma_w \frac{\partial U}{\partial s} = 0$$

(6.72)

Reorganize Eq. 6.72 by multiplying $\frac{de}{d\sigma'}$ on both sides:

$$\frac{de}{ds} + \frac{(\gamma_s - \gamma_w) + \frac{k_e}{k_h}\gamma_w \frac{\partial U}{\partial s}}{\frac{d\sigma'}{de}} = 0$$

(6.73)

Eq. 6.73 is the boundary condition for the impermeable boundary at the anode.

6.2.2.3. Settlement

The settlement of the tailing sample at any time, t, in Eulerian coordinate system can be calculated via the following equation:

$$S(t) = H_0 - \int_0^S [1 + e(s,t)]ds$$

(6.74)

where H_0 is the initial height of the sample in Eulerian coordinate system, S is the sample height in material coordinate system, e(s,t), is the sample void ratio at location, s, and time, t, in material coordinate system, and ds is the thickness of the layer in material coordinate system.

6.2.3. Experimental results for model verification

The model was verified and validated via experimental results on oil sands tailings, including the consolidation tests under 5 kPa alone and EK tests combined with 5kPa surcharge (DW tests). The experiments were carried in 1-D condition with the horizontally installed electrodes and reported in a M.Esc thesis by Guo (2012). The anode and cathode were placed at the top and bottom, respectively. The detailed experiments were described by Guo (2012) and Guo and Shang (2014). The conditions for modeling analysis are summarized in Table 6.1.

6.2.3.1. Boundary consideration and initial condition

In the first part of analysis, the oil sands tailings were consolidated via 5 kPa surcharge under two-way drainage.

In the second part of analysis, a surcharge pressure and EK were applied simultaneously. The configuration of the experiments is closed anode and open cathode, and water was driven from anode and drained from the cathode. Thus, the boundary conditions are the impermeable boundary at anode and free drainage boundary at the cathode.

As discussed before the initial condition is that the MFT has a constant void ratio of 4.3 (corresponding to a water content of 170% and solid content of 37%).

6.2.3.2. Constitutive relationship of void ratio and hydraulic conductivity

To solve Eq. 6.68, two relationships, i.e., void ratio-effective stress (e-σ'), and void ratio-hydraulic conductivity (e-k_h), are essential for the consolidation under surcharge. In addition, two constitutive relationships are needed for EK consolidaiton, i.e., void ratio-coefficient of electroosmotic permeability (e-k_e), and void ratio- electrical conductivity (e-κ).

The constitutive relationships for e-σ' and e-k_h have been reported by many researchers (Somogyi 1980, Suthaker 1995, Berilgen et al. 2006, Jeeravipoolvarn et at. 2008, and Bo et al. 2011). One of the commonly used relationships is presented in the forms of (Fox 2000, Jeeravipoolvarn et at. 2008, Ito and Azam 2013):

$$e = A\sigma'^{B} \tag{6.75}$$

$$k_h = Ce^{D} \tag{6.76}$$

where A, B, C, and D are parameters determined through experiments.

The Hydraulic conductivity of tailings has a wide range, depending on the void ratio. Jeeravipoolvarn (2010) measured the hydraulic conductivity of three types of oil sands tailings at different void ratio and reported piecewise regression relationships. It was also reported that the hydraulic conductivity of oil sand tailings was similar when the void ratio below about 3.

For oil sands tailings (MFT-A) studied in this research, the hydraulic conductivity k_h was measured at the void ratios from 0.9 to 3. It was noted that the measured hydraulic conductivity is consistent to the regression relationship by Jeeravipoolvarn (2010). In order to predict the relationship between hydraulic conductivity and void ratio (from 0.5 to 5) of oil sands tailings, the following equation is used by considering both experimental results from this analysis and data from Jeeravipoolvarn (2010), as seen in Fig. 6.7:

$$k_h = 6.00\times10^{-11}e^{3.91} \tag{6.77}$$

The relationship between the void ratio and effective stress is expressed based on the oedometer test on oil sands tailings, as seen in Fig. 6.8:

$$e = 2.40\sigma'^{-0.193} \tag{6.78}$$

Constitutive relationships for e-k_e and e-κ are obtained through regression of experiment data during EK dewatering tests, as seen in Figs. 6.9 and 6.10, and expressed as:

$$k_e = 0.00160\left(\frac{e}{1+e}\right)^{18.4} \tag{6.79}$$

$$\kappa = 0.689\left(\frac{e}{1+e}\right)^{7.21} \tag{6.80}$$

6.2.3.3. Model solution and verification

The finite difference method was selected to solve the large strain consolidation (Eq. 6.68). The detailed finite difference scheme is shown in Appendix 2 and the corresponding MATLAB code in Appendix 3.

Firstly, the model was verified and validated with the consolidation experiment under a surcharge of 5 kPa without applying EK treatment to ensure the model converging with Gibson's large strain consolidation theory. The input parameters are summarized in Table 6.2. For comparison, the normalized water discharge, V_w/V_0, and normalized sample height, H_t/H_0, were used, where V_w is the volume of water discharge, V_0 is the initial volume of sample, H_t is the height of the sample at consolidation time, t, H_0 is the initial height of the sample. The initial void ratio of 4.3 and average height of sample of 11 cm reported by Guo and Shang (2014) were used in the analysis. Fig. 6.11 shows the experimental results and model prediction during consolidation of oil sands tailings (MFT-A). It shows that the model is in agreement with experimental results in terms of the consolidation rate under the 5 kPa surcharge from 0 to 100 hours. At the end of consolidation (about 300 hours), the model slightly overestimated the total settlement, i.e. the normalized height, H_t/H_0(%), obtained through experiments was 54.1% (5.1 cm settlement) at 425 hours, while it was 51.3% (5.4 cm settlement) from model prediction. The difference between the model prediction and experimental result is 2.8%. In comparison with the experimental results, both the consolidation rate and final vertical strain were well predicted in the LSEK model under surcharge loading

In the 2nd step of validation, the experimental results reported by Guo and Shang (2014) were used to validate the proposed LSEK-1D model. The electrical current densities used in the analysis were 15 A/m^2, 10A/m^2 and 5A/m^2. The initial void ratio of 4.3 and average height of sample of 11 cm were used in the analysis. The input parameters of the model are listed in Table 6.3.

Figs. 6.12 to 6.14 show the model prediction and the experimental results for tests DW10, DW15 and DW5 respectively, reported by Guo and Shang (2014). It is observed that, from 0 to 25 hours, the experimental results are above the solid line, which are calculated through the model, as seen in Fig. 6.12(a). This indicates at the beginning of the test the rate of EK consolidation (1.5%/hr) is lower in the model prediction than those from experiments (2.3%/hour) at the current density of 10A/m^2. On the other hand, the model is in agreement with experimental results in terms of the final settlement, as shown in Fig. 6.12(b). The final settlement is 5.5 cm (H_t/H_0=51.4%), as calculated through the model, and 5.4 cm (H_t/H_0=50.7%), as observed in test DW10. The difference between the model prediction and experimental result is 0.7%. It is also noted that the rate of consolidation from model analysis reduces after about 25 hours, which is consistent with the experimental result.

Similar results are found on the test at current density of 15A/m^2. A slightly lower EK consolidation rate is observed in first 10 hours, as seen in Fig. 6.13(a), i.e., the strain rates due to EK consolidation are 2.2%/hour from model prediction and 3.0% from experimental result. The final settlement was 5.4 cm (H_t/H_0=50.9%) from test DW15 and 5.3 cm (H_t/H_0=51.5%) from model prediction, as shown in Fig. 6.13(b). The difference between the model prediction and experimental result is 0.6%. The model predicted that the settlement rate reduces after 25 hours, which is consistent with the experiment result.

For the current density of 5 A/m^2, the model is in excellent agreement on the consolidation rate from 0 to about 20 hours. Then the consolidation rate reduces from 25 to 50 hours, which again is consistent with experimental results. On the other hand, the final settlement predicted from the model was 5.4 cm (H_t/H_0=51.2%), which is higher than that obtained in the experiments, i.e. 3.5 cm (H_t/H_0=67.8%). The difference between the model prediction and experimental result is 16.6%.

In conclusion, the LSEK-1D model is in consistence with experimental results from EK consolidation tests at current density of 10 A/m^2 and 15 A/m^2. For the experiment at current density of 5 A/m^2, the model predicted higher settlement than the experimental observation. The overall performance of LSEK-1D model has shown to be satisfactory in predicting the rate and magnitude of settlement based on laboratory test results.

6.2.4. Discussion

6.2.4.1. Effects of initial height on consolidation time

In the Terzaghi's consolidation theory, the consolidation time is proportional to H_{dr}^2, where H_{dr} is the drainage path. With the large strain consideration, the drainage path decreases with time, leading to expedite the rate of consolidation (Gibson et al. 1981, Fox and Berles 1997, Fox and Pu 2012). Bromwell (1984) suggested that the consolidation time is proportional to $H_{dr}^{1.3}$ instead of H_{dr}^2 in the large strain analysis. In this analysis, the effects of initial drainage path on the LSEK-1D model performance are examined under conditions of surcharge alone and EK combined with surcharge loading.

In the first scenario of consolidation under surcharge alone, the drainage path is half of the sample height, H_0, because of two-way drainage from the top and bottom of the sample. An initial sample void ratio of 4 and a surcharge of 5 kPa were used in the analysis. The input parameters are listed in Table 6.4. Figs. 6.15 and 6.16 show the average degree of consolidation of the sample versus time at different initial height. The average degree of consolidation is calculated as:

$$U_{av} = \frac{S(t)}{S_{max}} \tag{6.81}$$

where S(t) is the settlement at consolidation time, t, and S_{max} is the maximum consolidation settlement.

As seen in Fig. 6.15, the time to reach the end of consolidation is over 300 hours (12.5 days) and 6000 hours (250 days) for the samples with initial heights of 0.1 and 0.5 m, respectively. Once the initial height increased to 2 m, the model predicted that the time to reach the end of the consolidation is over 2000 days (5.5 years) as seen in Fig. 6.16. The consolidation times at 30%, 50%, 70% and 90% consolidation is plotted with the initial drainage path in Fig. 6.17. It is shown that the consolidation time is proportional to $H_{dr}^{1.84}$ in average for oil sands tailings. Compared with the Terzaghi's consolidation theory, the large strain consolidation theory predicted a slightly higher rate of consolidation.

For consolidation under EK combined with surcharge, the drainage path is the height of the sample (one way drainage) because water is driven from anode and discharged at the cathode. An initial void ratio 4, current density $10A/m^2$ and surcharge of 5 kPa were used in the study. The detailed input parameters are summarized in Table 6.5. Fig. 6.18 shows the average degree of consolidation versus treatment time for EK combined with surcharge treatment. As shown in the figure, EK accelerated consolidation, which completed in about 100 hours (4.2 days) for 0.1m thick sample, which is three times faster than that only under 5 kPa alone. In the model prediction, for a sample with the initial height of 0.5 m, the time to complete consolidation is about 500 hours (21 days), which is over 10 times faster than the surcharge alone (250 days).

For better understanding of the influence of drainage path on EK consolidation, the consolidation times at 30%, 50%, 70% and 90% degrees of consolidation are plotted with the initial drainage path in Fig. 6.19. It can be seen that the time of EK consolidation is proportional to $H_{dr}^{1.12}$ (in average). Based on the small strain EK consolidation theory, the consolidation time is proportional to H_{dr}^2 (Wang and Mitchell 1967, Mitchell and Soga 2005). The LSEK-1D model developed in this study has shown that consolidation is much faster, considering nonlinearity of tailings properties, i.e., hydraulic conductivity, k_h, effective stress, σ', coefficient of electroosmotic permeability, k_e, and electrical conductivity, κ.

In conclusion, the application of EK can significantly reduce the consolidation time of oil sands tailings. The consolidation time is proportional to $H_{dr}^{1.12}$ for EK accelerated consolidation, compared to $H_{dr}^{1.84}$ under surcharge alone.

6.2.4.2. Effect of applied current density on EK consolidation time

The effect of applied current density on consolidation time as predicted in LSEK-1D model is analyzed similar to Section 6.2.4.1, the analysis used an initial void ratio 4, initial height of 15 cm and a surcharge of 5 kPa. The input parameters are summarized in Table 6.6. Fig. 6.20 shows the predicted water drainage and sample height change under current densities from 5 A/m^2 to 20 A/m^2. The average degrees of EK consolidation are plotted versus time in Fig. 6.21. The predicted times to complete consolidation were over 500 hours (21 days) for 5A/m^2 and 90 hours (3.75 days) for 20 A/m^2, for 15 cm thick tailings. The consolidation times at 30%, 50%, 70% and 90% degrees of consolidation are plotted with current density in Fig. 6.22. It is noticed that the time for EK consolidation is proportional to $i_c^{-0.94}$ in average, where i_c is current density (A/m^2). The results indicate that the high current density can shorten the treatment time, which has been observed in experiments. On the other hand, it should be recognized that electrochemical reactions at electrodes, as well as heating, are not considered in the LSEK-1D. Heating is more severe at higher current density, which reduces the efficiency of EK consolidation and dewatering.

6.3. Conclusion

In this study, a one-dimensional large strain EK consolidation model (LSEK-1D) is established via combining the Gibson (1967) large strain consolidation theory and Esrig (1968) EK excess pore water pressure theory. The governing equation was solved via finite difference method in MATLAB code. The following conclusions are drawn from the analysis:

1. The LSEK-1D model was assessed on experimental results on oil sands tailings, and a good consistency has been found between the model prediction and laboratory experimental results.

- For the consolidation under surcharge only

The LSEK-1D model predicted the total settlement of 5.4 cm (H_t/H_0=51.3%), while the settlement obtained in experiment was 5.1 cm (H_t/H_0=54.1%) for the sample with the initial height of 11cm. The LSEKS-1D for surcharge alone is in agreement with the experiment data for both consolidation time and final settlement.

- For consolidation under EK combined with surcharge

Generally, the LSEK-1D model is in consistence with experimental results for consolidation of MFT under EK combined with 5 kPa surcharge. The model predicted a slightly smaller EK consolidation rate at the beginning of EK treatment, whereas is in agreement on final consolidation settlement.

2. The LSEK-1D model predicted that the consolidation time is proportional to $H_{dr}^{1.84}$, where H_{dr} is initial drainage path, for oil sands tailings under surcharge alone. With EK treatment, the consolidation time of oil sands tailings is proportional to $H_{dr}^{1.12}$, based on the LSEK-1D model.

3. The model predicted that the consolidation time is proportional to $i_c^{-0.94}$ in average, where i_c is current density (A/m^2).

References

Bartholomeeusen G., Sills, G.C., Znidarčić, D., Van Kesteren, W., Merckelbach, L.M., Pyke, R., Carrier III, W.D., Lin, H., Penumadu, D., Winterwerp, H., Masala, S. and Chan, D. (2002). Sidere: numerical prediction of large-strain consolidation. Géotechnique, 52, No. 9, 639-648.

Berilgen, S. A., Berilgen, M. M., and Ozaydin, I. K. (2006). Compression and permeability relationships in high water content clays. Applied Clay Science, 31, No. 3, 249-261.

Biot, M. A. (1941). General theory of three- dimensional consolidation. Journal of applied physics, 12, No. 2, 155-164.

Bo, M. W., Choa, V., Wong, K. S., and Arulrajah, A. (2011). Laboratory validation of ultra-soft soil deformation model. Geotechnical and Geological Engineering, 29, No. 1, 65-74.

Bromwell, L.G. (1984). Consolidation of mining wastes. Sedimentation consolidation models: predictions and validation: In proceedings of a symposium, R.N. Yong and F.C. Townsend Eds, ASCE, New York, 275-295.

Cargill, K. W. (1982). Consolidation of soft layers by finite strain. U.S. Army Engineer Waterways Experimentation Station. Vicksburg, Mississippi, Miscellaneous Paper GL-82-3.

Das, B. M. (2013). Advanced soil mechanics. CRC Press.

Esrig, M.I. (1968). Pore pressures, consolidation and electrokinetics. Journal of the Soil Mechanics and Foundations Division, ASCE 94, No. SM4, 899–921.

Fox, P. J. (2000). CS4: A large strain consolidation model for accreting soil layers. In Geotechnics of high water content materials. ASTM International.

Fox, P. J., and Berles, J. D. (1997). CS2: A piecewise‐linear model for large strain consolidation. International Journal for Numerical and Analytical Methods in Geomechanics, 21, No. 7, 453-475.

Fox, P. J., and Pu, H. (2011). Enhanced CS2 model for large strain consolidation. International Journal of Geomechanics, 12, No. 5, 574-583.

Feldkamp, J. R., and Belhomme, G. M. (1990). Large-strain electrokinetic consolidation: theory and experiment in one dimension. Geotechnique, 40, No. 4, 557-568.

Gibson, R.E., England, G.L. and Hussey M.J.L. (1967). The theory of one-dimensional consolidation of saturated clays. I. Finite non-linear consolidation of thin homogeneous layers. Géotechnique, 17, No. 3, 261–273.

Gibson, R. E., Schiffman, R. L., and Cargill, K. W. (1981). The theory of one-dimensional consolidation of saturated clays. II. Finite nonlinear consolidation of thick homogeneous layers. Canadian geotechnical journal, 18, No. 2, 280-293.

Guo, Y. and Shang, J.Q. (2014). A study on electrokinetic dewatering of oil sands tailings. Environmental Geotechnics, 1, No.2, 121-134.

Guo, Y. (2012). Electrokinetic dewatering of oil sands tailing. MEsc. Thesis, The University of Western Ontario London.

Ito, M., and Azam, S. (2013). Large-strain consolidation modeling of mine waste tailings. Environmental Systems Research, 2, No. 1, 7.

Jeeravipoolvarn, S. (2010). Geotechnical behavior of in-line thickened oil sands tailings. PhD thesis, University of Alberta, Edmonton, Alberta.

Jeeravipoolvarn, S., Chalaturnyk, R. J., and Scott, J. D. (2008). Consolidation modeling of oil sands fine tailings: History matching. In Proceedings of 61st Canadian Geotechnical Conference, Edmonton, AB, September, 22-24.

Jones, C. J., Lamont-Black, J., and Glendinning, S. (2011). Electrokinetic geosynthetics in hydraulic applications. Geotextiles and Geomembranes, 29, No. 4, 381-390.

Lee, K., and Sills, G. C. (1981). The consolidation of a soil stratum, including self‐weight effects and large strains. International journal for numerical and analytical methods in geomechanics, 5, No. 4, 405-428.

Lo, K. Y., Inculet, I. I., and Ho, K. S. (1991). Electroosmotic strengthening of soft sensitive clays. Canadian Geotechnical Journal, 28, No.1, 62-73.

Malekzadeh, M., Lovisa, J., and Sivakugan, N. (2016). An overview of electrokinetic consolidation of soils. Geotechnical and Geological Engineering, 34, No. 3, 759-776.

Mitchell, J. K., and Soga, K. (2005). Fundamentals of soil behavior. John Wiley and Sons, Hoboken, New Jersey, USA.

Mohamedelhassan E and Shang JQ (2001). Effects of electrode materials and current intermittence in electroosmosis. Ground Improvement 5, No. 1, 3–11.

Mohamedelhassan, E., and Shang, J. Q. (2003). Electrokinetics-generated pore fluid and ionic transport in an offshore calcareous soil. Canadian Geotechnical Journal, 40, No. 6, 1185-1199.

Shang, J. Q. (1998). Electroosmosis-enhanced preloading consolidation via vertical drains. Canadian Geotechnical Journal, 35, No. 3, 491-499.

Shang, J. Q. (2011). Electrokinetics: engineering applications and recent development. In Advances in Unsaturated Soil, Geo-Hazard, and Geo-Environmental Engineering, GSP 217.

Somogyi, F. (1980). Large strain consolidation of fine grained slurries. Presented at the Canadian Society for Civil Engineering, Winnipeg, Manitoba, May 29-30.

Suthaker, N. N. (1995). Geotechnics of oil sand fine tailings, Ph.D. thesis, Department of Civil and Environmental Engineering, University of Alberta, Edmonton, AB.

Terzaghi, K. (1943). Theory of consolidation. John Wiley & Sons, Inc.

Table 6.1 The conditions for the large strain consolidation model of oil sands tailings

Conditions	Consolidation under surcharge	EK consolidation
Surcharge (kPa)	5 kPa	5 kPa
Applied current density (A/m^2)	0	5 to 20
Drainage condition	Two-way drainage	One way drainage (from anode to cathode)
Boundary condition	Free drainage condition at both the top and bottom	Impervious drainage condition at the anode Free drainage condition at the Cathode
Initial condition	Uniform distributed void ratio	

Table 6.2 Input parameters for model verification of 5 kPa surcharge consolidation

Parameters	
Unit weight of soil solid, γ_s (kN/m^3)	25.1
Unit weight of water, γ_w (kN/m^3)	9.81
Initial height of sample, H_0 (m)	0.11
Surcharge loading, P_s (kPa)	5
Initial void ratio, e_0	4.3
Current density, i_c (A/m^2)	0

Table 6.3 Input parameters for model verification of EK combined with 5 kPa surcharge consolidation

Parameters	
Unit weight of soil solid, γ_s (kN/m^3)	25.1
Unit weight of water, γ_w (kN/m^3)	9.81
Initial height of sample, H_0 (m)	0.11
Surcharge loading, P_s (kPa)	5
Initial void ratio, e_0	4.3
Current density, i_c (A/m^2)	10 and 15

Table 6.4 Input parameters for analysis of initial height effects on large strain consolidation with surcharge alone

Parameters	
Unit weight of soil solid, γ_s (kN/m^3)	25.1
Unit weight of water, γ_w (kN/m^3)	9.81
Initial height of sample, H_0 (m)	0.1; 0.2; 0.3; 0.4; 0.5; 0.75; 1.0; 1.25; 1.5; 2.0
Surcharge loading, P_s (kPa)	5
Initial void ratio, e_0	4.0
Current density, i_c (A/m^2)	0

Table 6.5 Input parameters for analysis of initial height effects on large strain consolidation with EK combined with surcharge loading

Parameters	
Unit weight of soil solid, γ_s (kN/m^3)	25.1
Unit weight of water, γ_w (kN/m^3)	9.81
Initial height of sample, H_0 (m)	0.1; 0.25; 0.5; 1.0; 2.0
Surcharge loading, P_s (kPa)	5
Initial void ratio, e_0	4.0
Current density, i_c (A/m^2)	10

Table 6.6 Input parameters for analysis of effects of applied current density on large strain consolidation with EK combined with surcharge loading

Parameters	
Unit weight of soil solid, γ_s (kN/m^3)	25.1
Unit weight of water, γ_w (kN/m^3)	9.81
Initial height of sample, H_0 (m)	0.15
Surcharge loading, P_s (kPa)	5
Initial void ratio, e_0	4.0
Current density, i_c (A/m^2)	5; 10; 15; 20

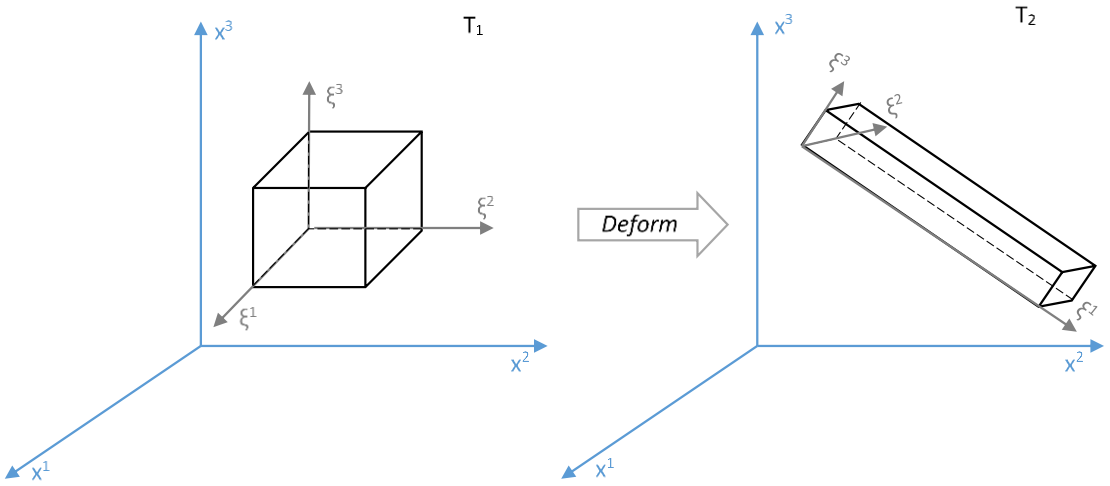

Figure 6.1Deformation of Lagrangian and Eulerian coordinate systems

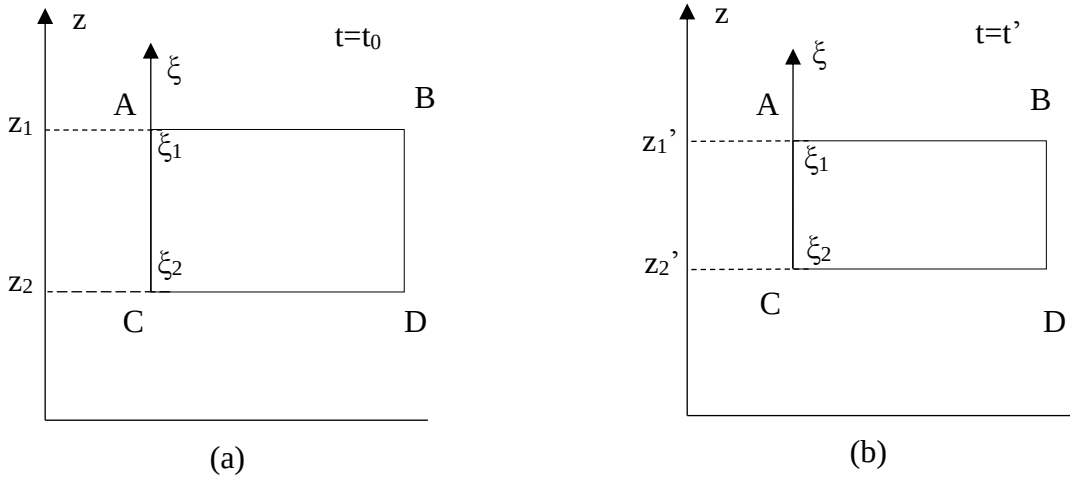

Figure 6.2 The deformation of body ABCD from t_0 to t' in the Eulerian (spatial) and Lagrangian coordinate systems

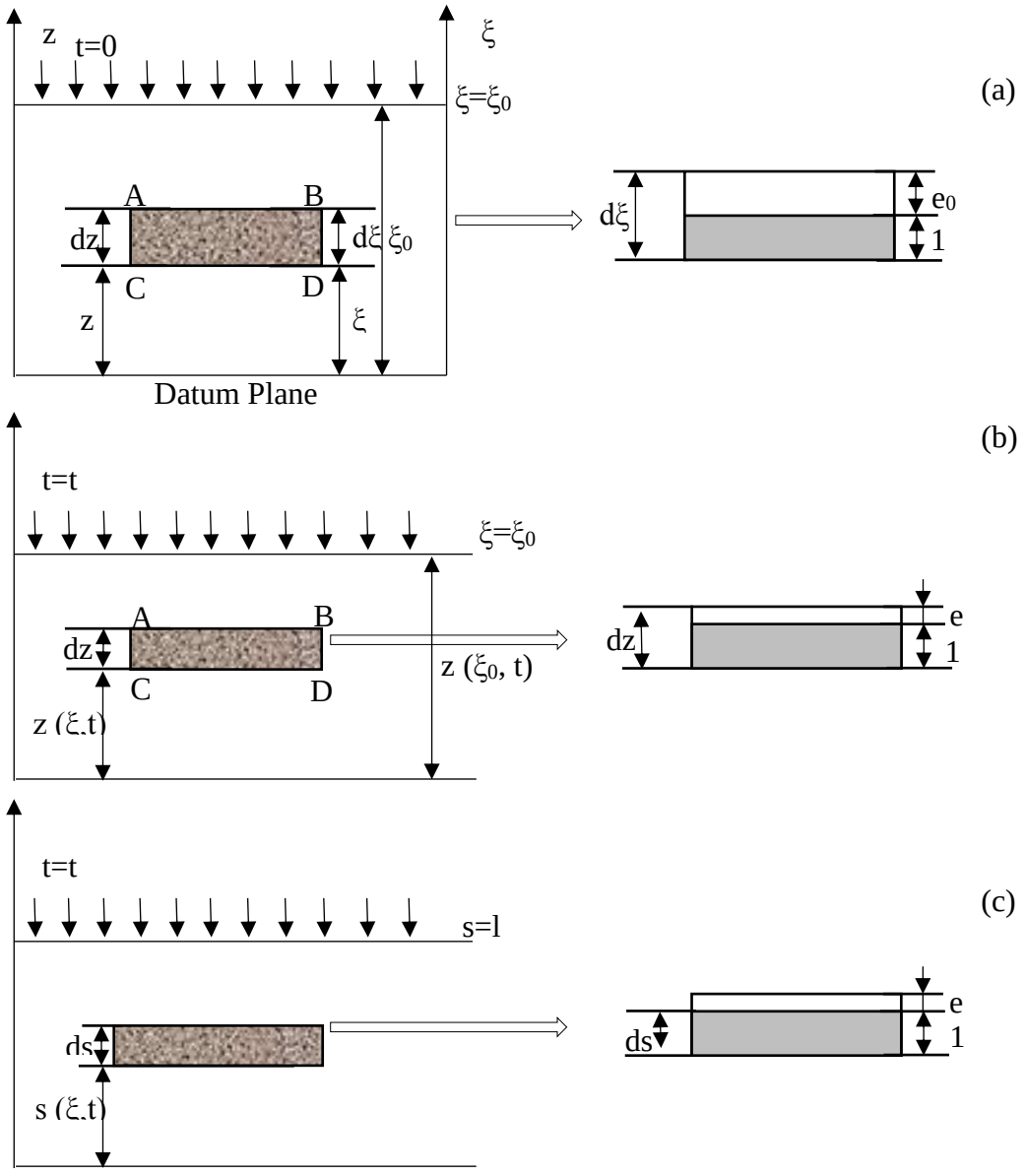

Figure 6.3 Coordinate system used in Gibson's theory (a) the Eulerian and Lagrangian coordinate system at initial time; (b) the Eulerian coordinate system at an arbitrary time, t; (c) the material coordinate system defined in Gibson's theory

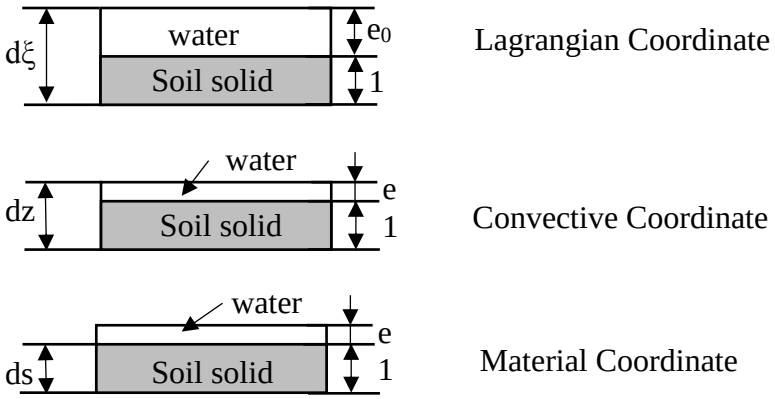

Figure 6.4 Soil phase volume relationship for REV ABCD

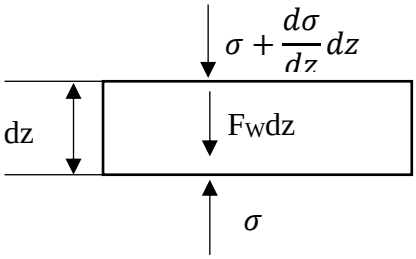

Figure 6.5 Force Equilibrium for REV

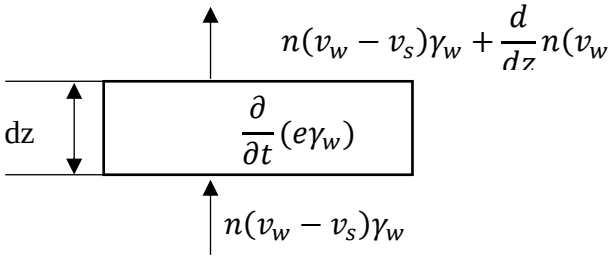

Figure 6.6 Fluid Continuity of REV ABCD

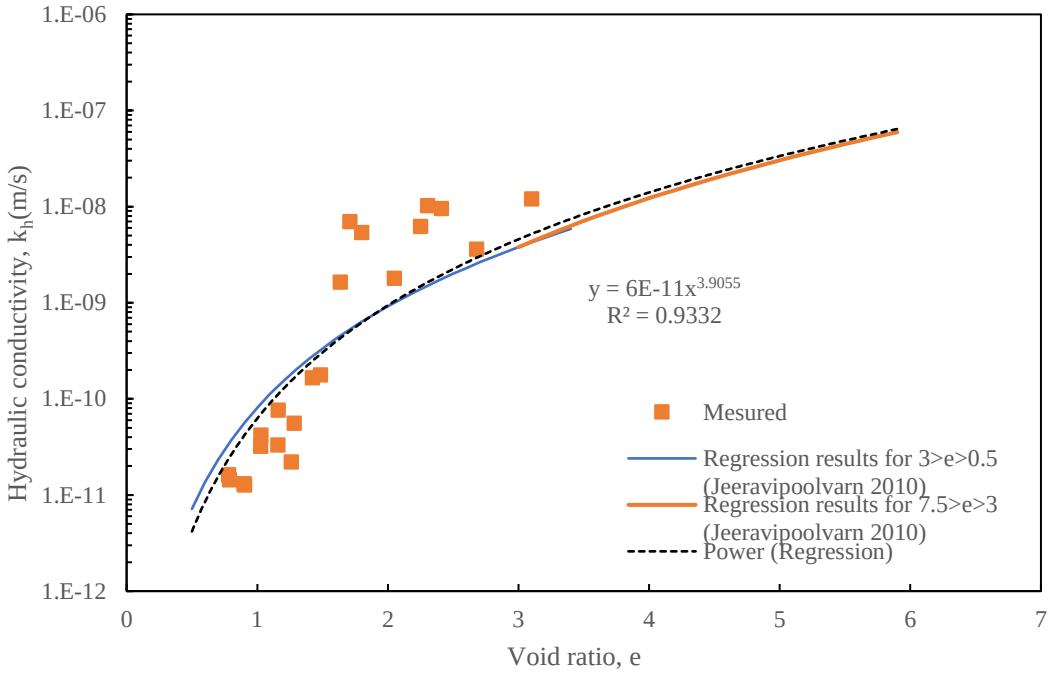

Figure 6.7 Relation between hydraulic conductivity and void ratio (k_h-e) for oil sands tailings

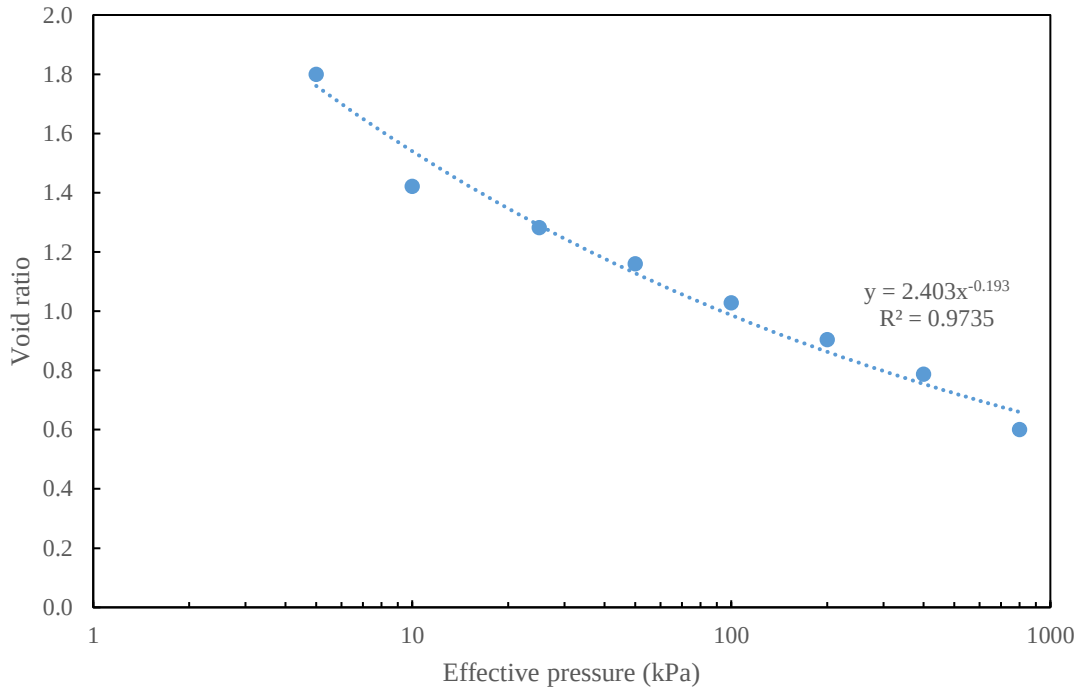

Figure 6.8 Relation between effective stress and void ratio (σ'-e) for oil sands tailings

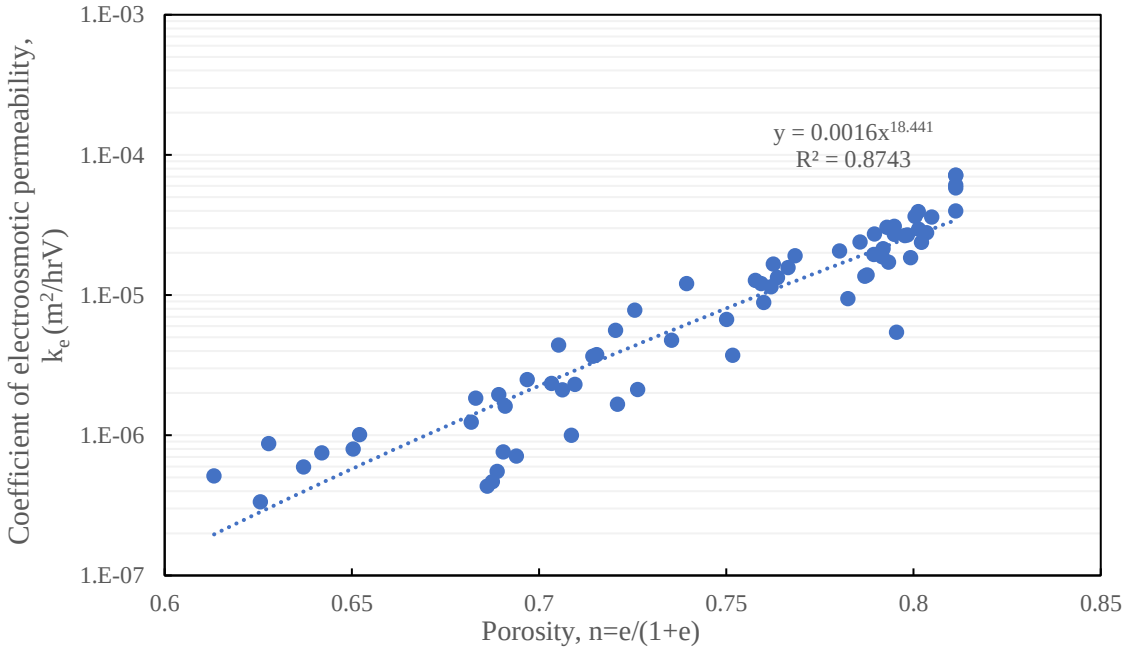

Figure 6.9 Relation between coefficient of electroosmotic permeability and porosity (k_e-n) for oil sands tailings calculated based on (Guo and Shang 2014)

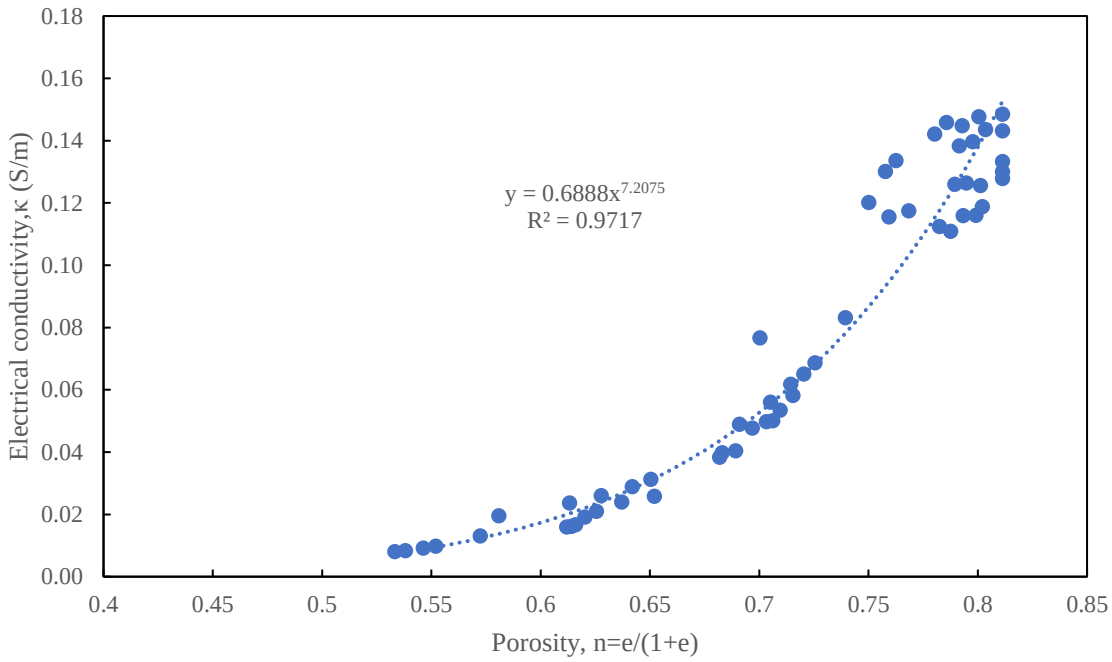

Figure 6.10 Relation between electrical conductivity and porosity (k_e-n) for oil sands tailings calculated based on (Guo and Shang 2014)

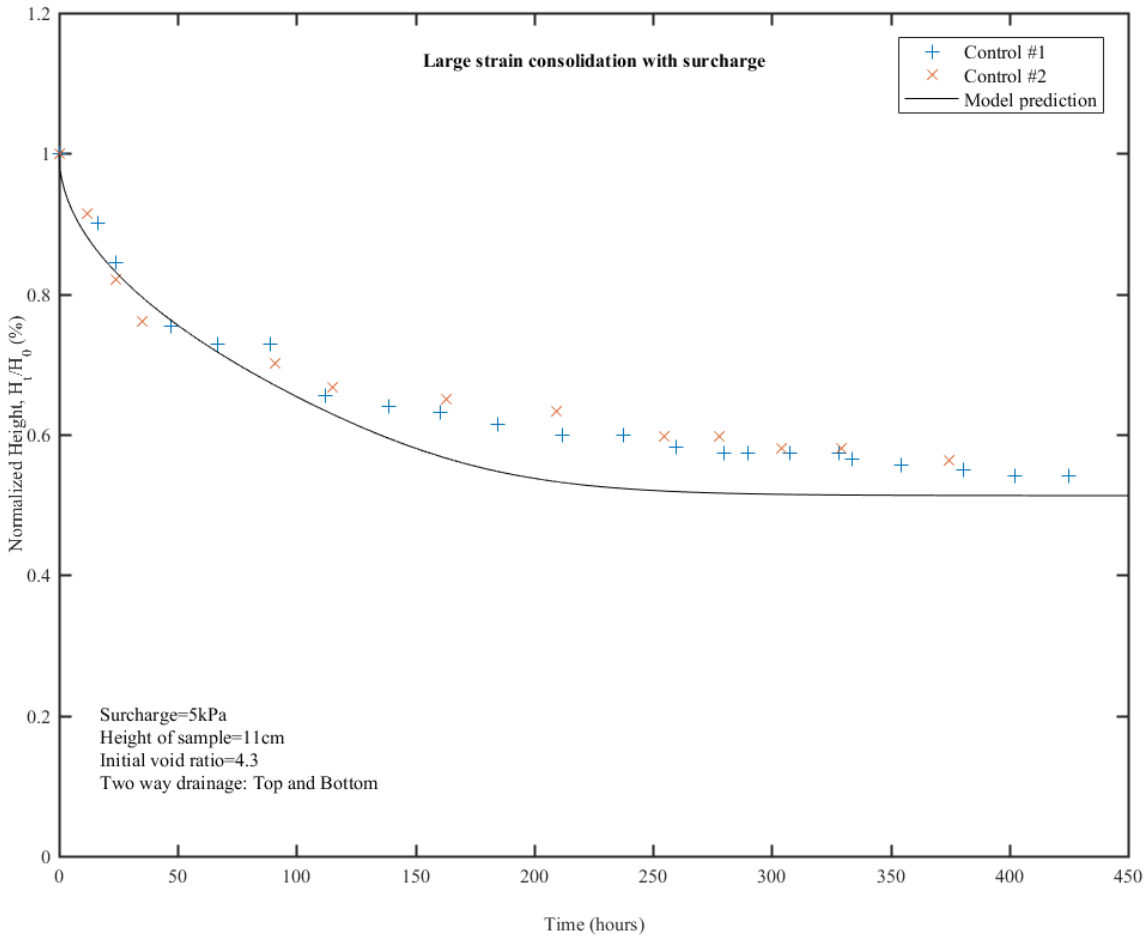

Figure 6.11 Experimental results and LSEK-1D model prediction of tailings consolidation under 5 kPa surcharge alone

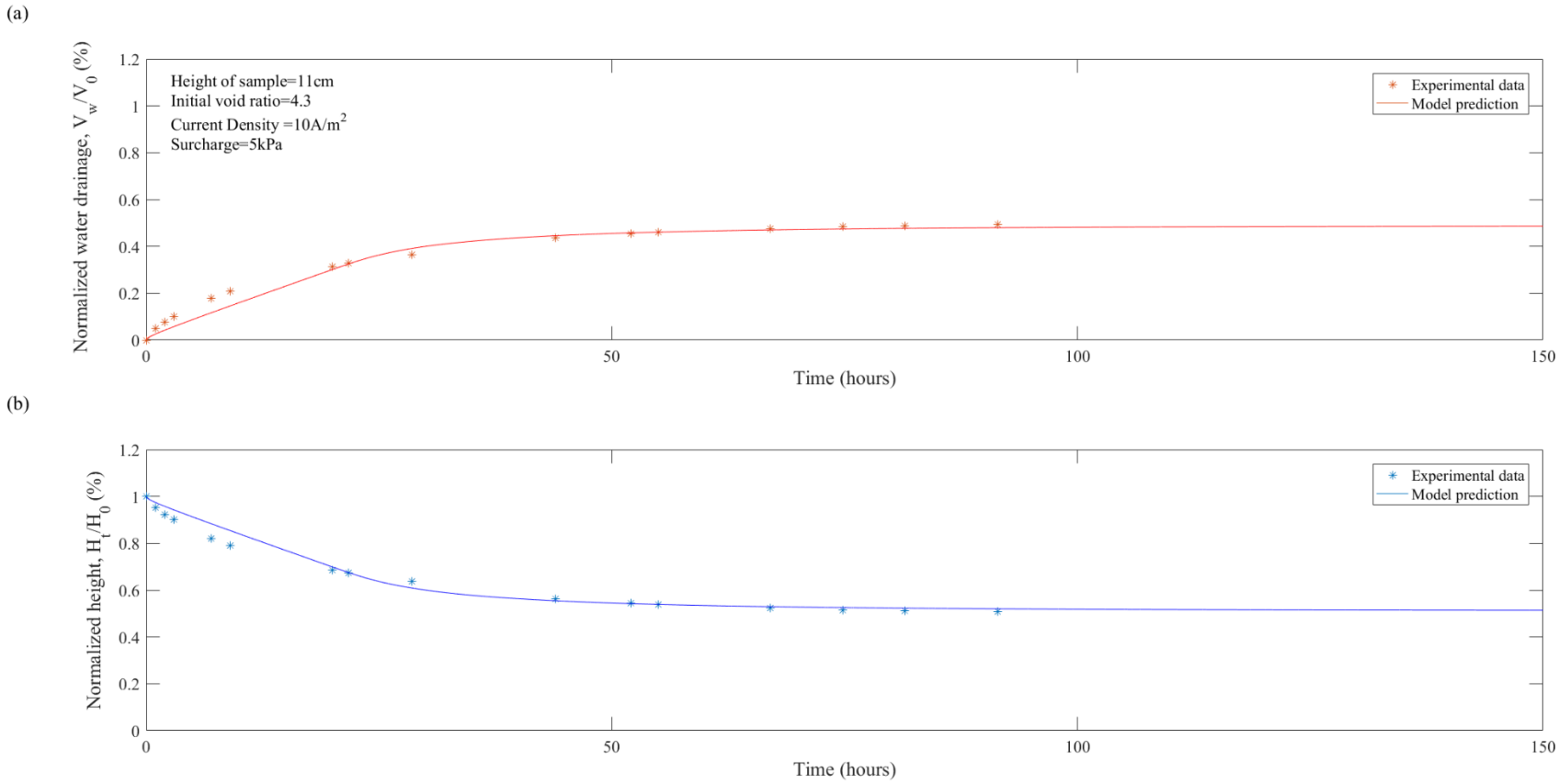

Figure 6.12 Experimental results and LSEK-1D model prediction of tailings consolidation under EK (with current density of 10A/m^2) combined with 5 kPa surcharge alone in terms of (a) Normalized water drainage, V_w/V_0 (%); (b) Normalized height change, H_t/H_0 (%)

(a)

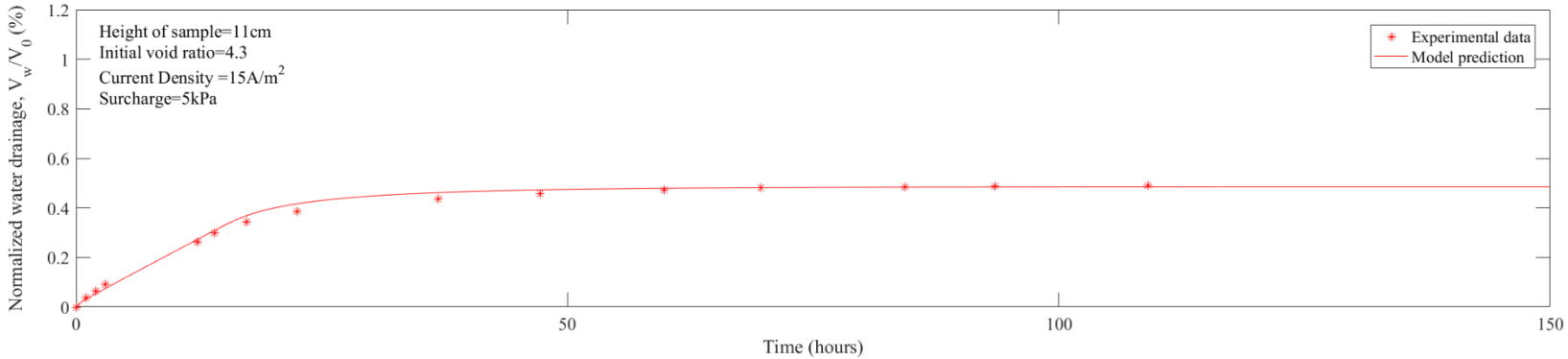

(b)

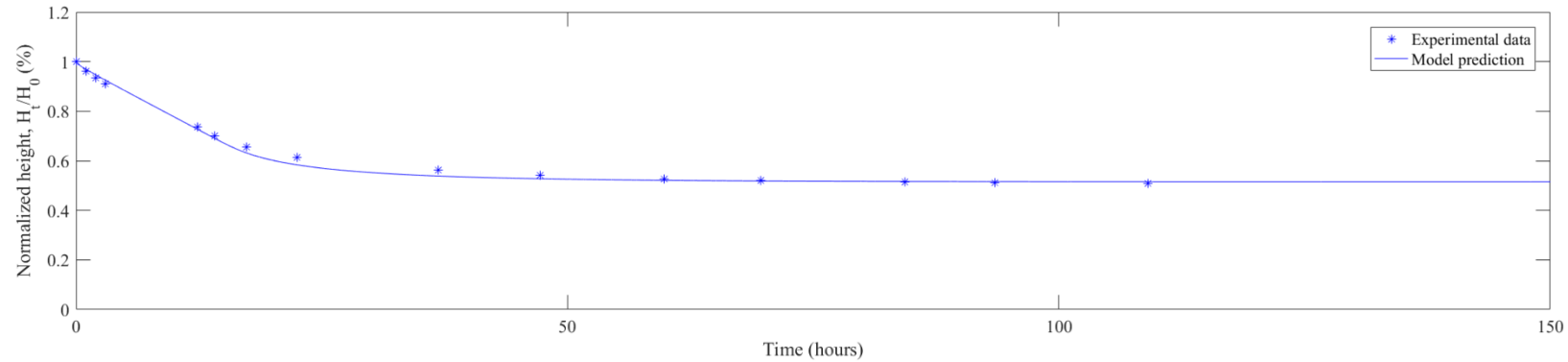

Figure 6.13 Experimental results and LSEK-1D model prediction of tailings consolidation under EK (with current density of 15A/m^2) combined with 5 kPa surcharge alone in terms of (a) Normalized water drainage, V_w/V_0 (%); (b) Normalized height change, H_t/H_0 (%)

(a)

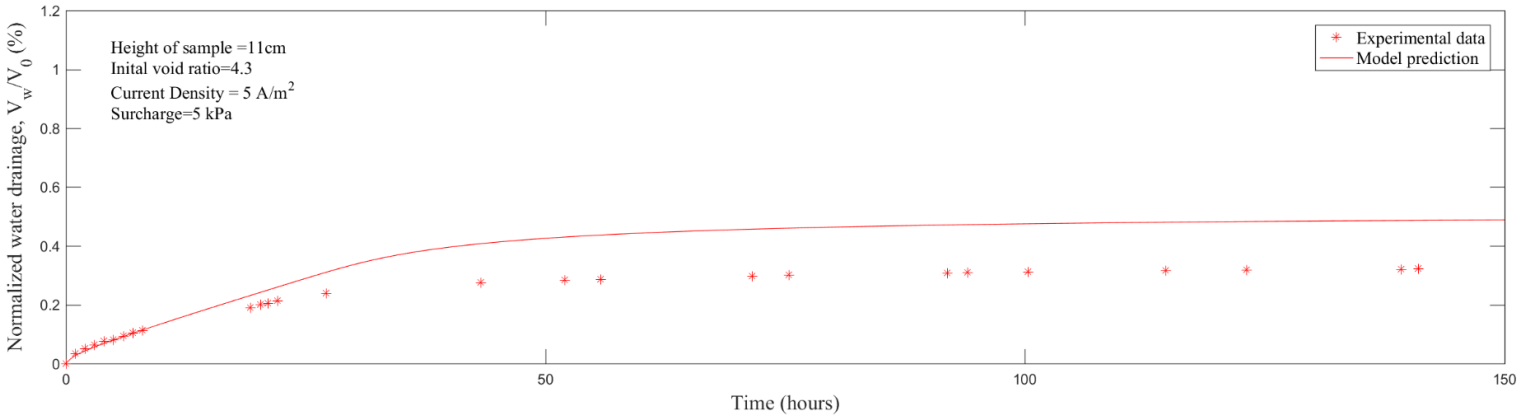

(b)

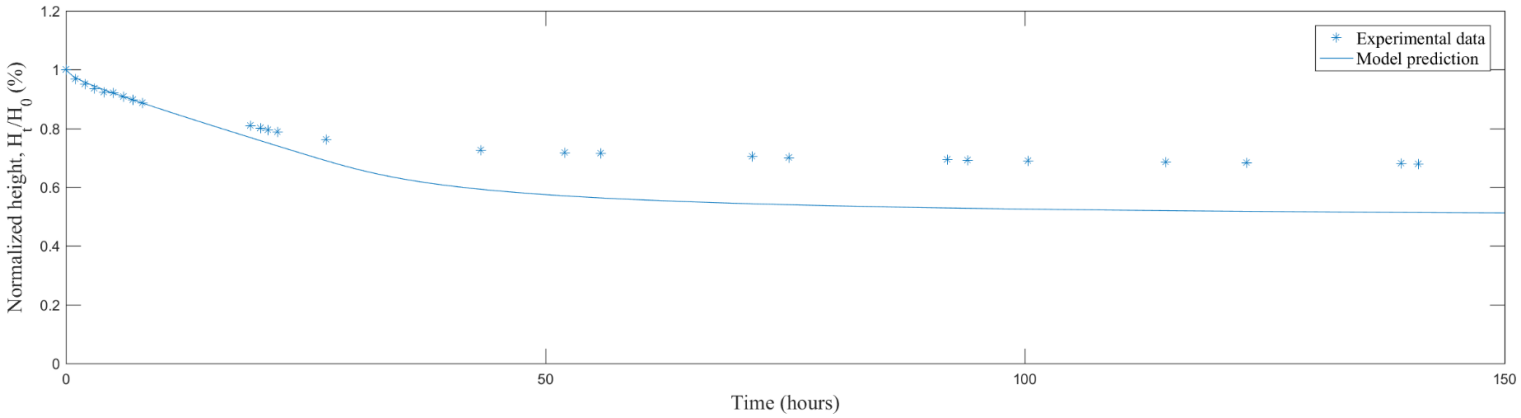

Figure 6.14 Experimental results and LSEK-1D model prediction of tailings consolidation under EK (with current density of 5A/m^2) combined with 5 kPa surcharge alone in terms of (a) Normalized water drainage, V_w/V_0 (%); (b) Normalized height change, H_t/H_0 (%)

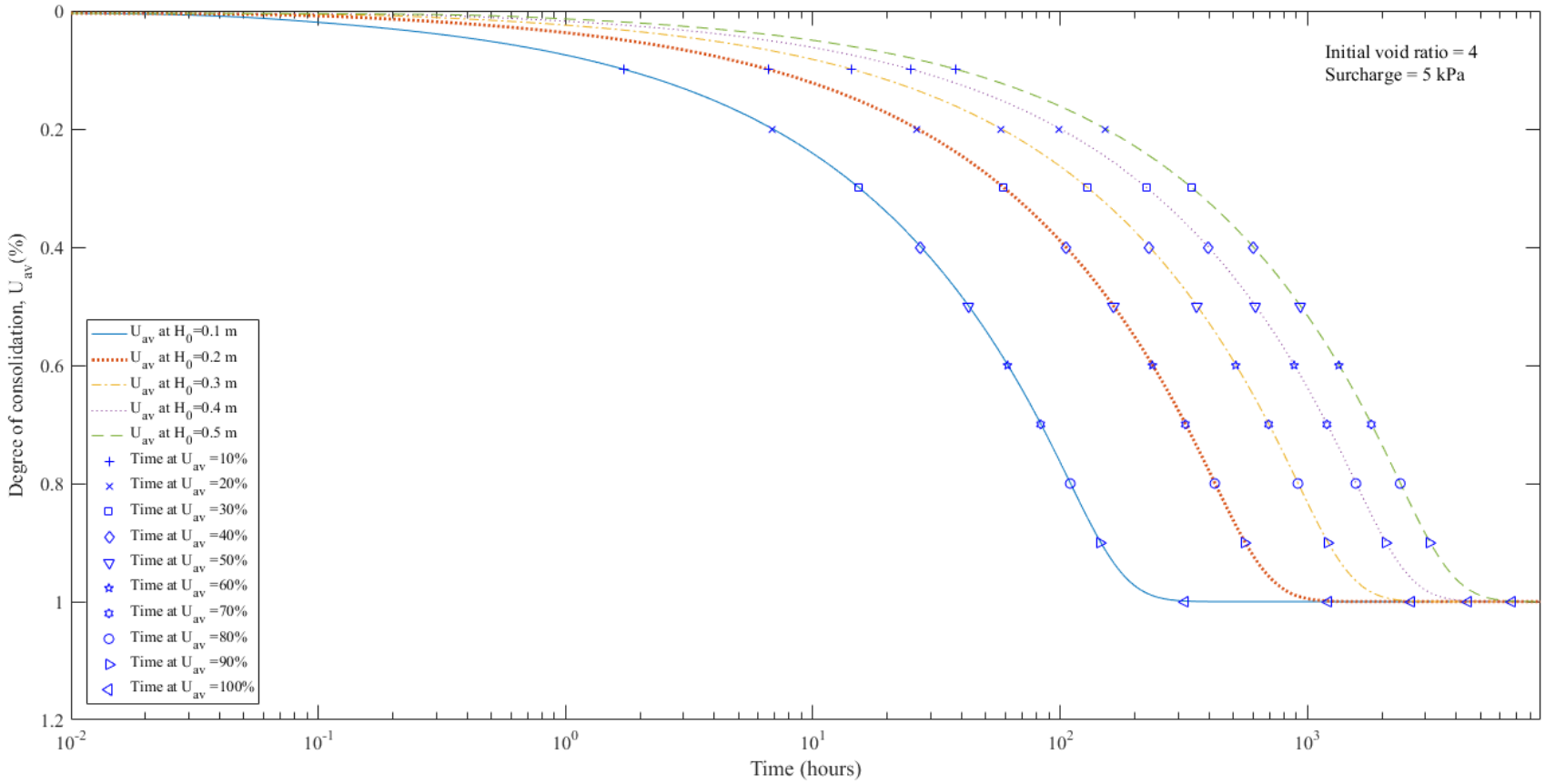

Figure 6.15 LSEK-1D model predicted average degree of consolidation of the sample with the initial height from 0.1 to 0.5m under 5 kPa surcharge consolidation

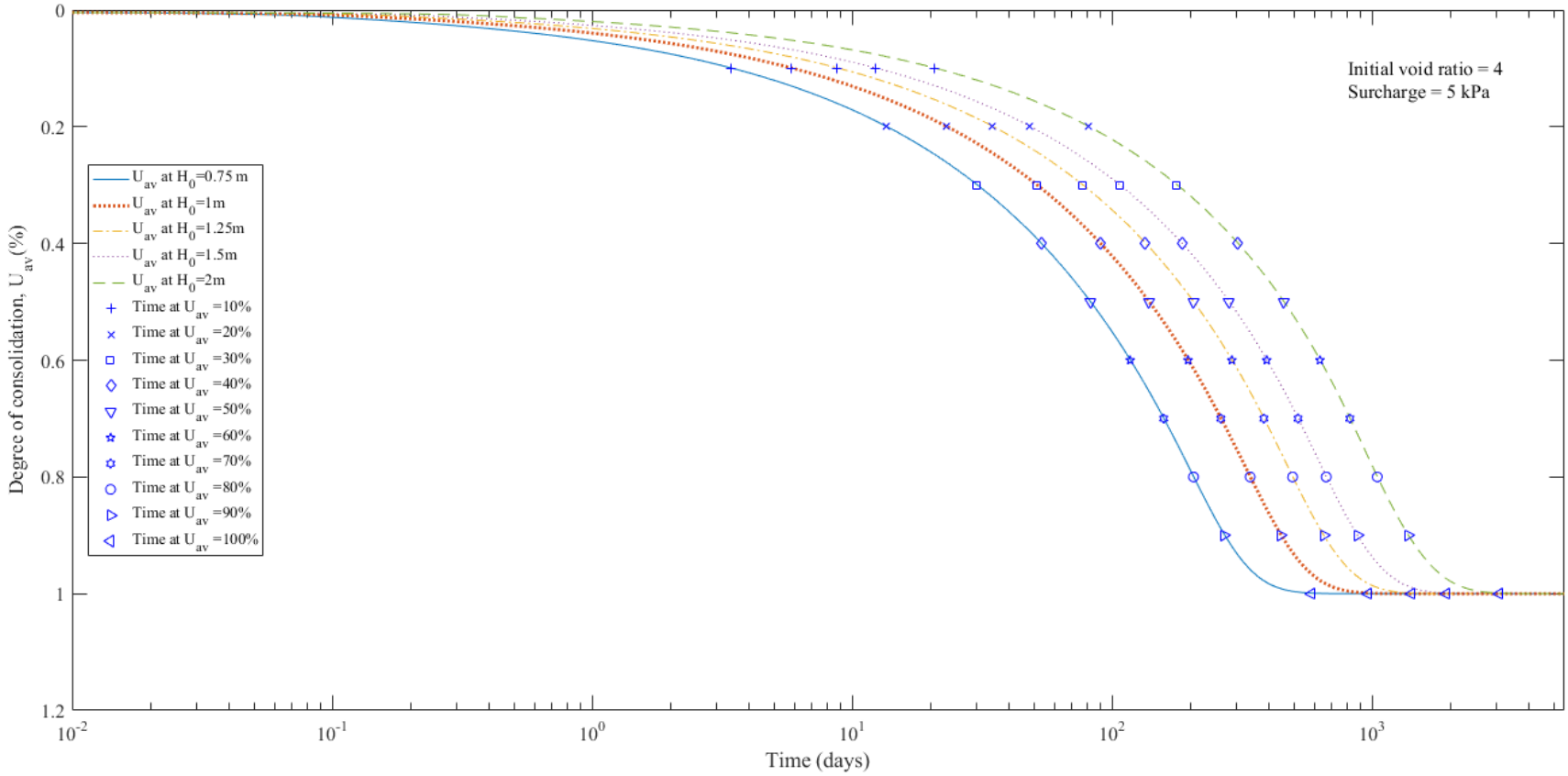

Figure 6.16 LSEK-1D model predicted average degree of consolidation of the sample with the initial height from 0.75 to 2m under 5 kPa surcharge consolidation

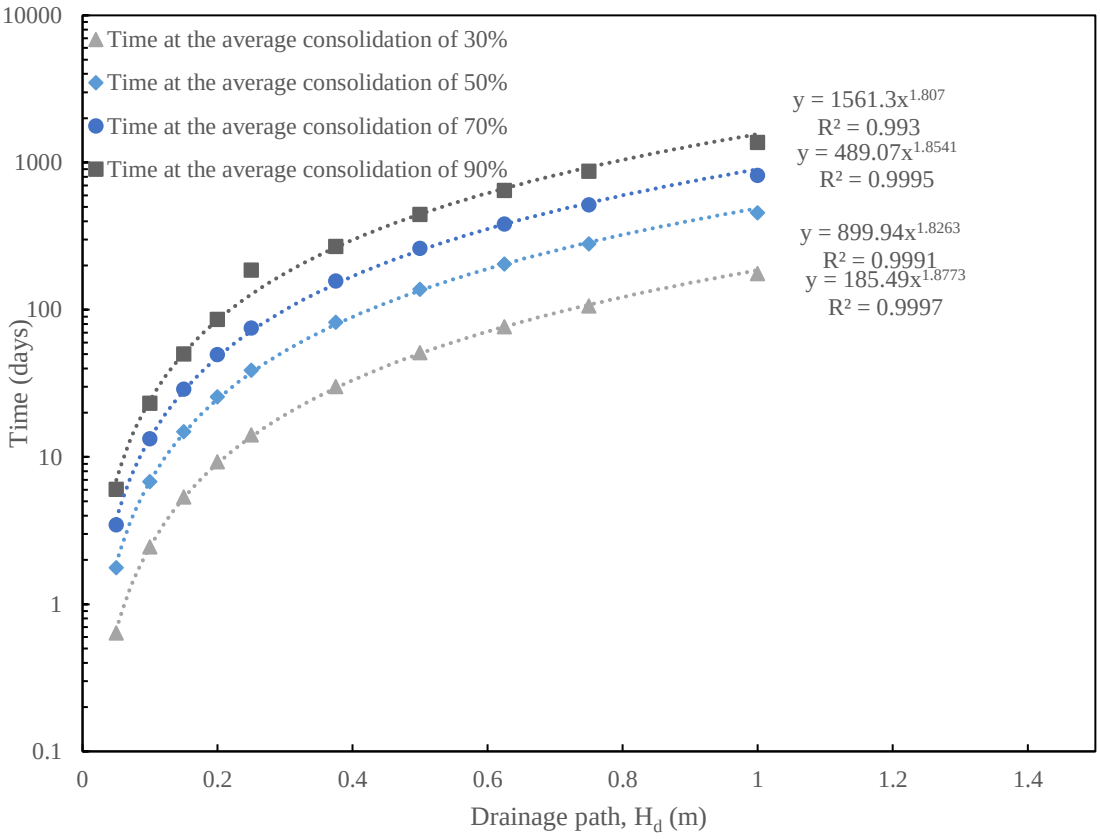

Figure 6.17 Drainage path versus consolation time under 5 kPa surcharge alone obtained in LSEK-1D model

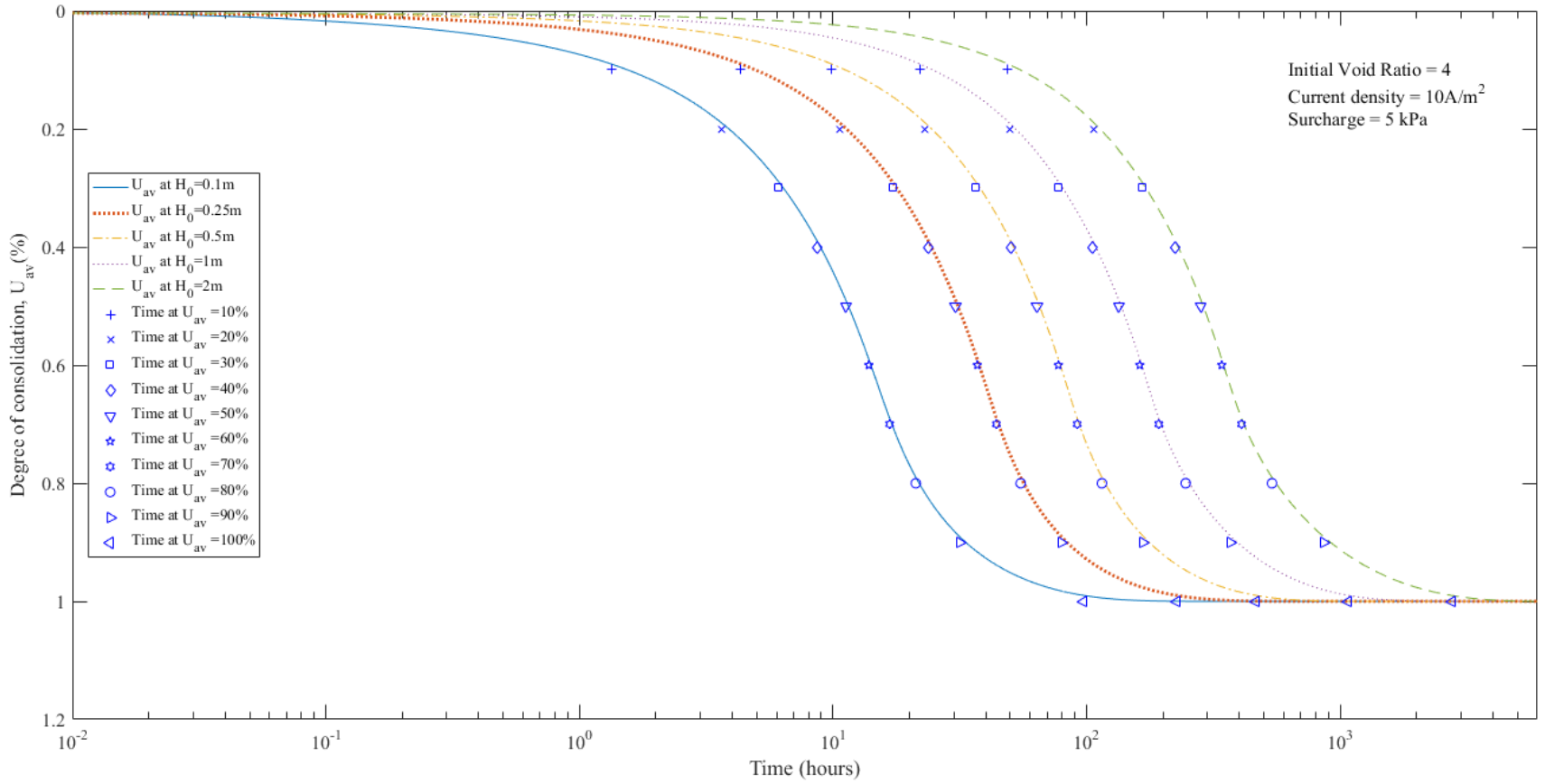

Figure 6.18 LSEK-1D model predicted average degree of consolidation of the sample with the initial height from 0.1 to 2m under EK (at current density of 10A/m^2) combined with 5 kPa surcharge consolidation

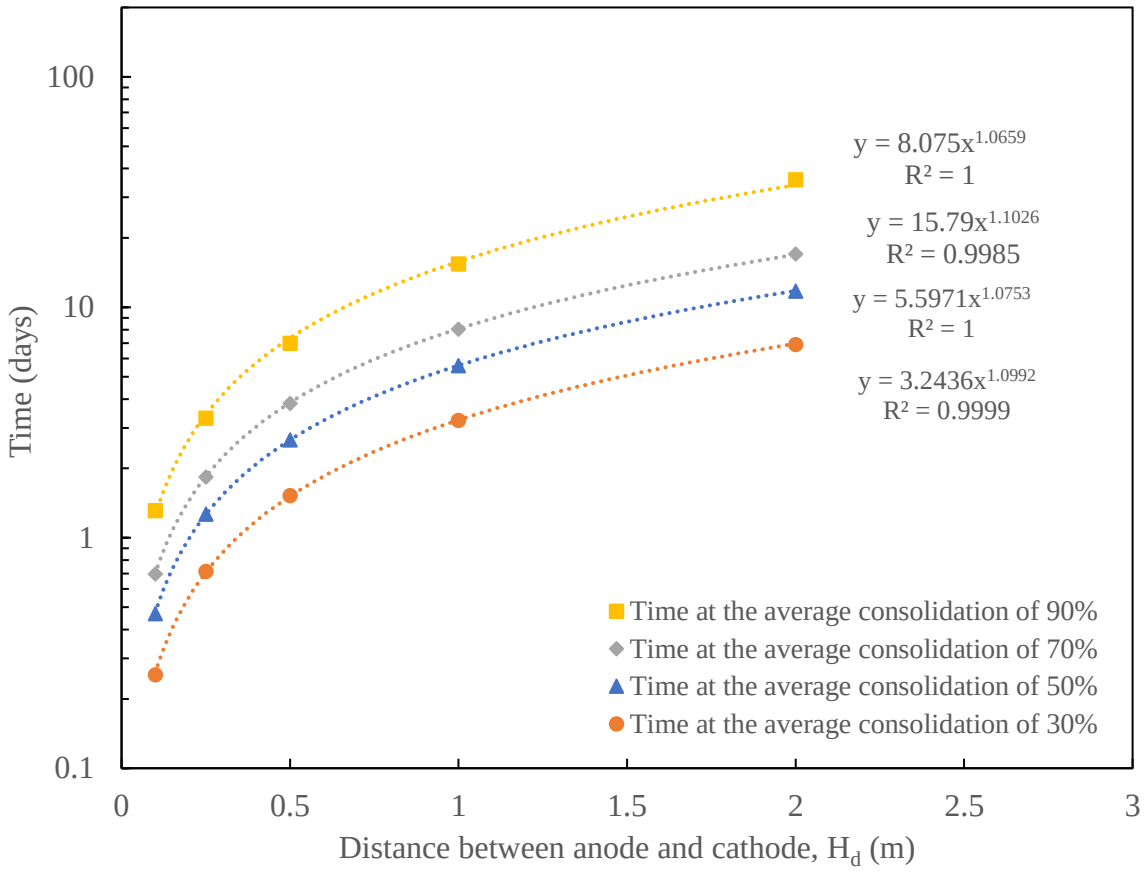

Figure 6.19 Drainage path versus consolation time under EK (at current density of 10A/m^2) combined with 5 kPa surcharge consolidation obtained in LSEK-1D model

(a)

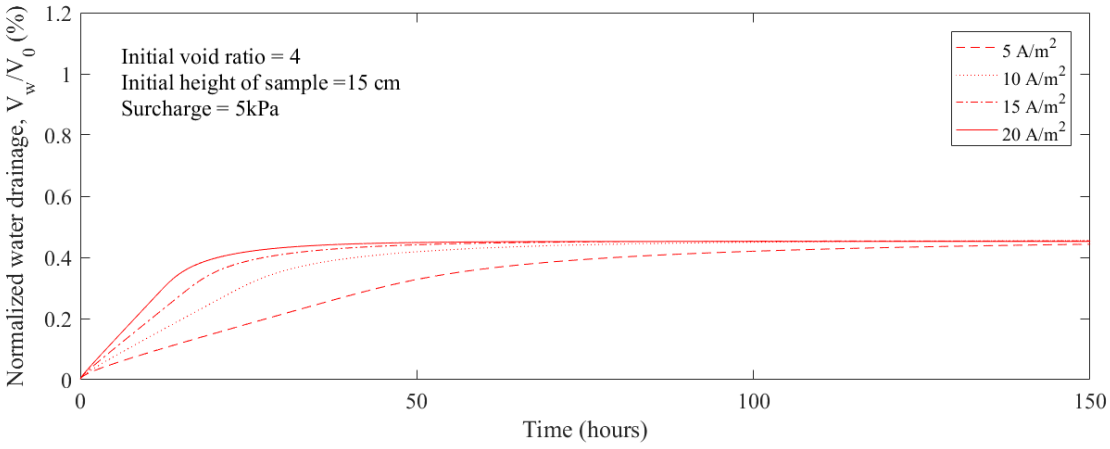

(b)

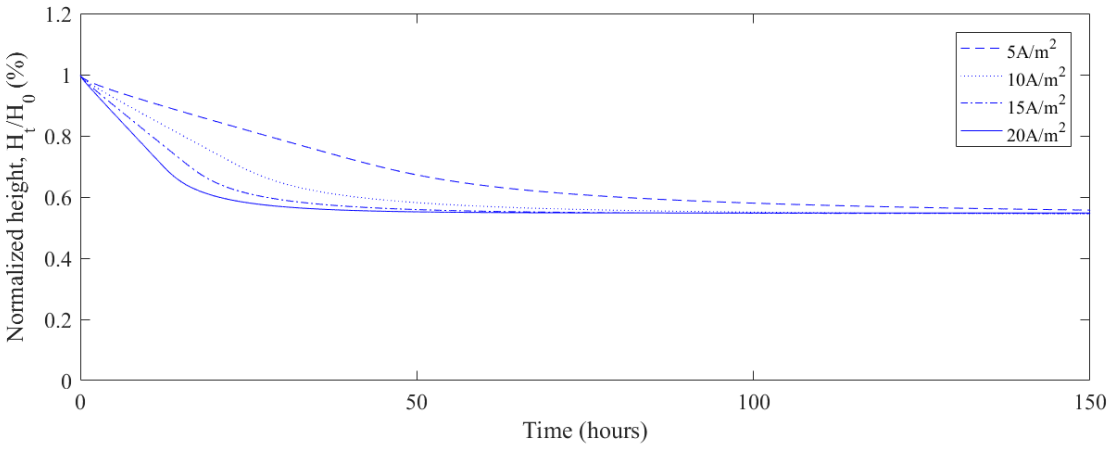

Figure 6.20 LSEK-1D model prediction of tailings consolidation under EK combined with 5 kPa surcharge alone in terms of (a) Normalized water drainage, V_w/V_0 (%); (b) Normalized height change, H_t/H_0 (%) with the current density from 5A/m^2 to 20A/m^2

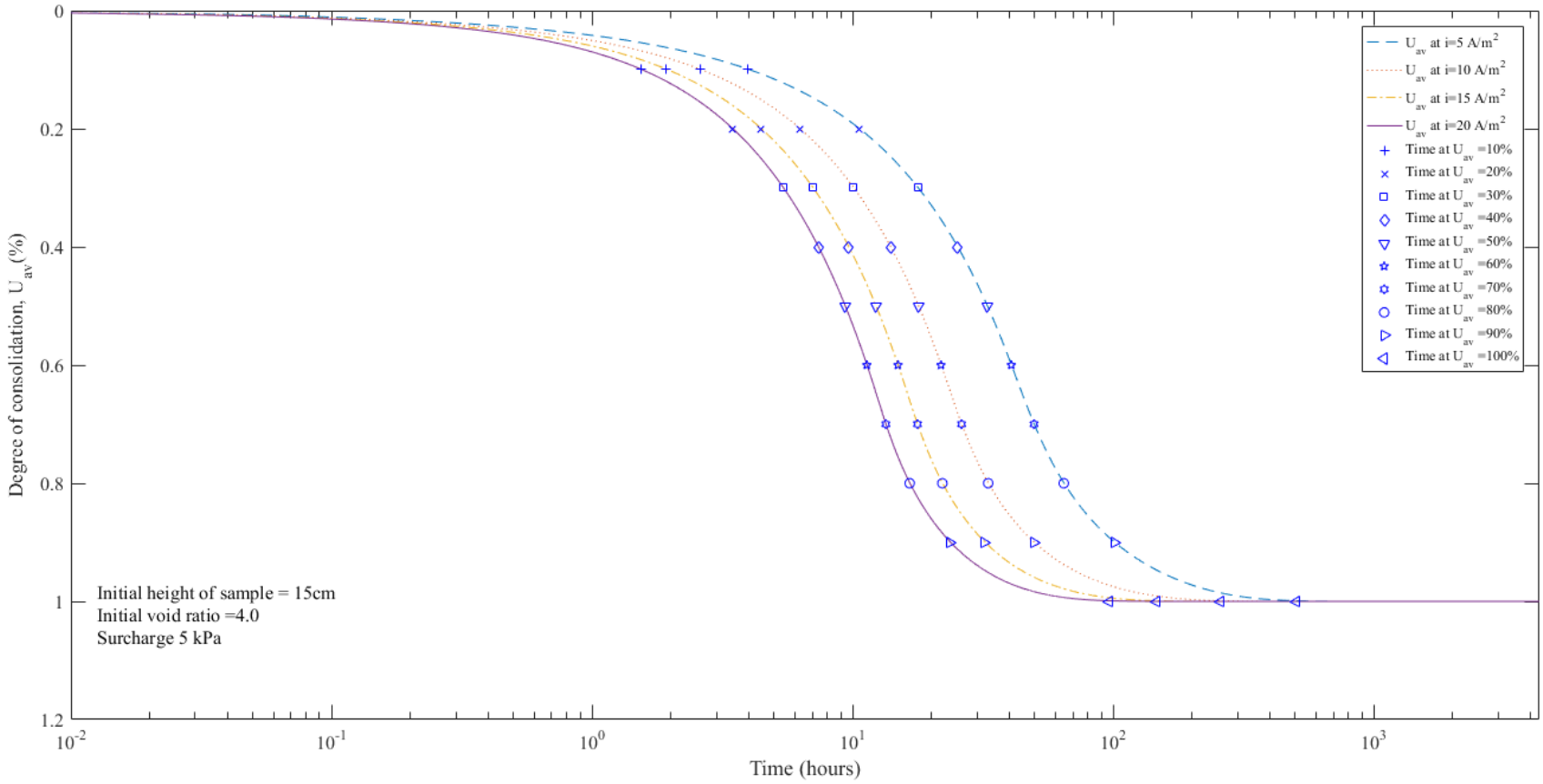

Figure 6.21 LSEK-1D model predicted average degree of consolidation of the sample under EK (at current density from 5A/m^2 to 20A/m^2) combined with 5 kPa surcharge consolidation

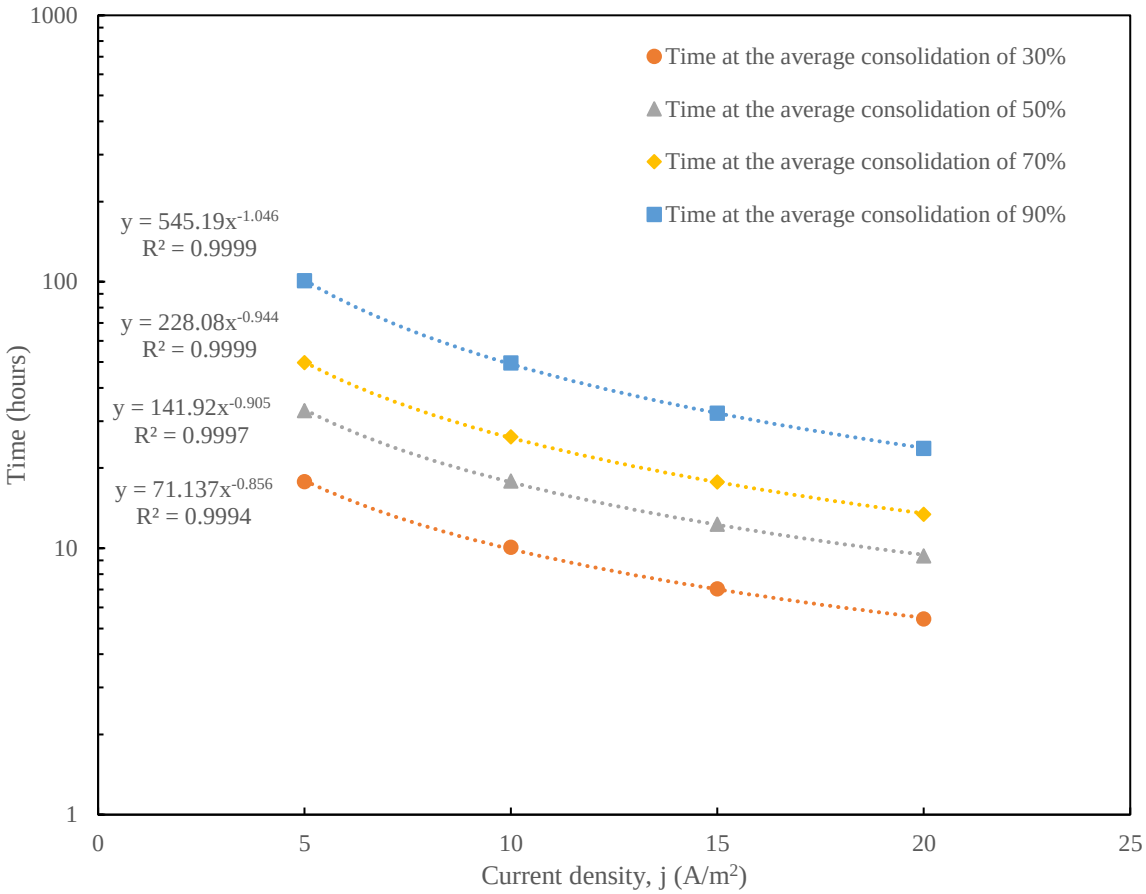

Figure 6.22 Current density versus consolation time under EK (at current density from 5A/m^2 to 20A/m^2) combined with 5 kPa surcharge consolidation obtained in LSEK-1D

Chapter 7 Summary, conclusions and recommendations

7.1. Summary

In this thesis, experiments were designed to study EK dewatering of oil sands tailings and kaolinite slurry with vertically installed electrodes. The data analysis method, involving normalization and regression, was used to find the general trends of EK dewatering. It was identified that the material saturation is the key controlling factor for termination of the EK flow, which was verified via experiments on oil sands tailings and kaolinite slurries. The combined treatment of EK and chemical stabilization using quicklime and Portland cement was studied via changes in the water content, undrained shear strength, plasticity, porewater pH and EC, and zeta potential. The combined treatment of EK and quicklime and Portland cement significantly reduced the property difference of the sample between the anode and the cathode, whereas the EK dewatering effects was minimized by addition of chemicals. Finally, a one dimensional large strain EK consolidation model (LSEK-1D) was developed and assessed via the experimental data of EK treatment on oil sands tailings. The model predicted results are in agreement with those from experiments. The LSEK-1D model is proven to be valid for both surcharge loading alone and EK treatment combined with surcharge loading.

The results in this thesis help for a better understanding of the EK dewatering on oil sands tailings. Even though the regression equations obtained from this research cannot be used directly for field application, the data analysis method and general forms of the regression equations are useful for future works. For the field application, the degrees of saturation of the tailings especially at the anode can served as a guideline to determine the most efficient stage for EK dewatering process. The development of LSEK-1D model for oil sands tailings is necessary and important for field applications to predict the consolidation and dewatering time. The chemical stabilization may apply only at the weak zone closed to the cathode to receive the benefits for both EK and chemical stabilization.

7.2. Conclusions

The main conclusions in this thesis are highlighted and listed below:

- After normalization, the changes in properties over the time for oil sands tailings and kaolinite, including EK water flow, water content, material electrical conductivity, and power consumptions, can be expressed via regression equations obtained in this study for EK dewatering process.

- Non-uniform water content distributions were found after EK treatment of oil sands tailings. The water content of MFT sample reduced significantly at the anode and remained unchanged at the vicinity of cathode.

- The effects of applied voltage gradient and initial water content on EK induced water flow were studied quantitatively by using the regression equations. It was found that the maximum water discharge is governed by the initial water content of kaolinite slurry governs, whereas the voltage gradient controls the rate of dewatering.

- The water flow generated by EK can be classified in three stages, i.e., 1) the linear flow, 2) the transitional flow, and 3) the end flow, and the EK dewatering is most efficient in the linear flow stage. It is identified that the flow rate was controlled by the saturation status of the sample. The linear flow stage lasted from beginning of the treatment until the material saturation reached 80% at the anode for both oil sands tailings and kaolinite. Hence the degree of saturation of tailings may serve as a guideline in large scale applications to estimate effective treatment time.

- With the same initial water content and experimental configuration, the treatment under high voltage gradient needs more energy but less treatment time than those with low voltage gradient to reach the same post-treated water content. At the meantime, there are significant strengthening effects for the sample at the anode after the treatment under the high voltage gradient.

- For the chemical treatment on oil sands mature fine tailings, the water content of MFT reduced immediately after mixing with quicklime and cement, due to hydration reaction. The post-treatment water content of MFT samples reduced linearly with the increase in the chemical dosage.

- For the combined treatment of EK and chemical stabilization, the addition of quicklime and cement reduced the EK flow, hence reduced dewatering effects. The EK flow completely stopped at the chemical dosage of 10%. In contrast, at a low chemical dosage (1% cement or quicklime), the EK treatment is beneficial for the strength gain of MFT and can significantly reduce the property differences of the sample between the anode and cathode, such as the water content and undrained shear strength. In general, Portland cement is more effective in generating strength gain than quicklime.

- A one dimensional large strain EK consolidation model (LSEK-1D) was developed and verified for oil sands tailings, and validated with the experimental data on oil sands tailings in the first time.

- The LSEK-1D model predicted that the consolidation time is proportional to $H_{dr}^{1.84}$, in which H_{dr} is the initial drainage path for oil sands tailings under surcharge alone. The EK consolidation time of oil sands tailings is proportional to $H_{dr}^{1.12}$, based on the LSEK-1D model, indicating that EK can significantly accelerate consolidation.

7.3.Limitations of the research

Some of the limitations for the research in this thesis are listed as follows:

- Ideally, the electric field, which was generated via two parallel plates, was considered to be uniform. However, the boundary effects of the experimental apparatus on the electric field were not considered and studied. The electric field is expected to be weak closed to the wall of the EK dewatering cell and strong at the center. The difference in electric field will affect the distributions of the tailings properties, such as final water content, after the treatment.

- Compared with other methods in geotechnical engineering, such as unconfined compression test and triaxial test, the laboratory vane shear tester for the strength measurement is not very precise, especially at low undrained shear strength. But due to the difficulties for MFT sample preparation, the vane shear test is the most convenient method to assess the strength of the tailings sample.

- In the regression analysis, the time is not normalized. The scale effects need to be studied for normalization of the dewatering time.

7.4. Recommendations for further research

Base on the experiments and modelling analysis presented in this thesis, the recommendations for the further studies are listed as follows:

- Carry out large scale tests on EK dewatering on oil sands tailings to find the scale effects on EK dewatering.

- Study the effects of residual bitumen and other hydrocarbons on MFT for better understanding the behavior of oil sands tailings.

- Develop a 2D large strain model for EK consolidation to facilitate the design of in-situ applications.

- Establish a database of oil sands tailings properties for validation of the EK large strain consolidation model.

Appendix 1 Supplementary figures

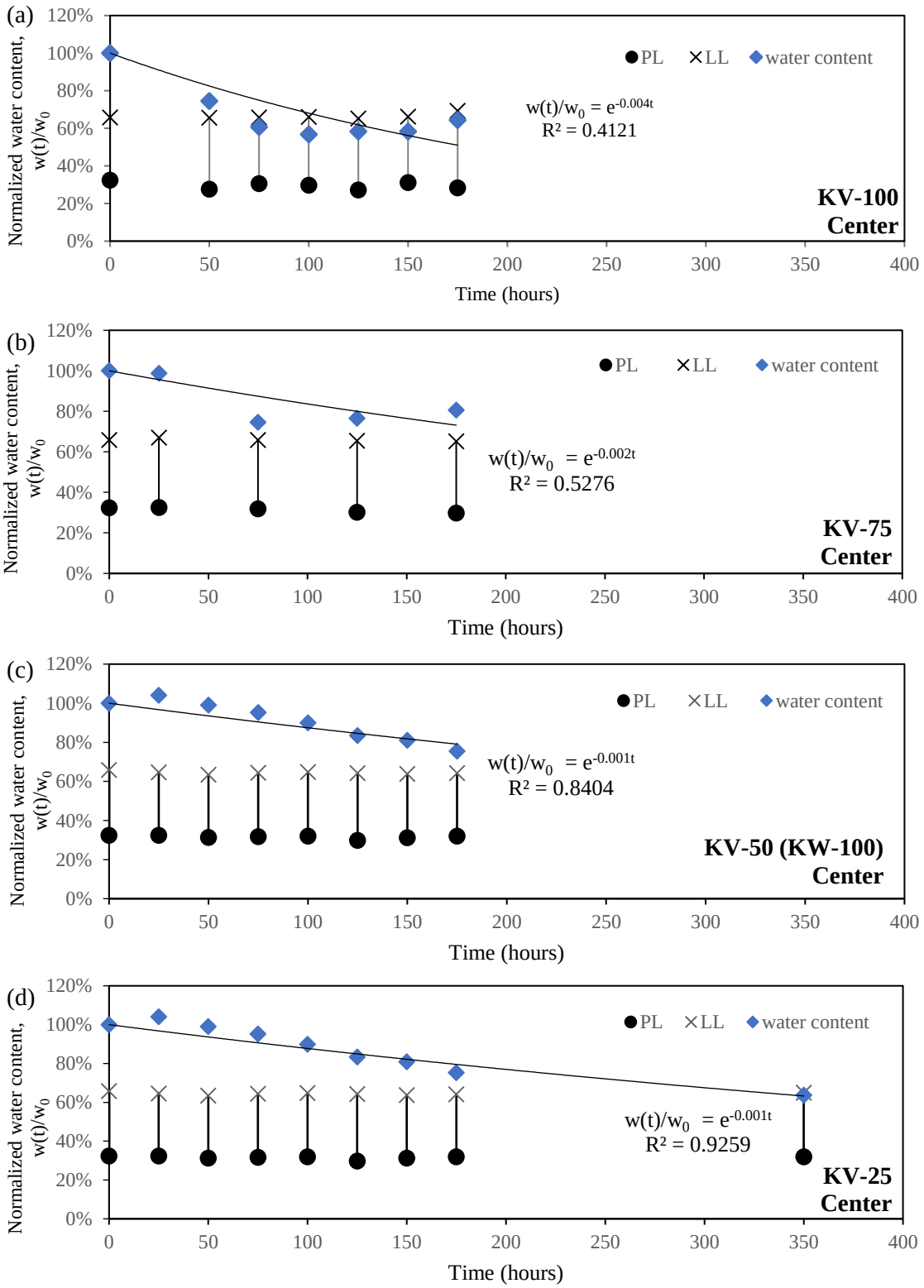

Figure A1. 1 Normalized water content, w(t)/w0, of the kaolinite sample at center for KV series tests (a) KV-100; (b) KV-75; (c) KV-50; (d) KV-25.

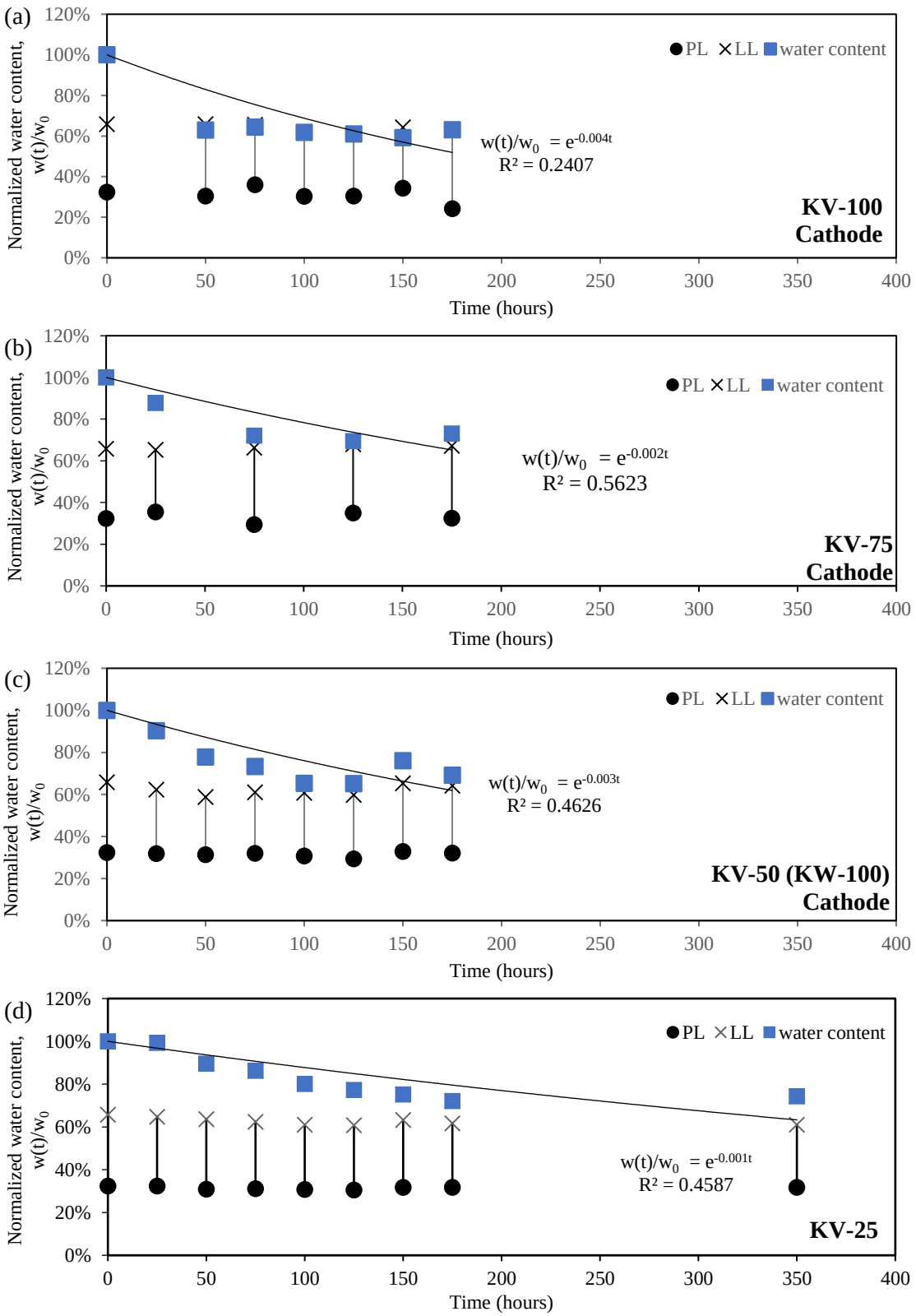

Figure A1. 2 Normalized water content, w(t)/w0, of the kaolinite sample at cathode for KV series tests (a) KV-100; (b) KV-75; (c) KV-50; (d) KV-25.

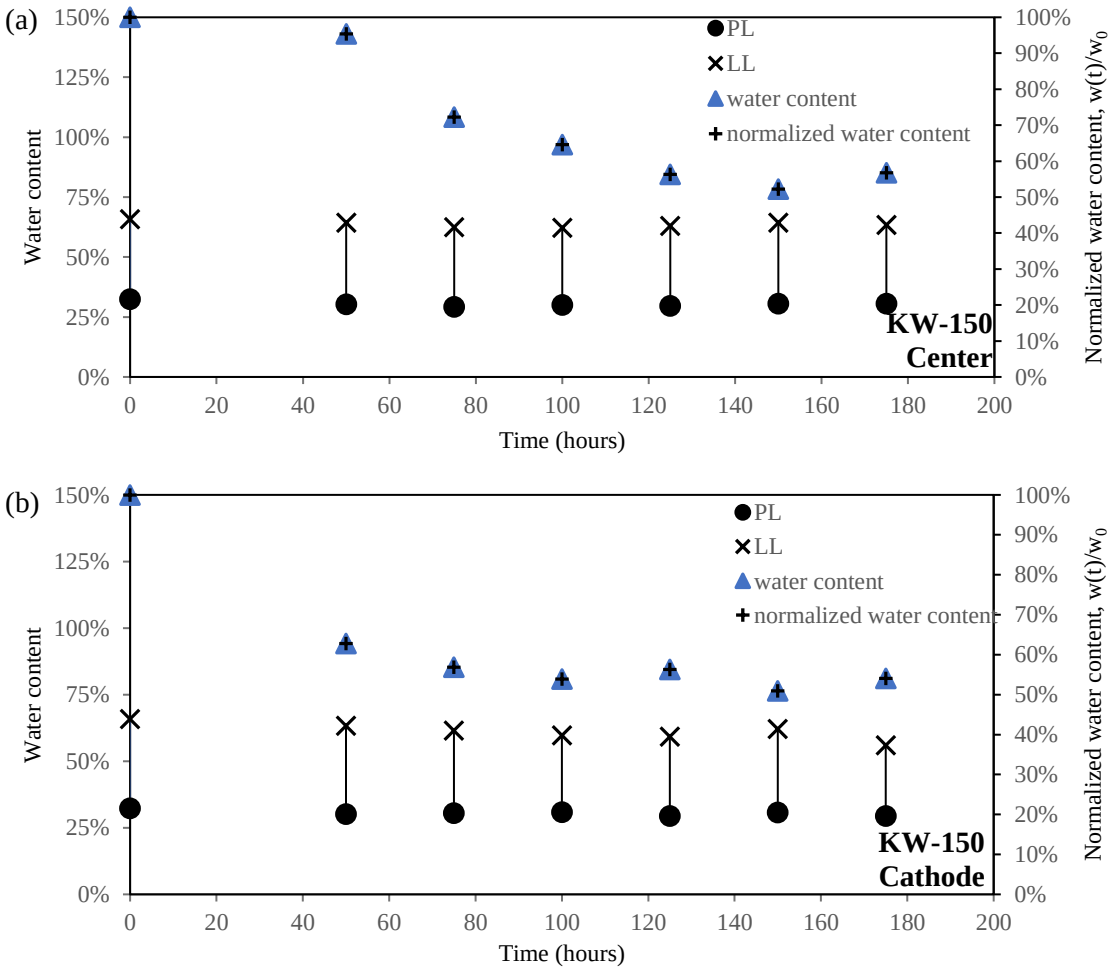

Figure A1. 3 Normalized water content, w(t)/w0, of the kaolinite sample at (a) center and (b) cathode for KW-150 tests

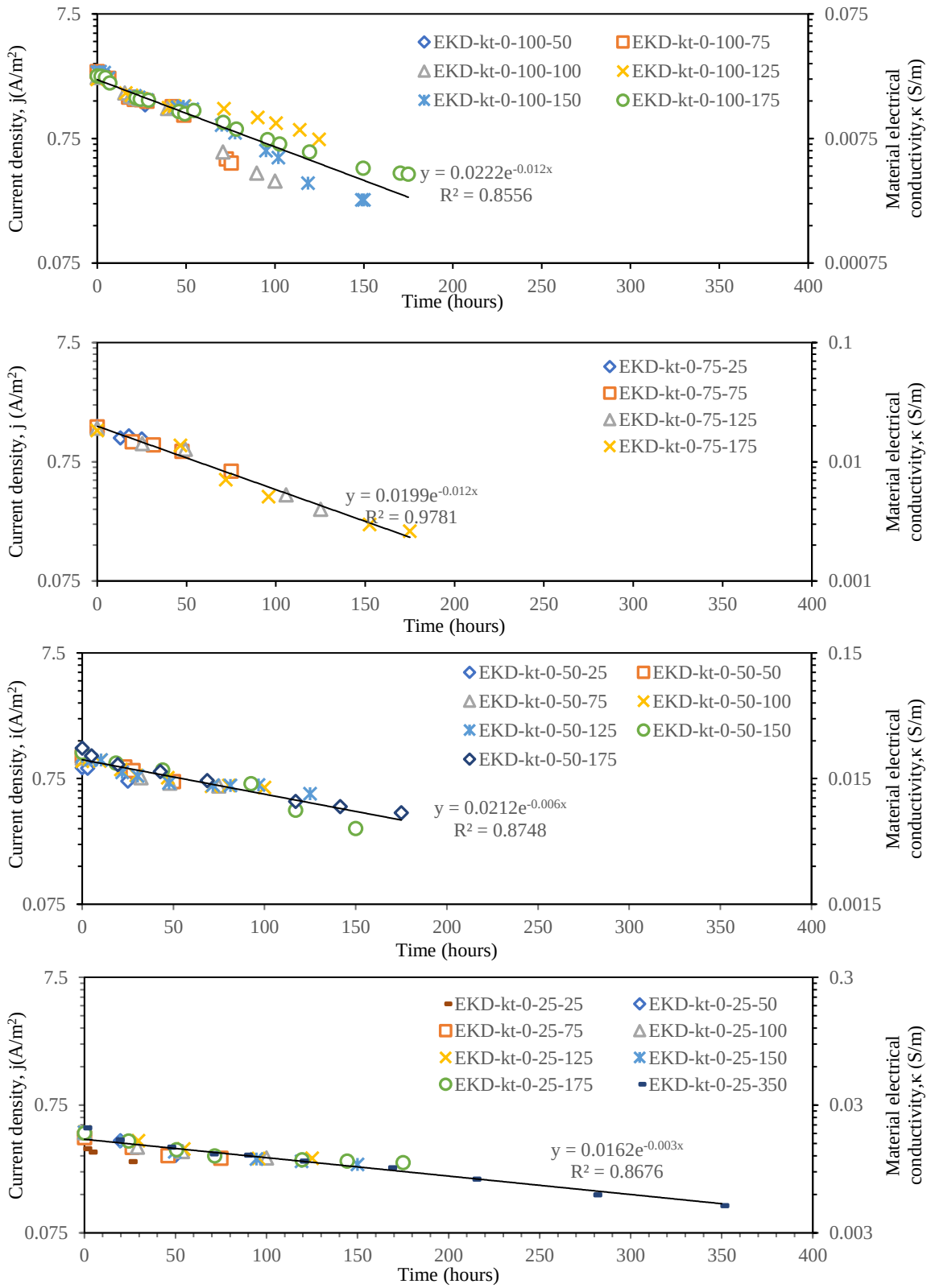

Figure A1. 4 Current density and material conductivity vs time of Kaolinite slurry for KV series tests (a) KV-100; (b) KV-75; (c) KV-50; (d) KV-25.

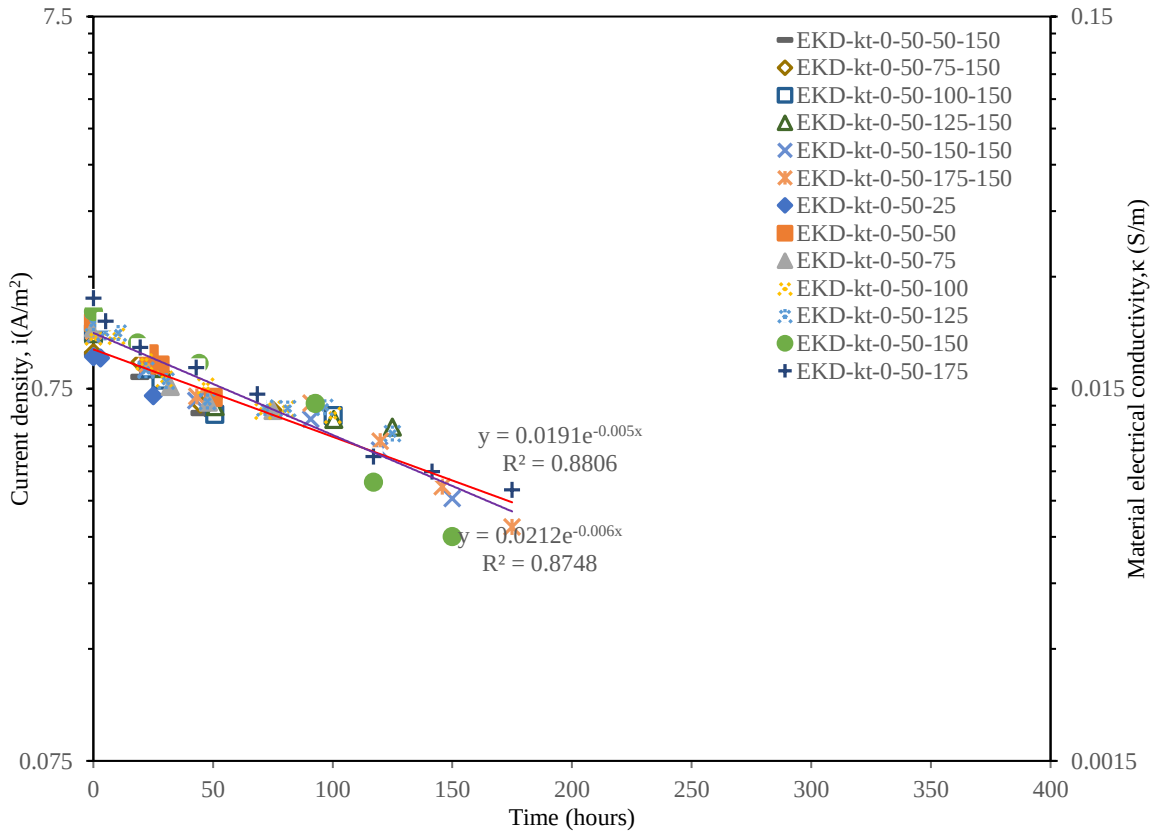

Figure A1. 5 Current density and material conductivity vs time of Kaolinite slurry for KW series test

Appendix 2 Finite difference scheme

Finite difference method was selected used to solve the one dimensional large strain consolidation problem of oil sands tailings via MATLAB.

In order to solve the governing equation, rewrite Eq. 6.68 in the form of

$$\left(\frac{\gamma_s}{\gamma_w}-1\right)\frac{d}{de}f\frac{\partial e}{\partial s}+\frac{1}{\gamma_w}\frac{d}{de}\left[f\cdot dsigma\frac{\partial e}{\partial s}\right]\frac{\partial e}{\partial s}+i\frac{d}{de}\left[\frac{k_e}{\kappa(e)}\right]\frac{\partial e}{\partial s}+\frac{\partial e}{\partial t}=0 \tag{6.82}$$

where,

$$f=\frac{k_h(e)}{1+e} \tag{6.83}$$

$$dsigma=\frac{d\sigma'}{de} \tag{6.84}$$

Expanding second and third term in Eq. 6.82,

$$\left(\frac{\gamma_s}{\gamma_w}-1\right)df\frac{\partial e}{\partial s}+\frac{1}{\gamma_w}[df\cdot dsigma+dsigma2\cdot f]\left(\frac{\partial e}{\partial s}\right)^2+\frac{1}{\gamma_w}\cdot f\cdot dsigma\frac{\partial^2 e}{\partial s^2}+i\left(\frac{dke}{\kappa}+ke\cdot dkappa\right)\frac{\partial e}{\partial s}+\frac{\partial e}{\partial t}=0 \tag{6.85}$$

where

$$df = \frac{df}{de} = \frac{d}{de}\left[\frac{k_h(e)}{1+e}\right]$$

(6.86)

$$dsigma2 = \frac{d}{de}(dsigma) = \frac{d^2\sigma'}{de^2}$$

(6.87)

$$dke = \frac{dke}{de}$$

(6.88)

$$dkappa = \frac{d}{de}\left(\frac{1}{\kappa}\right)$$

(6.89)

Simplify Eq. 6.85,

$$A(e)\frac{\partial e}{\partial s} + B(e)\left(\frac{\partial e}{\partial s}\right)^2 + b(e)\frac{\partial^2 e}{\partial s^2} + C(e)\frac{\partial e}{\partial s} = -\frac{\partial e}{\partial t}$$

(6.90)

where,

$$A(e) = \left(\frac{\gamma_s}{\gamma_w} - 1\right) df$$

(6.91)

$$B(e) = \frac{1}{\gamma_w}[df \cdot dsigma + dsigma2 \cdot f]$$

(6.92)

$$b(e) = \frac{1}{\gamma_w} \cdot f \cdot dsigma$$

(6.93)

$$C(e) = i\left(\frac{dke}{\kappa} + ke \cdot dkappa\right)$$

(6.94)

Rearrange Eq. 6.90,

$$AC(e)\frac{\partial e}{\partial s} + B(e)\left(\frac{\partial e}{\partial s}\right)^2 + b(e)\frac{\partial^2 e}{\partial s^2} = -\frac{\partial e}{\partial t}$$

(6.95)

where,

$$AC(e) = A(e) + C(e)$$

(6.96)

To solve Eq. 6.95, the explicit convection (centered difference) with implicit diffusion method was used. The difference form of the governing equation (Eq. 6.95) is written as:

$$AC\left(e_{n,j}\right)\frac{e_{n,j+1} - e_{n,j-1}}{2h} + B\left(e_{n,j}\right)\left(\frac{e_{n,j+1} - e_{n,j-1}}{2h}\right)^2 + b\left(e_{n+1,j}\right)\frac{e_{n+1,j+1} - 2e_{n+1,j} + e_{n,j-1}}{h^2} = -\frac{e_{n+1,j} - e_{n,j}}{\Delta t}$$

(6.97)

where

$$n - index\ number\ of\ time\ grid$$

$$j - index\ number\ of\ space\ grid$$

$$h - step\ size\ in\ space\ direction$$

$$\Delta t\ - step\ size\ in\ time\ direction$$

$$e_{n,j} - void\ ratio\ of\ MFT\ at\ time\ n\ and\ space\ j$$

The matrix form of Eq. 6.97 is written as:

$$\frac{\Delta t}{2h}\begin{bmatrix} AC(e_{n,1}) & 0 & 0 & 0 & 0 \\ 0 & AC(e_{n,2}) & 0 & 0 & 0 \\ \vdots & \vdots & \ddots & \vdots & \vdots \\ 0 & 0 & 0 & AC(e_{n,j-1}) & 0 \\ 0 & 0 & 0 & 0 & AC(e_{n,j}) \end{bmatrix}\begin{bmatrix} -1 & 0 & 1 & 0 & \cdots & \cdots & 0 \\ 0 & -1 & 0 & 1 & \ddots & \ddots & \vdots \\ \vdots & \ddots & \ddots & \ddots & \ddots & \ddots & \vdots \\ \vdots & \ddots & \ddots & -1 & 0 & 1 & 0 \\ 0 & \cdots & \cdots & 0 & -1 & 0 & 1 \end{bmatrix}\begin{bmatrix} e_{cb} \\ e_{n,1} \\ e_{n,2} \\ \vdots \\ e_{n,j-1} \\ e_{n,j} \\ e_{ab} \end{bmatrix} +$$

$$\frac{\Delta t}{4h^2}\begin{bmatrix} B(e_{n,1}) & 0 & 0 & 0 & 0 \\ 0 & B(e_{n,2}) & 0 & 0 & 0 \\ \vdots & \vdots & \ddots & \vdots & \vdots \\ 0 & 0 & 0 & B(e_{n,j-1}) & 0 \\ 0 & 0 & 0 & 0 & B(e_{n,j}) \end{bmatrix}\begin{bmatrix} e_{cb} - e_{n,2} & 0 & 0 & 0 & 0 \\ 0 & e_{n,1} - e_{n,3} & 0 & 0 & 0 \\ \vdots & \vdots & \ddots & \vdots & \vdots \\ 0 & 0 & 0 & e_{n,j-2} - e_{n,j} & 0 \\ 0 & 0 & 0 & 0 & e_{n,j-1} - e_{n,ab} \end{bmatrix}\begin{bmatrix} e_{cb} - e_{n,2} \\ e_{n,1} - e_{n,3} \\ \vdots \\ e_{n,j-2} - e_{n,j} \\ e_{n,j-1} - e_{ab} \end{bmatrix} +$$

$$\frac{\Delta t}{h^2}\begin{bmatrix} \mathrm{b}(e_{n,1}) & 0 & 0 & 0 & 0 \\ 0 & \mathrm{b}(e_{n,2}) & 0 & 0 & 0 \\ \vdots & \vdots & \ddots & \vdots & \vdots \\ 0 & 0 & 0 & \mathrm{b}(e_{n,j-1}) & 0 \\ 0 & 0 & 0 & 0 & \mathrm{b}(e_{n,j}) \end{bmatrix}\begin{bmatrix} 1 & -2 & 1 & 0 & \cdots & \cdots & 0 \\ 0 & 1 & -2 & 1 & \ddots & \ddots & \vdots \\ \vdots & \ddots & \ddots & \ddots & \ddots & \ddots & \vdots \\ \vdots & \ddots & \ddots & 1 & -2 & 1 & 0 \\ 0 & \cdots & \cdots & 0 & 1 & -2 & 1 \end{bmatrix}\begin{bmatrix} e_{cb} \\ e_{n+1,1} \\ e_{n+1,2} \\ \vdots \\ e_{n+1,j-1} \\ e_{n+1,j} \\ e_{ab} \end{bmatrix} =$$

$$-\begin{bmatrix} e_{n+1,1} - e_{n,1} \\ e_{n+1,2} - e_{n,2} \\ \vdots \\ e_{n+1,j-1} - e_{n,j-1} \\ e_{n+1,j} - e_{n,j} \end{bmatrix}$$

(6.98)

Rewrite Eq. 6.98,

$$0.5r * ACoefM * DDmatrix * W2 + 0.25 * R * BCoefM * diag(DDmatrix * W2) * DDMatix * W2 + R * bCoefM * K * E_{n+1} + Boundaryterm = -(E_{n+1} - E_n)$$

(6.99)

where,

$$r = \frac{\Delta t}{h}$$

(6.100)

$$R = \frac{\Delta t}{h^2}$$

(6.101)

$$ACoefM = \begin{bmatrix} AC(e_{n,1}) & 0 & 0 & 0 & 0 \\ 0 & AC(e_{n,2}) & 0 & 0 & 0 \\ \vdots & \vdots & \ddots & \vdots & \vdots \\ 0 & 0 & 0 & AC(e_{n,j-1}) & 0 \\ 0 & 0 & 0 & 0 & AC(e_{n,j}) \end{bmatrix}$$

(6.102)

$$BCoefM = \begin{bmatrix} B\left(e_{n,1}\right) & 0 & 0 & 0 & 0 \\ 0 & B\left(e_{n,2}\right) & 0 & 0 & 0 \\ \vdots & \vdots & \ddots & \vdots & \vdots \\ 0 & 0 & 0 & B\left(e_{n,j-1}\right) & 0 \\ 0 & 0 & 0 & 0 & B\left(e_{n,j}\right) \end{bmatrix}$$

(6.103)

$$bCoefM = \begin{bmatrix} \mathrm{b}(\mathrm{e}_{n,1}) & 0 & 0 & 0 & 0 \\ 0 & \mathrm{b}(\mathrm{e}_{n,2}) & 0 & 0 & 0 \\ \vdots & \vdots & \ddots & \vdots & \vdots \\ 0 & 0 & 0 & \mathrm{b}(\mathrm{e}_{\mathrm{n,j-1}}) & 0 \\ 0 & 0 & 0 & 0 & \mathrm{b}(\mathrm{e}_{\mathrm{n,j}}) \end{bmatrix}$$

(6.104)

$$diag(DDmatrix * W2) = \begin{bmatrix} e_{cb} - e_{n,2} & 0 & 0 & 0 & 0 \\ 0 & e_{n,1} - e_{n,3} & 0 & 0 & 0 \\ \vdots & \vdots & \ddots & \vdots & \vdots \\ 0 & 0 & 0 & e_{n,j-2} - e_{n,j} & 0 \\ 0 & 0 & 0 & 0 & e_{n,j-1} - e_{n,ab} \end{bmatrix}$$

(6.105)

$$DDmatrix * W2 = \begin{bmatrix} e_{cb} - e_{n,2} \\ e_{n,1} - e_{n,3} \\ \vdots \\ e_{n,j-2} - e_{n,j} \\ e_{n,j-1} - e_{ab} \end{bmatrix}$$

(6.106)

$$DDmatrix = \begin{bmatrix} -1 & 0 & 1 & 0 & \cdots & \cdots & 0 \\ 0 & -1 & 0 & 1 & \ddots & \ddots & \vdots \\ \vdots & \ddots & \ddots & \ddots & \ddots & \ddots & \vdots \\ \vdots & \ddots & \ddots & -1 & 0 & 1 & 0 \\ 0 & \cdots & \cdots & 0 & -1 & 0 & 1 \end{bmatrix}$$

(6.107)

$$K = \begin{bmatrix} -2 & 1 & 0 & \cdots & \cdots \\ 1 & -2 & 1 & \ddots & \ddots \\ \ddots & \ddots & \ddots & \ddots & \ddots \\ \ddots & \ddots & 1 & -2 & 1 \\ \cdots & \cdots & 0 & 1 & -2 \end{bmatrix}$$

(6.108)

$$Boundaryterm = \frac{\Delta t}{h^2} \begin{bmatrix} \mathrm{b}(\mathrm{e}_{n,1}) & 0 & 0 & 0 & 0 \\ 0 & \mathrm{b}(\mathrm{e}_{n,2}) & 0 & 0 & 0 \\ \vdots & \vdots & \ddots & \vdots & \vdots \\ 0 & 0 & 0 & \mathrm{b}(\mathrm{e}_{\mathrm{n,j-1}}) & 0 \\ 0 & 0 & 0 & 0 & \mathrm{b}(\mathrm{e}_{n,\mathrm{j}}) \end{bmatrix} \begin{bmatrix} e_{cb} \\ 0 \\ \vdots \\ 0 \\ e_{ab} \end{bmatrix}$$

(6.109)

$$W2 = \begin{bmatrix} e_{cb} \\ e_{n,1} \\ e_{n,2} \\ \vdots \\ e_{n,j-1} \\ e_{n,j} \\ e_{ab} \end{bmatrix}$$

(6.120)

$$E_n = \begin{bmatrix} e_{n,1} \\ e_{n,2} \\ \vdots \\ e_{n,j-1} \\ e_{n,j} \end{bmatrix}$$

(6.121)

$$E_{n+1} = \begin{bmatrix} e_{n+1,1} \\ e_{n+1,2} \\ \vdots \\ e_{n+1,j-1} \\ e_{n+1,j} \end{bmatrix}$$

(6.122)

Rearrange Eq. 6.99,

$$(I + Diffuterm)E_{n+1} = E_n - ACterm - Bterm - Boundaryterm$$

(6.123)

where,

$$I = j \times j\ identity\ matrix$$

$$ACterm = 0.5r * ACoefM * DDmatrix * W2$$

$$Bterm = 0.25 * R * BCoefM * diag(DDmatrix * W2) * DDMatix * W2$$

$$Diffuterm = (R * bCoefM * K)$$

Then the void ratio at the new time interval, n+1, can be solved via MATLAB.

Appendix 3 MATLAB code example
Appendix 3.1 Large strain consolidation for 5 kPa surcharge

Materials: oil sands tailings (MFT-A)

```
clear
clc
```

Configuration of tailings

```
H0=0.11; % initial height of tailings (unit m)
e0=4.0; %initial void ratio of tailings
surcharge=5; %surcharge pressure (unit kPa)
gammas=25.1; %unit weight (kN/m^3) of MFT-A solid
gammaw=9.81; %unit weight (kN/m^3) of water
```

Definition of variables

```
s0=1/(1+e0)*H0; % initial height in material coordinate
j=250; % grid in s-direction;
dels=s0/(j+2); %thickness of each layer
t=450; % time in hours
delt=0.1; %time interval
n=t/delt; % grid in time-space n time steps

r=delt/dels; % r coefficient
R=delt/dels^2; % R coefficient
e=zeros(j,n); % void Ratio matrix with size of j by n
e(:,1)=e0; % initial value of void ratio defined as e0

I=sparse(eye(j)); % Define an identity matrix with js '1' in its diagonal
K=sparse(toeplitz([-2 1 zeros(1, j-2)])); % Generate a 1-D 2 order difference
matix
D=sparse(-diag(ones(j-1,1),-1)+diag(ones(j-1,1),1)); % Generate a 1-D 1 order
difference matix
feo=zeros(1,n); % feo matix in boundary term
Aboundary=zeros(1,n); % Boundary matrix at anode in boundary term
Cboundary=zeros(1,n); % Boundary matrix at Cathode in boundary term
ACterm=zeros(size(e)); % generate matrix for convection term
Bterm=zeros(size(e)); % generate matrix for square of 1st order difference
Diffuterm=zeros(size(e)); % generate matrix for diffusion term
H=zeros(1,n); % generate a vector for height changes
```

```
S=zeros(1,n); % generate a vector for settlement changes
T=zeros(1,n); % generate a vector for plotting time
sigmaeff=zeros(1,n); % generate a vector for effective stress
KAb=[zeros(1,j-1) 1]'; % anode boundary matrix
KCb=[1 zeros(1,j-1)]'; % cathode boundary matrix
KDmatrix=[KCb K KAb]; % 2nd order difference matrix with boundary value
DDmatrix=[-KCb D KAb]; % 1st order difference matrix with boundary value
A=zeros(size(e)); % Coefficient matrix
b=zeros(size(e)); % Coefficient matrix
B=zeros(size(e)); % Coefficient matrix
W1=zeros(j+1,n); % generate a vector for void ratio with cathode boundary
W2=zeros(j+2,n); % generate a vector for void ratio with two side boundary
```

Function of parameters

Hydraulic conductivity-void ratio function

```
chydrau=6*10^-11*3600; % coefficient ch1 (m/h)
ahydrau=3.9055; % coefficient a1
kh= @(e) chydrau*e.^ahydrau; % function of kh(e)
dkh=@(e) ahydrau*chydrau*e.^(ahydrau-1); % 1st derivative of kh(e) to e
f=@(e) (chydrau*e.^ahydrau)./(e + 1); % function of f=kh=@((e)/(e+1)
df= @(e) chydrau*ahydrau*e.^(ahydrau-1)./(1+e)-
(chydrau*e.^ahydrau)./((1+e).^2);  % 1st derivative of f(e) to e
```

Effetive stress (sigma)-void ratio function

```
csigma=2.403;
asigma=-1/0.193;
sigma= @(e) (e./csigma).^asigma;
dsigma= @(e) (asigma.*(e./csigma).^asigma)./e;
dsigma2= @(e) (asigma^2.*(e./csigma).^asigma)./e.^2-
(asigma2.*(e./csigma).^asigma)./e.^2;
```

Time loop for differential equation in time space grid

```
for l=1:n

   % Boundary condition for free top
   sigmaboundaryA=surcharge;
   Aboundary(l)=csigma*sigmaboundaryA^(1/asigma);
   AB=[zeros(1,j-1) Aboundary(l)]';

   % Boundary condition for free bottom
```

```
    sigmaboundaryC=surcharge+H0/(1+e0)*(e0*gammaw+gammas);
    Cboundary(l)=csigma*sigmaboundaryC^(1/asigma);
    CB=[Cboundary(l) zeros(1,j-1)]';
    W1(:,l)=[Cboundary(l) e(:,l)']';
    W2(:,l)=[Cboundary(l) e(:,l)' Aboundary(l)]';
    % Term A-convection term for hydraulic flow
    A(:,l)=(2.51-1)*df(e(:,l));
    ACoefM=diag(A(:,l));
    % Term b&B-diffusion term of flow
    b(:,l)=(1/gammaw)*f(e(:,l)).*dsigma(e(:,l));
    B(:,l)=(1/gammaw)*(df(e(:,l)).*dsigma(e(:,l))+f(e(:,l)).*dsigma2(e(:,l)));
    BCoefM=diag(B(:,l));
    bCoefM=diag(b(:,l));
    % Coefficient matrix for differential equation
    ACterm(:,l)=0.5*r*(ACoefM)*(DDmatrix*W2(:,l));
    Bterm(:,l)=0.25*R*(BCoefM)*(diag(DDmatrix*W2(:,l))*(DDmatrix*W2(:,l)));
    Diffuterm(:,l)=R*(bCoefM)*(KDmatrix*W2(:,l));
    Boundaryterm=R*bCoefM*(AB+CB);
    % Backward in time-Centered in space
    Newtimeterm=I+R*(bCoefM)*K;
    Oldtimeterm=-ACterm(:,l)-Bterm(:,l)+e(:,l)-Boundaryterm;
    e(:,l+1)=(Newtimeterm)\(Oldtimeterm);
    % Settlement and Height changes
    T(l)=l*delt;
    H(l)=dels*sum(W2(:,l))+(j+2)*dels;
    S(l)=H0-H(l);

end
```

Plot the results

```
Height=H./H0;
Verti=S./H0;
plot(T, Height);
axis([0 inf 0 1.2]);
xlabel('Time (hours)','FontName','Times New Roman','FontSize',12);
ylabel('Normalized height, H_t/H_0 (%)','FontName','Times New
Roman','FontSize',12);
hold on
```

Appendix 3.2 Large strain consolidation for EK combined with 5kPa surcharge

Materials: oil sands tailings (MFT-A)

```
clear
clc
```

Configuration of tailings

```
H0=0.11; % initial height of tailings (unit m)
e0=4.3; %initial void ratio of tailings
surcharge=5; %surcharge pressure (unit kPa)
gammas=25.1; %unit weight (kN/m^3) of MFT-A solid
gammaw=9.81; %unit weight (kN/m^3) of water
ic=15; %current density (unit A/m^2)
```

Definition of variables

```
s0=1/(1+e0)*H0; % initial height in material coordinate
j=150; % grid in s-direction;
dels=s0/(j+1); %thickness of each layer
t=1000; % time in hours
delt=0.1; %time interval
n=t/delt; % grid in time-space n time steps

r=delt/dels; % r coefficient
R=delt/dels^2; % R coefficient
e=zeros(j,n); % void Ratio matrix with size of j by n
e(:,1)=e0; % initial value of void ratio defined as e0

I=sparse(eye(j)); % Define an identity matrix with js '1' in its diagonal
K=sparse(toeplitz([-2 1 zeros(1, j-2)])); % Generate a 1-D 2 order difference
matix
D=sparse(-diag(ones(j-1,1),-1)+diag(ones(j-1,1),1)); % Generate a 1-D 1 order
difference matix

feo=zeros(1,n); % feo matrix in boundary term
Aboundarydelta=zeros(1,n); % Aboundarydelta matrix (anode side) in boundary
term
Aboundary=zeros(1,n); % Boundary matrix at anode in boundary term
Cboundary=zeros(1,n); % Boundary matrix at Cathode in boundary term
```

```
Aterm=zeros(size(e)); % generate matrix for convection term
Bterm=zeros(size(e)); % generate matrix for square of 1st order difference
Diffuterm=zeros(size(e)); % generate matrix for diffusion term
H=zeros(1,n); % generate a vector for height changes
S=zeros(1,n); % generate a vector for settlement changes
T=zeros(1,n); % generate a vector for plotting time
sigmaeff=zeros(1,n); % generate a vector for effective stress
KAb=[zeros(1,j-1) 1]'; % anode boundary matrix
KCb=[1 zeros(1,j-1)]'; % cathode boundary matrix
KDmatrix=[KCb K KAb]; % 2nd order difference matrix with boundary value
DDmatrix=[-KCb D KAb]; % 1st order difference matrix with boundary value
A=zeros(size(e)); % Coefficient matrix
b=zeros(size(e)); % Coefficient matrix
B=zeros(size(e)); % Coefficient matrix
f2=zeros(size(e)); % Coefficient matrix
c=zeros(size(e)); % Coefficient matrix
C=zeros(size(e)); % Coefficient matrix
W1=zeros(j+1,n); % generate a vector for void ratio with cathode boundary
W2=zeros(j+2,n); % generate a vector for void ratio with two side boundary
```

Function of parameters

Hydraulic conductivity-void ratio function

```
chydrau=6*10^-11*3600; % coefficient ch1 (m/h)
ahydrau=4.1947; % coefficient a1
kh= @(e) chydrau*e.^ahydrau; % function of kh(e)
dkh=@(e) ahydrau*chydrau*e.^(ahydrau-1); % 1st derivative of kh(e) to e
f=@(e) (chydrau*e.^ahydrau)./(e+1); % function of f=kh=@((e)/(e+1)
df= @(e) chydrau*ahydrau*e.^(ahydrau-1)./(1+e)-(chydrau*e.^ahydrau)./((1+e).^2); % 1st derivative of f(e) to e
```

Electrical conductivity-void ratio function

```
ck1=0.6888;
ck2=7.2075;
kappa=@(e) ck1.*(e./(1+e)).^ck2;
dkappa=@(e) -ck2/ck1.*(1-e./(1+e))./(e.*(e./(1+e)).^ck2);
```

Coefficient of electroosmotic-void ratio function

```
ake3=18.441;
ke0=0.0016;
ke=@(e) ke0.*(e./(1+e)).^ake3;
```

```
dke=@(e) ke0.*(ake3.*((e./(1+e)).^ake3).*(1./(1+e)-e./(1+e).^2).*(1+e))./e;
```

Effective stress (sigma)-void ratio function

```
csigma2= 2.403;%1.9803;
asigma2= -1/0.193;%-1/0.147;
sigma= @(e) (e./csigma2).^asigma2;
dsigma= @(e) (asigma2.*(e./csigma2).^asigma2)./e;
dsigma2= @(e) (asigma2^2.*(e./csigma2).^asigma2)./e.^2-
(asigma2.*(e./csigma2).^asigma2)./e.^2;
desigma= @(sigma) csigma2*(1/asigma2)*sigma.^(1/asigma2-1);
```

Time loop for differential equation in time space grid

```
for l=1:n

   feo(l)=gammaw*ic*ke(e(j,l))/(kh(e(j,l))*kappa(e(j,l)));
   Aboundarydelta(l)=(-gammas+gammaw-feo(l)*(1+e(j,l)))*desigma(sigma(e(j,l)));
   Aboundary(l)=e(j-1,l)-2*dels*Aboundarydelta(l);
   AB=[zeros(1,j-1) Aboundary(l)]';

   % Boundary condition for free bottom

   sigmaboundaryC=surcharge+H0/(1+e0)*(e0*gammaw+gammas);
   Cboundary(l)=csigma2*sigmaboundaryC^(1/asigma2);
   CB=[Cboundary(l) zeros(1,j-1)]';
   W1(:,l)=[Cboundary(l) e(:,l)']';
   W2(:,l)=[Cboundary(l) e(:,l)' Aboundary(l)]';
   % Term A-convection term for hydraulic flow
   A(:,l)=(2.51-0.981)*df(e(:,l));
   ACoefM=diag(A(:,l));
   % Term b&B-diffusion term of flow
   b(:,l)=(1/gammaw)*f(e(:,l)).*dsigma(e(:,l));
   B(:,l)=(1/gammaw)*(df(e(:,l)).*dsigma(e(:,l))+f(e(:,l)).*dsigma2(e(:,l)));
   BCoefM=diag(B(:,l));
   bCoefM=diag(b(:,l));
   % Term C-electroosmotic convection term
   f2(:,l)=ic.*(((ke(e(:,l)))).*dkappa(e(:,l))+dke(e(:,l))./kappa(e(:,l)));
   C(:,l)=f2(:,l);
   CCoefM=diag(C(:,l));
   % Coefficient matrix for differential equation
   Aterm(:,l)=0.5*r*(ACoefM+CCoefM)*(DDmatrix*W2(:,l));
   Bterm(:,l)=0.25*R*(BCoefM)*(diag(DDmatrix*W2(:,l))*(DDmatrix*W2(:,l)));
```

```
    Diffuterm(:,l)=R*(bCoefM)*(KDmatrix*W2(:,l));
    Boundaryterm=R*bCoefM*(AB+CB);

    % Backward in time-Centered in space
    Newtimeterm=I+R*(bCoefM)*K;
    Oldtimeterm=-Aterm(:,l)-Bterm(:,l)+e(:,l)-Boundaryterm;
    e(:,l+1)=(Newtimeterm)\(Oldtimeterm);

    % Settlement and Height changes
    T(l)=l*delt;
    H(l)=dels*sum(W1(:,l))+(j+1)*dels;
    S(l)=H0-H(l);
end
```

Plot the results

```
Height=H./H0;
Verti=S./H0;
subplot(2,1,1);
plot(T, Verti,'-r');
axis([0 inf 0 1.2]);
xlabel('Time (hours)','FontName','Times New Roman','FontSize',12);
ylabel('Normalized water drainage, V_w/V_0 (%)','FontName','Times New
Roman','FontSize',12);
str1={'(a)'};
text(-15,1.4,str1,'FontName','Times New Roman','FontSize',12)
hold on;
subplot(2,1,2);
plot(T, Height,'-b');
axis([0 inf 0 1.2]);
xlabel('Time (hours)','FontName','Times New Roman','FontSize',12);
ylabel('Normalized height, H_t/H_0 (%)','FontName','Times New
Roman','FontSize',12);
str2={'(b)'};
text(-15,1.4,str2,'FontName','Times New Roman','FontSize',14)
hold on;
```

Published with MATLAB® R2016a

Curriculum Vitae

Name: Yu Guo

Post-secondary Education and Degrees:

University of Science and Technology Beijing
Beijing, China
2006-2010 B.E.

The University of Western Ontario
London, Ontario, Canada
2010-2012 M.E.Sc

Western University
London, Ontario, Canada
2013-2017 Ph.D.

Honours and Awards:

John Booker Award, GRC
2014

R.M. Quigley Award
2016

Related Work Experience

Teaching and Research Assistant
The University of Western Ontario
2010-2016

Publications:

Guo, Y. and Shang, J.Q. (2014) A study on electrokinetic dewatering of oil sands tailings. Environmental Geotechnics, 1, No.2, 121-134.

Luo, X., Shang, J.Q. and *Guo, Y.* (2013). An Experimental Study on Landslide Mechanisms in Three-Gorges Reservoir Area, China. Proceedings of the 23rd International Offshore and Polar Engineering, Anchorage, Alaska, USA, June 30–July 5, 2, 698-702.

Guo, Y., Shang, J.Q., Luo, X. and Lo, K.Y. (2015). Landslides in the Three Gorges Reservoir Area. Proceedings, The 3rd IACGE International Conference on Geotechnical and Earthquake Engineering (IACGE2015), Los Angeles, USA, May 14 to 16.